THE ROLE AND REGULATION OF NUCLEAR MYOSINS IN DNA DAMAGE

Alexander William Cook

A thesis submitted for degree of doctor of philosophy

DEPARTMENT OF BIOSCIENCES
UNIVERSITY OF KENT
2019

An understanding of the natural world and what's in it, is
a source of not only a great curiosity, but great fulfilment.

Sir David Attenborough

Declaration

No part of this thesis has been submitted in support of an application for any degree or other qualification of the University of Kent, or any other University or Institution of learning.

Alexander Cook

Date. 22nd October 2019

Acknowledgements

My thanks go to my supervisor Dr. Christopher P. Toseland, he has taught me how to become a scientist. He gave me, a person he had never met before, an opportunity to undertake a PhD within his lab, allowing me to fulfil a dream of mine. I also wish to thank my supervisory chair Prof. Mike Geeves, a man who knows everything there is to know about myosins and who has helped shape my PhD. The Toseland lab all members past and present, in particular, Ália, Yukti, Rosie, and Natali. You have all made this experience amazing, you made every day in the lab enjoyable. A specific thanks to Ália and Yukti, for providing feedback about this thesis, and pointing out how little I know about English grammar!

At the University of Kent, I have made friends who have provided support; everyone in the Goult lab and Kad lab have been with me since the start. Luke, Jamie, Elliot, Diego and Austin have been a constant source of entertainment, and made me realise how important it is to have laugh.

I also wish to thank the collaborators that have helped to produce this work, in particular Prof. Piergiorgio Percipalle at NYU Abi Dhabi, and Tomáš Venit. Thanks to Kevin Howland at UKC for help with the proteomics, and Dr. Peter Ellis for the chromosome paints and help with FISH.

Finally I have to thank my parents, my sister and Katie. Katie, you have been with me since the very start of my PhD, and have been there for me, even when we had to bury my gerbil! Emily, thank you for calling me a nerd throughout my teenage years, I think I am exactly that. Dad, you have allowed me to do things that I could only have dreamt to do, and for that I am forever grateful. Mum, every time I speak to you on the phone, I feel at home, your advice, support and supply of food “to take home as a treat”, got me through 7 years of studying. I hope I can become the parents you have been for me.

Table of Contents

CHAPTER 1. FOREWORD 16

1.1 RESEARCH CONTRIBUTIONS 17
1.1.1 PUBLICATIONS 17

1.1.2 POSTERS 17

1.2 ABSTRACT 18
1.3 TABLE OF ABBREVIATIONS 19

CHAPTER 2. INTRODUCTION 21

2.1 GENERAL MYOSINS 22
2.2 THE VARIATION OF MYOSIN STRUCTURES 23
2.3 MYOSIN IC 25
2.3.1 OVERVIEW 25

2.3.2 MICS CROSS BRIDGE CYCLE 26

2.3.3 REGULATING MIC THROUGH ITS IQ REGIONS 28

2.3.4 MICS TAIL DOMAIN DEFINES ITS FUNCTION 29

2.3.5 MICS BINDING PARTNERS 29

2.4 MYOSIN VI (MVI) 30
2.4.1 MVI STRUCTURE 30

2.4.2 MVIS CROSS BRIDGE CYCLE 30

2.4.3 MVIS IQ DOMAINS 31

2.4.4 MVIS TAIL 31

2.4.5 MVIS BINDING PARTNERS 33

2.5 ACTIN INSIDE THE CELL 34
2.5.1 CYTOPLASMIC ACTIN 34

2.5.2 NUCLEAR ACTIN 35

2.6 NUCLEAR MYOSINS 37
2.6.1 THE IMPORT AND EXPORT OF NUCLEAR MYOSINS 37

2.6.2 MIC IMPORT AND EXPORT 38

2.6.3 MVI IMPORT AND EXPORT 39

2.7 FUNCTION OF NUCLEAR MYOSINS 39

2.7.1 NUCLEAR MYOSINS IN TRANSCRIPTION 40

2.7.2 NM1'S ROLE IN TRANSCRIPTION 40

2.7.3 MVIS ROLE IN TRANSCRIPTION 41

2.8 DNA DAMAGE 42

2.9 SIGNALLING DOUBLE STRANDED BREAKS (DSBS) 44

2.9.1 ACTIVATION OF PROTEIN KINASES 44

2.9.2 ΓH2AX SIGNALLING 44

2.10 REPAIRING DOUBLE STRAND BREAKS 45

2.10.1 HOMOLOGOUS RECOMBINATION 45

2.10.2 NON-HOMOLOGOUS END JOINING 46

2.10.3 IRREPARABLE DSB DAMAGE 47

2.11 NUCLEAR MYOSINS IN DNA DAMAGE 48

2.11.1 MVI AND P53 48

2.11.2 GLOBAL CHROMOSOME RE-ARRANGEMENTS BY NM1 49

2.11.3 CHROMOSOME REARRANGEMENTS BY OTHER NUCLEAR MYOSINS 50

2.12 THE NUCLEAR MYOSIN FIELD 51

CHAPTER 3. MATERIALS AND METHODS 52

3.1 CHEMICALS AND REAGENTS 53

3.1.1 RECOMBINANT PROTEIN EXPRESSION CONSTRUCTS 53

3.1.2 PRIMERS 54

3.1.3 2.4 OLIGONUCLEOTIDES 54

3.1.4 NM1 PEPTIDE 55

3.1.5 DRUG STOCKS AND ANTIBODIES 56

3.1.6 WHOLE CHROMOSOME PAINTS 58

3.2 METHODS 59

3.2.1 BACTERIAL TRANSFORMATION 59
3.2.2 BACTERIAL PROTEIN EXPRESSION 59
3.2.3 BACULOVIRUS BACTERIAL TRANSFORMATION 59
3.2.4 ISOLATION AND ANALYSIS OF RECOMBINANT BACMID DNA 60
3.2.5 INSECT CELL TRANSFECTION AND PROTEIN EXPRESSION 61
3.2.6 FULL LENGTH NM1 PURIFICATION FROM SF21 CELLS 61
3.2.7 SDS-PAGE ANALYSIS 62
3.2.8 WESTERN BLOTTING 62
3.2.9 RECOMBINANT PROTEIN PURIFICATION 63
3.2.10 CIRCULAR DICHROISM 64
3.2.11 NM1 N-TERMINAL PEPTIDE FLUORESCENT LABELLING 64
3.2.12 FLUORESCENCE MEASUREMENTS 65
3.2.13 MAMMALIAN CELL CULTURE 65
3.2.14 MVI KNOCKDOWN 66
3.2.15 RNA-SEQ SAMPLE PREPARATION 67
3.2.16 RNA SEQUENCING AND ANALYSIS 67
3.2.17 MVI CO-IMMUNOPRECIPITATION 68
3.2.18 MVI PROTEOMICS PREPARATION 69
3.2.19 LC- MS/MS AND PROTEOMICS ANALYSIS 70
3.2.20 CONFOCAL IMMUNOFLUORESCENCE 71
3.2.21 HIGH CONTENT SCREENING 72
3.2.22 STORM IMAGING 73
3.2.23 CLUS-DOC ANALYSIS 73
3.2.24 2D-FISH 74
3.2.25 APOPTOSIS ASSAY 75

CHAPTER 4. PROPERTIES OF NUCLEAR MYOSIN 1 76

CHAPTER 1 ..... **77**
CHAPTER 2 ..... **77**
4.1 INTRODUCTION 77
4.1.1 NUCLEAR MYOSIN I 77
4.1.2 REGULATION OF MIC 78
4.1.3 NM1S IMPORT INTO THE NUCLEUS 80
4.1.4 NM1S FUNCTION IN THE NUCLEUS 82
4.1.5 DNA BINDING BY NM1 84
4.1.6 AIMS OF THIS STUDY 84
4.2 RESULTS 84
4.2.1 FULL LENGTH NM1 PURIFICATION REQUIRES FURTHER OPTIMISATION 84
4.2.2 NM1 TAIL CONSTRUCT CONTAINS STRUCTURE 87
4.2.3 THE N-TERMINUS OF NM1 COMPETES WITH CAM TO BIND TO ITS OWN TAIL 89
4.2.4 THE TAIL DOMAIN OF NM1 HAS NANO-MOLAR AFFINITY FOR DSDNA 92
4.2.5 THE TAIL DOMAIN OF NM1 BINDS SSDNA AS WELL 92
4.2.6 NM1 AND CAM COLOCALISE WITHIN THE NUCLEUS 95
4.3 DISCUSSION 97
4.3.1 THE PURIFICATION OF FULL LENGTH NM1 REQUIRES FURTHER OPTIMISATION 97
4.3.2 RECOMBINANT NM1 TAIL IS A STABLE CONSTRUCT FOR *IN VITRO* STUDIES 98
4.3.3 N-TERMINAL – TAIL INTERACTION PROVIDES AN EXPLANATION FOR ALTERED MOTOR ACTIVITY 98
4.3.4 N-TERMINAL REGULATION MAY PLAY A ROLE IN NUCLEAR IMPORT 99
4.3.5 NM1S ABILITY TO BIND DNA IS POTENTIALLY REGULATED BY CAM 100
4.3.6 DNA BINDING MUST OCCUR THROUGH ELECTROSTATIC INTERACTIONS 101
4.3.7 NM1S ROLE AND REGULATION 101

CHAPTER 5. MYOSIN VIS' RESPONSE TO DNA DAMAGE 103

5.1 INTRODUCTION. 104

5.1.1 MYOSIN VI. 104
5.1.2 MVI IN THE NUCLEUS. 105
5.1.3 DNA DAMAGE INDUCING DRUGS. 107
5.1.4 DNA DAMAGE AND MVI. 109
5.1.5 THE FIRST STAGES OF THE DOUBLE STRAND BREAK RESPONSE. 111
5.1.6 HIGH CONTENT SCREENING (HCS). 114
5.1.7 RNA-SEQ, THE METHOD TO STUDY TRANSCRIPTOMICS. 114
5.1.8 LIQUID CHROMATOGRAPHY – MASS SPECTROMETRY, THE METHOD TO STUDY PROTEOMICS. 116
5.1.9 THE AIMS OF THIS STUDY. 117
5.2 RESULTS 118
5.2.1 MVI LEVELS IN THE NUCLEUS CHANGE AFTER DNA DAMAGE 118
5.2.2 LIPOFECTAMINE AND SCRAMBLED SIRNA HAS AN EFFECT ON THE TRANSCRIPTOMICS OF A CELL. 120
5.2.3 CISPLATIN TREATMENT ITSELF HAS THE LARGEST EFFECT ON GENE REGULATION. 123
5.2.4 CISPLATIN TREATMENT ALTERS A DIVERSE SET OF GENES. 125
5.2.5 MVI KD EFFECTS THE TRANSCRIPTOME DIFFERENTLY TO CISPLATIN TREATMENT. 128
5.2.6 MVI KD WITH CISPLATIN TREATED CELLS BEHAVES SIMILAR TO THAT OF CISPLATIN ONLY TREATED CELLS. 130
5.2.7 MVI KD WITH CISPLATIN TREATMENT DOES NOT AFFECT EXPRESSION OF GENES REQUIRED FOR THE DNA DAMAGE RESPONSE 133
5.2.8 THE MVI INTERACTOME BEFORE TREATMENT, IS CELL LINE INDEPENDENT. 135
5.2.9 THE MVI INTERACTOME AFTER CISPLATIN TREATMENT IS CELL LINE DEPENDENT. 136
5.2.10 HELA MVI INTERACTS WITH A MULTITUDE OF DNA DAMAGE REPAIR PROTEINS. 139
5.2.11 CISPLATIN CAUSES MVI TO INTERACT WITH CHROMATIN REMODELLING COMPLEXES. 142
5.2.12 MVI INTERACTS WITH THE SAME DNA DAMAGE PROTEINS IN HELA AND MCF10A BEFORE DNA DAMAGE 144

5.2.13 MCF10A MVI DOES NOT INTERACT WITH DSB SPECIFIC PROTEINS IN MCF10A AFTER DNA DAMAGE 146

5.3 DISCUSSION 149

5.3.1 THE MVI LOCALISATION CHANGES OBSERVED AFTER CISPLATIN TREATMENT SHOWS A SPECIFIC PROTEIN RESPONSE TO DNA DAMAGE 149

5.3.2 TRANSFECTIONS CHANGE THE TRANSCRIPTOME OF CELLS. 150

5.3.3 DNA DAMAGE ITSELF DOES NOT CHANGE THE EXPRESSION OF DNA REPAIR PROTEINS. 151

5.3.4 MVI KD DOES NOT HAVE THE SAME TRANSCRIPTIONAL EFFECT AS CISPLATIN TREATMENT. 152

5.3.5 HELA CELLS STILL TRANSCRIPTIONALLY RESPOND TO DNA DAMAGE AFTER MVI KD. 153

5.3.6 MVI DOES NOT HAVE A ROLE TRANSCRIPTIONALLY IN THE DNA DAMAGE RESPONSE. 155

5.3.7 MVI BINDING PARTNERS ARE SIMILAR BETWEEN CANCEROUS AND NON-CANCEROUS CELL LINES. 156

5.3.8 MVI HAS A ROLE IN DNA REPLICATION 157

5.3.9 MVI RESPONDS TO DNA DAMAGE BY BINDING TO DNA DAMAGE PROTEINS 158

5.3.10 MVI MAY PLAY A ROLE IN CHROMATIN REORGANISATION AFTER DNA DAMAGE 160

5.3.11 MVI RESPONDS TO DNA DAMAGE AT A PROTEIN-PROTEIN LEVEL AND NOT BY REGULATING TRANSCRIPTION 160

CHAPTER 6. MVI INVOLVEMENT IN DSB SIGNALLING 162

6.1 INTRODUCTION 163

6.1.1 HISTONES AND THEIR MODIFICATIONS 163

6.1.2 ΓH2AX SIGNALLING. 165

6.1.3 DSB REPAIR FOCI 166

6.1.4 2,4,6-TRIIODOPHENOL (TIP) THE SMALL MOLECULE INHIBITOR OF MVIS MOTOR DOMAIN. 168

6.1.5 KU55933 AN ATM INHIBITOR. 169

6.1.6 CONFOCAL MICROSCOPY 169

6.1.7 STOCHASTIC OPTICAL RECONSTRUCTION MICROSCOPY (STORM) 170

6.1.8 CLUSTER ANALYSIS WITH DEGREE OF COLOCALIZATION (CLUS-DOC) 173

6.1.9 STUDYING APOPTOSIS.....175

6.1.10 THE AIMS OF THIS STUDY 176

6.2 RESULTS 177

6.2.1 MVI INHIBITED HELA, RESPOND TO DNA DAMAGE. 177

6.2.2 THE MOTOR ACTIVITY OF MVI IS REQUIRED FOR DNA DAMAGE SIGNALLING IN MCF10A CELLS.181

6.2.3 MVI IS CAPABLE OF ENTERING THE NUCLEUS OF HELA CELLS AFTER TIP TREATMENT. 183

6.2.4 MCF10A CELL LINE REQUIRES MVI FOR PHOSPHORYLATION OF H2AX. 186

6.2.5 MVI INHIBITION CAUSES A GREATER CHANGE TO DNA DAMAGE HISTONE MODIFICATIONS THAN DAMAGE ITSELF. 189

6.2.6 USING CLUS-DOC FOR DATA ANALYSIS ON MCF10A CELLS. 193

6.2.7 MVI FORMS LARGER CLUSTERS AFTER DNA DAMAGE IN MCF10A CELLS.....195

6.2.8 CLUS-DOC PROVIDES INFORMATION ON THE COLOCALIZATION OF PROTEIN CLUSTERS IN MCF10A CELLS 197

6.2.9 ГH2AX CLUSTERS VARY WITHIN THE NUCLEUS IN MCF10A CELLS. 199

6.2.10 MVI CLUSTERING INCREASES AROUND AREAS OF DENSE ГH2AX IN MCF10A CELLS.....200

6.2.11 STUDYING APOPTOSIS REQUIRES FURTHER WORK 205

6.3 DISCUSSION..... 206

6.3.1 MVI MOTOR DOMAIN INHIBITOR TIP PREVENTS NUCLEAR LOCALISATION OF MVI. 206

6.3.2 MCF10A CELLS RELY ON NUCLEAR MVI TO SIGNAL DSBS. 208

6.3.3 MVIS MOTOR IS REQUIRED TO REGULATE HISTONE MODIFICATIONS. 209

6.3.4 MVI CAN BE FOUND AT ГH2AX REPAIR FOCI. 210

CHAPTER 7. LINKING THE ROLES OF NM1 AND MVI IN THE NUCLEUS 212

7.1 INTRODUCTION 213

7.1.1 CHROMOSOME TERRITORIES.....213

7.1.2 HISTONE MODIFICATIONS SHAPE CHROMATIN 214

7.1.3 ACTIN HAS A DIRECT INTERACTION WITH CHROMATIN ORGANISERS 215

7.1.4 NM1 BINDS DIRECTLY TO CHROMATIN REMODELLING COMPLEXES. 218

7.1.5 NUCLEAR MYOSINS ARE INVOLVED IN LONG-RANGE CHROMATIN MOVEMENTS 218

7.1.6 MYOSIN I AND MVI COOPERATE WITHIN THE CYTOPLASM OF THE CELL. 220

7.1.7 USING FLUORESCENCE IN SITU HYBRIDISATION (FISH) FOR STUDYING CHROMOSOME LOCATIONS. 221

7.1.8 THE AIMS OF THIS STUDY. 222

7.2 RESULTS 222

7.2.1 HELA AND MCF10A CELLS MODIFY THEIR HISTONES DIFFERENTLY AFTER DNA DAMAGE 222

7.2.2 NUCLEAR MVI IS RESPONSIBLE FOR CORRECT HISTONE MODIFICATIONS 223

7.2.3 HELA CHROMOSOME TERRITORIES DIFFER TO HUMAN DERMAL FIBROBLASTS 227

7.2.4 MVI IS REQUIRED FOR CT ORGANISATION BOTH BEFORE AND AFTER DNA DAMAGE 228

7.2.5 NEITHER NM1 OR MVI NUCLEAR CLUSTERING IS AFFECTED BY TIP 231

7.2.6 MVI AND NM1 CLUSTERS ARE OFTEN SEGMENTED 233

7.3 DISCUSSION 236

7.3.1 SCIENTIFIC RESEARCH IS CELL LINE DEPENDENT 236

7.3.2 NM1 AND MVI MAY BOTH PLAY A ROLE IN TRANSCRIPTION REGULATION 237

7.3.3 HELA CELLS DO NOT REQUIRE FUNCTIONING MVI FOR THEIR HISTONE RESPONSE TO DNA DAMAGE 238

7.3.4 MVI IS REQUIRED FOR CT RELOCATIONS AFTER DNA DAMAGE 239

7.3.5 NM1 AND MVI ARE KEPT APART FROM EACH OTHER 240

CHAPTER 8. GENERAL DISCUSSION 243

8.1 SUMMARY 244
8.2 MYOSIN SELF-REGULATION AIDS ITS NUCLEAR LOCALISATION 244
8.3 MVI IS VITAL TO THE DNA DAMAGE RESPONSE 245
8.4 NUCLEAR MYOSINS PLAY A SIGNIFICANT ROLE IN CHROMOSOME ORGANISATION 248
8.5 DNA DAMAGE RESPONSE IS CELL LINE DEPENDENT 249
8.6 IMPROVING RESEARCH PRACTICES 250
8.7 FURTHER WORK 251

CHAPTER 9. REFERENCES 252

CHAPTER 10. APPENDIX 288

Table of figures

Figure 2.1. The myosin repertoire of eukaryotes 22

Figure 2.2. Comparitive diagram of mammalian myosins. 25

Figure 2.3. Schematic diagram of myosin IC. 26

Figure 2.4. The myosin cross bridge cycle. 27

Figure 2.5. A simplified diagram of MVI. 30

Figure 2.6. The isoforms of MVI exists in four isomers. 33

Figure 2.7. Actin inside the nucleus 36

Figure 2.8. MVI within RNAPII transcription. 42

Figure 2.9 Diagrams of the DNA damage repair pathways. 47

Figure 4.1. Representation of the three isoforms of myosin IC. 78

Figure 4.2. A crystal structure of myosin IBs' N-terminus. 79

Figure 4.3. A cartoon representation of NM1 nuclear localisation. 81

Figure 4.4. NM1 binds to RNAPI and DNA. 83

Figure 4.5. Purification of the full length NM1. 86

Figure 4.6. Circular Dichroism of recombinant NM1 tail. 88

Figure 4.7. NM1 tail constructs bind to the N-terminus of NM1. 91

Figure 4.8. 4 NM1 tail is able to bind dsDNA. 93

Figure 4.9. NM1 tail can bind ssDNA. 94

Figure 4.10. Colocalisation of NM1 and CaM. 96

Figure 4.11. A new model of NM1 regulation. 102

Figure 5.1. Mechanism of DNA damage drugs. 109

Figure 5.2. Double strand break response. 113

Figure 5.3. A cartoon to depict the RNA-seq procedure. 115

Figure 5.4. A cartoon to depict this studies proteomics procedure. 117

Figure 5.5. MVI moves into the nucleus after DNA damage. 119

Figure 5.6. PCA analysis of the RNA-seq data. 122

Figure 5.7. Volcano plots of upregulated and downregulated genes. 124

Figure 5.8. GO terms to distinguish gene expressions changed by DNA damage. 127

Figure 5.9. Gene expression changes caused by MVI KD. 130

Figure 5.10. GO terms to distinguish gene expressions caused by MVI KD with cisplatin treatment. 132

Figure 5.11. P53 KEGG pathways of the RNA-seq data. 134

Figure 5.12. A comparison of proteomics between healthy and damaged cell lines. 138

Figure 5.13. Protein network map of MVI interactions in WT HeLa. 141

Figure 5.14. Protein network map of MVI interactions in HeLa cells treated with cisplatin. 143

Figure 5.15. Protein network map of MVI interactions in MCF10A WT cells. 145

Figure 5.16. Protein network map of MVI interactions in MCF10A cells treated with cisplatin. 147

Figure 6.1. The current map of histone modifications. 165

Figure 6.2. An example of visible repair foci. 167

Figure 6.3. A simplified Jablonski diagram. 172

Figure 6.4. A work flow of Clus-DoC. 173

Figure 6.5. A comparison of clustering analysis and colocalisation analyses. 175

Figure 6.6. Confocal microscopy of HeLa cells with single treatments. 178

Figure 6.7. Confocal microscopy of HeLa cells with double treatments 179

Figure 6.8. A western blot of DNA damage proteins in HeLa. 179

Figure 6.9. Confocal microscopy of MCF10A cells with single treatments. 181

Figure 6.10. A western blot of DNA damage proteins in MCF10A cells. 182

Figure 6.11. Confocal microscopy of MCF10A cells after double treatments. 182

Figure 6.12. HCS of HeLa cells. 185

Figure 6.13. HCS analyses of MCF10A cells. 188

Figure 6.14. HCS analyses of DSB histone modifications in HeLa. 191

Figure 6.15. HCS analyses of DSB histone modifications in MCF10A cells. 192

Figure 6.16. A workflow of Cluster analyses. 194

Figure 6.17. The effect of cisplatin on MVI nuclear clustering. 196

Figure 6.18. A work flow of DoC analyses. 198

Figure 6.19. Violin plots showing the colocalisation of MVI and γH2AX. 203

Figure 6.20. A cartoon depicting MVI inside repair foci. 204

Figure 6.21. Apoptosis report of HeLa cells. 205

Figure 7.1. A generalised map of chromosome territories. 214

Figure 7.2. Chromatin remodelling complexes in DSBs. 217

Figure 7.3. Acting and myosins translocating DSBs. 220

Figure 7.4. An illustration of Myosin I and MVI cooperating. 221

Figure 7.5. HCS of acetyl histone modifications. 226

Figure 7.6. HCS of methyl histone modifications. 226

Figure 7.7. 2D FISH of whole painted chromosome 12 (blue) and 19 (pink). 230

Figure 7.8. NM1 and MVI clustering analysis. 232

Figure 7.9. Clus-DoC analysis of the colocalisation of MVI and NM1 clusters. 235

Table of equations

Equation 3.1. Mean residue ellipticity equation.....64

Equation 3.2. Quadratic binding equation.....65

Equation 6.1 Abbes resolution criteria 170

Equation 6.2. Ripley K function.....174

Table of tables

Table 3.1. A table of recombinant protein expression plasmids. 53

Table 3.2. A table of primers used. 54

Table 3.3. A table of oligonucleotides used. 54

Table 3.4. A table of NM1 N-terminus peptides used. 55

Table 3.5. A table of drugs used both stocks and final concentrations. 56

Table 3.6. A table of antibodies and their dilutions.....58

Table 3.7. Chromosome paints purchased from cytocell. 58

Table 3.8. A table of PCR conditions for baculovirus preparation. 60

Table 5.1. A Table of MVI nuclear localisation and nuclear export sequences 106

Table 5.3. A table of MVI protein interactions involved in the DNA damage response. 148

Chapter 1. Foreword

1.1 Research Contributions

1.1.1 Publications

1) Fili, N., Hari-Gupta, Y., dos Santos, A., **Cook, A.,** Poland, S., Ameer-Beg, S., Parsons, M., and Toseland, C. P. 2017. "NDP52 Activates Nuclear Myosin VI to Enhance RNA Polymerase II Transcription." Nature Communications 8(1):1871.

2) **Cook, A**., Hari-Gupta, Y. and Toseland, C. P. (2018) 'Application of the SSB biosensor to study in vitro transcription', *Biochemical and Biophysical Research Communications*, 496(3), pp. 820–825. doi: 10.1016/j.bbrc.2018.01.147.

1.1.2 Posters

1) Nuclear myosins in the DNA damage response – International Chromosome Conference, Prague (2018). **Alexander Cook**, Yukti Hari-Gupta, Christopher P. Toseland

2) Myosin VI is vital for the DNA damage response – Annual Meeting, The Biophysical Society, Baltimore (2019). **Alexander Cook**, Yukti Hari-Gupta, Tomas Venit, Piergiorgio Percipalle, Christopher P. Toseland.

3) Myosin VI and the DNA damage response – Nucleic Acids Forum, London (2019). **Alexander Cook**, Yukti Hari-Gupta, Tomas Venit, Piergiorgio Percipalle, Christopher P. Toseland.

1.2 Abstract

Unconventional myosins have often been characterised within the cytoplasm of the cell, however little work has been done to characterise their role within the nucleus. The first nuclear myosin was identified within the 1990s and since then eight types of myosin have been found within the nucleus. The first to be found and the one myosin that has been heavily characterised is nuclear myosin 1. This myosin has a role in transcription, as well as chromatin movement after DNA damage. Myosin VI another myosin recently found in the nucleus has also been attributed to stable transcription, and, like nuclear myosin 1 can also bind to the RNA polymerase II complex.

So far, a full length structure of nuclear myosin I is yet to be defined, here in this thesis, using typical biochemical techniques, an interaction between the N-terminus of the protein and the nuclear localisation sequence has been identified, along with disassociation constants, that finally show a direct interaction between DNA and the myosin. As well as this, MVI has had another role in the nucleus, which is observed after the induction of double strand breaks within DNA. This thesis discusses why MVI is vital for double strand break signalling, as cellular biology techniques have shown the lack of γH2AX signalling the motor domain of MVI is inhibited. Not only is a working MVI necessary for when signalling DNA damage, this thesis has also found direct interactions with histones and their modifiers.

As both nuclear myosins are involved in transcription, this thesis has looked at how these two myosins interact, and looks further into their nuclear import, roles in the DNA damage response, and how they are regulated within these roles.

1.3 Table of Abbreviations

Arp	Actin related protein
ATM	Ataxia-Telangiectasia-Mutated
CBD	Cargo binding domain
CD	Circular Dichroism
CT	Chromosome territory
dH_2O	Distilled water
DSB	Double stranded breaks
DNA	Deoxyribonucleic acid
DTT	Dithiothreitol
ECM	Extracellular matrix
EGF	Epidermal growth factor
F-actin	Filamentous actin
FBS	Fetal bovine serum
FISH	Fluorescence in Situ Hybridisation
FRAP	Fluorescence recovery after photobleaching
FRET	Fluorescence resonance energy transfer
GLOX	Glucose oxidase
GO	Gene Ontology
HAT	Histone acetyl transferases
HCS	High Content Screening
HMT	Histone methyl transferases
HR	Homologous recombination
HRP	Horse radish peroxidase
IPTG	Isopropyl-β-D-thiogalactopyronoside
JACoP	Just another colocalisation plugin
LB	Lysogeny broth

LC/MS-MS	Liquid Chromatography/ Mass Spectrometry-Mass Spectrometry
MS	Mass-Spectrometry
MIC	Myosin IC
MVI	Myosin VI
NaCl	Sodium Chloride
NER	Nucleotide excision repair
NHEJ	Non-homologous end joining
PCA	Principle component analysis
PH	Pleckstrin homology
PTM	Post translational modifications
PBS	Phosphate buffered saline
PCR	Polymerised chain reaction
PFA	Paraformaldehyde
RNAP	RNA polymerase
SSC	Saline-sodium citrate
STORM	Stochastic Optical Reconstruction Microscopy
TBS	Tris-Buffered Saline
WT	Wild Type

Chapter 2. Introduction

2.1 General Myosins

Myosins are motile proteins within a cell that utilise actin to produce movement and tension. The myosin superfamily can be divided into 79 classes and can be found throughout the eukaryotic evolutionary tree (Kollmar and Mühlhausen, 2017). So far, the study of myosin domain architectures and species phlyogenies has identified 7859 myosins within these defined classes. (Figure 2.1).

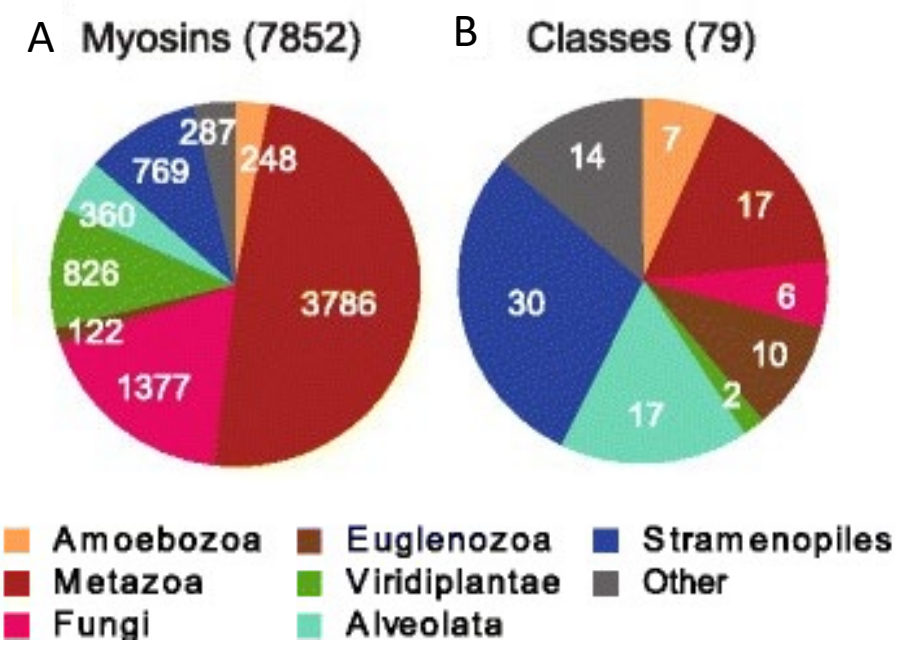


Figure 2.1. The myosin repertoire of eukaryotes

A) The amount of myosins found within each taxon of the eukaryotic evolutionary branch.

B) Number of classes identified within each taxon. Taken from Kollmar and Mühlhausen (2017).

One well characterised myosin class is the muscle myosin II found within cardiac and skeletal muscles (Eddinger and Meer, 2007; Frontera and Ochala, 2015; Somlyo *et al.,* 2004). The research carried out into these motors has provided information on how myosins are able to

generate force. This type of force generation requires the turnover of ATP into ADP, allowing the myosin to "step" along actin filaments, with the distance each myosin moves with one ATP turned over being defined as the step size (Houdusse and Sweeney, 2016). After the discovery of muscle myosins, other myosin types began to be identified within the cytoplasm and nucleus of cells. Myosins are now known to be responsible for a vast array of cellular functions such as actin based protrusions, cargo transport and cell division (Woolner and Bement, 2009). It is these non-muscle myosins that have formed the basis of my research.

2.2 The variation of myosin structures

The diversity of the myosin superfamily is down to small variations within a mostly conserved structure (Hartman and Spudich, 2012). The motor domain between myosins of different classes shows little variation; all contain an actin binding site closely aligned with an ATPase, the site that powers the myosin. A neck region dictates step size and allows binding of regulators that are able to manipulate a myosin into open and closed conformations (Burgess *et al.,* 2002). This neck domain contains IQ regions that bind to calmodulin (CaM) in a regulatory manner. An IQ sequence is defined as, [I,L,V]QxxxRGxxx[R,K], in which a hydrophobic amino acid is required at position 1, glutamine at position 2 and basic residues at position 6 and 11; X refers to any amino acid residue (Bahler and Rhoads, 2002). Depending on the type of myosin, the neck region can contain a varying number of IQ regions that are separated by 9-16 amino acids. This separation allows spacing for multiple regulatory CaMs to bind. The number of IQ domains defines the number of bound CaMs; which will stabilise a long rod conformation and dictate the myosin's step size (Sakamoto *et al.,*2005). The neck region is then followed by a C-terminal tail domain. This tail domain varies completely between different myosins and has evolved for their specific functions. It houses the cargo binding domain (CBD), pleckstrin homology (PH), which bind phosphoinositides,

and FERM domains, which provide a scaffold for linking membrane to cytoskeleton (Korn, 2000).

Some myosins also contain coiled-coil domains. These are often found immediately after the IQ regions to allow dimerization, which activates the myosin for step-wise processivity along an actin track. In the dimeric form, these myosins function together to share a cargo where each myosin head sequentially rotates into the forward position (Yu *et al.,* 2009). The same coiled-coil domains also allow for the formation of myosin filaments, where multiple myosins can form thick filaments resulting in synchronised contraction such as seen in muscle myosin II (Ikebe *et al.,* 2001).

As discussed, all myosins have some variation of these three structural domains; the motor, the neck and tail, and it is this variation that allows a plethora of roles. From this point onwards this thesis will focus on two myosins in particular, myosin IC (MIC) and myosin VI (MIV) as shown in Figure 2.2.

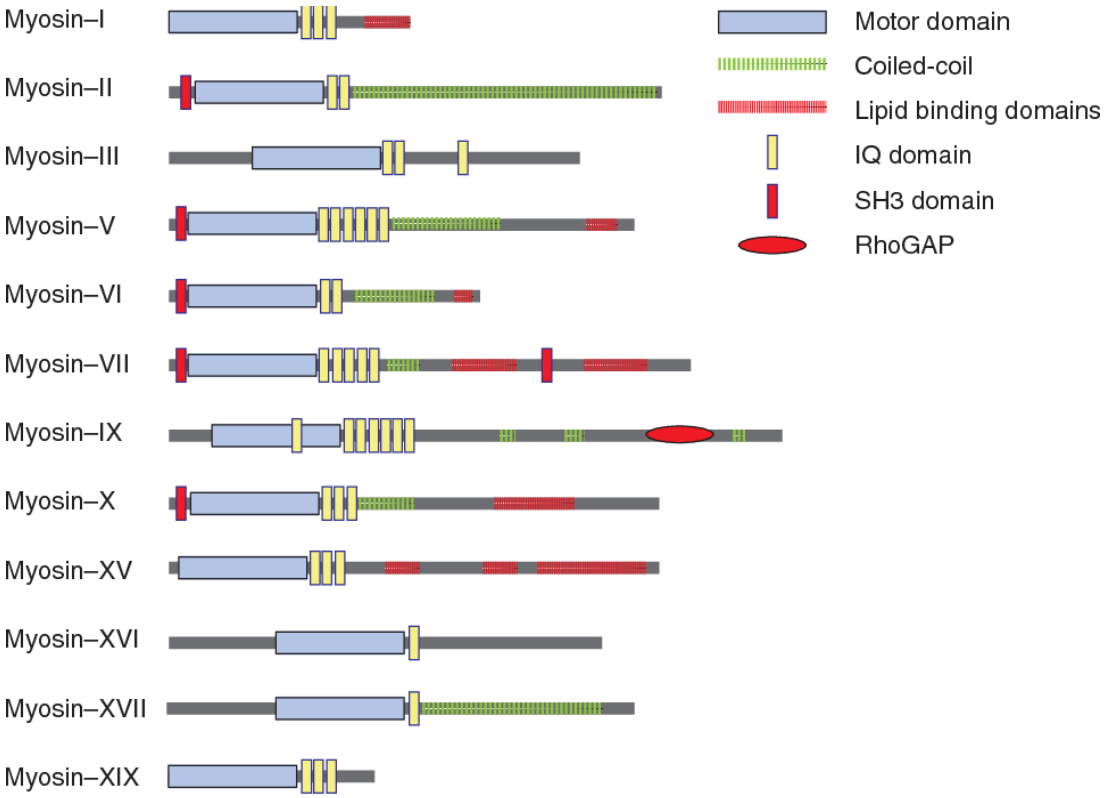


Figure 2.2. Comparitive diagram of mammalian myosins.

The general structure of each mammalian myosin taken from (Batters and Veigel, 2016).

2.3 Myosin IC

2.3.1 Overview

MIC is a myosin found abundantly within the cell and is part of the non-conventional myosin I family. It functions as a single headed motor, and its roles include linking the actin cytoskeleton to the cellular membrane, endocytosis, glucose uptake and transcription (Zattelman *et al.,* 2017). The structure of MIC is shown in Figure 2.3. It contains a conventional motor domain, a neck region that contains three flexible IQ regions and a tail domain, which houses a PH domain.



Figure 2.3. Schematic diagram of myosin IC.
A blue N-terminus showing a motor domain, followed by three IQ domains shown in yellow and the tail domain in green which contains PH domain near the C-terminus.

2.3.2 MICs cross bridge cycle

All myosins are specifically adapted to their function through the variation in their motor, neck and tail domains. Beginning with the motor domain, the ATP turnover tunes the myosin for its function. The ATPase activity of a myosin can be defined by the cross-bridge cycle described in Figure 2.4 (Geeves and Holmes, 1999). There are eight states in which the myosin can be found in. In the absence of ATP, myosin is tightly bound to actin through the actin binding domain (rigor complex). ATP then binds to the ATPase domain creating an acto-myosin-ATP complex; this complex then disassociates from the actin in a two-step manner, which can be defined by the two constants - $K_{S/W}$, for complex formation and K_{det} for detachment. Once detached from the actin, the myosin is in a recovery-like state, which leads to ATP hydrolysis and the formation of a myosin-ADP-P_i complex which allows rebinding to actin (Walklate *et al.,* 2016). With the rebinding of actin, the inorganic phosphate leaves the complex, resulting in the power stroke of the myosin pulling on the actin. Once this power stroke is complete the change in conformation allows the release of the ADP returning the cross-bridge cycle to the initial actin-myosin rigor state complex.

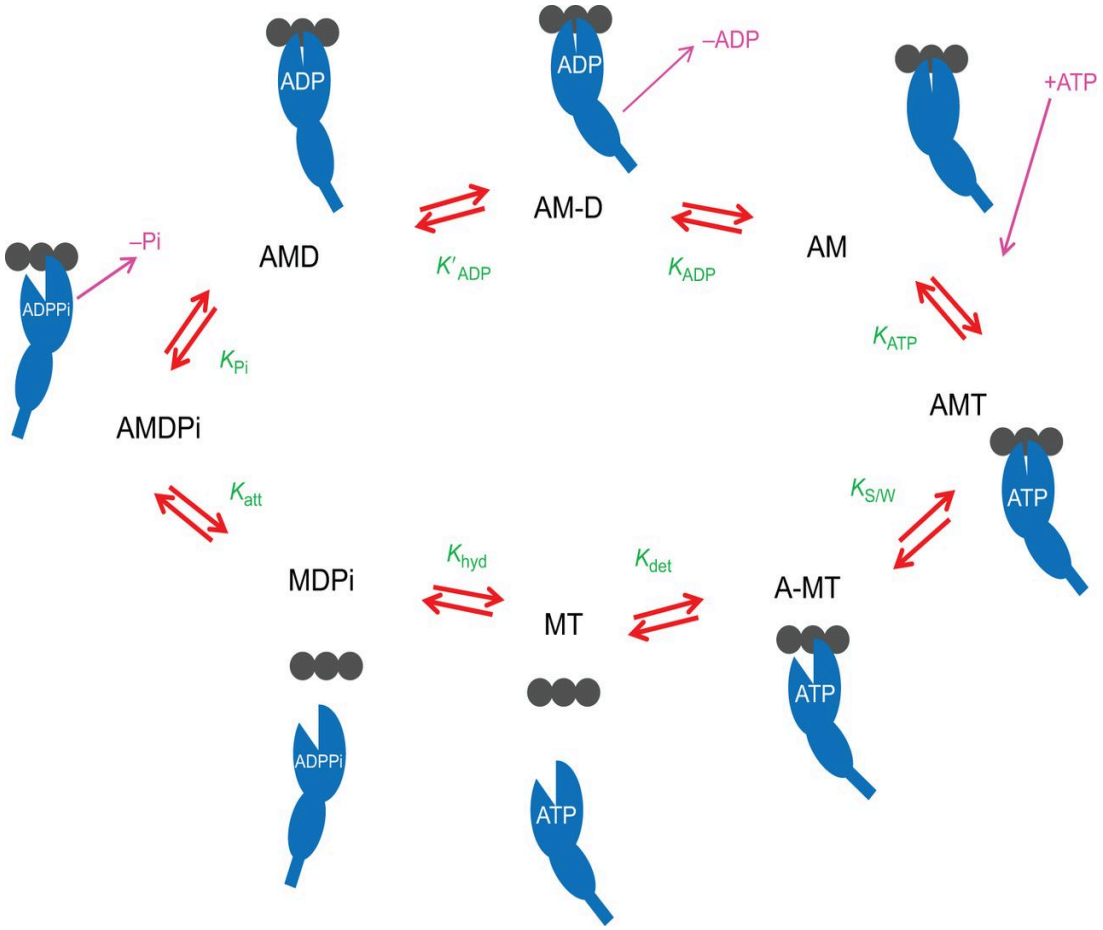


Figure 2.4. The myosin cross bridge cycle.

Starting from the myo-actin complex (AM), there is the addition of ATP, leading to the detachment of myosin off the actin (MT), the hydrolysis of ATP to ADP causing the acto-myosin complex to reform ($AMDP_i$), then the loss of the ingorganic phosphate Pi to form the tightly associated myo-actin complex (AMD). Taken from (Walklate *et al.,* 2016)

Like most myosins, myosin IC is sensitive to forces applied through cargo binding. These forces are able to dictate the cross bridge cycle kinetics of a motor protein. At low forces, less than 1pN, ADP release limits the detachment of myosin from actin, however at forces above 1pN, the myosin detachment from actin is limited by the binding of ATP. This differs from another myosin I isoform, isoform 1B, in which its cross bridge cycle is incredibly sensitive to force below 1pN, which allows longer attachment lengths once bound to cargo. This type of attachment length can be attributed to myosin 1Bs role as a molecular force

sensor (Greenberg *et al.,* 2012). Yet MIC remains as a stable transporter over a range of forces.

Once again to fully study the function of a myosin, an understanding of its structure and its motor domain is required.

2.3.3 Regulating MIC through its IQ regions

IQ regions are contained within the neck of a myosin. This region, as previously described, is defined as [I,L,V]QxxxRGxxx[R,K] (Terrak *et al.,* 2003). Whilst all myosins must contain at least one IQ motif (Cameron, Liu, and Pihkala, 2013), it can be repeated up to six times leading to multiple IQ regions adjacent to each other (Nishikawa *et al.,* 2006). Each IQ region can bind to an essential light chain which can act as a myosin regulator such as CaM and CaM-like proteins (Houdusse, Silver, and Cohen, 1996). Structurally, an IQ region is comprised of amphiphilic seven turn α-helices. These turns can contain phosphorylation sites that once again aid in the regulation of myosins (Li *et al.,* 2017).

The essential light chain, CaM, is a well characterised myosin binding protein that can regulate the activity of a specific myosin. It is a small 16.7kDa protein that is highly conserved with a simple structure where both the N and C terminus form two EF hand motifs, which are helix-loop-helix domains that bind specifically to calcium ions (Denessiouk *et al.,* 2014). These two motifs are then joined by a flexible linker which allows the protein to wrap around the IQ region (Babu, Bugg, and Cook, 1988).

In the case of myosin IC, CaM disassociates from the 1st IQ region, in the presence of calcium, whilst in the complete absence of calcium, apo-CaM can then bind (Manceva *et al.,* 2007). The effect of apo-CaM differs between myosins, with their ATPase activity being inhibited, or stimulated, by the addition of calcium. However, this effect should not be seen as an all or nothing: with the variation of IQ domain numbers there is also a variation in how many

CaMs bind and unbind, depending on calcium concentrations. It is this fine tuning that has made MIC highly adapted to its functions.

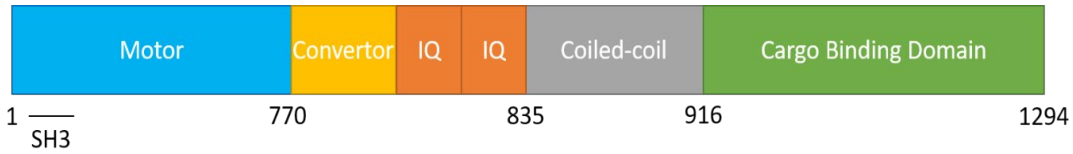
2.3.4 MICs tail domain defines its function

Within the tail of MIC, is a pleckstrin homology domain (PH). This domain is utilised for the transportation of vesicles in and out of the cell for both endo and exocytosis that occurs at the cellular membrane (Boguslavsky *et al.,* 2012; Bose *et al.,* 2004). At the membrane, MIC binds to phospholipids to aid in insulin stimulated GLUT4 translocation to a cell membrane and aids in membrane ruffling (Boguslavsky *et al.,* 2012). This lipid binding role is regulated by calcium, where a low concentration of calcium is required, to allow tight binding of apo-CaM to the IQ region, which frees the PH domain (Lu, *et al.,* 2014). When this PH domain is inhibited in zebrafish embryos there is a complete loss of membrane shape, highlighting the importance of MIC and its tail (Gupta *et al.,* 2017).

2.3.5 MICs binding partners

By studying the binding partners of myosins, their roles can be elucidated. These binding partners allow the motor to become activated in a specific pathway. As MIC is heavily localised at the cellular membrane, the most characterised binding partners that can control MICs function are often vesicle related (Hokanson and Ostap, 2006; Kittelberger *et al.,*2016). It is known that MIC binds directly to Neph1, a signalling protein required for fully functioning kidney podocytes, to stabilise cell shape, linking MIC to the actin cytoskeleton (Arif *et al.,* 2016). It also functions as a stabiliser of lipid rafts through its lipid binding properties which can then form cell adhesions or allow the recruitment of GTPases for cell signalling (Brandstaetter, Kendrick-Jones, and Buss, 2012). Here, it is likely that the binding partners

do not change the functionality of the MIC but that the structure of MIC itself dictates its role.



2.4 Myosin VI (MVI)

This diagram shows the SH3 domain found at the beginning of the motor domain, with the unique convertor that is linked with an IQ region. The coiled-coil domain which allows for dimerization and the cargo binding domain

2.4.1 MVI structure

MVI is the only myosin that travels from the barbed end of actin (+) to the pointed end of actin (-) (Wells *et al.,* 1999). This reversal of direction makes it vital in cellular exo and endocytosis as well as stabilisation of the Golgi-apparatus (Buss, Spudich, and Kendrick-Jones, 2004). Whilst both MIC and MVI have lipid binding domains within their tails, MVI contains an SH3 domain at the N-terminus before the motor, and only two IQ regions, compared to MICs three. A coiled-coil region within the neck of MVI allows for dimerization in a cargo dependent fashion (Yu *et al.,* 2009), and a convertor region dictates the reversal of direction (Ménétrey *et al.,* 2005).

Figure 2.5. A simplified diagram of MVI.

2.4.2 MVIs cross bridge cycle

Myosin VI is an example where both ATP turnover and the force of the myosin affect its functionality. Optical trapping experiments have shown that up to 2pN of force, MVI has a large stepping step size, between 35nm to 27nm, to which ATP concentration has little effect. Once a load larger than 2pN is added to the myosin, the myosin stalls. This stalling is down

to an increased rate of ADP binding, and a decrease in ATP affinity at the trailing head (Altman, Sweeney, and Spudich, 2004). This creates a biphasic myosin that is able to act as a transporter when necessary, but at a certain force can also become an anchor, linking the actin filament to its cargo.

The motor domain dictates not only the length of time a myosin can spend on an actin track but also the step size it can take and the forces the myosin can withstand. These forces are not only external forces deriving from cargo binding, but also internal forces that occur during dimerization of two myosin heads, leading to the human-like stepping characteristic that myosins display.

2.4.3 MVIs IQ domains

All known myosins use their motor domain to travel towards the plus end of actin, except myosin VI. Myosin VI contains a small domain between its convertor domain and the IQ motif (Ménétrey *et al.,* 2005). This domain provides an additional CaM binding site outside of its traditional IQ motif. This small CaM binding motif has been coupled to the convertor domain just after the motor domain. It is this small motif that allows the repositioning of the lever arm in the opposite direction towards the minus end of the actin. CaM is able to bind to this convertor domain independently of calcium concentration, whilst the remaining IQ region bind apo-CaM only in the absence of calcium, similarly to MIC (Batters *et al.,* 2016).

This simple conserved IQ domain controls not only the direction of travel of a myosin, but its activity through stabilisation of structure.

2.4.4 MVIs tail

Coiled-coil domains are prevalent within myosins and allow the formation of myosin bundles and myosin filaments. These domains have been heavily characterised in the muscle myosin

II due to the formation of the myosin filaments by two heavy chains (Dasbiswas *et al.,*2018). This filament formation creates the energy needed to move a muscle. Within a cell, however, coiled-coil domains are utilised for myosin dimerization which are then able to create a stepping motion required for transportation. This provides MVI with enough energy to transport large cargoes throughout the cytoplasm, as well as withhold the large forces placed upon it when acting as an anchor (Mukherjea *et al.,* 2014). Non-muscle myosin IIA and IIB utilises its coiled-coil domain for complete filamentous formation, like that as seen in the muscle myosin; yet these particular filaments can be dynamic along cellular actin (Melli *et al.,* 2018). This type of filamentous formation of myosins is yet to be seen in MVI and is unlikely to occur.

Similar to MIC, MVI contains a lipid binding domain within its tail region. One role where it utilises this feature is during endocytosis. In this case, MVI is targeted to clathrin-coated structures, which are then invaginated when MVI binds to Dab2 - a clathrin-associated sorting protein. As well as endocytosis, MVI has a role in exocytosis in neurosecretory cells. The myosin binds to secretory granules and tethers them to the cortical actin network linking the myosins cargo to its function (Tomatis *et al.,* 2013).

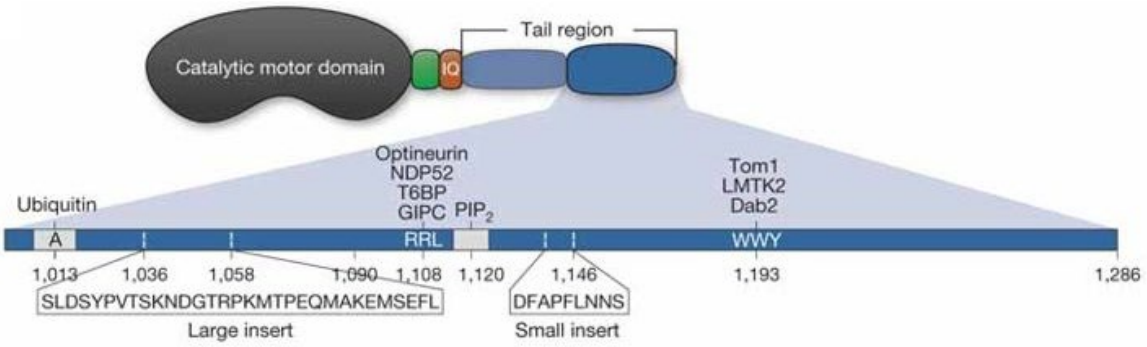
MVI exists as four different isoforms, all of which differ within the tail region of the protein. The four isoforms contain either a short insert, large insert, both inserts, or no inserts (Wollscheid *et al.,* 2016) (Figure 2.6). These isoforms provide differing affinities for MVIs binding partners and allow a variation of function, whilst maintaining the motor characteristics of the protein.

This variation in the tail and myosin's structural differences define their functionality. To understand how a myosin functions within the cell, the motor domain, the neck region and the tail domains must be taken into consideration, for these form the basis of the cargo they

bind, the forces they can withstand, the processivity of the motor and the regulation of that myosin.

2.4.5 MVIs binding partners

Binding partners are the key to understanding a myosin's role within a system. In the case of MVI there are a multitude of well characterised binding partners, all within distinct cellular



pathways. During receptor-mediated endocytosis, MVI binds to disabled homolog 2 (Dab2) through its WWY motif, positioned between residues 1193 and 1195 (Morris *et al.,* 2002). This complex then binds to lipoproteins for signal transduction, where MVI is recruited solely

Figure 2.6. The isoforms of MVI exists in four isomers.
The short insert, the large insert, both inserts and no insert. Within the tail region are the two binding motifs, the RRL motif, which binds to GIPC, NDP52 and others, and the WWY motif, which binds to Dab2. Taken from Tumbarello *et al.,*(2012).

by the presence of Dab2. Another binding partner is the tumor necrosis receptor-associated factor 6 binding protein (T6BP), a protein involved in NF- κB signalling, which controls cytokine dependent cell signalling. MVI binds this protein through another motif found in its cargo binding domain: the RRL motif found at position 1108-1110 (Morriswood *et al.,* 2007). These two domains have differing affinities within the four isoforms of MVI (Figure 2.6). The short insert isoform has a much higher affinity for proteins that bind to the RRL motif, compared to the large insert due to slight blocking of the motif by itself (Fili *et al.,* 2019). However, further work is required to fully understand the functions of all four isoforms.

2.5 Actin inside the cell

2.5.1 Cytoplasmic actin

When discussing myosin, the state of actin also needs to be discussed. Actin is a 43kD monomer that can oligomerise into polymeric and then filamentous actin. The actin itself rotates at each monomer to allow for binding, thus leading to a helical structure. It is this helical structure that defines the barbed (+) and pointed (-) ends of actin and is important in defining which direction a myosin is travelling (Holmes *et al.,* 1990). In physiological ionic strength, actin spontaneously polymerises and does not require any external proteins. Yet, in the presence of ATP, actin polymerisation can be accelerated and treadmilling can occur, where the actin depolymerisation at the minus end matches the polymerisation at the plus end (Chesarone and Goode, 2009). Due to the spontaneous nature of actin filaments, the cell is able to control filament formation through the use of cofilin, a protein that promotes the disassociation of monomeric actin, and profilin, a protein which aids in the association of monomeric actin (Bamburg and Bernstein, 2010). Arp2/3 (actin related proteins) is a complex that creates nucleation sites by binding to an actin filament and causing a new filament to form at 60° from the original. This forces the actin to polymerise in certain directions, thus resulting in rearrangement of the actin cytoskeleton within the cell (Goode *et al.,* 2001). To stabilise actin filaments (F-actin) the F-actin capping protein binds to the fast growing plus end which then blocks further transfer of actin monomers. If the cell requires the actin filaments to be cut, gelsolin and villin, can undertake this process (Friederich *et al.,* 1999; Sun *et al.,* 1999).

Actin polymerisation and regulation creates a cytoskeleton within the cell to act against the cell membrane to retain the cell's shape and size (Bezanilla *et al.,* 2015), provide actin tracks for myosins to transport cargo (Cramer, 2008) and cellular polarity through the generation

of membrane protrusions (Caswell and Zech, 2018). All myosins require actin for their role as a motor, and many of them use actin filaments for their function.

2.5.2 Nuclear actin

Once again, whilst discussing nuclear roles for myosins it is always important to understand the state of actin within the local environment of a myosin. Nuclear actin was discovered long before nuclear myosins (Lestourgeon, *et al.,* 1975); however, the form it takes in the nucleus has always been hotly discussed due to the different imaging techniques utilised by different labs (Kelpsch and Tootle, 2018).

This variation in actin formation is down to the observation of actin stress filaments that are formed in the nucleus during serum starvation, heat shock, DMSO treatment and other stress causing conditions (Serebryannyy, *et al.,* 2016). Interestingly, this journal article, is the only time the presence of long actin filaments has been observed in the nucleus; more commonly, actin can be found as monomers (Kapoor *et al.,* 2013) and polymeric (Gieni and Hendzel, 2009) rather than the well characterised filaments observed in the cytoplasm. After labelling cells with actin phalloidin, actin rods can be distinguished under stress conditions, but only when the cytoplasmic actin is saturated in the image (Belin, Lee, and Mullins, 2015). This provides evidence that even though the actin rods are being stained, it is likely that they have a distinct structure compared to that of their cytoplasmic counterparts.

It is generally agreed that the mechanisms that require nuclear actin, use actin as small polymeric molecules or monomeric. Actin plays vital roles in transcription (Hofmann *et al.,* 2004), chromatin organisation and movement (Xie *et al.,* 2018) and is utilised by the human cytomegalovirus during nuclear egress of viral capsids (Wilkie, Lawler, and Coen, 2016). In transcription, actin co-purifies with RNA polymerase (RNAP) I (Philimonenko *et al.,* 2004), RNAPII (Hofmann *et al.,* 2004) and by blocking actin binding through anti-actin antibodies, RNAPII transcription is inhibited (Hofmann *et al.,* 2004). Anti-actin antibodies also block

chromosome condensation and the actin-related proteins Arp4 and Arp8, along with monomeric actin, all bind to the chromatin remodelling complex INO80 (Zhang *et al.,* 2019). When studying chromatin movement, Chuang *et al.,* (2006) used a non-polymerisable actin mutant actin-G13R, to delay chromatin movement for transcriptional activation, and this movement can inversely be enhanced by the F-actin stabilising mutant actin -S14C.

The different forms of actin all have varying functions and are highly regulated in the nucleus by cofilin, Arp proteins and profilin, like cytoplasmic actin. As previously discussed, for a myosin to have complete function, actin also has to be present. Therefore, to understand a myosin's function within the nucleus, the state of nuclear actin also has to be taken into account.

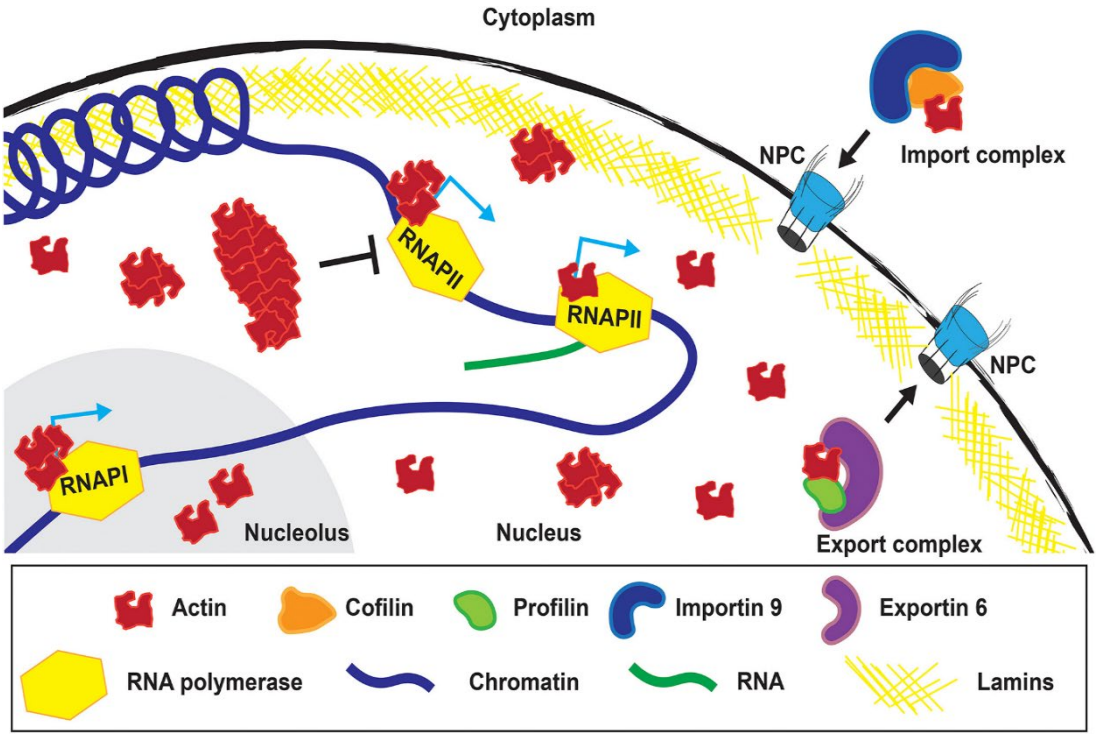


Figure 2.7. Actin inside the nucleus

A cartoon showing the role actin has in both RNAPI and RNAPII transcription, as well the import complex of actin containing cofilin, and the export complex containing exportin 6. Taken from (Kelpsch and Tootle, 2018).

2.6 Nuclear myosins

So far, cytoplasmic myosins are the most characterised myosins other than muscle myosins. A relatively recent field has begun to focus on the role myosins play within the nucleus. This field first begun with a single myosin in 1997 (Nowak *et al.,* 1997) . It was first though this discovery was through accidental leakage of cytoplasmic proteins into the nuclear extract. However, after this, the myosin was discovered to be a MIC isoform, isoform B, referred to as nuclear myosin 1 (NM1) (Pestic-Dragovich *et al.,* 2000), and the nuclear myosin field began to increase in traction. Now it is known that there are at least 8 myosin families with one or two isoforms within the nucleus (de Lanerolle, 2012). Nuclear myosins have been characterised within a few fields, with a heavy bias towards transcription and NM1. To fully understand how nuclear myosins are involved in a collaborative effort within the nucleus it is important to discuss them in a wider picture, rather than focusing on a single myosin. So far, the nuclear myosin field have covered a broad range of topics from DNA damage repair and transcription to viral infections, as reviewed by de Lanerolle, (2012). The work published within these topics are limited and often prescribe an obvious phenotype with a deletion of a nuclear myosin. To truly understand nuclear myosins, the regulation and activation, import and export control, and their binding partners need to be known. As well as this, if there is a specific isoform localised within the nucleus, the properties that differ it from its cytoplasmic counterpart need to be discovered.

2.6.1 The import and export of nuclear myosins

Whilst cytoplasmic myosins do not need to cross any membranes, nuclear myosins require nuclear localisation signals or binding partners to allow them to cross into the nucleus and differentiate from their cytoplasmic roles. Understanding how these myosins are selectively transported across the nucleus will then allow the study of the nuclear pool only. As the majority of nuclear myosins have cytoplasmic roles, knock-outs and knock-downs have a

drastic effect on the cell and often a phenotype observed may be down to a loss of multiple pathways in addition to the one being studied. To understand this movement may also open a new set of binding partners required for transportation.

2.6.2 MIC import and export

Myosin IC isoforms all contain a nuclear localisation signal embedded amongst the IQ region; however, only two of the isoforms, A and B, can be identified in the nucleus (Dzijak *et al.,* 2012). Interestingly, these isoforms differ in their N-terminal sequence, where NM1 (isoform B) contains a unique 16 amino acid sequence that is required for its nucleolar localisation. The NLS itself, however, is enough for the myosins to enter the nucleus. With the NLS sequence being conserved it is recognised by importin 5, importin 7 and importin β. For importin β to recognise this NLS sequence, the IQ regions need to be freely available and so CaM must disassociate before the NM1 is imported into the nucleus (Maly and Hofmann, 2016).

In another pathway, NM1 may be taken into the nucleus through the phosphoinositide-dependent pathway that requires the PH domain, found in the tail of all MIC isoforms (Nevzorov *et al.,* 2018). This domain allows binding of phospholipids found on vesicles and, in this case, NM1 requires no energy to be transported into the nucleus as it simply binds to the endoplasmic reticulum and diffuses into the nucleus through the nuclear membrane. With the use of fluorescence recovery after photobleaching, GFP tagged NM1 recovers in the nucleus after only one minute. This contradicts the previous published hypothesis and produces a mechanism for NM1 shuttling, and removes the need for calcium regulated import. It is possible both these mechanisms can work in tandem, where the PH domain provides basal levels of NM1 and the calcium regulated importin dependent pathway, allows the cell to react to an increase in calcium levels.

2.6.3 MVI import and export

Myosin VI also contains an NLS sequence within the IQ regions of the protein like that of NM1. There are also seven other NLS sequences throughout the myosin, which signals are relevant is yet to be seen (Majewski *et al.,* 2018), as binding partners can also affect the myosin VI distribution throughout the cell (Fili *et al.,* 2017). Myosin VI has four isoforms and the nuclear localisation, like that of NM1, is found to be isoform specific. Only with the non-insert myosin VI do we see nuclear localisation, and this is beginning to be attributed to the availability of the protein binding motifs, RRL and WWY, found in the cargo binding domain (Fili *et al.,* 2017). These binding domains can bind to two nuclear proteins, hnRNPU, a protein responsible for pre-mRNA transport and nucleolin, a nucleolar specific protein. Majewski *et al.,* (2018) have attributed these binding capabilities to the shuttling of myosin VI across the nuclear membrane. Myosin VI also binds to hormone receptors such as the androgen receptor (Loikkanen *et al.,* 2009) and knocking out myosin VI causes a loss of gene expression controlled by these receptors. One hypothesis is that myosin VI is responsible for transporting these receptors the full distance from membrane to DNA and once bound to these receptors it piggy-backs through the nuclear membrane. This hypothesis is yet to be tested.

So far, it seems that there is no one-fits-all mechanism for import and export, and it is dependent on the myosin itself. The variation could be due to binding partners, NLS sequences, and location of NLS sequence. If more information on these differences is available, then experiments can be undertaken to specifically remove nuclear myosins from the nucleus, whilst keeping the cytoplasmic pool, thus only interfering with their nuclear roles.

2.7 Function of nuclear myosins

2.7.1 Nuclear myosins in transcription

Nuclear myosins have been the most characterised within the transcription field. So far NM1, myosin VI and myosin Vb have been identified to play a role within transcription (Lindsay and McCaffrey, 2009; Philimonenko *et al.,* 2004; Vreugde *et al.,* 2006). The prevalence of nuclear myosin research in transcription is due to the vital role they play. With the removal of NM1, transcription levels within the cell deplete, and this observation has been repeated with myosin VI as well.

2.7.2 NM1's role in transcription

NM1 is the most studied of the myosins in terms of transcription. Like actin, as previously discussed, NM1 has also been found in complex with all three RNAPs within eukaryotic cells. Both chromatin immunoprecipitation (ChIP) and co-immunoprecipitation assays have shown that NM1 has a direct interaction with RNAPI and rRNA genes (Sarshad *et al.,* 2013). This direct interaction relies on the cargo binding domain of NM1 to bind to the chromatin and actin to the motor domain. RNAPI binds actin directly and thus NM1 creates a cross link between the RNAPI-actin complex and the DNA itself. As well as binding to RNAPI, NM1 also binds to the chromatin remodelling complex WSTF-SNF2h (Percipalle *et al.,* 2006), recruiting the complex to the site of rDNA transcription to create the pre-initiation complex. Not only is NM1 found within the pre-initiation complex for RNAPI transcription, it has also been found directly bound to the DNA through ChIP-seq data at class II promoters for RNAPII transcription (Almuzzaini *et al.,* 2015). Similarly, NM1 also interacts with the same WSTF-SNF2h at RNAPII sites for the opening of chromatin. If actin is not present, these complexes dissociate, and so there is a hypothesis that NM1 is able to work as an auxiliary motor for the

polymerases, where small actin polymers are generated rapidly alongside the transcribing polymerase. This hypothesis has some backing with NM1 not only being found at the initiation complexes but also during elongation and termination of transcription (Ye *et al.,* 2008).

2.7.3 MVIs role in transcription

MVI also has the potential to be an auxiliary motor or an anchor during transcription. This is possible as the cargo binding domain of MVI can bind to DNA, regulated by the binding of nuclear dot protein 52 (NDP52). Here the binding of NDP52 causes an unfolding of the protein, from its inactive backfolded state to its active state, allowing dimerisation of two myosin VI heads. The binding partner is the regulator of the myosins functionality in this process. The motor domain binds to the actin bound to the RNAPII complex itself and, like NM1, the tail binds to DNA. By inhibiting myosin VI using the small molecule inhibitor TIP, a 75% reduction of RNAPII transcription *in vitro* occurs, showing the importance of myosin VI as well as the potential for myosin redundancy as not all transcription is inhibited (Fili *et al.,* 2017; Cook *et al.,* 2018). This redundancy could be, in part, due to NM1 also being found at RNAPII sites. One point in discussion is how these two myosins could work together at the site of transcription and whether they are both required for complete transcription - from pre-initiation to termination. With NM1 binding the SNF2h-WSTF chromatin remodelling complex, MVI can also remodel chromatin. MVI has been shown to be responsible for the homologous pairing of TNF alleles (Zorca *et al.,* 2015) during transcription, which allows for simultaneous expression of genes and requires chromatin rearrangement that is lost after knock out of the MVI gene.

Another myosin that is found involved in RNAPI transcription but will not be studied in this thesis is Mysoin Vb, which is found localised within the nucleoli. Here, the molecular motor is found co-localised to the RNAPI complex as well as newly synthesised rRNA and co-purifies

with actin (Lindsay and McCaffrey, 2009). Once again, we see a molecular motor binding directly to an RNAP as well actin, showing the need for actin within the nucleus. Interestingly, this interaction is isoform specific where myosin Va, whilst nuclear, is not found in the nucleoli, like MVI and NM1 where nuclear and nucleolar localisation is isoform specific.

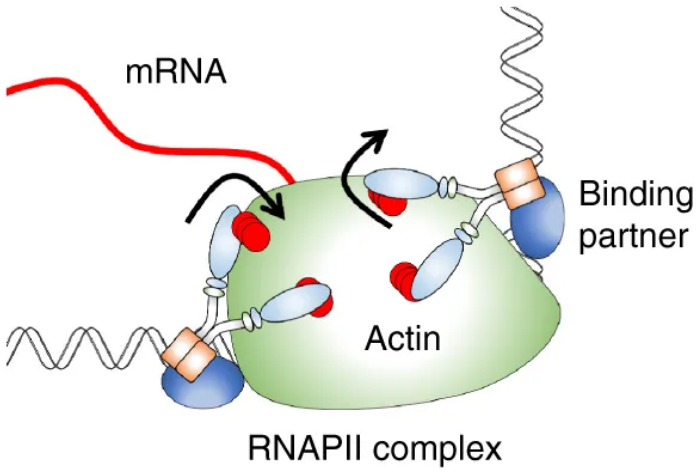


Figure 2.8. MVI within RNAPII transcription.
Myosin VI utilises a binding partner to dimerise where it then binds to the RNAPII complex through actin. Taken from (Fili *et al.,* 2017).

2.8 DNA damage

To discuss the role of nuclear myosins in DNA damage, it is important to understand the types of DNA damage that can occur and the different pathways within a cell that signal and repair this damage. By understanding these mechanisms, novel myosin roles can be elucidated.

DNA damage can take multiple forms depending on the damage inducer. The different types of DNA damage are: single stranded breaks (Zhou and Doetsch, 1993);, double stranded breaks (Jackson, 2002); base mismatches (Xu, Fu, and Xiao, 2018); insertion-deletion of bases (Lee *et al.,* 1995); as well as oxidation (Fleming, Ding, and Burrows, 2017), alkylation (Xu *et al.,* 2017) and deamination of bases (Duncan and Miller, 1980). All of these generate a

different response within the nucleus and all have different repair pathways. If the cell is unable to repair the damage or the damage is prevalent along the chromatin, then senescence, where a cell ceases to divide (Venkatachalam, Surana, and Clément, 2017), or apoptosis, forced cell death, is induced (Roos and Kaina, 2006). If the cell is unable to control the DNA damage, mutations become incorporated in vital regulatory genes, this leads to mis-regulation of the genome, leading to cellular transformation, where they undertake uncontrollable growth and division (Aparicio, Baer, and Gautier, 2014).

Due to the large variety of damage and repair mechanisms, I will be focussing on double stranded breaks (DSBs) within DNA and how they are signalled and repaired. DSBs are particularly dangerous to a cell's genome, as they can lead to a complete shear in the DNA, which can then lead to whole genome rearrangements (So *et al.*, 2017). Spontaneous DSBs occur during DNA replication, often caused by the stalling of replication forks (Alexander and Orr-Weaver, 2016) .

It is important to remember that the genome is covered in DNA binding proteins, all of which are performing a variety of functions to aid in stability, transcription, replication and structure. With all these different proteins being bound to DNA, at any one time, it is likely during DNA replication for any of the machinery - the topoisomerase, DNA polymerases, and the helicases - to encounter other DNA bound proteins. If an unusual structure occurs in the DNA, or a collision between DNA bound proteins occurs, a DSB has the potential to form (Pomerantz and O'Donnell, 2008) . However, not only can DSBs form naturally, they can also be induced by external sources such as radiation (Vignard, Mirey, and Salles, 2013), for example UV and Infra-red, and chemotherapeutics, such as cisplatin (Hu *et al.,* 2016) and bleomycin, which have been used in this thesis. In fact, it is this function of chemotherapeutics to inhibit DNA replication that leads to the generation of DSBs which makes them suitable for cancer treatments.

2.9 Signalling double stranded breaks (DSBs)

2.9.1 Activation of protein kinases

At the point of damage, a selection of proteins begins to signal to the cell that a damaging event has occurred. Phosphatidylinositol-3 kinase-related kinases (PIKK) are responsible for the initial signalling of any DSBs. Specifically, it is the Ataxia-Telangiectasia-Mutated protein (ATM) (Hartlerode *et al.,* 2015), and the DNA-dependent protein Kinase catalytic subunits (DNA-PKcs) (Y. Zhou *et al.,* 2017) that signal a response. However, the proteins responsible for first binding to a DSB-end are part of the MRN complex; made up of the MRE11, Rad50 and NBS1. The MRN complex binds to a free DSB and tethers the broken ends (Lee and Paull, 2004). If an alternative repair pathway is required, a different complex binds to the damaged DNA strands, known as the Ku70/Ku80 complex (Jin, 1997). This threads itself onto the DSB and then slides along the break, allowing space for more Ku70/ku80 complexes to slide on. This type of collaborative binding provides the scaffold for the repair mechanisms.

The MRN or Ku70/Ku80 complex once bound recruits ATM to the site of damage through its N-terminal domain and causes the activation of ATM. ATM normally resides as an inactive dimer, yet under damage the ATM is autophosphorylated on the serine at position 1981 (So, Davis, and Chen, 2009). This autophosphorylation causes the disassociation of this dimer, resulting in two monomeric active ATM proteins that stabilise the DSB.

2.9.2 γH2AX signalling

γH2AX signalling forms the basis of DSBs signalling. It occurs through the phosphorylation of the serine-139 found on the tail of the H2AX histone. This histone is a variant of the H2A histone, and is found within 10% of nucleosomes (Rogakou *et al.,* 1998). All three signalling proteins, DNA-PKcs and phosphorylated ATMs and phosphorylated Ataxia telangiectasia and Rad3 related kinases (ATRs), which are similar to ATMs, are able to phosphorylate this

residue once DNA damage is discovered (Wang *et al.,* 2005). This phosphorylation then forms a cascade of phosphorylation of H2AX histones that can travel up to 2 Mbp with clusters of γH2AX signals forming around the break point (Burma *et al.,* 2001).

MDC1, a mediator of DNA damage checkpoint 1, recognises these γH2AX sites which in turn recruits more MRN complexes to the damage site, leading to an increase in activated ATM kinases (Eliezer *et al.,* 2014). This process creates a positive feedback cascade event where the occurrence of a repair protein leads to the increase in signalling proteins, which in turn upregulates the activation of repair proteins.

These proteins and post-translational modifications at the site of a DSB decide where a break has occurred, how to signal a break and from this then decide how the break can then be repaired.

2.10 Repairing double strand breaks

2.10.1 Homologous recombination

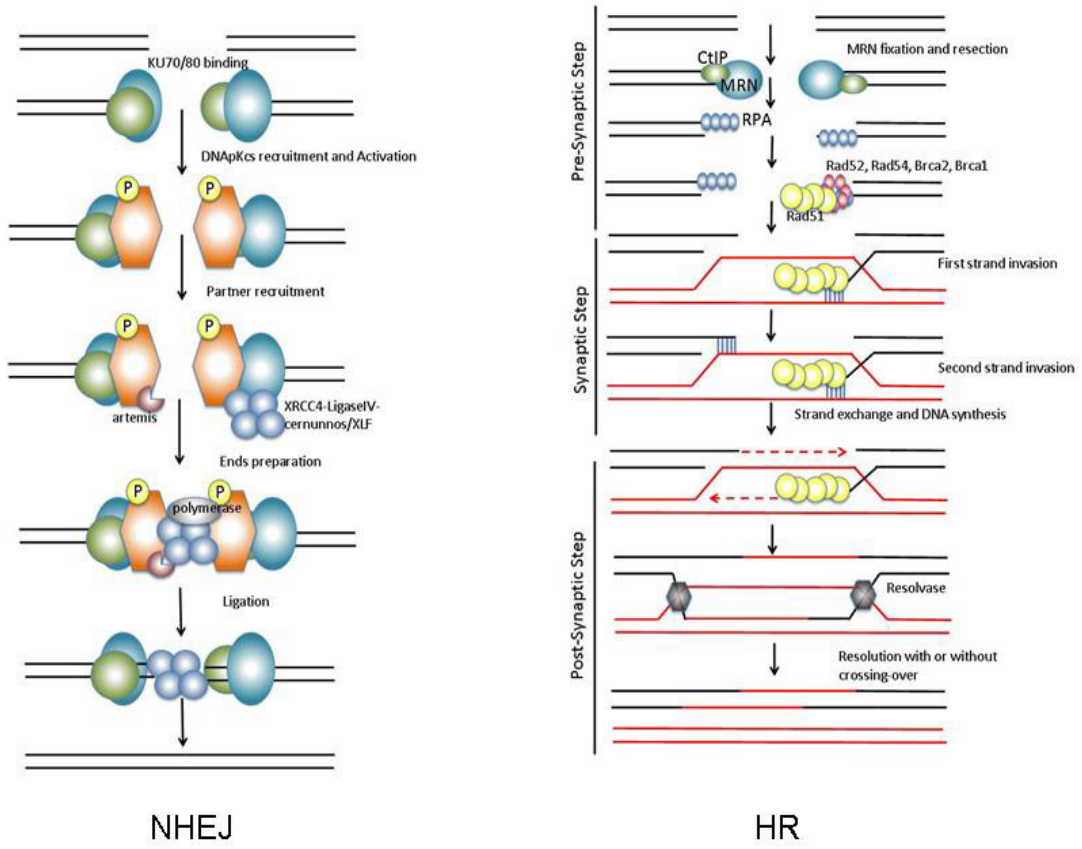
To repair DSB, the cell has three main options: homologous recombination (HR) (Morrical, 2015), HR with single-strand annealing (Ramakrishnan *et al.,* 2018), and non-homologous end joining (NHEJ) (Takata *et al.,* 1998). HR is the least error prone of the repair mechanisms and relies on the sister chromatid or a homologous chromosome to act as a template to repair the DNA. This type of repair only comes within the S and G_2 phases of the cell cycle as the sister chromatids need to be readily available (Zhao *et al.,* 2017). Once MRN is bound and the damage is signalled, the DNA is cut back by the nuclease Artemis, this then releases a 5' end oligonucleotide (Beucher *et al.,* 2009) . The 5' end acts as the invading strand, acting as a primer for the repair filaments moderated by the recombinase, Rad51 (Lu *et al.,* 2018). This primer has an identical sequence to that of the target homologue, where Rad51, then causes the separation of the double helix and the annealing of one of the ssDNA damaged

parts to a complete section of DNA, called the D loop extrusion (Mazloum and Holloman, 2009). DNA synthesis is initiated and, through the formation of Holliday junctions, the cell can repair the DNA without any lasting damage. This type of repair requires movement of chromosomes within the nucleus to repair factories, so that the homologous pair can be identified and is in close enough proximity to allow Holliday junctions to form (Bugreev, Mazina, and Mazin, 2006).

A variation of HR is when single strand annealing can occur through annealing homologous repeat sequences flanking a DSB. This process can be inhibited by the HR activating protein Rad51, most likely to force the DNA into HR as single strand annealing causes major deletions (Bae *et al.,* 2019). After the ends are resected, the repeat sequences can pair with each other, like in HR, thus leaving anything in front of these repeats out of the repair site. DNA ligase III then joins the two strands together. The main issue with this repair pathway is that a large loss of genetic information occurs, and this repair pathway is often selected against when others are available.

2.10.2 Non-homologous end joining

Finally, NHEJ does not require any type of homologous template for repair to occur. This type of repair is independent of the cell cycle and for it to be induced requires the Ku70/Ku80, and not the MRN complex, to bind to the DSB. The Ku70/Ku80 complexes provide a scaffold for the whole repair mechanism. Like all repair processes, first the broken strands are cut, in this process the DNAPKcs:Artemis complex has both a 5' endonuclease as well as a 3' endonuclease, allowing it to cut both parts of the break. If now the two ends are not compatible to be ligated, the DNA polymerases λ and μ produce two compatible ends. Once ligation can occur, DNA ligase IV and its cofactor XRRC4 are recruited by the Ku70/ku80 complex and the DNA is repaired (Kurosawa *et al.,* 2013). This type of DNA repair however



NHEJ HR

causes a loss of genetic material or an insertion of the wrong bases by the DNA polymerases, which could in turn have a dramatic effect on the cell.

2.10.3 Irreparable DSB damage

After the induction of damage, the activated ATM has many downstream effects on the cell. Most importantly, the cells enter cell cycle arrest through DNA damage checkpoints. CHEK2 is phosphorylated by the ATM kinase at threonine-68, which results in the prevention of

A simple comparison of the proteins required for non-homologous end joining and homologous recombination. In NHEJ, the Ku70/80 complex binds to the break, recruits DNApKcs which in turn activates Artemis and the ligase IV complex which prepares the ends and allows for ligation. HR however relies on the MRN complex to bind to a break, which then acts as a scaffold for other repair proteins to bind, Rad52, Brca2 etc. Then homologous recombination occurs. Taken from Renodon-Corniere *et al.,* (2013.)

Figure 2.9 Diagrams of the DNA damage repair pathways.

mitosis. CHEK2 phosphorylation is not only required for mitosis prevention but also for stalling the cell in S-phase through its interaction with CDC25 (Einarsdóttir *et al.,* 2006) .

Both the ATM kinase and CHEK2 can also interact with p53, the well characterised tumour suppressor, cell cycle controller and apoptotic marker (Chrisanthar *et al.,* 2008). If the cell is unable to repair the genome damage, then p53 becomes activated through phosphorylation by ATM and its destabilising protein, Mdm2, which marks the protein for degradation, is released from p53 (Kang *et al.,* 2005). The apoptotic pathway then becomes cytoplasmic with the release of cytochrome C from the mitochondria, which forms with other proteins, the apoptosome, leading to apoptosis of the cell (Leoni *et al.,* 1998) . As p53 can act as a transcriptional factor, the activation of the protein leads to a large cascade of activation and inactivation of proteins. It is also identified as the most mutated protein within cancerous cells, therefore the activating ATM kinase becomes significant to research (R. Zhao *et al.,* 2000). If it becomes mutated, then there is activation of tumour development genes and a repression of tumour repressor genes. If p53 is linked with any of the nuclear myosins then it becomes possible these myosins could act in either tumour growth or suppression making them a vital cog in the oncogenic machinery.

2.11 Nuclear myosins in DNA damage

2.11.1 MVI and p53

So far, little interaction between DNA damage proteins and nuclear myosins has been discovered, except for a regulatory link between p53 and myosin VI (Jung *et al.,* 2006) . The gene for MVI can be regulated by p53, where phosphorylated p53 can cause an increase in expression of MVI. MVI then binds to p53 and stabilises the protein, inhibiting degradation of the protein and allowing it to carry out cell cycle stalling and DNA repair. Interestingly, once MVI is bound to p53 there is a negative feedback loop where this complex inhibits

further MVI expression. This has been confirmed in RKO, colon cancer cell line, LS174T, another colon cancer cell line and H1299, a lung cancer cell line. However, in other cancer cell lines such as MCF7, a breast cancer cell line, and LNCaP, a prostate cancer cell line, DNA damage causes a reduction in MVI levels. Knock down of myosin VI in RKO de-sensitises the cell to DNA damage-induced apoptosis and overexpression of MVI stabilises p53, and so MVI could only be used as a therapeutic on certain cell lines and not to treat cancers globally (Cho and Chen, 2010). However, these studies do not comment on whether this myosin VI is cytoplasmic or nuclear. Further work will allow us to understand if MVI plays a vital role in p53 stabilisation, through its cytoplasmic or nuclear interactions.

2.11.2 Global chromosome re-arrangements by NM1

So far, DNA damage and its response at the point of damage has been discussed. However, whilst DSBs go under local repair, there is also a global rearrangement of chromosomes, to allow for not only the pairing of genes for homologous recombination but also to bring the points of damage to a defined location to form repair factories.

Chromosome territories have been well discussed since the 1950s where it was first defined that chromatin was diffuse across the nucleus, with no spatial organisation during interphase. However, in 1977, Stack *et al.* (Stack, Brown, and Dewey, 1977) began to define that each chromosome has a specific arrangement within the nucleus. Since then, in 2005 a full map of chromosome locations was defined (Bolzer *et al.,* 2005). There are multiple reasons why a cell would still maintain organisation of their chromosomes even during interphase, as it allows the expression of related genes and the easy compaction of chromosomes once entering metaphase. This map has allocated a space each chromosome can fill and defined the territory of each chromosome. Now, this theory is common practice and it has allowed observations of complete chromatin rearrangement under stimulating

conditions such as with the use of hormones (Q. Hu *et al.,* 2008), serum starvation (Mehta *et al.*, 2010) and DNA damage (Mehta *et al.,* 2013).

When these chromosomes move, they have the potential to move great distances from 5-10 µm to allow for the expression of genes and thus making gene movements cell cycle specific (Chuang *et al.,* 2006). Due to the length of movement and the density of nuclear proteins, motion cannot be attributed to simple Brownian motion and must be the result of an active mechanism. During DNA damage, these long-range movements can also be observed. After cisplatin treatment, some but not all chromosomes relocate their territories. So far, it is noted that chromosomes 19, 17, 20, and 12 all relocate from the nuclear periphery to the nuclear interior or vice-versa. After knocking down NM1 this relocation was not observed, and the chromosomes remained in their original territories. This relocation coincides with an upregulation of NM1 into the nucleus and the increased amount of NM1 found directly bound to chromatin (Kulashreshtha *et al.,* 2016). If the cell is unable to activate γH2AX signalling for DNA damage or the ATM is inactivated, this chromosome movement does not occur and therefore there must be cross talk between NM1, γH2AX and ATM (Kulashreshta *et al.,* 2016). Also, after DSBs occur, NM1 allows for the contact of homologous chromosomes providing a template for gene repair (Evdokimova *et al.,* 2018). This recruitment also requires ATM, thus making NM1 a key player in the DNA damage response.

2.11.3 Chromosome rearrangements by other nuclear myosins

Myosin V has also been attributed to moving heterochromatic breaks within *Drosophila* cells (Caridi *et al.,* 2018). Heterochromatin consists of satellite repeats and transposons. Due to their repetitive nature it is vital the cell can repair any breaks as fast as possible to stop large chromatin recombination and the mixing of chromosomes.

Mre11, the DSB repair protein, recruits not only myosin V but also myosin Ia and myosin Ib through the myosin activator Unc45 and the heterochromatin protein 1a (HP1a). After this

recruitment long actin filaments form from repair foci to the periphery of the heterochromatin domain. This allows the breaks to be transported to repair factories within the nucleus (Caridi *et al.,* 2018). Surprisingly, repair foci have also been observed travelling along these actin filaments however this movement has not yet been attributed to a myosin. Here the myosins are acting as traditional transporters of cargo and not as anchoring proteins.

2.12 The nuclear myosin field

As a relatively new field, there are still many mechanisms that need to be defined. So far, in the field, obvious phenotypic results have been attributed to a loss of a nuclear myosin, however this should not be used to define a role for the nuclear myosin. The reason for this is due to the inability to differentiate between nuclear and cytoplasmic pools of myosins, and due to their multiple responsibilities within a cell, a knockdown or knockout can have drastic effects on the cell not just within the focus of the experimenter but also on transcription, cells susceptibility to DNA damage and the effect on chromatin organisation.

To further build on the research done so far it is important to tackle the issues of how these myosins shuttle between the nuclear membrane allowing researchers to isolate the two pools of myosin. Along with this, the binding partners of nuclear myosins, their mechanical properties and their differences to their cytoplasmic counterparts all need to be considered. The aim of this project is to build on what is known about the roles and regulation of nuclear myosins, in particular NM1 and MVI, keeping in mind their already well characterised properties within the cytoplasm.

Chapter 3. Materials and Methods

3.1 Chemicals and reagents

All chemicals have been purchased from Sigma Aldrich and ThermoFisher, unless specified. The antibodies have been purchased from Abcam, unless specified. Bleomycin sulphate (Sigma, Cat no.B1141000) was prepared to a stock concentration of 100µM is dH_20. Cisplatin (Sigma, Cat no. C2210000) was prepared in 0.9% NaCl solution to a stock concentration of 1mg.mL^{-1}. Ku55933 (Sigma, Cat no. SML1109) was prepared in DMSO, to a stock concentration of 5mg.mL^{-1}. Human epidermal growth factor (EGF) (Sigma, Cat no. E9644) is dissolved in 10mM acetic acid. Paclitaxel (abcam, 120143) is dissolved to a concentration of 100mM in DMSO.

3.1.1 Recombinant protein expression constructs

Name	Amino acids	Tags	Plasmid	Origin
Homo sapien NM1 Full length	1-1044	Histidine x6	pFastBac^{TM} 1	Gifted by N. Fili
Homo sapien NM1 tail co-expressed with CaM	698-1044; 1-148	Histidine x6	pET21	Kindly gifted by M. Zhang
Xenopus Laevis CaM	1-148	Histidine x6	pET21	Gifted by N. Fili

Table 3.1. A table of recombinant protein expression plasmids.

3.1.2 Primers

Name	Sequence (5’ to 3’)	Origin
pUC/M13 Forward	CCCAGTCACGACGGTTGTAAAACG	Invitrogen
pUC/M13 Reverse	AGCGGATAACAATTTCACACAGG	Invitrogen

Table 3.2. A table of primers used.

3.1.3 2.4 Oligonucleotides

Name	Sequence	Modification	Origin
$ssDNA_{15}$	CCGGGCGGGGGCCGG	5’ fluorescein	Integrated DNA tech.
$ssDNA_{40}$	TTAGTTGTTCGTAGTGCTCGTCTGGCTCTGGATTACCCGC	5’ Fluorescein	Integrated DNA tech.
$ssDNA_{15}$	GGCCCGCCCCCCGGCC	None	Integrated DNA tech.
$ssDNA_{40}$	AATCAACAAGCATCACGAGCAGACCGACCTAATGGGCG	None	Integrated DNA tech.

Table 3.3. A table of oligonucleotides used.

3.1.4 NM1 peptide

Name	Sequence (aa)	Modification	Origin
NM1 wild type (WT)	CMRYRASALGSDGVRV	N-terminus cysteine	GL Biochem (Shanghai) Ltd
NM1 R2L2	CMLYRASALGSDGVRV	N-terminus cysteine	GL Biochem (Shanghai) Ltd
NM1 R4L4	CMRYLASALGSDGVRV	N-terminus cysteine	GL Biochem (Shanghai) Ltd
NM1 R2L2-R4L4	CMLYLASALGSDGVRV	N-terminus cysteine	GL Biochem (Shanghai) Ltd

Table 3.4. A table of NM1 N-terminus peptides used.

3.1.5 Drug stocks and Antibodies

Table 3.5. A table of drugs used both stocks and final concentrations.

Name	Stock concentration (mM)	Final concentration (µM)	Incubation period
TIP	0.1	25	4 hours, except with cisplatin treatments, 24 hours.
Bleomycin	1	0.5	4 hours
Cisplatin	3.3	25	24 hours restocked every 4 hours.
Ku55933	12.6	20	4 hours
Paclitaxel	100	0.1	Stated length of apoptosis assay.

Name	Origin and Cat. No.	Use	Dilution
Anti-Myosin Iβ (Nuclear) antibody produced in rabbit	Sigma-Aldrich, M3567	Western Blot, Immunofluorescence	1 in 200, 1 in 100
Myosin Ic Antibody produced in mouse	Santa-Cruz, sc-136544	Immunofluorescence	1 in 200
Anti-Lamin β1 produced in rabbit	Abcam, ab16048	Western Blot	1 in 500
Anti-β-actin produced in rabbit	Abcam, ab8227	Western Blot	1 in 5,000
Anti-MVI produced in rabbit	Sigma-Aldrich, ABT42	Western Blot, Immunofluorescence	1 in 500, 1 in 200
Anti-phospho-Histone H2A.X (Ser139) Antibody produced in mouse	Sigma-Aldrich, 05-636	Western Blot, Immunofluorescence	1 in 1,000, 1 in 500
Goat Anti-Rabbit IgG HandL (HRP)	Abcam, ab6721	Western Blot	1 in 15,000
Rabbit Anti-Mouse IgG HandL (HRP)	Abcam, ab6728	Western Blot	1 in 10,000
Anti-CaM 1/2/3 antibody produced in mouse	Abcam, ab2860	Immunofluorescence	1 in 50
Anti-Histone H3 (tri methyl K9) antibody produced in rabbit	Abcam, ab8898	Immunofluorescence	1 in 500
Anti-Histone H3 (acetyl K27) antibody produced in rabbit	Abcam, ab4729	Immunofluorescence	1 in 500
Anti-Histone H3 (acetyl K9) antibody produced in rabbit	Abcam, ab4441	Immunofluorescence	1 in 200
Anti-Histone H3 (mono methyl K4) antibody produced in rabbit	Abcam, ab8895	Immunofluorescence	1 in 200
Anti-Histone H3 (di methyl K36) antibody produced in rabbit	Abcam, ab9049	Immunofluorescence	1 in 500
Goat anti-Rabbit IgG (H+L) Highly Cross-Adsorbed Secondary Antibody, Alexa Fluor Plus 488	ThermoFisher, A32723	Immunofluorescence	1 in 500

Goat anti-Rabbit IgG (H+L) Highly Cross-Adsorbed Secondary Antibody, Alexa Fluor Plus 488	ThermoFisher, A32731	Immunofluorescence	1 in 500
Goat anti-Rabbit IgG (H+L) Highly Cross-Adsorbed Secondary Antibody, Alexa Fluor Plus 555	ThermoFisher, A32732	Immunofluorescence	1 in 500
Goat anti-Rabbit IgG (H+L) Highly Cross-Adsorbed Secondary Antibody, Alexa Fluor Plus 647	ThermoFisher, A32733	Immunofluorescence, specifically STORM	1 in 250

Table 3.6. A table of antibodies and their dilutions.

3.1.6 Whole Chromosome paints

All chromosome paints were purchased from Cytocell (Cambridge).

Cat. No.	Name
LPP12R	Chromosome 12 Whole Chromosome Painting Probe Red
LPP19G	Chromosome 19 Whole Chromosome Painting Probe Green

Table 3.7. Chromosome paints purchased from cytocell.

3.2 Methods

3.2.1 Bacterial transformation

Plasmid DNA for the NM1 recombinant tail and CaM were transformed into *Escherichia coli* B21 cells. 3µL of pure plasmid DNA was added to the cells and gently stirred before incubating on ice for 30 minutes. The cells were then heat shocked for 45 secs at 42°C and allowed to cool on ice for 2 minutes. 200µL of commercial lysogeny broth (LB) was added and incubated for 1 hour at 37°C whilst shaking (220rpm). The mixture was then plated onto an LB agar plate containing 100µgmL^{-1} ampicillin and then incubated at 37°C overnight.

3.2.2 Bacterial protein expression

A single colony was chosen from the *E. coli* transformation that contained the NM1 tail plasmid and were grown overnight at 37°C in 100mL of LB containing 100µgmL^{-1} of ampicillin. A 1 in 100 dilution was then added to 1 litre of LB containing 100µgmL^{-1} ampicillin and grown at 37°C at 220rpm. Once the optical density OD_{595} reached 0.5 the cells were induced with 1mM IPTG. Cells were then allowed to grow overnight at 18°C. Cells were then collected by centrifugation at 4°C at 4000rpm in a JS 4.2 swing bucket rotor (Beckman Coulter) for 20 mins. The supernatant was then discarded and the cell pellets resuspended in 50mM Tris.HCl (pH 7.5), 1mM Dithiothreitol (DTT), 200mM NaCl, 10% (w/v) sucrose. The resuspension was frozen at -80°C.

3.2.3 Baculovirus bacterial transformation

Baculovirus transfection and expression followed the protocol provided by the Bac to Bac® system (Invitrogen™). Briefly, the plasmid is transformed into DH10Bac™ chemically competent cells. 1ng of DNA is added to 100µL of cells at 4°C and allowed to incubate for 30mins. Cells are then heat shocked for 45 secs at 42°C. Then immediately chilled at 4°C for two minutes. 900µL of S.O.C medium provided, was then added and the cells were incubated

at 37°C at 225rpm for 4 hours. Cells were then plated on LB agar plates containing 50µgmL^{-1} kanamycin, 7µgmL^{-1} gentamicin, 10µgmL^{-1} tetracycline, 100µg^{-1} Bluo-gal and 40µgmL^{-1} IPTG. The plates were incubated at 37°C for 48 hours and single white colonies were then restreaked on LB plates containing the same antibiotics and allowed to grown at 37°C for 24 hours.

3.2.4 Isolation and analysis of recombinant bacmid DNA

Once suitable colonies had been identified by their white colour, the colonies were picked and grown in 100mL LB containing all selective antibiotic except bluo-gal, overnight at 37°C. The cells were then collected through centrifugation at 4000rpm for 5 mins. The DNA was then isolated using the PureYield™ Midiprep system. Following DNA extraction, PCR analyses was undertaken. A PCR reaction contained 100ng of purified DNA, 1X Platinum® Taq polymerase buffer, 0.2mM dNTP mix, 0.05mM $MgCl_2$, 1.25µL of each 10µM stock of forward and reverse primers, 2.5 units of Platinum® Taq polymerase, made to a final volume of 50µL using sterile H_2O. The PCR reaction was set up as follows:

Step	Time	Temperature	Cycles
Initial Denaturation	3 minutes	93°C	1X
Denaturation	45 seconds	94°C	30X
Annealing	45 seconds	55°C	
Extension	5 minutes	72°C	
Final Extension	7 minutes	72°C	1X

Table 3.8. A table of PCR conditions for baculovirus preparation.

Gel electrophoresis was carried out using 1% agarose prepared in TAE buffer (40mM Tris-acetate, 1mM EDTA), and stained with SYBR™Green.

3.2.5 Insect cell transfection and protein expression

Sf9 insect cells were grown in Sf-900 media to a logarithmic phase of $2x10^6$ cells at 27°C. Cells were then plated on a 6-well tissue culture plate, with a total of $2x10^6$ cells per well. 1µg of DNA per well was mixed with 8µL of Cellfectin® in Sf-900 media and mixed gently then left at RT for 30 minutes. The DNA mixture was then added dropwise to each well and the cells were incubated for 72 hours at 27°C. Cells were then observed for infection by the cessation of cell growth, a granular appearance and detachment from the cell base. Once this phenotype had occurred the medium was collected including the cells which was then centrifuged at 500 x g for 5 minutes at 4°C. The supernatant is then collected and stored in the dark at 4°C for further amplification of the virus.

Once a suitable amount of viral stock is created, 1 litre flasks of sf21 cells were prepared at a concentration of $1x10^6$ cells/mL in Spodipan (Lonza) at 27°C at 250rpm and infected with virus at a dilution of 1:25mL. The cells and virus mixture was then incubated for 72 hours at 27°C, after which the viability of the cells were measured. A viability of less than 50% showed infection and the mixture was centrifuged at 4°C at 4000rpm in a JS 4.2 swing bucket rotor (Beckman Coulter) for 20 minutes. The pelleted cells were then resuspended in 50mM Tris.HCl (pH 7.5), 1mM DTT, 200mM NaCl, 10% (w/v) sucrose and stored at -80°C.

3.2.6 Full length NM1 purification from Sf21 cells

Sf21 cells containing the full length NM1 were defrosted, 1µM PMSF, 1µM ATP, 2mM EDTA and a protease inhibitor cocktail were added. The solution was then sonicated for 15 seconds on, 15 seconds off, for 10 cycles. The slurry was then centrifuged at 20,000rpm at 4°C for 1 hour in a Beckman Avanti J-26S using a J 25.50 rotor. The supernatant was then loaded onto a 5mL His-Trap HP column (GE Healthcare) which had been equilibrated in 50mM Tris.HCl pH 7.5, 250mM NaCl and 1mM DTT. Once loaded the column was washed by 5 column volumes in the equilibration buffer. The proteins were then eluted using the equilibration buffer

except an increase of imidazole from 0mM to 400mM stepwise was implemented. The elution fractions were then collected and stored at 4°C for SDS-PAGE and western blotting analysis.

3.2.7 SDS-PAGE analysis

Polyacrylamide gel electrophoresis was used to analyse the presence and purity of the full length NM1. Gels were made using the Bio-Rad minigel system. The resolving section was made using 6mL 30% Acrylamide/Bis 20:1, 3.75mL 1.5M Tris.HCl pH 8.8, 150µL 10% SDS (w/v), 4.72mL ddH_2O, 100µL 10% (w/v) ammonium persulfate, and 5µL TEMED (Bio-Rad). The stacking was made with 2mL 30% Acrylamide/Bis 20:1, 1.5mL 1.5M Tris.HCl pH 6.8, 100µL 10% SDS, 5.4mL ddH_2O, 100µl 10% ammonium persulfate and 5µL TEMED. Samples for analysis were mixed with 4x NuPAGE™ LDS sample buffer, 0.1mM DDT to make a final concentration of protein sample in a 2X loading buffer. To analyse whole mammalian cell samples for western blotting, $1x10^6$ cells were mixed with 200µL of a loading buffer containing 4x NuPage™ LDS sample buffer, 1xPBS, 1M DTT at a ratio of 2:2:1. The samples are then boiled at 95°C for 10 minutes. Gels were then ran at 200 volts for 60 minutes in a running buffer containing 25mM Tris, 1.44% (w/v) glycine and 0.1% SDS. The gels were then put aside for western blotting or stained with Coomassie brilliant blue R-250 (Bio-Rad) for 30 mins. The gels were then de-stained at RT for 1-2 hours in 10% (v/v) acetic acid and 50% (v/v) methanol.

3.2.8 Western blotting

Once samples had been separated using SDS-PAGE analysis, the gels were incubated with the SDS-PAGE gel running buffer supplemented with 1% (v/v) methanol. A single PVDF membrane was cut to fit the size of the gel which was first activated in 100% methanol for 10 secs, rinsed three times with ddH_2O and then left at RT for 10-15 mins in Pierce™ 1 step transfer buffer. 8 Whatman® filter paper were cut to size and also incubated at RT for 10-15

mins in the same transfer buffer. Using a semi-dry Power Blotter system from Thermo the samples were left to transfer to the membrane for 12 mins at 25V, 1.3A. Once transferred the gel is discarded and the membrane is washed in 20% (v/v) methanol and rinsed thoroughly with ddH_2O and is then incubated in blocking buffer (0.1% Tween, 5% dried skimmed milk powder, 1x TBS) for at least 45 min at RT or overnight at 4°C. After blocking the membrane is incubated with the primary antibody specific to the protein of interest which is prepared in blocking buffer for 2 hrs at RT. Membrane is then washed thrice with washing buffer (10 min each wash) (Washing Buffer: 0.1% Tween, 1% dried skimmed milk powder, 1x TBS) followed by incubating with the secondary antibody containing an attached horse radish peroxidase (HRP), which is prepared in blocking buffer for 1 hour at RT. The membrane was then washed with washing buffer as before (3 times, 10 min each) and finally washed with TBS only. It was then imaged using the Pierce™ ECL western blotting substrate kit, where 1mL of solution A and 1mL of solution B are mixed and added to the membrane. The membrane is then incubated for 1 min at RT and imaged using a G:Box (Syngene) where the exposure was adjusted for each membrane.

3.2.9 Recombinant protein purification

E. coli cells containing the NM1 tail with CaM plasmid, and CaM were defrosted and supplemented with 1µM PMSF, if purification with the CaM was required then 5mM EGTA was also added. The cells were then sonicated for 5 minutes and centrifuged at 18,000rpm at 4˚C for 30 mins in a Beckman Avanti J-26S using a J 25.50 rotor. The supernatant was then collected and stored at 4˚C. A 5mL His-Trap HP column (GE healthcare) was equilibrated in 50mM Tris.HCl pH 7.5, 40mM imidazole, 500mM NaCl, 1mM DTT and 5mM EGTA if necessary. The stored supernatant was loaded onto the column and the column was washed with the equilibration buffer. The protein was eluted using the same buffer with increasing imidazole concentrations from 40mM to 400mM. Fractions were collected and analysed

using SDS-PAGE, those containing the NM1 tail protein, or CaM were carried forward for further work.

3.2.10 Circular Dichroism

1 $mgmL^{-1}$ of NM1 tail with or without CaM were analysed using far UV spectra (190nm-270nm) measured by a Jasco J715 Circular Dichroism Spectrometer (Jasco Inc.). Spectra were taken at 20˚C. 4 readings were taken for each measurement and averaged by the software provided. Each sample was measured in 5mM EGTA or prepared with 1mM $CaCl_2$

For spectra analysis the following equation was used.

Equation 3.1. Mean residue ellipticity equation

$$[\theta]_{MRW} = \frac{\frac{MW}{(n-1)} \times \theta}{l \times c \times 10}$$

Where ϑ_{MRW} is the mean residue ellipticity, *MW* is the molecular weight of the protein, *n* is the number of amino acids, ϑ is the degrees in ellipticity, *l* is the path length and *c* is the concentration.

3.2.11 NM1 N-terminal peptide fluorescent labelling

The N-terminal peptides containing an extra cysteine on the N-terminus were labelled to a ratio of 1 fluorescein-5-maleimide (Fisher) to 1 cysteine. 1mg of peptide was solubilised in 20mM Tris.HCl pH 7.5, 1mM EDTA and 200mM NaCl and mixed with 1M DTT for 20 mins at RT. Excess DTT was removed using a PD10 column (GE Healthcare) equilibrated in the solubilisation buffer. 1mg of fluorescein-5-maleimide was added to the eluted peptide and was left on rotation in the dark at 4°C overnight. Complete labelling was assumed and the now labelled peptide was carried forward for further work.

3.2.12 Fluorescence measurements

All measurements were done in solution. Fluorescein NM1 N-terminal peptide in 20mM Tris.HCl pH 7.5, 1mM EDTA and 200mM NaCl was diluted to 100nM and added to 10 wells of a 96 well FluoroNunc™ plate. NM1 tail and CaM also in 20mM Tris.HCl pH 7.5, 1mM EDTA and 200mM NaCl were serial diluted against the N-terminal peptides. Fluorescence emission was measured using a ClarioStar® (BMG Labtech) using an excitation at 495nm and emission at 519nm. Fluorescence was then normalised to fluorescein only and the data was fitted using the quadratic binding equation;

Equation 3.2. Quadratic binding equation.

$$[Complex] = \frac{([Pep]_t + [Pro]_t + K_d) - \sqrt{([Pep]_t + [Pro]_t + K_d)^2 - 4[Pep]_t[Pro]_t}}{2}$$

For NM1 tail binding to DNA, first the dsDNA was produced by mixing 100nM of each appropriate ssDNA oligonucleotides, one fluorescein labelled, the other not in 10mM Tris.HCl pH7.5, 50mM NaCl, 1mM DTT, 1mM $MgCl_2$ and 5mM EGTA if necessary for NM1 with tail binding assays. The DNA was heated to 95°C for 10 minutes and allowed to cool for 1 hour. The DNA was added to a 96 well plate at a 100nM concentration and the NM1 tail with CaM or without CaM was serial diluted into the DNA. Analysis was carried out as done previously for NM1 peptide binding. All experiments were carried out in triplicate.

3.2.13 Mammalian cell culture

All cells were maintained at 37°C and 5% CO_2. HeLa wells were maintained in MEM Alpha media with GlutaMAX (no nucleosides) supplemented with 10% heat inactivated Fetal bovine serum (FBS) and a penicillin-streptomycin mix diluted to 50 units mL^{-1}. MCF10A cells

were maintained in 50% MEM Alpha media with GlutaMAX (no nucleosides) and 50% Ham's F-12 nutrient mixture, where a 500mL mixture is then supplemented with 5% FBS, 5% horse serum, penicillin-streptomycin mix diluted to 100 units mL^{-1}, 50µg Cholera toxin, 5µg insulin, 20ngmL^{-1} human EGF and 0.5µgmL^{-1} hydrocortisone. Removal of cells from cell culture dishes was carried out first by washing the cells three times in PBS, then Trypsin-EDTA (0.25%), phenol red, was added directly to the cells and incubated at 37°C for 5 mins for HeLa and 20 mins for MCF10A cells. Cells were then centrifuged at 500 x g for 5 mins at RT and the supernatant was discarded and the cells resuspended in their respective growth mediums. The table below shows the stock concentrations and final concentrations of drugs that supplemented the media for each experiment.

3.2.14 MVI knockdown

Cells were seeded to a 30% confluency in a 24 well cell culture plate in their respective media and incubated at 37°C and 5% CO_2 overnight. The media is removed and the cells are then grown in their respective media without antibiotics. 50nM Human Myosin VI siRNA duplex (Ambion) or 50nM All Stars Negative Control siRNA duplex (Qiagen) is then prepared in 50µL of Opti-MEM per reaction. Alongside 1.5µL per reaction of lipofectamine-2000 transfection reagent is added to 50µL of Opti-MEM. Both are incubated at RT for 10 mins. The siRNA and lipofectamine is then mixed at left to stand at RT for 20 mins. The KD mixture is then added to the cells dropwise. After 24 hours cells the media was changed to re-introduce the antibiotics and any drug treatments that were required. After another 24 hours the cells were fixed or collected for further analysis.

3.2.15 RNA-seq sample preparation

1mL of ice cold TRIzol™ reagent was added to each cell culture. The lysate was then mixes using a pipette to homogenise. The mixture was then incubated for 5 mins at RT 0.2mL of chloroform was added to the lysis and incubated for 3 mins. The samples were then centrifuged at 12,000 x g at 4°C. Once the mixture has separated the colourless aqueous phase is collect and placed in a new clean Eppendorf tube. The RNA is then precipitated using 0.5mL of isopropanol and incubated for 10 mins and centrifuged for a further 10 mins at 12,000 x g at 4 °C. The supernatant is then discarded and the pellet is washed in 75% (v/v) ethanol, vortexed and centrifuged for 5 mins at 7500 x g at 4°C. The supernatant is removed and the RNA pellet is air dried for 10 mins. The pellet is then resuspended in 50µL of RNase-free water containing 0.1mM EDTA and incubated at 55°C for 15 mins to allow the RNA to dissolve. The RNA was then quantified using then 260nm absorbance, ensuring the A260/A280 ratio was approximately 2, implying the sample is pure. The sample was then further purified using the RNeasy kit (Qiagen) where the manufacturers protocol was followed exactly. To ensure purity and stability of the RNA, a 1% agarose TAE gel was ran, after which it was then stained using SYBR™gold to identifying the two rRNA bands, 28S and 18S. Once the purity and stability had been measured the RNA was then stored at -80°C and shipped on dry ice to Prof. Percipalles laboratory at New York University Abu Dhabi for further analysis.

3.2.16 RNA sequencing and analysis

RNA sequencing and analysis was carried out by Tomáš Venit from Prof. Percipalles lab. Total RNA extracted from three replicates of WT, MVI KD, MVI KD Cisplatin, Scrambled and scrambled cisplatin was analysed. The RNA seq library was prepared by using the TruSeq Stranded mRNA Library Prep Kit (Illumina) and sequenced with the HiSEq 2500 sequencing platform (performed at the NYUAD Sequencing Center). All of the subsequent analysis,

including quality trimming, was executed using the BioSAILs workflow execution system. The raw reads were quality trimmed using Trimmomatic (version 0.36) to trim low quality bases, systematic base calling errors, as well sequencing adapter contamination. FastQC was used to assess the quality of the sequenced reads pre/post quality trimming. Only the reads that passed quality trimming in pairs were retained for downstream analysis. The quality trimmed RNAseq reads were aligned to the Homo sapiens GRch38 genome using HISAT2 (version 2.0.4). The resulting SAM alignment files for each sequenced sample were then converted to BAM format and sorted by coordinate using SAMtools (version 0.1.19). The BAM alignment files were processed using HTseq-count using the reference annotation file to produce raw counts for each sample. The raw counts were then analyzed using the online analysis portal NASQAR (http://nasqar.abudhabi.nyu.edu/) in order to merge, normalize and identify differentially expressed genes. Differentially expressed genes by at least 2-fold log2(FC)≥1 and adjusted p-value of <0.05 for upregulated genes and log2(FC)≤-1 and adjusted p-value of <0.05 for downregulated genes) between the samples which were then subjected to Gene Ontology (GO) enrichment using ShinyGo v0.60 (http://bioinformatics.sdstate.edu/go/). Venn diagram was produced by Bioinformatics and Evolutionary Genomics platform (http://bioinformatics.psb.ugent.be/webtools/Venn/).

3.2.17 MVI co-immunoprecipitation

Cells were either left untreated or treated with cisplatin for 24 hours in triplicate for each condition. They were then washed three times in PBS and then collected using Trypsin-EDTA (0.25%), phenol red. Once the cells were detached the solution was centrifuged at 500 x g for 5 mins at 4 °C. The supernatant was discarded and the pellet was resuspended in 200µL of lysis buffer per $1x10^6$ cells. The lysis buffer contained, 10mM Hepes pH 7.5, 2mM $MgCl_2$, 25mM KCl, 0.1mM DTT, 0.1mM PMSF, 0.1% (v/v) Triton X-100, 0.1 % (v/v) NP40 and a protease inhibitor cocktail. The cells were left to lyse on ice for 1 hour. 0.075mg of protein A

agarose beads (Sigma Aldrich, Cat No. PROTAA-RO) were then washed three times and equilibrated in lysis buffer, the buffer was then removed and the cell lysis was added to the beads and incubated at 4°C for 10 mins, this identified any non-specific proteins that bound to the beads. The cell lysis was then removed and placed in a clean tube where the Anti-MVI antibody as described previously was added at a dilution of 1 in 100. This antibody and cell lysis was left rotating at 4°C overnight. 0.15mg of protein A agarose beads were then added to the cell lysis and was left to rotate at 4°C for 2 hours. The beads are then collected using a MagRack 6 (GE Healthcare) and the supernatant was removed.

3.2.18 MVI Proteomics preparation

Once the agarose beads were collected from the co-immunoprecipitation NuPage™ LDS sample buffer, 1xPBS, 1M DTT at a ratio of 2:2:1 was added to the beads. The beads were then boiled at 95°C for 10 mins before being loaded onto an SDS-PAGE gel. The gel was ran for 10 mins at 200V and stopped when the dye front had reached the resolving segment of the gel. The gel was then stained and destained as previously described leaving a single band containing all proteins elucidated from the previous steps. 0.5mL tubes were cleaned with 100% methanol and left to dry covered in a dust free environment. In a sterile laminar flow hood, each band for each sample was cut into $1mm^2$ segments using a clean scalpel which were then placed into the cleaned tubes. The gel segments were then washed with 50mM ammonium bicarbonate and acetonitrile in a 1:1 ratio at RT for 15 mins and then centrifuged at 500 x g for 1 min, and the supernatant was removed. The gels were then washed in acetonitrile, incubated for 15 mins and centrifuged as previously described, and the acetonitrile was removed. The gel was then washed in 10mM DTT, 50mM ammonium bicarbonate and incubated at 56°C for 30 mins. The gels were centrifuged and the wash removed. Acetonitrile was then washed over the pieces to shrink them and then taken off and 55mM iodoacetamide in 50mM ammonium bicarbonate was added and the gel pieces

were incubated at RT in the dark for 20 mins. The supernatant was removed and the gels were washed as previously described in the ammonium bicarbonate-acetonitrile solution, ammonium bicarbonate and finally acetonitrile. The gel pieces were then rehydrated in digestion buffer (25mM ammonium bicarbonate, 10% acetonitrile and 10ng.μL^{-1} of recombinant trypsin (Sigma Aldrich, EMS0006)). The reaction was incubated on ice for 30 mins and the supernatant was then removed. The gel pieces were covered in digestion buffer without trypsin and left at RT overnight.

5µl of acetonitrile was added to each sample in digestion buffer and the samples were then sonicated in an ultrasonic bath (Thermo) for 15 minutes at RT. The gel pieces were centrifuged at 500 x g for 2 mins and the supernatant was collected and stored at 4°C. 50% acetonitrile and 5% formic acid were added to the pieces which were then sonicated again as before. The gel pieces were centrifuged as before and the supernatant was collected and added to the previous supernatant stored at 4°C. This mixture is then vacuum dried using a benchtop CentriVap™ (Thomas Scientific) until the protein pellet is dry. 10µL of 10% acetonitrile and 0.1% trifluoroacetic acid resuspended the protein pellets. The samples were collected and loaded onto the liquid chromatography – mass spectrometry/mass spectrometry (LC-MS/MS) apparatus.

3.2.19 LC- MS/MS and proteomics analysis

Each sample, WT-precleared beads, WT-MVI co-immunoprecipitation, Cisplatin-precleared beads and Cisplatin-MVI co-immunoprecipitation, were subjected to nanoLCMS: peptides were separated on a HSS T3 Acquity column (Waters) 75 µm i.d. x 15 cm (1.8 µm, 100A) using an Acquity M-Class UPLC (Waters), elution was performed with a linear gradient from 3 to 40% B over 40 mins (solvent A = 0.1% formic acid, solvent B = 0.1% formic acid, acetonitrile) and the eluate directed via a nanospray source to a Synapt G2-Si (Waters) with data collected in UDMSe mode. The mass spec data was imported into a software package from Non-Linear

Dynamics called Progenesis QI for and searched against a protein database using an MSe Search algorithm with a false detection rate of 4%. Progenesis QI software (Waters) provided quality control information and quantification of peptides. The peptides were assigned using the following criteria. The human proteome including enolase v5 2017 from UNIPROT was used as the reference library with trypsin cleavage being included. The maximum protein mass was limited to 500kDa and only a maximum of 1 missed cleavage was allowed. Due to the sample preparations the carbamidomethyl modification to cysteine residues and the oxidation of methionine residues were accounted for. The peptide mass tolerance was set at 1 along with the fragmentation mass tolerance at 1. The false discovery rate was set at 4 with the minimum of fragments per peptide was required to be above 3 and the minimum fragments per protein were required to be above 5. Initially the minimum of peptides per allocated protein was set at 1. Further analysis was completed on the allocated proteins, by removing any proteins that did not have a 2 fold increase of abundance compared to the samples bound non specifically to agarose beads, and proteins that had an ANOVA p value of >0.05. All assigned proteins also had to contain at least 1 unique peptide in its assignment. Finally protein networks were plotted using STRING V11 (https://string-db.org)

3.2.20 Confocal immunofluorescence

Cells were maintained as previously described however were directly grown on coverslips in their required media and drug treatments. The cells were washed three times in TBS and fixed with 4% (w/v) paraformaldehyde (PFA) in TBS for 12 mins. The fixed cells were then washed three times in TBS. Residual PFA and cell autofluorescence was then quenched using 50mM NH_4Cl for 15 mins. Cells were then washed three times with TBS. Cells were then permeabilised and simultaneously blocked for 30 mins with 2% (w/v) Bovine Serum Albumin (BSA) in TBS supplemented with 0.1 (v/v) Triton X-100. Without washing the cells were then incubated with the designated primary antibody in 2% (w/v) BSA in TBS for 1 hour. The

coverslips were then washed three times in TBS. The appropriate fluorophore-conjugated anti mouse or anti rabbit secondary was then prepared in 2% (w/v) BSA in TBS and placed onto the coverslips, the coverslips were then incubated at RT for 1 hour in the dark. The coverslips were washed three times in TBS followed by nuclear staining using Hoechst 33342 solution (62249) for 10 mins at RT in the dark. The coverslips were then washed three times in TBS and once with ddH_2O. The coverslips were mounted onto microscope slides using Mowiol® 4-88, supplemented with 2.5% (w/v) of the antifading reagent 1,4-diazabicyclo[2.2.2]octane (DABCO). The slides were incubated overnight at RT and then stored at 4°C until imaged. The slides were then imaged using a Zeiss LSM980 with Airyscan 2 using a 60X oil-immersion objective and analysed using the manufacturer's software Zeiss Black. Colocalisation of NM1 and CaM, was analysed using Just another colocalisation plugin (JACoP) (Bolte and Cordelieres, 2006) following the published protocol and then plotted using Prism 8, Graphpad.

3.2.21 High Content Screening

High content screening was undertaken by myself at the imaging suite at New York University Abu Dhabi under the supervision of Prof. Percipalle and Dr. Venit. Cells were maintained as previously described, however they were grown directly onto Corning® 384 well microplates at a density of 5,000 cells per well. The cells were grown for 24 hours, followed by the necessary treatments. The cells were fixed and immunofluorescence was undertaken as described above, due to the cells being grown directly on the plates no mounting of coverslips was required. Stained cells in plate were scanned via Cellomics ArrayScan™ XTI High Content Analysis (HCS) platform (Thermo Fisher Scientific), with a 20x Objective. Compartment Analysis Bio Application software (Cellomics) was applied to quantitatively analyse the immunostaining spots in the nucleus based on a mask created using the nuclear Hoechst staining. For each experiment, at least 1000 valid single cells per culture well were

quantified and at least 10 independent culture wells (10 biological replicates) were analysed, fluorescence intensities were then plotted using Prism 8, Graphpad.

3.2.22 STORM imaging

Cells were cultured in 6 well Corning™ Costar™ Flat Bottom Cell Culture Plates (10578911). A total of 150,000 cells were plated and allowed to grow for 24 hours in previously stated growth conditions. Drug treatments were then undertaken for their respective time courses. The cells were fixed and labelled as previously described. Fixed coverslips were then transported to The Research Complex at Harwell, Harwell, UK. STORM imaging was carried out by myself. A STORM buffer was added onto the coverslips during imaging, this contained 400µL of a dilution buffer, 100µL of a glucose stock, 5µL of Beta-mercaptoethanol (63689) and 10µL of a glucose oxidase (GLOX) solution. The dilution buffer consisted of 50mM NaCl, 200mM Tris.HCl pH 8.0. The GLOX solution was made in dilution buffer, supplemented with 0.07mgµL^{-1} glucose oxidase (G7141) and 5mgmL^{-1} of catalase (C9322). Imaging was undertaken using the following illumination lasers, 642 nm (Vortran), 561 nm, 488 nm (Coherent, Sapphire), and 405 nm (Coherent, Cube) and imaged using a Zeiss Elyra 7 microscope with an EM-CCD camera attached. Imaging was completed as per the manufacturer's instructions, processing of the images and STORM data was undertaken using the Zeiss Black software. A minimum of 10 cells were analysed for each condition.

3.2.23 Clus-Doc analysis

The single molecule positions were exported from Zeiss Black and imported into the Clus-DoC analysis software (https://github.com/PRNicovich/ClusDoC) taken from Pageon *et al.,* (2016). The region of interest was determined by the nuclear staining. First the Ripley K function was completed on each channel identifying the r max. The r max was then assigned for DBSCAN if one channel was being analysed or Clus-Doc if two channel colcalisation was being analysed. The clustering size was set to a minimum of 5 molecules within a cluster with

a smoothing of a cluster being set at 7nm. All other analyses parameters remained at default settings. Data concerning each clusters was exported and graphed using Prism 8, GraphPad.

3.2.24 2D-FISH

Cells were cultured as previously described, where KD and drug treatments were completed when necessary. Once all treatments had been completed cells were washed with PBS, which was then collected and then removed using Trypsin-EDTA as before. The Trypsin-EDTA cell solution was diluted in PBS and then collected and added to the previous PBS wash. The collected cells were centrifuged at 500 x g at RT for 10 mins. The supernatant was then removed and the cell pellet was resuspended in 5mL of 0.075M KCl and incubated at 37°C for 20 mins. 3 drops of the fix solution (3 parts methanol : 1 part glacial acetic acid) was added to the samples which were then centrifuged at 500 x g for 10 mins at RT. The supernatant was discarded except for 0.5mL, the pellet was resuspended in this supernatant to which 5mL of fix solution was added, the samples were then centrifuged at 500 x g for 10 mins. This process was repeated three times to wash the cells into the fix solution. Finally the cells were then centrifuged at 500 x g for 10 mins, the supernatant removed except for 0.5mL which was used to resuspend the cells.

A Vysis HYBrite Hybridization System was preheated to 37°C. 10µL of cells in fix solution were dropped directly onto a microscope slide followed by 10µl of fix solution only. The slide was left to dry at RT and then immersed into 2x saline-sodium citrate solution (SSC) for 2 mins at RT without agitation. The slides were then dehydrated in an ethanol series (2 mins in 70%, 85% and 100% ethanol) at RT. They were then air dried and placed on the hybridisation system at 37°C. Cover slips were prepared with 10µL of the necessary chromosome paints and placed onto the slides. The coverslips were sealed using rubber cement and placed back onto the hybridisation system at 75°C for 2 mins. The samples were left within a hybridisation chamber over night in the dark at 37°C. The rubber cement and coverslips were removed

and the slides were immersed into 0.4xSSC pH 7.0 at 72°C for 2 mins, without agitation. The slides were drained and then placed into 2xSSC supplemented with 0.05% Tween-20 at RT for 30 secs. The slides were air dried and 10µl of DAPI (D9542) was placed onto each sample and a coverslip was placed and sealed onto the samples. Images were taken using an Olympus BX53 with a 40X oil-immersion objective. Approximately 50 nuclei per condition were then analysed using the nuclear morphology analysis software, (https://bitbucket.org/bmskinner/nuclear_morphology/wiki/Home).

3.2.25 Apoptosis assay

Cells were seeded in a 96 well cell culture dish (Corning) and allowed to grow for 24 hours in standard conditions. The RealTime-Glo™ Annexin V Apoptosis assay was utilised to provide real time measurements of apoptosis after samples had been treated with their designated drugs. The protocol follows the manufacturer's protocol. Briefly, a 2x Detection reagent is produced using the reagents provided in the kit, Annexin V NanoBiT™, $CaCl_2$, Annexin V-SmBiT and Annexin V LgBiT. This 2x detection reagent is diluted to 1x in the cells growth medium supplemented with cisplatin, bleomycin, TIP or Ku55933 at the concentrations stated previously. The cells are then incubated at 37°C with 5% CO_2 for 7 hours within a ClarioStar™ (BMG Labtech) multiplate reader. The multiplate reader was set to measure luminescence following the manufacturer's protocol as well as GFP fluorescence, with an excitation of 485nm and an emission of 525nm. These measurements were taken every 10 mins and were completed in triplicate for each cell growth condition. The graphs were then plotted using Excel, Microsoft.

Chapter 4. Properties of Nuclear Myosin 1

4.1 Introduction

Nuclear myosin 1 (NM1) is the most characterised of the nuclear myosins. Whilst this is the case, there are still questions regarding to the role of CaM and its interactions with NM1 in the nucleus, as well as if NM1 binds directly to the DNA. This chapter will focus on the biochemical properties of NM1 to further understand its nuclear functions.

4.1.1 Nuclear myosin I

NM1 is a monomeric processive motor with a unique 16 amino acid sequence at its N-terminus, a traditional motor domain, a neck region that contains three IQ regions, and finally a tail domain which contains a plecktstrin homology (PH) domain (Venit *et al.,* 2013). NM1 is an isoform of Myosin IC (MIC). MIC has three isoforms, A, B and C. These three isoforms differ through their N-terminal sequences, isoform C is the original single headed myosin known as MIC, isoform B is known as NM1 and isoform A, the most recent to be discovered and is yet to be characterised (Dzijak *et al.,* 2012). The expression of these isoforms is dependent on the cell type and it has been shown that both the C isoform and the B isoform can localise to the nucleus. It is important to note that all three of these isoforms contain an embedded NLS sequence within their IQ regions and so it is possible for all these isoforms to shuttle in and out of the nucleus. However, this NLS sequence does not allow any of these isoforms into the nucleolar region (Sielski *et al.,* 2014). NM1 can localise to the nucleolar spots to function in RNA polymerase I (RNAPI) transcription, therefore it is believed whilst all isoforms are able to enter the nucleus through their NLS sequence, the unique amino acids present at the N-terminus allows for NM1 to be the sole myosin IC in the nucleolar region (Dzijak *et al.,* 2012).

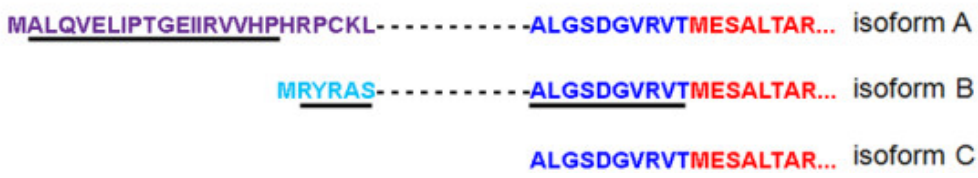


Figure 4.1. Representation of the three isoforms of myosin IC.
All the three isoforms differ at their N-termini through the transcription of upstream exons. Adapted from (Sielski *et al.,* 2014)

4.1.2 Regulation of MIC

For the myosins to be controlled within the cell, their activity needs to be tightly regulated. This regulation can come in the form of calmodulin (CaM) interactions with the IQ regions, back folding so that binding domains are blocked, and association with binding partners in their tail domains. In the case of MIC, apo-CaM can bind to the first two IQ domains through the typical CaM-IQ mode, where C-terminal lobes of the CaMs and the CaMs hydrophobic pocket links with the hydrophobic side chain found on the isoleucine within the IQ motif. Here the CaMs' N-terminal lobes are closed. The third IQ region of MIC slightly differs due to an arginine replacing a glutamine within the motif, yet CaM can still bind resulting in three CaMs bound to three regulatory regions (Lu *et al.,* 2014). Apo-CaM binding to these regions provides mechanical stiffness to the myosins structure. Once calcium is introduced to the system there is a weakening of the CaMs affinity to the IQ regions, where the IQ1 is highly calcium sensitive where it is lost in the presence of calcium, whilst the other binding regions have significantly lower dissociation rates, which in turn, inhibits actin gliding and increases the ATPase of MIC (Adamek, Coluccio and Geeves, 2008). Translating this to its role in the

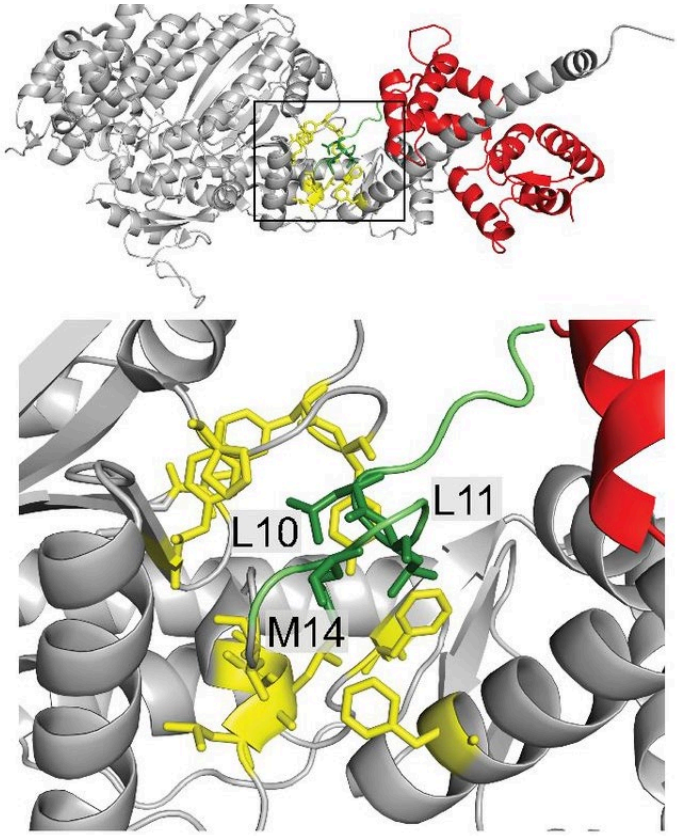


Figure 4.2. A crystal structure of myosin IBs' N-terminus.

A crystal structure showing the N-terminus (green) of apo-myosin IB being embedded at the beginning of the neck domain. Where two lysines-10,11 and methionine-14 interact adjacent to the IQ domains. Taken from Greenberg *et al.,* (2015) (PDB ID Code 4L79).

cell, so far myosin IC has been shown to bind to hair cell receptors through its IQ motif which is regulated by CaM binding (Cyr, Dumont and Gillespie, 2002) .

The N-terminal region of myosin IB, a myosin similar to myosin IC, is embedded within the hydrophobic pocket found within the motor domain and the lever arm helix. This position is then stabilised by interacting with the first CaM light chain (Figure 4.2. Greenberg *et al.,* 2015) . This positioning of the N-terminal region may provide a platform where the lever arm is able to respond to calcium regulation and ATP concentrations. This hydrophobic pocket also exists within MIC and so this N-terminal regulation may be possible. Greenberg *et al.,* (2015) have shown that the N-terminal region of MIC is able to tune the myosins motor

activity. By removing the N-terminal region, the rate of actin detachment, which is usually found to be force sensitive above 2pN, is no longer force sensitive until forces higher than 5pN. This is also supported by the fact the removal of the N-terminal region slows the rate of ADP release and accelerates ATP-induced actin disassociation. Force reversals, where the myosin is unable to maintain the post-power stroke conformation, also become more regular, showing this region stabilises the post-power-stroke conformation.

4.1.3 NM1s import into the nucleus

There are currently two distinct proposed models NM1 utilises to import itself into the nucleus. The first of which requires the NLS embedded within the second IQ region. Here the NLS itself and not the unique 16 amino acid N-terminus is required for nuclear localisation (Dzijak *et al.,* 2012). As all of the myosin IC isoforms contain this NLS, there is a redundancy amongst the isoforms, where NM1 knockout mice that are still able to express myosin IC A, show strong nuclear localisation of this protein (Venit *et al.,* 2013). This NLS sequence binds directly with importin 5, importin 7 and importin-β1, all well characterised nuclear pore complexes that utilise the GTPase Ran nuclear import pathway, however the NM1 does not seem to follow this specific pathway.

The second mechanism for NM1 import, relies on the PH domain found within the tail region. This domain allows the myosin to bind to phosphoinositides and so the NM1, can locate to the nucleus through a novel phosphoinositide pathway (Nevzorov *et al.,* 2018). Here, NM1 shuttles between the nucleus and the cytoplasm through its interaction with the endoplasmic reticulum, where it is able to diffuse through the nuclear pore complexes in a passive manner, even though the myosin is much larger than the characterised molecular weight cut off of around 40kDa. They also found no interaction between the myosin and the importins as previously published.

Whilst these two mechanisms differ, what is generally agreed on is that calcium effects the nuclear import of NM1. First by mutating the IQ binding region so that CaM is unable to bind, myosin IC has higher nuclear localisation, and by using a calcium ionophore, mimicking a calcium increase, nuclear import of NM1 is induced (Maly and Hofmann, 2016). By containing the NLS sequence within the IQ region it is postulated that the importins previously identified, compete with CaM and by increasing the calcium concentration and so weakening the CaM-IQ binding, the NLS becomes free for importin binding. As there is clear evidence for both pathways, I would suggest that both these pathways are required, the phosphoinositide pathway provides a cell with basal levels of NM1 and the NLS allows for rapid nuclear localisation for a cellular stimulus response, such as increase in calcium levels.

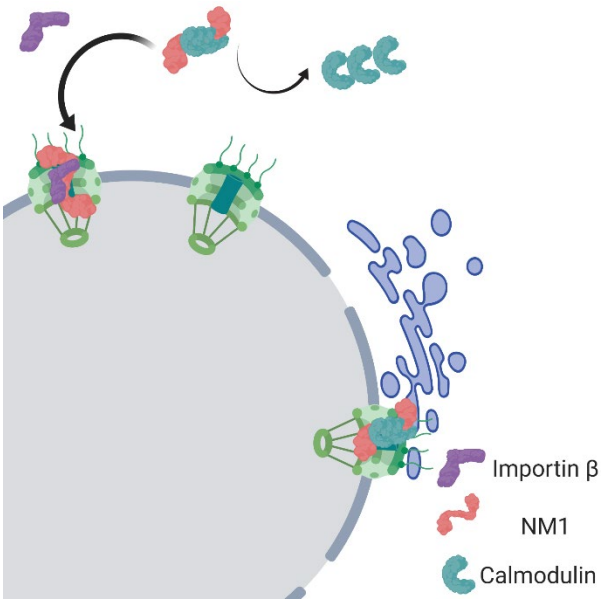


Figure 4.3. A cartoon representation of NM1 nuclear localisation.

NM1 (red) travelling either through the nuclear pore complex that requires the loss of CaM and the binding of an importin (purple) and NM1 travelling through the endoplasmic reticulum and diffusing into the nucleus through a nuclear pore complex. It is possible that these can occur simultaneously.

4.1.4 NM1s function in the nucleus

3.1.1.1 Transcription

NM1 has multiple roles within the nucleus, one of its first characterised roles is within transcription. NM1 has a role an interaction with RNA polymerases, RNAPI (Philimonenko, 2004), for rRNA synthesis, and RNAPII (Hoffman *et al.,* 2004) for mRNA synthesis. In RNAPI transcription, NM1 binds to the transcription factor TIF-IA and is found with actin alongside transcriptionally active RNAPI complexes (Sarshad *et al.,* 2013). Here NM1 binds directly to the rDNA, in RNAPII transcription NM1 also binds to the DNA, in both cases the biding has only been observed through chromatin immunoprecipitation (Sarshad *et al.,* 2013; Almuzzaini *et al.,* 2015). Actin is also found in RNAPII transcription where it binds directly to the subunit Rpb6, and it has been shown that NM1 associates with RNAPII with actin acting as linker protein between the two. During RNAPII transcription NM1 also acts as a chromatin re-modeller protein through its interactions with the B-WICH assembly (Vintermist *et al.,* 2011). The B-WICH assembly causes the activation of PCAF, a histone acetyl transferase which results in the unravelling of heterochromatin to euchromatin and the activation of transcription. The interaction between NM1 and this assembly, is directly with SNF2h stabilising it's binding to WSTF. These two roles of NM1, in RNAPII transcription alone, shows how important it is not just for the RNAPII machinery but also the organisation of chromatin.

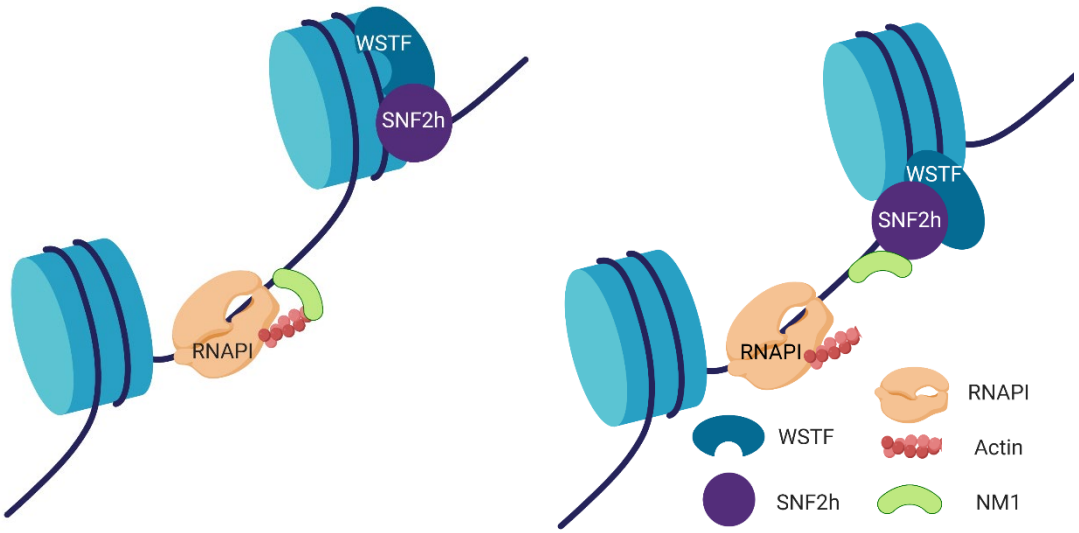


Figure 4.4. NM1 binds to RNAPI and DNA.

This occurs at its C-terminus at the initial stage of rDNA transcription. For transcription to then proceed NM1 unbinds actin and whilst still bound to DNA binds to the chromosome remodelling complex made up of SNF2h and WSTF.

DNA damage

NM1 plays a vital role in the DNA damage response. It is established that chromosomes are able to travel long distances within the nucleus by utilising NM1 and with removal of NM1 from the system long range chromosome movements are not observed (C. H. Chuang *et al.,* 2006). Interestingly, after the induction of DNA damage using cisplatin, there is movement of interphase chromosomes within the nucleus. These mobile chromosomes are able to move long distances from the periphery of the nucleus to the interior of the nucleus (Mehta *et al.,* 2010). This movement after DNA damage requires both the DNA damage signal γH2AX and NM1 (Kulashreshtha *et al.,* 2016). If either the signal does not occur, or NM1 is knocked down, then the chromosomes do not move as expected.

4.1.5 DNA binding by NM1

It is thought that NM1 is able to bind to DNA, due to its localisation within the nucleus and its role in DNA-based processes, however the question of, does NM1 bind directly to DNA is yet to be answered. Within this model, the cargo binding domain of NM1 has been implemented to bind DNA, however this has only been hypothesised by ChIP-seq data and RNA-seq data where the removal of the C-terminus causes loss of transcription and loss of chromatin associated proteins (Almuzzaini *et al.,* 2015). Nuclear myosins binding to DNA is not a new concept, as myosin VI (MVI) has been seen to bind directly to DNA through its C-terminus (Fili *et al.,* 2017). Therefore it is of importance to identify if NM1 does bind DNA directly and if so, what are the kinetics of this binding.

4.1.6 Aims of this study

Biochemically NM1 still remains elusive, the full length protein is yet to be purified recombinantly, therefore no full structure has been defined. This study aims to understand how its N-terminus, like that of myosin IB, interacts with the IQ region. Also DNA binding has been implied multiple times but is yet to be seen *in vitro*. Finally if NM1 does indeed lose CaM to enter the nucleus, how does this happen? And does NM1 rebind to CaM once inside the nucleus.

4.2 Results

4.2.1 Full length NM1 purification requires further optimisation

To begin the biochemical characterisation of NM1, a recombinant protein must first be produced, however the full length NM1 protein is yet to be purified for *in vitro* analysis. NM1 expression requires complex folding chaperones and the protein was expressed in the insect cell - baculovirus system. Expression was confirmed (Figure 4.5A), however, in the first purification most of the protein remained insoluble and so could not undergo further

purification (Figure 4.5B). A larger batch of protein expression provided small amount of soluble protein which could be isolated. The NM1 was tagged with a 6x histidine tag and the 5% of protein that was in the soluble fraction was further purified using a nickel column. Due to the lack of imidazole, which allowed binding of the protein to the column, in the loading buffer there was a large amount of impurities that also bound to the column (Figure 4.5C). After elution a small fraction of NM1 could be identified using western blot within an impure fraction (Figure 4.5C). Due to the low levels of soluble pure protein I decided it would be more efficient in studying the NM1 in terms of its domains which have already been published.

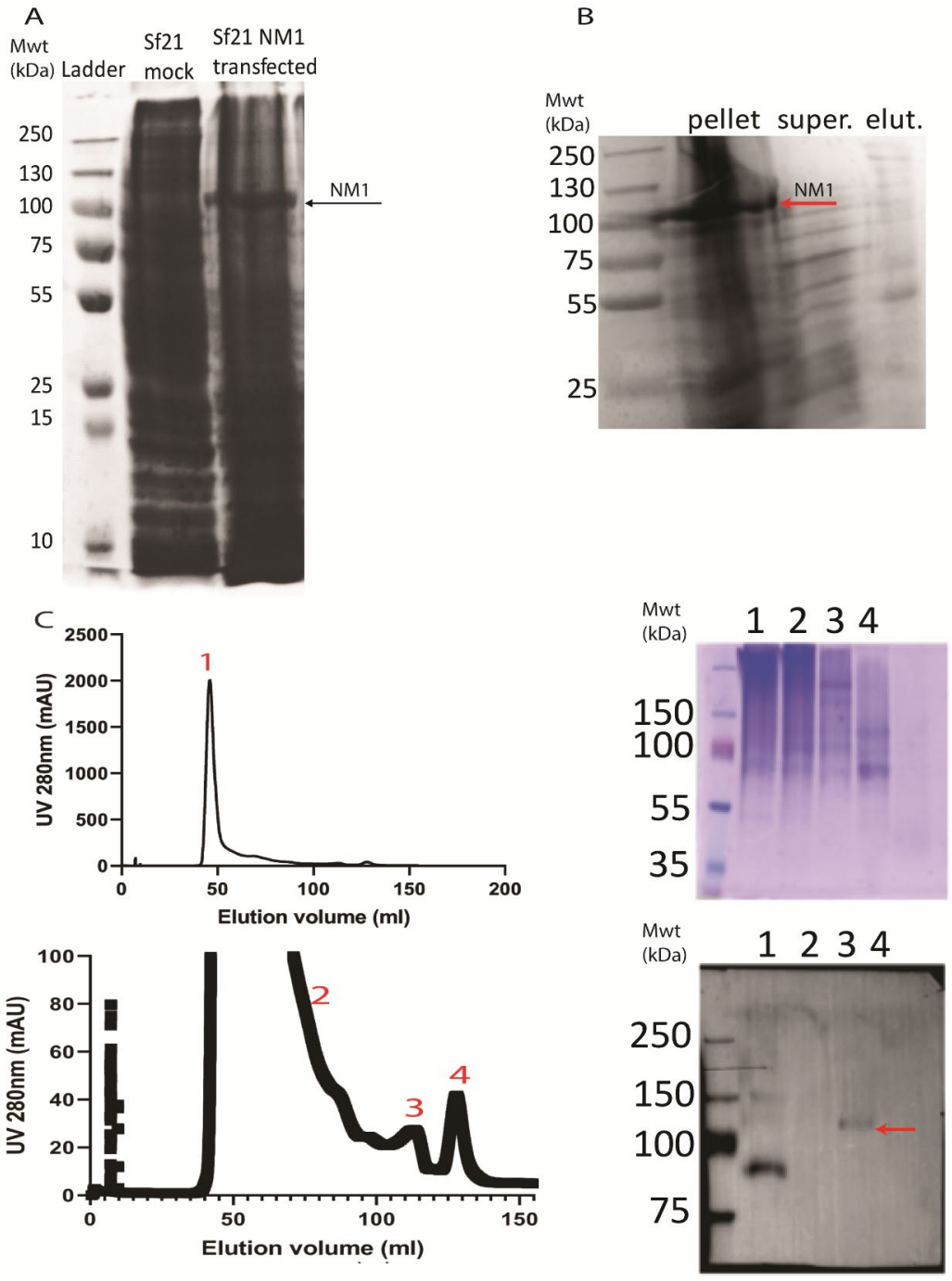


Figure 4.5. Purification of the full length NM1.

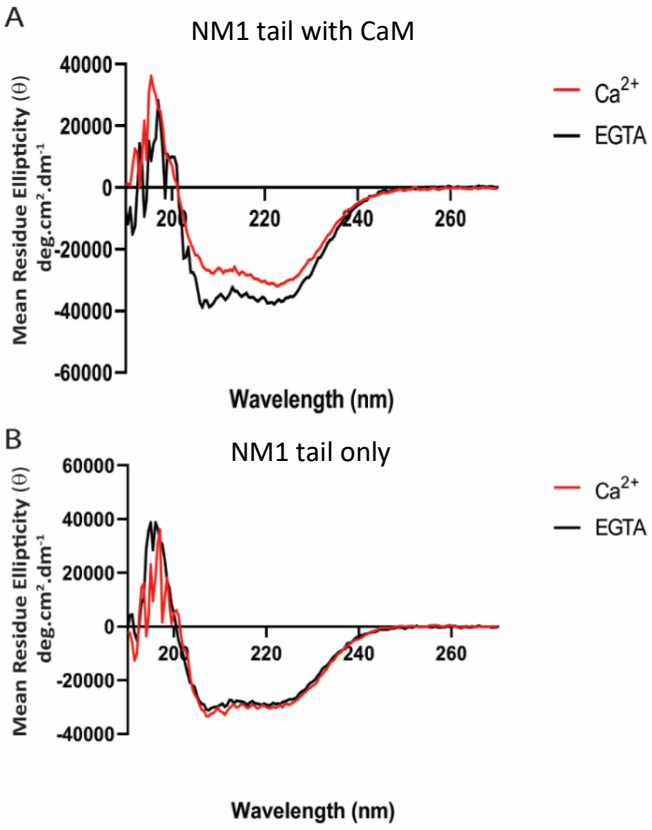
NM1 is successfully expressed in the baculovirus (A) however it is incredibly insoluble as shown by the presence of the protein in the pellet, with little being present in the supernatant (super.) and the elution fraction from the column (elut.) (B). After further attempts of purification only a negligible amount of NM1 can be purified as shown in the western blot as shown by the sequential fractions 1,2,3,4 from the chromatogram (C).

4.2.2 NM1 tail construct contains structure

After attempting to purify full NM1, the NM1 tail containing the three IQ regions and the cargo binding domain was purified from *E. coli* instead. This construct is made from the valine-732 position to the leucine-1060 and on the same plasmid there is also the gene for CaM, under the same promotor. This construct has previously been used to produce a crystal structure of three calmodulins binding to the tail region and so has been heavily characterised for stability (Lu *et al.,* 2015). During the initial purification it was only possible to purify the NM1 tail without CaM. To understand if the tail domain had structure following purification without CaM, circular dichroism was used (Figure 4.6). The structure was then determined using K2D3, a protein secondary structure prediction programme (Louis-Jeune et al., 2012), which showed that approximately 78% of the structure was α helical and approximately 1% of the structure is β sheets. As expected due to the absence of CaM, this structure was independent of the calcium levels within the buffer, as the addition of calcium led to a minimal change of 1% overall. This however differs from the crystal structure of the tail which has defined 44% helical residues and 20% β-sheet. However the K2D3 prediction software and circular dichroism is not as sensitive as using the crystal structure, and so the constructs were continued for further analysis.

To purify the NM1 tail with CaM an excess of EGTA was required. This EGTA chelates Ca^{2+} ions thus leaving only apo-CaM and therefore tight binding between the IQ regions and the CaM. This construct, co-purified with CaM, also has structure. Using the same analysis software in a buffer containing 5mM EGTA, the structure was made up of 78% α helixes and 1% β sheets similar to that of the NM1 tail on its own (Figure 4.6 C). With the addition of calcium altering the confirmation of the NM1 tail, there is a shift in circular dichroism spectra and a slight change of structure of 2%. This change in structure of the NM1 tail occurs due to

the release of CaM from the tail, caused by the shifting from apo-CaM to calcium bound CaM which loosens its binding to the IQ regions of the construct.



C

	NM1 tail-CaM (Ca^{2+})	NM1 tail-CaM (EGTA)	NM1 tail (Ca^{2+})	NM1 tail (EGTA)
α helix (%)	76.61	78.79	78.79	78.72
β strand (%)	1.1	1.08	1.08	1.1

Figure 4.6. Circular Dichroism of recombinant NM1 tail.
The NM1 tail can be purified with or without CaM (A, B) and there is clear structural change after the addition of calcium with the protein purified with CaM (A). Their structures have suitable percentages of α helices and β sheets (C).

Both tail constructs are stable and the presence of excess calcium on the tail co-purified with CaM can be observed. It is these purified recombinant proteins that have been carried on for further studies, which will focus on the role of the N-terminus extension and subsequently DNA binding.

4.2.3 The N-terminus of NM1 competes with CaM to bind to its own tail

Attention was first given to understanding how the N-terminus of NM1 may regulate nuclear localisation of the protein, in combination with the NLS sequence. Here the N-terminus is hypothesised to interact with the NLS sequence found within the IQ regions. To assess this, four peptides were designed, the wild type, one with the 2nd arginine replaced with a leucine, another where the 4th arginine is replaced with a leucine and the final peptide where both arginines had been replaced with leucines (Figure 4.7A).

These peptides were labelled with a maleimide coumarin dye, 7-Diethylamino-3-((((2-Maleimidyl)ethyl)amino)carbonyl)coumarin (MDCC) which binds to an extra cysteine residue added to the N-terminus sequence. These arginines were chosen as *in silico* modelling completed by our collaborators Percipalle *et al.,* (unpublished), had identified these positively charged amino acids necessary for the interaction between the N-terminus and the NLS embedded within the IQ region. The binding of the peptide to a protein construct, was measured through the increase in fluorescence and was then fitted to a quadratic binding equation, as previously described in the Chapter 3.

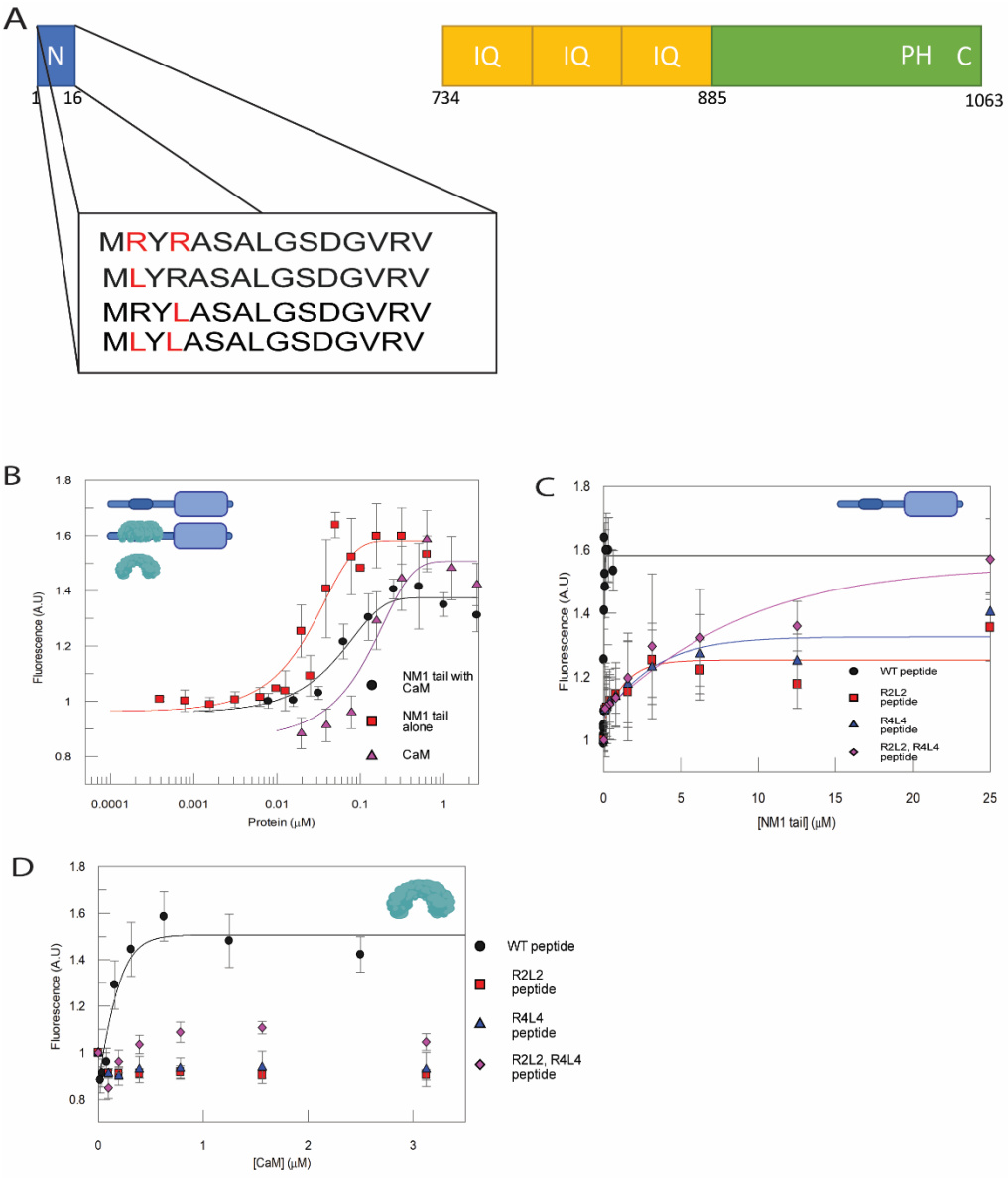
Equation 3.2. Quadratic binding equation.

$$[Complex] = \frac{([Pep]_t + [Pro]_t + K_d) - \sqrt{([Pep]_t + [Pro]_t + K_d)^2 - 4[Pep]_t[Pro]_t}}{2}$$

Where Pep is the concentration of peptide and Pro is the concentration of protein. Here the equilibrium dissociation constants (K_d) have been studied by looking at the NM1 tail with and without CaM and the binding of the peptides to CaM itself.

The NM1 tail without CaM binds very tightly to the wild type peptide at K_d of 0.03µM ±0.01. The CaM has a K_d of 0.2±0.07µM and the NM1 tail with CaM has a weaker K_d of 0.55±0.1µM (Figure 4.7 B). All of these bindings are within the nanomolar range and so are likely to occur within the nucleus assuming CaM is present, which will be discussed later. These bindings show that the N-terminus itself is capable of binding both to the tail region of NM1, as well as CaM albeit with different affinities. The capability for the NM1 tail without CaM to bind to N-terminus peptide can be disrupted through the two mutated arginines. All three mutated peptides, the two single and one double mutations, are unable to have their K_d defined at the low concentrations used for the wild type peptide and all the K_ds are over 1µM. These data show that both arginines are required for the N-terminus to bind to the tail (Figure 4.7 C).

Overall, the data shows that the absence of CaM leads to a more stable complex before the NLS and N-terminus can combine. This fits with the model that CaM needs to be removed for correct localisation into the nucleus. A weaker interaction between the N-terminus with the tail bound to CaM also occurs. This suggests that the CaM bound structure is also stable but for a yet unknown function.



E

Peptide	NM1 tail	NM1 tail$_C$	CaM
Wild type	0.03±0.01μM	0.55±0.1μM	0.2±0.07μM
R2L2	ND	ND	ND
R4L4	ND	ND	ND
R2L2R4L4	ND	ND	ND

Figure 4.7. NM1 tail constructs bind to the N-terminus of NM1.

The diagrams represent the NM1 tail (Blue), CaM (Green) and the NM1 tail with CaM. The N-terminus peptide binds to the NM1 tail with or without CaM as well as CaM itself. The fluorescence intensity was measured using fluorescein labelled peptide at a concentration of 100nM and titrating in the constructs from 0.0005 to 1.5μM (A). By replacing any of the arginines in this N-terminal sequence all binding is weakened significantly, as shown naked tail (C,D,E). N=3

4.2.4 The tail domain of NM1 has nano-molar affinity for dsDNA

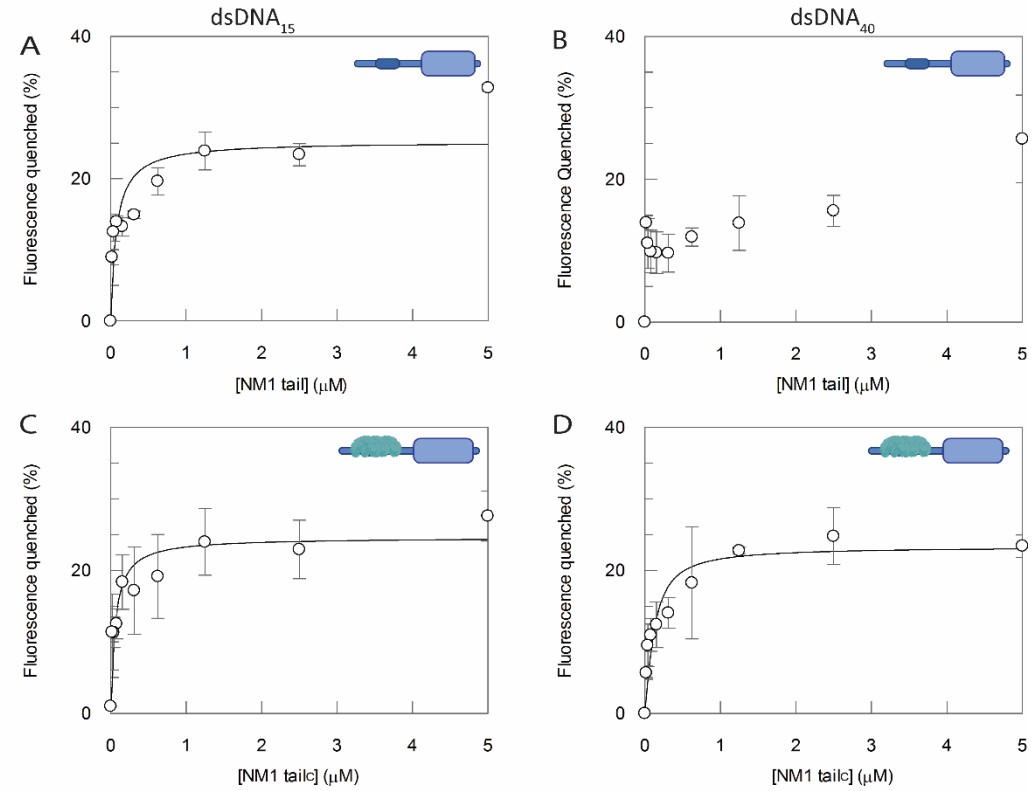
As discussed previously, it has been suggested by ChIP that NM1 is able to bind DNA through its C-terminus, however no biochemical measurements have been undertaken to understand if it directly binds dsDNA. By using two double stranded DNA lengths 15bp ($dsDNA_{15}$) and 40bps ($dsDNA_{40}$) both containing a fluorescein dye at their 5' ends it is possible to undertake such binding kinetics by studying the quenching of fluorescein fluorescence. This quenching occurs due to the changing of environment by the binding of a protein. This quenching is then fitted with using the quadratic binding equation (Equation 3.2).

The NM1 tail without CaM is able to bind to $dsDNA_{15}$ with a K_d of 75±33.1nM however the K_d is not able to be determined for $dsDNA_{40}$. When CaM is present the NM1 tail has a similar binding affinity for $dsDNA_{15}$ of 56±21nM. A K_d can also be defined for NM1 tail with CaM binding $dsDNA_{40}$ as 73.6±37.7nM (Figure 4.8). These results now add to the mechanism of NM1 binding to DNA where CaM may stabilise the protein enabling DNA bound to a more stable NM1. Moreover, direct DNA binding does occur through the C-terminus of NM1.

4.2.5 The tail domain of NM1 binds ssDNA as well

To identify if the binding of the tail domain to DNA is specific to the type of DNA, ssDNA substrates 15bp ($ssDNA_{15}$) and 40bp ($ssDNA_{40}$) long were also labelled with fluorescein at their 5' end. The binding was overall weaker compared to that of the NM1 tail with dsDNA, however it is still in the nanomolar range. NM1 tail without CaM has a K_d 399±145nM for $ssDNA_{15}$ and a K_d 148±69nM for $ssDNA_{40}$. These binding affinities are similar to that of NM1 tail with CaM where the binding to $ssDNA_{15}$ has a K_d 114.6±24nM and $ssDNA_{40}$ had a K_d 109.5±72nM (Figure 4.9). These binding affinities imply that NM1 binding to DNA is not

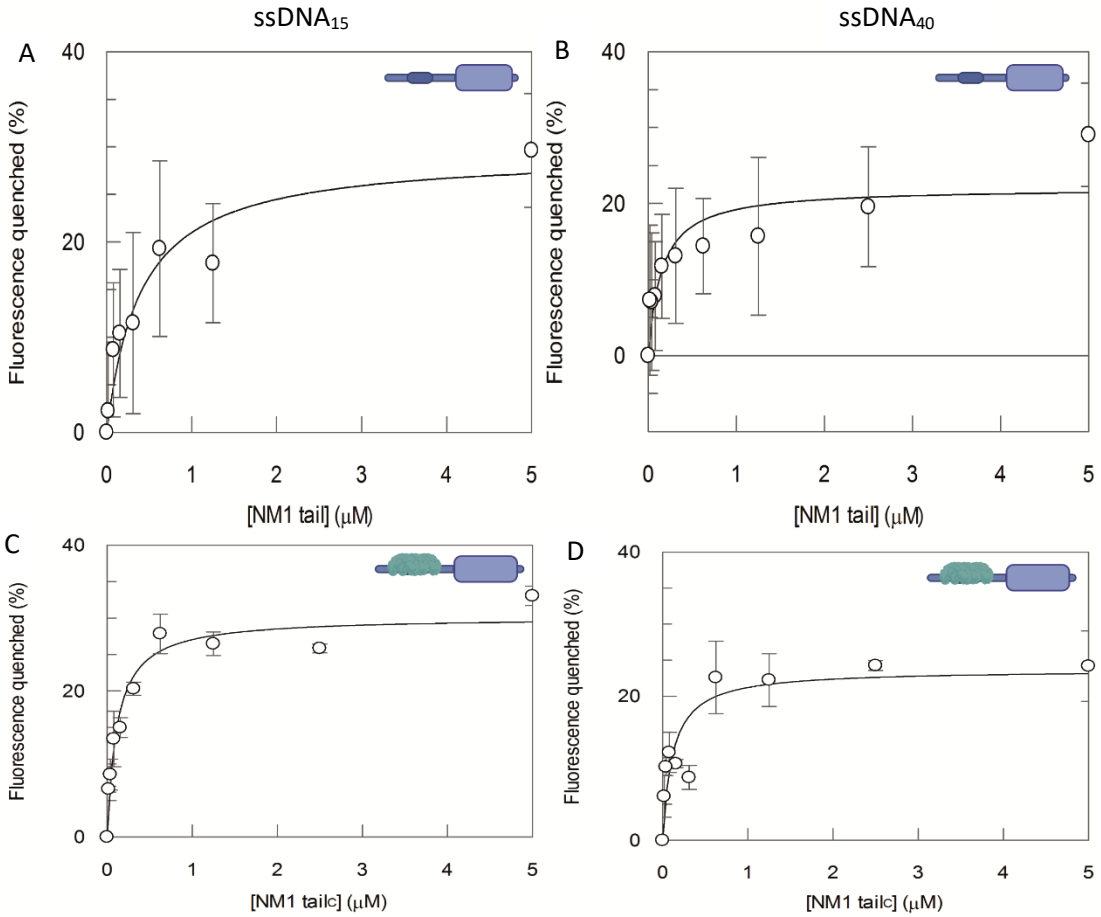
specific to the structure of said DNA and is likely down to electrostatic forces, and that CaM may have a stabilising affect on this DNA binding.



	NM1 $tail_C$ ($dsDNA_{15}$)	NM1 $tail_C$ ($dsDNA_{40}$)	NM1 tail ($dsDNA_{15}$)	NM1 tail ($dsDNA_{40}$)
K_d	56±21nM	73.6±37.7nM	75.0±33.1nM	ND

Figure 4.8. 4 NM1 tail is able to bind dsDNA.

The cartoons depict NM1 tail (blue) with or without CaM (green). NM1 tail can bind without CaM to $dsDNA_{15}$, K_d 75± 33.1nM (A), but not $dsDNA_{40}$ (B). However, in the presence of CaM the NM1 tail (NM1 $tail_C$) can bind both dsDNA lengths with a K_d of 56±21nM to $dsDNA_{15}$ and a K_d of 73.6± 37.7nM to $dsDNA_{40}$ (C,D).



	NM1 tail$_C$ (ssDNA$_{15}$)	**NM1 tail$_C$ (ssDNA$_{40}$)**	**NM1 tail (ssDNA$_{15}$)**	**NM1 tail (ssDNA$_{40}$)**
K_d	114.6±24nM	109.5±72nM	399±145nM	148±69nM

Figure 4.9. NM1 tail can bind ssDNA.

The cartoons depict NM1 tail (blue) with or without CaM (green).NM1 tail can bind ssDNA weaker than that of dsDNA. NM1 tail without CaM binds to ssDNA$_{40}$, K_d 399±145nM (A) and ssDNA$_{15}$, K_d 148 ±69nM (B). With the presence of CaM the is lowered and so the NM1 tail$_C$ can also bind ssDNA$_{40}$, K_d 109.5±72nM (C) and ssDNA$_{15}$, K_d

4.2.6 NM1 and CaM colocalise within the nucleus

Nuclear import suggests CaM is not bound to NM1 once inside the nucleus, however these data shown, suggests that CaM is required for DNA binding. Therefore it is possible that NM1 is able to rebind to CaM once it has entered the nucleus. Using confocal microscopy (Figure 4.10, A), alongside the JACoP analysis software, this study has identified that when an image of NM1 is imposed onto CaM, the average Manders' coefficient is 0.833. Manders' coefficients range from 0, where there is no colocalisation to 1, which is equal to 100% colocalisation. This means that the majority of NM1 molecules can be found colocalised to CaM (Figure 4.10 B). When CaM is overlapped onto NM1, the average Manders' coefficient is less, at 0.72. This suggests that the majority of CaM is associated with NM1 in the nucleus, however there is a portion of the population that is not colocalised to NM1. Overall, this provides evidence that after entering the nucleus, NM1 may be able to regain CaM or localised near CaM, which most likely regulates its roles within the nucleus, similar to that in the cytoplasm.

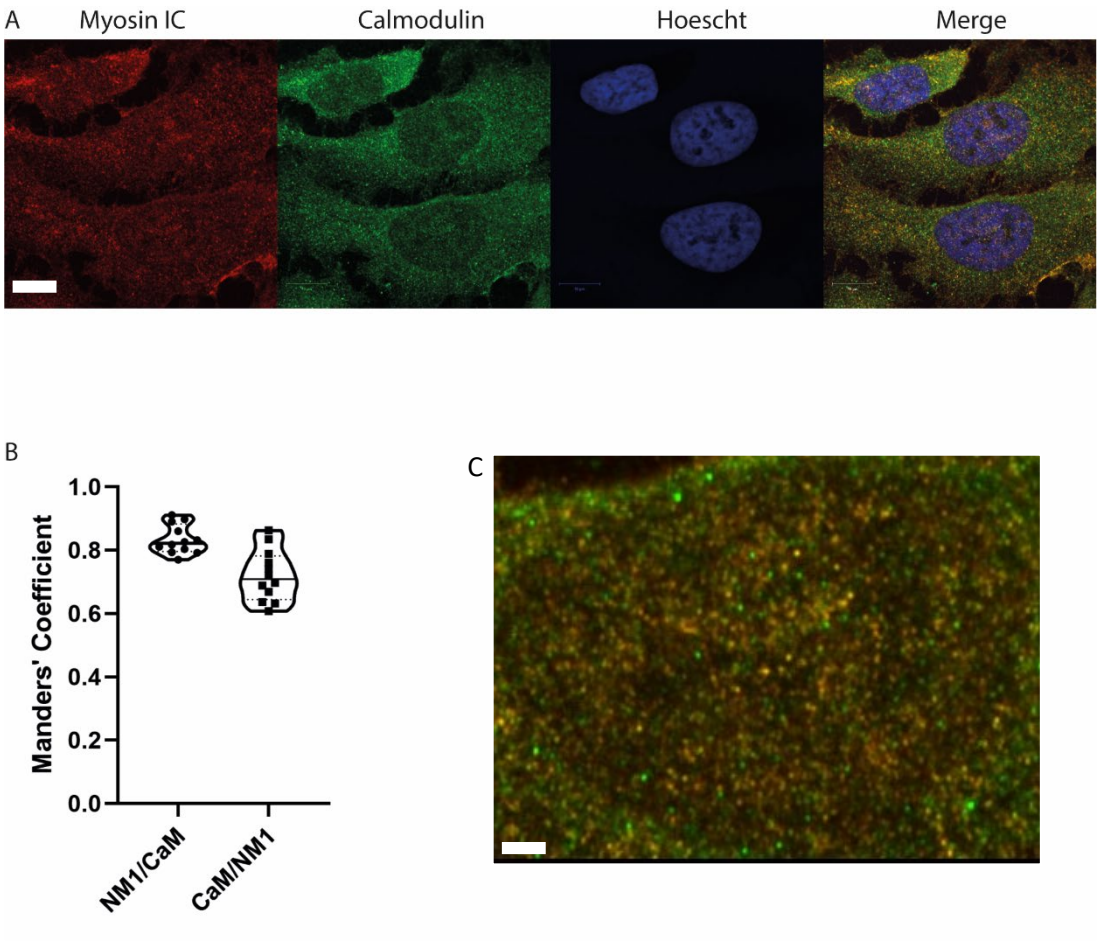


Figure 4.10. Colocalisation of NM1 and CaM.

(A) Confocal microscopy of NM1 and CaM within HeLa showing a population of both proteins within the nucleus. Scale bar = 10µm. After analysing the images using the colocalisation software JACoP, Manders' coefficients were produced for each nuclei of a cell. When NM1 is overlapped onto CaM the average Manders' coefficient is 0.833. When CaM is overlaid onto NM1 the average Manders' coefficient is 0.72. N of nuclei analysed = 12. Zooming in on the bottom nucleus in image A (C) shows the yellow colour of the overlapping channels of red for Myosin IC and green of CaM, scale bar =1µm.

4.3 Discussion

4.3.1 The purification of full length NM1 requires further optimisation

NM1 is yet to be purified as a full-length protein recombinantly and so many biochemical techniques such as actin gliding assays and structural techniques such as crystallography have yet to be undertaken. Using the baculovirus system the full-length protein has been successfully expressed, however its purification became difficult. The largest fraction of protein was insoluble, this is most likely due to the PH domain of myosin IC that is required for its membrane binding properties. This membrane binding causes the protein to be insoluble as these interactions are maintained following sonification and clarification. With further optimisation of the purification technique such as the use of detergents, for example triton or NP-40, to break down the membrane further, it would be possible to release the NM1 into the soluble fraction. However, these detergents would need to be removed for further purification of the protein using affinity chromatography. Alternative methods such as a mutation in the PH binding domain could also ease solubility of the protein, although this method may alter the structure or function of NM1. It may also be that these cells do not contain enough CaM, which may lead to aggregation of the protein.

To introduce further optimisation to the protocol, imidazole concentrations may be altered. During this study the full soluble fraction of proteins from the sf21 cells was loaded onto a nickel affinity column, knowing the histidine tag would bind, without any imidazole. This loading without imidazole leads to higher nonspecific binding of various proteins to the column as well the protein of interest, however increased imidazole leads to no binding of the NM1. Therefore, the concentrations of imidazole can be altered to reduce nonspecific binding.

Overall the full-length purification remains unsolved, this study however has shined a new light on how to express NM1. This could lead to a better understanding of its functional and structural properties and allow for easy *in vitro* characterisation of the protein. In the interest of time, the decision was taken to focus upon the tail domain.

4.3.2 Recombinant NM1 tail is a stable construct for *in vitro* studies

The motor domain of NM1 has been well characterised, however many of the binding capabilities of the tail region have yet to be studied *in vitro.* Using a construct that has been previously published, the NM1 tail including all three IQ regions, was purified and then studied for its structure. To understand the effect of CaM binding on the function of the tail domain, it was important to understand a structural role the CaM may play in the tail. The circular dichroism has shown that the NM1 tail has structure with or without CaM, as well as in the presence or absence of calcium. The circular dichroism data matches that of the published work when altering the calcium levels of NM1 tail purified with CaM (Lu *et al.,* 2015). This data also shows that the NM1 tail itself without CaM is unaffected structurally by calcium levels. Due to this stability, it was possible to take the recombinant tail onwards for further studies with and without CaM.

4.3.3 N-terminal – tail interaction provides an explanation for altered motor activity

As previously published the N-terminus of myosin IC alters the motor activity of the protein (Greenberg *et al.,* 2015). By simply removing the N-terminus the ADP release is slowed and the ATP induced disassociation of actin is increased. With this theory and the proof of an alternative myosin I, myosin IB having an N-terminal interaction close to the IQ region, I have shown that NM1 has this interaction as well. As the N-terminus peptide is able to bind to NM1 when CaM is present at a K_d of 0.55µM and can bind CaM itself with a K_d of 0.2µM. As CaM regulates the activity of NM1 as well as the N-terminus there is potential for the NM1

to backfold around the CaM, where CaM may act as a bridge between the tail and the N-terminus. This then can explain how the removal of the N-terminus then affects the motor activity.

The fact the binding of N-terminus peptide is weaker to NM1 tail with CaM than CaM itself may be occurring due to the peptide being able to bind both CaM and the tail domain and so it is difficult to predict which protein the peptide is binding too. However it does show that the interaction between the peptide with CaM or the tail recombinant protein is relatively unaffected by the binding of NM1 tail with CaM. This shows that all three are able to interact thus providing structural information without the ability to express and purify the full length protein.

4.3.4 N-terminal regulation may play a role in nuclear import

The N-terminus of NM1 has been shown to be required for nucleolar localisation of NM1 and for the myosin to enter the nucleus the CaM must dissociate from the IQ regions (Dzijak *et al.,* 2012). It has been hypothesised that the CaM is blocking the NLS region within the IQ domain and so importins are unable to transport the myosin into the nucleus.

The data shows that the unique 16 amino acid sequence found at the N-terminus of NM1 binds tightly to the tail domain of NM1 with a K_d of 0.03µM. Whilst we are unable to identify the precise location of N-terminal binding we have shown this binding can be disrupted by either a single point mutation of the arginine found at position two or the arginine at position 4 of the N-terminus, showing that both amino acids are necessary for a complete interaction.

Due to the fact the N-terminus binds tightest to the NM1 tail without CaM but also the N-terminus binds CaM, as previously stated, there is potential for competitive binding with the N-terminus having a preference to bind to the tail directly. This competitive binding could be

regulated by the local calcium concentration, as this would aid in the either the IQ region being free for N-terminal binding or CaM being bound instead.

It is likely that once CaM is removed, by high calcium levels, from the IQ regions the motor domain folds over and the N-terminus interacts with the NLS region of the tail. This interaction may compete with CaM, blocking the CaM from rebinding to the IQ region and allowing NM1 to interact with the nuclear pore complexes using its NLS, finally transporting it into the nucleus. Once transported some other conformational change must occur to reset the folding to then allow CaM to rebind.

4.3.5 NM1s ability to bind DNA is potentially regulated by CaM

Whilst it has been known that NM1 is able to associate with the genome through ChIP-seq data (Almuzzaini *et al.,* 2015), the data shown here is the first to provide biochemical characterisation for direct binding. The NM1 tail can bind to a variation of dsDNA lengths with and without CaM with K_ds of 56 to 75nM except for when no CaM is present when the NM1 tail is binding to $dsDNA_{40}$ where the K_d is undefined. In the binding assay it is possible that the K_d is not determined due to it not being reached within the system.

The fact that the NM1 tail is able to bind to $dsDNA_{15}$ with or without CaM with a K_d of 75nM and 56nM respectively shows that the IQ domains do not have an effect on the tail binding and it is likely that closer to the PH domain is the DNA binding domain. This binding also shows that NM1 must bind to DNA that is at least 15bp long, however the actual length of DNA needed for binding could be far below that and so short DNA strands could be used and smaller recombinant fractions of just the tail without IQ domains and just the PH domain could be used to identify the exact amino acids required for DNA binding.

The fact that NM1 is able to bind DNA in the nano-molar range and it binds RNAPII through actin it is possible that the CaM more affects the binding to actin and RNAPII rather than the

DNA binding. However the ssDNA binding affinity was far stronger when CaM was present in the system, and the colocalisation has shown that CaM and NM1 are present together within the nucleus.

4.3.6 DNA binding must occur through electrostatic interactions

The tail domain not only binds to dsDNA but also ssDNA. These strands are made up of guanine and cytosine residues and with no discernible structure. The binding assays have shown reduced binding constants with and without CaM compared to that of dsDNA, and all are able to be defined with a K_d all above 100nM. The fact that the NM1 tail can bind to both substrates, it is likely that the phosphate backbone of the DNA is providing a negative charge and the positive charges found in the tail domain, allow an electrostatic interaction thus making the sequence of DNA irrelevant.

4.3.7 NM1s role and regulation

The identification of the N-terminus binding the tail domain and CaM provides evidence of how NM1 can be imported and why it is important for the protein to have high local calcium levels and that the loss of CaM is required. The colocalisation analysis suggests once NM1 enters the nucleus it is likely that apo-CaM rebinds to the NM1 tail, thus allowing for the NM1 to become regulated by CaM once again. It seems as though the presence of CaM may affect DNA binding but could also play a classical regulation of the motor domain which may help NM1 act as an auxiliary motor to the RNAPII machinery. This DNA binding role also helps link NM1 to the chromatin remodelling complexes containing WTSF and SNF2h where NM1 could potentially bind DNA to allow for the opening of closed chromatin, or move the DNA to transcriptionally active areas (Vintermist *et al.,* 2011). This study has shown that whilst it is not possible to purify the full length myosin, by using the recombinant tail further biochemical and structural characterisation can be undertaken.

The next step in this study would be to purify the full length protein so as to study its regulation by CaM and to produce a crystal structure highlighting the embedded N-terminus with the IQ regions To further study the gain and loss of CaM, live cell imaging using fluorescence resonance energy transfer (FRET) would provide information on the state of CaM during transcription and would further confirm the loss of CaM to allow NM1 translocation into the nucleus.

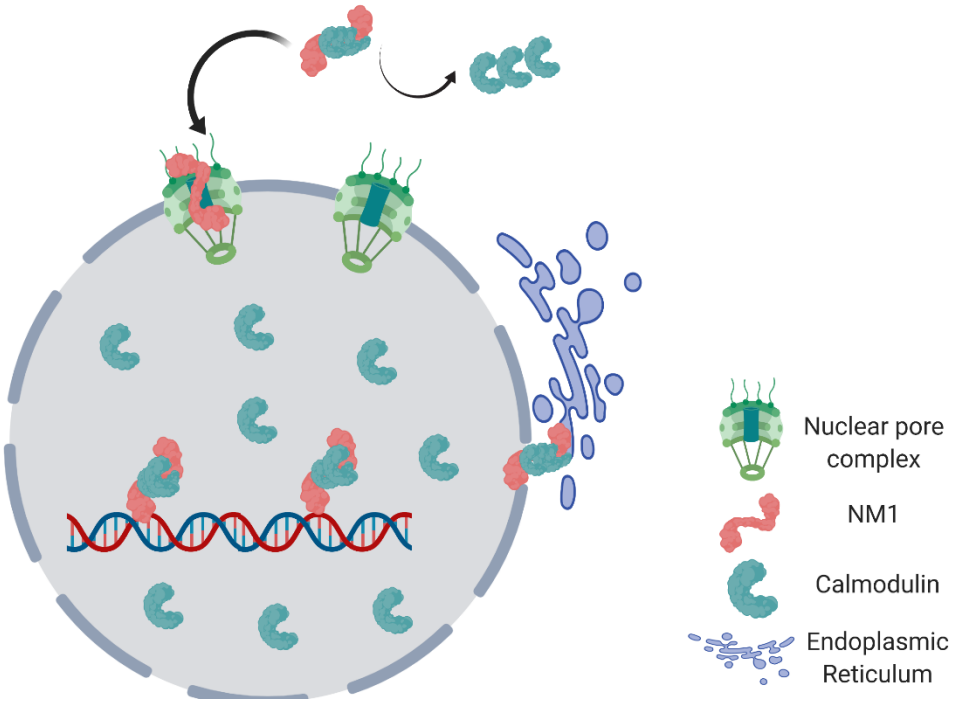


Figure 4.11. A new model of NM1 regulation.

NM1 releases CaM allowing the N-terminus of NM1 to bind to the tail domain. This allows translocation through the nuclear pores. NM1 then rebinds to CaM in the nucleus where it then binds DNA for its role in transcription.

Chapter 5. Myosin VIs' response to DNA damage

5.1 Introduction.

To understand further how nuclear myosins can be regulated and to further elucidate their roles in the nucleus, a stimulus can be used. Use of a stimulus along with gene silencing technology can be availed to identify phenotypic and genotypic responses by the protein of interest in a cellular pathway. In this study, double stranded breaks were used to identify how a nuclear myosin, in particular MVI, responds to these breaks and if it is required for DNA damage. It is already known that NM1 responds to DNA damage and brings about the movement of chromosomes after DNA damage (Kulashreshta *et al.,* 2016) and so it is possible for MVI to also have a role in the DNA damage response.

5.1.1 Myosin VI.

MVI is commonly found as both monomeric and dimeric and travels along actin filaments in the opposite direction to all other known cellular myosins, from the barbed end, to the pointed end of actin. This ability to move in reverse means that within the cytoplasm of the cell, it is utilised for endocytosis, golgi membrane maintenance and cell migration (Chibalina *et al.,* 2009). Its structure follows all other myosins with a globular motor domain, a neck region and finally a tail domain for cargo binding. The motor domain allows for a step size of 30-36nm when the protein is dimeric, as well as the ability for MVI to act as either a processive motor at low forces or an anchor at high molecular forces above 2pN (Altman *et al.,* 2004). This duality of function between anchor and motor shows that MVIs function can be regulated by external forces, cargo binding and other binding partners.

The neck region contains only one IQ domain as well as the unique insert, thus MVI binds two CaMs, that regulate the stability of the protein. The binding partners of MVI, such as GIPC (Buss *et al.,* 2001), involved in clathrin coated vesicles and endocytosis, Dab2, involved in tumour suppression and cell signalling (Morris *et al.,* 2002), and SAP97, used at cell-cell

adhesion sites all define its function (Nash *et al.,* 2010). These studies suggest that the binding partners might be involved in regulation of MVI as well as provide evidence of its various functions within the cytoplasm.

5.1.2 MVI in the nucleus.

MVI in the nucleus is a relatively new discovery, having been found in 2006, where it was associated with newly transcribed mRNA and RNAPII complexes (Vreugde *et al.,* 2006). Fili *et al.* (2017), then took this work further and showed that one of its binding partners NDP52 activates MVI, allowing it to unfold from its back folded state and then dimerise through the NDP52 intermediate. This then creates a mechanism where MVI binds to a DNA binding protein, NDP52 as well as the RNAPII complex itself, acting as a potential stabiliser of the transcription machinery. Here it is likely due to the large forces the RNAPII complex generates, that MVI is acting within an anchoring role rather than that of the cytoplasmic transporter it is often characterised as.

For MVI to enter the nucleus there are multiple putative nuclear localisation signals that have been identified, these sites are yet to be experimentally proven and with six sites it is difficult to predict if they are all active or if there is one specific site only (Majewski *et al.,* 2018). These sites are shown in the table below.

Putative Sites	Amino acid residues predicted by bioinformatic tools	Location within the MVI heavy chain (residues/domains)
NLS - nuclear localization signal	PRKSKLA	559-566, motor domain
	RRHK	831-834, IQ motif
	RKRR	937-940, putative coiled-coil domain
	RRRK	946-949, putative coiled-coil domain
	RKKR	971-974, putative coiled-coil domain
	RRLKVYHAWKSKNKKRN	1116-1132, globular tail domain
	PQNKKKG	1185-1191, globular tail domain
NES - nuclear export sequence	LALRI	1012-1016, putative coiled-coil domain

Table 5.1. A Table of MVI nuclear localisation and nuclear export sequences

Taken from Majewski *et al.,*(2018)

There is also one export sequence that has been identified within the coiled-coil domain of the MVI. These multiple import and single export sequences allow MVI to shuttle across the nuclear membrane, which shows that there are no specific and separate cytoplasmic and nuclear pools and the exchange of MVI proteins is much more dynamic.

This type of dynamic nature is observed when neurosecretory cells are stimulated with KCl that leads to a large movement of MVI into the nucleus (Majewski *et al.,* 2018). This movement into the nucleus is associated with the increase of cellular transcription levels and so it is believed that this movement of MVI, is down to the cell requiring an increase in gene

expression. If nuclear export or import is blocked using leptomycin B and ivermectin respectively there is no movement of MVI.

These data suggest that an increase in MVI expression within the nucleus comes after stimulating the cell, and also that the MVI shuttles in and out of the nucleus. To fully understand other stimulations that may cause MVI nuclear localisation, DNA damage inducing drugs have been used in this study.

5.1.3 DNA damage inducing drugs.

This study has used two well characterised drugs, bleomycin and cisplatin, to understand the DSB response.

Cisplatin generates double stranded breaks indirectly through intra and interstrand cross linking, which leads to fork stalling during the DNA replication process of the cell cycle (Dasari and Tchounwou, 2014). It is a common cancer therapeutic used for the treatment of testicular, ovarian, lung, and cervical cancer; where it is directly given to a patient through injection into the bloodstream. It is a platinum-based drug covalently bonded to two NH_3 molecules and two Cl atoms. This bonding allows the platinum drug to preferentially bind to guanine bases, inter-chelating within the DNA helix, and then blocking the DNA helicase from unwinding DNA during replication. This inability to unwind can cause replicative stress which generates double stranded breaks within the DNA, that then must be repaired otherwise the cell enters apoptosis. Cisplatin not only induces double stranded breaks but also can induce the nucleotide excision repair pathways in around 3-5% of the cases where interstrand cross linking occurs (Dasari and Tchounwou, 2014). However, this study will focus on the main cause of damage through double strand breaks.

Bleomycin is another drug that has been used in this study. This is also a well-known cancer therapeutic used to treat Hodgkin and non-Hodgkin lymphomas, testicular and ovarian

cancers. It is a glycopeptide antibiotic that is produced by *Streptomyces verticillus*, which forcibly breaks double stranded DNA (Dorr, 1992). The bleomycins activity differs from that in cisplatin, where the main damage is caused during replication, here the damage can be caused at any time during the cell cycle. The damage mechanism starts with the molecule first inter-chelating within the DNA, separating the strands, it then, using oxygen and iron molecules, generates damaging free radicals that are able to break the double strand open. With a half-life of up to 21 hours this was deemed a suitable drug for this study. By using two drugs the responses observed would be dependent on the double stranded break of DNA, and not down to other side effects of that drug, also by using common cancer therapeutics it allows us to further study the effect of MVI nuclear localisation and cancer treatments together.

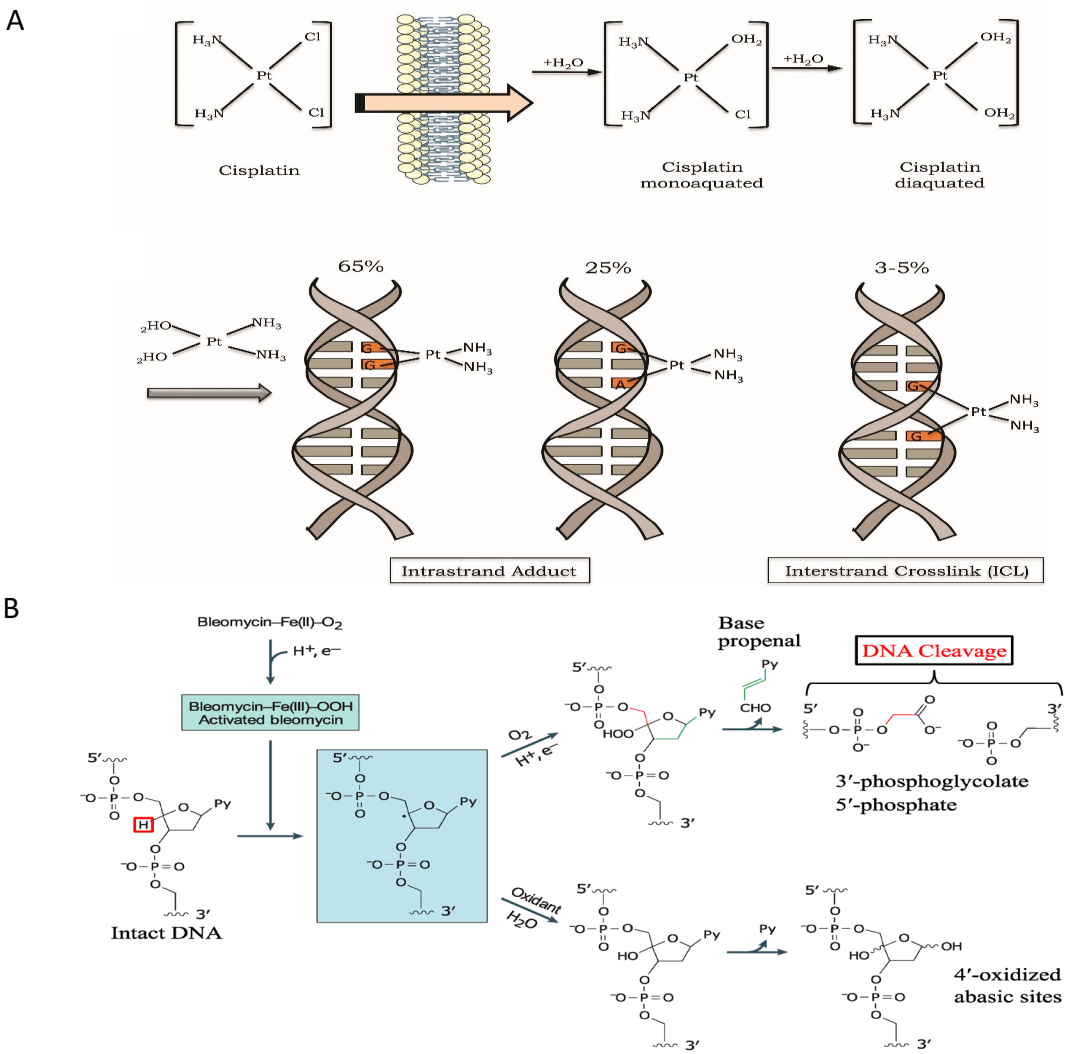


Figure 5.1. Mechanism of DNA damage drugs.

Cisplatin (A) is able to form intrastrand adducts as well as interstrand cross links. Bleomycin (B) creates reactive free radicals that lead to DNA cleavage. Taken from Rocha *et al.,* (2017) and Murray, Chen and Chong. (2018)

5.1.4 DNA damage and MVI.

So far little is known about the role of MVI in the DNA damage response, except for its ability to interact with the cell cycle inhibitor and tumour suppressor p53 (Jung *et al.,* 2006). It was originally thought that expression of MVI is increased after DNA damage and this increase in protein levels is dependent on a functional p53, if the cells do not have p53 then MVI expression remains constant. It was later found that p53 itself can be found bound to the

promotor region of the *MVI* gene (Chung *et al.,* 2006). Interestingly this study also identified the movement of MVI away from membrane ruffles and endocytic vesicles, towards the golgi apparatus and into the nucleus.

MVI has been reported to bind directly to p53, however the actual binding site has not been elucidated (Chung *et al.,* 2006). With the knocking down of MVI, p53 stabilisation is also reduced after DNA damage, which could be down to the fact that phosphorylation of p53 by the DNA damage response protein, ATM or that the golgi apparatus is not stable enough without the MVI thus leading to quick breakdown of p53.

All this work was carried out in RKO, LS174T, and H1299 cell lines, however further work has shown that this MVI expression increase due to DNA damage is cell line dependent and that MCF7 and LNCaP cell lines (a breast cancer and a prostate cancer cell line respectively) do not exhibit an increase of MVI expression after DNA damage and that after DNA damage there is in fact a repression of MVI levels (Cho and Chen, 2010). This repression however seems to be independent of p53 through another pathway. If MVI is knocked down in these cell lines, compared to those that have an increase of MVI expression levels, the cell lines become less responsive to DNA damaging drugs. This is important for therapeutic research as whilst in some cell lines MVI inhibition will cause great susceptibility to cancer therapeutics, in others, it will reduce the therapeutics efficacy.

For this reason, this study will use two different cell lines, HeLa and MCF10A cells. HeLa cells are cervical cancer immortal cell lines that contains, the viral protein E6 which suppresses p53 (DeFilippis *et al.,* 2013), and the viral protein E7 which causes DNA aneuploidy (Yaginuma et al., 2015) as well as centrosome duplication errors (Duensing and Münger, 2002) leading to chromosome instabilities. On the other hand, MCF10A cells are non-cancerous epithelial mammary gland cells that will serve as controls in this study with no mutations or defects in the DNA damage signalling and repair.

5.1.5 The first stages of the double strand break response.

To understand how else MVI might be involved in the DNA damage response, it is important to fully appreciate the complexity of the first stages of this response.

Immediately after the double strand break, if the cell is able to complete homologous recombination, the MRN complex binds to the break. This binding allows for the resection of the DNA from 5' to 3' (Paudyal *et al.,* 2017). This complex is made up of Mre11, which houses a single strand endonuclease component and the double strand specific 3' to 5' exonuclease, Rad50 that binds to the DNA and helps the two linear segments of DNA close together. As well as these subunits, NBS1, allows for the localisation of this complex, and contains a phosphorylation site for the ATM complex (H. Zhou *et al.,* 2017).

If, the cell is unable to perform homologous recombination due to no template being available, the cell then turns to using non-homologous end joining (NHEJ). Here the first to bind to the double stranded break are the Ku70/Ku80 proteins that bind to the ends of the DNA, blocking the MRN complex, until activation of the DNA dependent protein kinase (DNA-PKcs) which acts in a similar manner to that of the ATM kinase (Fragkos, Jurvansuu, and Beard, 2009). Where it is able to then phosphorylate and activate the downstream proteins required for signalling and repair.

During the scaffold complex formation, to directly repair the broken strands further, signalling cascades begin around the DSB. This signalling cascade all relies on the self-activation of the ATM kinase through automatic phosphorylation. This phosphorylation occurs when a dimer of ATM proteins releases and the ATMs become monomers where they auto-phosphorylate at the serine-1981 residue (S. So, Davis, and Chen, 2009). From here the ATM then phosphorylates the histone variant H2A at the serine-139 position (Burma *et al.,*

2001). This phosphorylation can then spread rapidly throughout the chromatin and at multiple points of damage providing a signal of a DSB throughout the nucleus.

Once ATM is activated, a complex and diverse pathway is activated that contains; BRCA1, a DNA damage repair and tumour suppressor protein, that can form the BRCA1 associated genome surveillance complex (Cortez *et al.,* 1999), p53, the tumour suppressor protein that controls cell cycle and apoptotic pathways (Saito *et al.,* 2002), tumour protein 53 binding protein 1 (TP53BP1), a protein that alongside BRCA1 decides which route the repair should take with the majority being NHEJ or HR (Iwabuchi *et al.,* 1998). Both the DNA-PKcs and ATM activate similar pathways in the response to DNA damage.

With the list of ATM activated proteins being so large, it becomes apparent that MVI may have some involvement amongst the cellular response. This study will only focus on the first stages of the DSB response and the signallers required rather than that of the whole ATM pathway.

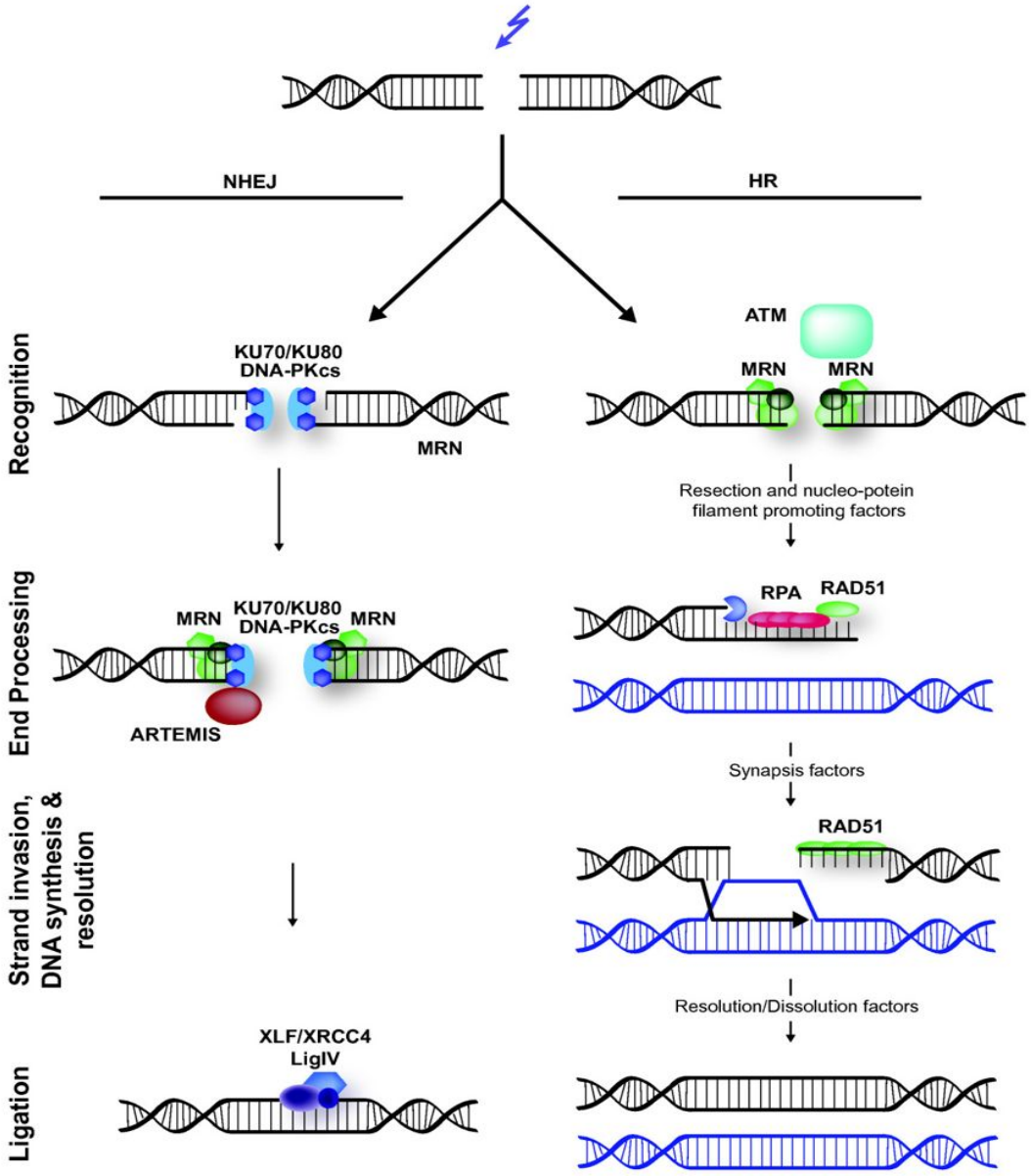


Figure 5.2. Double strand break response.

After DSBs have occurred the two most common repair pathways are the non-homologous end joining (NHEJ) and homologous recombination (HR). Taken from Lans, Martejn and Vermeulen, (2012).

5.1.6 High Content Screening (HCS).

Whilst confocal imaging provides a degree of information about localisation of proteins, due to the length of time that is required for each image and the processing alongside it, it is not suitable in providing statistical information using large sample sizes. Therefore, HCS is used to image and analyse hundreds of images in a short space of time. This method uses a low magnification of around 20X to 60X objectives, due to this low magnification multiple images of a sample can be taken rapidly providing images of thousands of cells in a short period of time using a microplate.

The images are then analysed with a defined region of interest, and within this region it is possible to measure the intensity of a fluorescent signal. By keeping the capture settings the same throughout, the relative intensities can be compared and thus provide information on the abundance of a protein within your region of interest. Whilst this technique relies on equal labelling of samples with primary and secondary antibodies, due to the large sample size any minor differences between labelling errors can be discounted.

This type of imaging provides evidence that what is seen within one cell, can be seen across the whole sample within a short timescale.

5.1.7 RNA-seq, the method to study transcriptomics.

As previously mentioned MVI has an involvement in successful transcription within cells. Fili *et al.,*(2017) showed that by inhibiting MVI there is a 75% decrease in total transcription, *in vitro*. With this information in mind it is important to understand that MVI may increase the expression levels of DNA damage proteins and thus responsible for the DSB response through its interactions with the RNAPII machinery. In this study to understand if this is the case, RNA-seq was employed.

RNA-seq is the method in which small mRNA transcripts are sequenced and can be aligned to identify the cells response to DSBs. This method begins with the purification of the total RNA transcripts from the cells either non-treated, or treated with cisplatin for 24 hours. Once the RNA is extracted and purified it is then checked for quality through gel electrophoresis to identify the 28S and 18S rRNA. Only high quality mRNA is selected and is used to create the cDNA library which is subjected to next generation sequencing. Once sequenced the genes can be aligned to the known human transcriptome using the *De Novo* approach and then quantitative expression and expression networks can be formed. This type of quantification allows the identification of the global effects of cisplatin treatment to cells, and the effect MVI KD has on this expression signature.

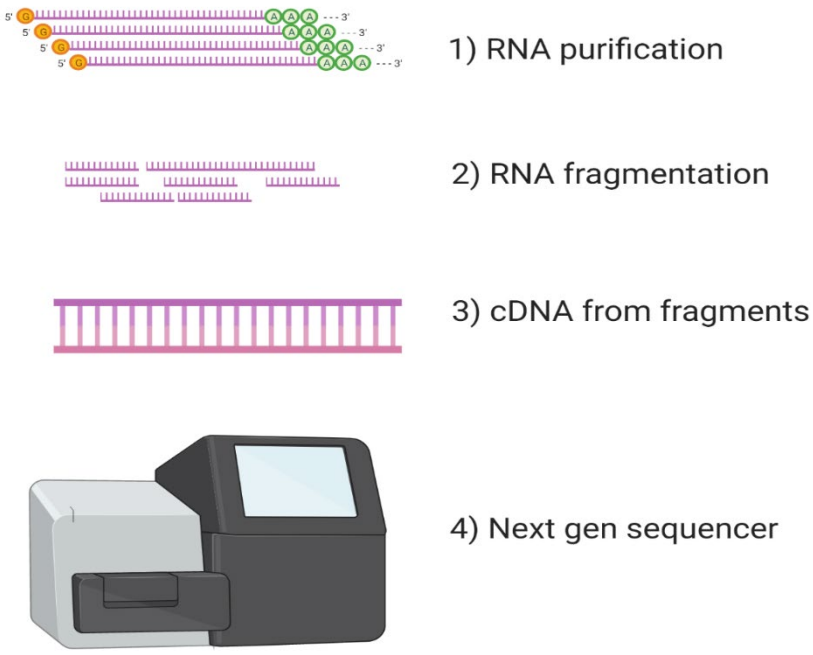


Figure 5.3. A cartoon to depict the RNA-seq procedure.

5.1.8 Liquid Chromatography – Mass spectrometry, the method to study proteomics.

To understand if there is a direct interaction between MVI and any of the DSB proteins either required for repairing the break or signalling a break, Liquid Chromatography-Mass spectrometry/Mass Spectrometry (LC-MS/MS) was used to identify precisely, a list of proteins MVI is interacting with before and after damage.

This method requires total protein isolation from the treated or untreated cells. Once isolated the proteins are then precipitated using immunoprecipitation (IP). Here protein A beads, which bind to the heavy chain within the Fc region, with high specificity to immunoglobulin G (IgG) antibodies (Skvaril, 1976), can be used to bind specifically the MVI antibody used in the study. These beads can be linked with the MVI antibody which then binds any MVI in the cell lysate which in turn also precipitates out any protein that directly or indirectly interacts with MVI. After IP the eluted proteins along with the MVI are purified using 2D gel electrophoresis. The proteins are digested using trypsin which is able to cut proteins at carboxyl end of the amino acids, lysine and arginine. Once digested the proteins are solubilised out of the gel and then maintained in a solvent. This solvent is then passed through a liquid chromatography column that separates these protein peptides depending on their affinity for the column. Once eluted the peptides pass through the electrospray vaporising them, allowing for ionisation of the peptides, which then collide with the mass spectrometer detector differently depending on their mass.

To provide higher sensitivity for assigning the correct peptides to the correct protein, another round of mass spectrometry can be performed. Here another ionisation step occurs on a collision photon surface, breaking the parent peptides further into multiple daughter ions. These daughter ions then travel through the mass spectrometer again and their weight

can be identified. Through this process each protein peptide can have its molecular weight detected and then assigned followed by another round of assignment of its daughter ions.

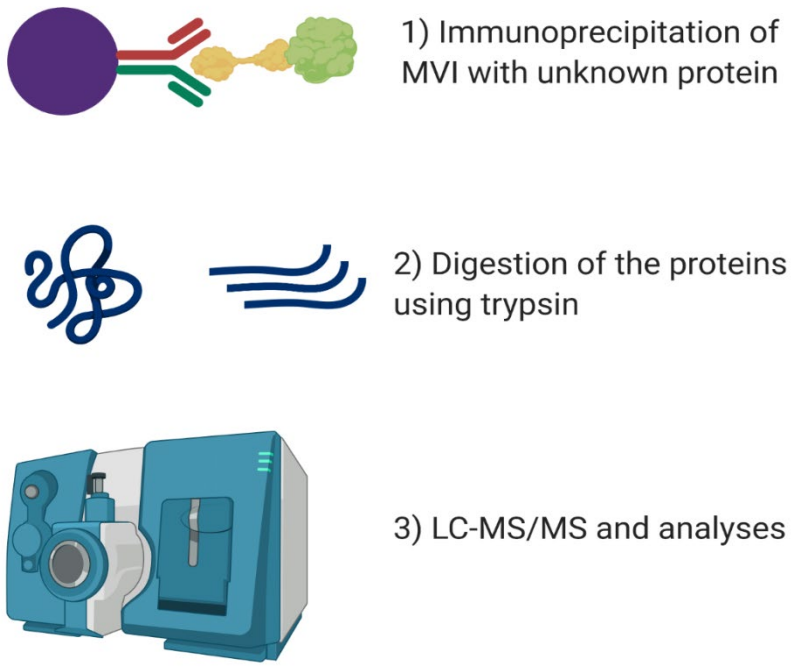


Figure 5.4. A cartoon to depict this studies proteomics procedure.

5.1.9 The aims of this study.

To fully appreciate how MVI might be involved in the DNA damage response in particular DSBs, it is important to investigate how the localisation of MVI changes after DNA damage; does the cell utilise MVI to produce mRNA transcripts relating to DNA damage proteins so that the cell can respond to the damage? And does MVI itself directly interact with any of the DSB signalling proteins or DSB repair proteins?

5.2 Results

By using a simple work flow of identifying where MVI is after DNA damage and then proceeding with transcriptomics and then proteomics, it is possible to identify potential roles it may play in the DNA damage response. This study has used both RNA-seq and LC-MS/MS proteomics procedures to unveil the potential roles, and also look at MVI signatures globally in response to the damage inducing drugs.

5.2.1 MVI levels in the nucleus change after DNA damage.

To understand how MVI changes after DNA damage, HeLa cells were treated with 25µM cisplatin for 24 hours or 4 hours of 0.5µM bleomycin. Immunofluorescence was then undertaken. It is common that MVI localisation is predominantly within the cytoplasm of untreated cells, where it resides around the golgi-apparatus as well as at the cell periphery (Figure 5.5). Using immunofluorescence it is possible to identify the nucleus through MVI staining due to the low amounts that are present. After treating the cells with cisplatin, the amount of MVI found within the nucleus increases. Here, it becomes difficult to distinguish the nucleus through the MVI staining. This increase of MVI in the nucleus coincides with the appearance of γ-H2AX, the histone modification that signals double stranded breaks, showing that the cisplatin treatment is causing direct damage to the DNA.

HCS has provided statistical data behind these images, where the intensity of MVI increases by 50% in the nuclei of HeLa cells and 27% in MCF10A cells. Within HeLa cells there is also a 27% increase of MVI around the external nuclear membrane but in MCF10A cells there is a decrease of 15% (Figure 5.5). This could be due to MVI translocating across the nuclear membrane into the nucleus of the cell in both cell lines. These data provide evidence that MVI has some response to DNA damage and that either the amounts of MVI increase with

DNA damage, or the cytoplasmic pool of MVI moves into the nucleus after damage. These images gave purpose into proceeding with the transcriptomics.

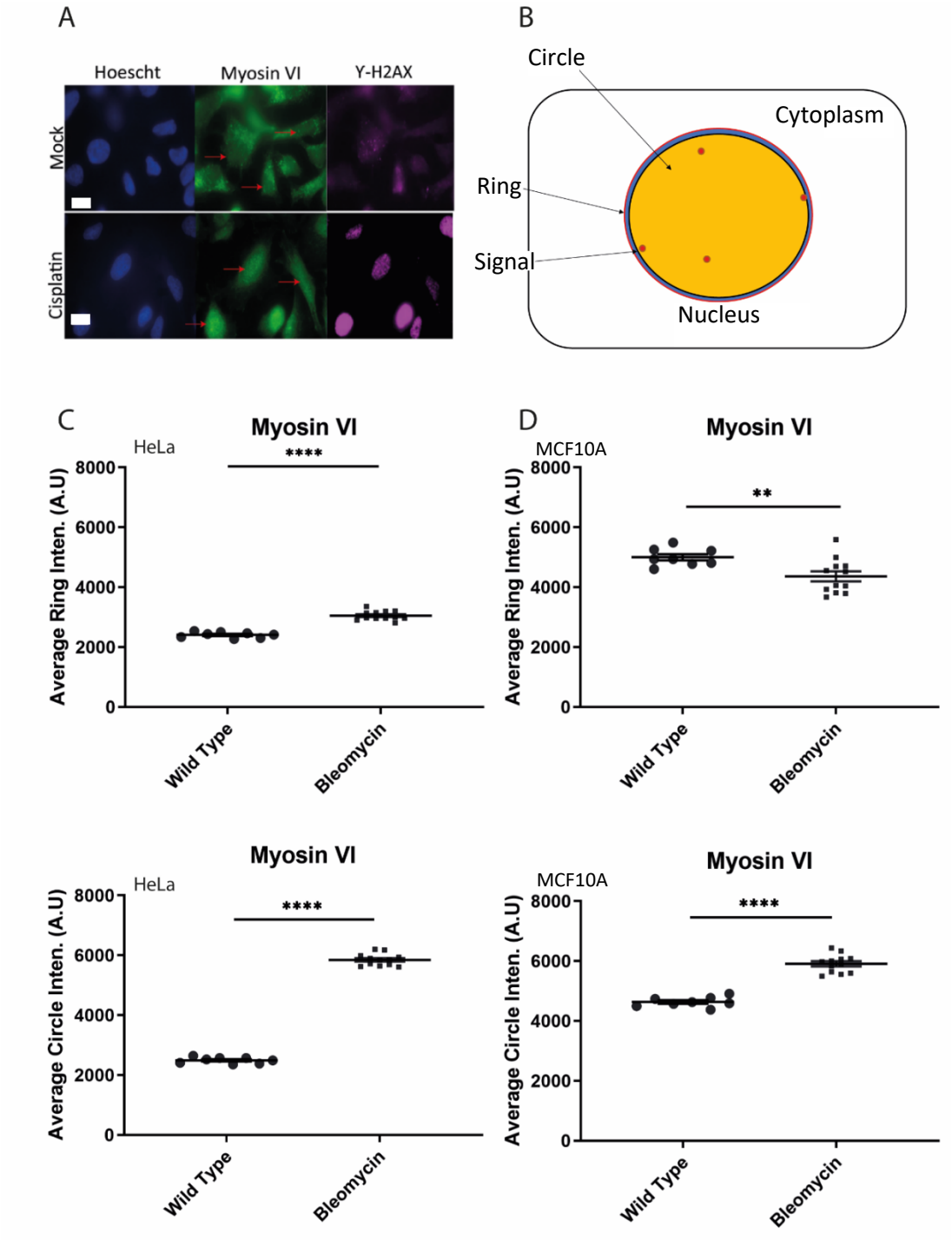


Figure 5.5. MVI moves into the nucleus after DNA damage.

Immunofluorescence (A) shows an increase of MVI within the nucleus after 24 hours of cisplatin treatment. Scale bar 10µM. HCS is able to analyse the images using two masks, the ring (nuclear external periphery) and the circle (the nucleus) (B). HCS of cells treated with bleomycin for 4 hours, shows an increase of MVI signal both at the nuclear periphery and inside the nucleus in HeLa (C). It also shows the decrease of MVI at the nuclear periphery and an increase of MVI in the nucleus in MCF10A cells. Significance was calculated using the students T test where ** $p<0.01$ and **** $p<0.0001$.

5.2.2 Lipofectamine and scrambled siRNA has an effect on the transcriptomics of a cell.

MVI has been shown to play a role in transcription, where it binds to DNA and has an interaction with NDP52 (Fili *et al.,* 2017). It has previously been shown that MVI binds to RNAPII during mRNA transcription and by introducing a stress such as DNA damage, one of the aims of this study was to investigate if MVI has a role in regulation of DNA damage genes. To ascertain if this is in fact the case, RNA-seq was used to identify if any DNA damage response genes are affected by the knock down of MVI.

RNA-seq was performed on RNA extracted from untreated cells, treated with scrambled siRNA, or MVI siRNA. After siRNA transfections using lipofectamine, the cells were grown in either MEM, or MEM with 25µM cisplatin for 24 hours. MVI transcription levels were first checked to ensure the MVI KD was successful (Figure 5.6). The MVI KD was successful, as the level of MVI mRNA was significantly reduced by three fold in both the MVI KD and the MVI KD treated with cisplatin, whilst all other conditions maintained the normal level of MVI transcript.

There was no increase of MVI expression in HeLa cells after DNA damage in both WT cells and those treated with a control siRNA. Therefore the increase of MVI inside the nucleus

after DNA damage is due to the movement of the cytoplasmic pool of MVI into the nucleus, and not due to an increase of total MVI inside the cell.

Principle component analysis (PCA) showed that out of the triplicates of conditions, the majority of them were clustered to each other, this shows that these samples can be carried forward for further analysis (Figure 5.6). A PCA plot, is a dimension reduction plot that allows the correlation of each sample to be plotted onto a single graph, where samples that contain similar gene expression are clustered together. PCA plots are also ranked, where the difference in the samples 1st principle component is of greater importance than the difference in 2nd principle components. One replicate for cells treated with scrambled siRNA and cisplatin was deemed as an outlier due to its large difference in principle component score, compared to the other replicates from that condition. This sample was then taken out of the dataset and was not analysed any further (Figure 5.6 C).

Interestingly cells treated with scrambled siRNA and cisplatin behaved different to wild type cells treated with cisplatin. This placed the transcriptomics of scrambled siRNA cisplatin treated cells significantly distant in terms of PCA score from the no siRNA cisplatin treated cells. Therefore the dataset was reduced so that only scrambled siRNA, and MVI siRNA treated cells with and without cisplatin were compared, and the wild type samples were removed, keeping the focus on the effect of MVI KD and cisplatin treatment to be studied, from here when discussing cells treated with scrambled siRNA, I will be referring to these as mock samples.

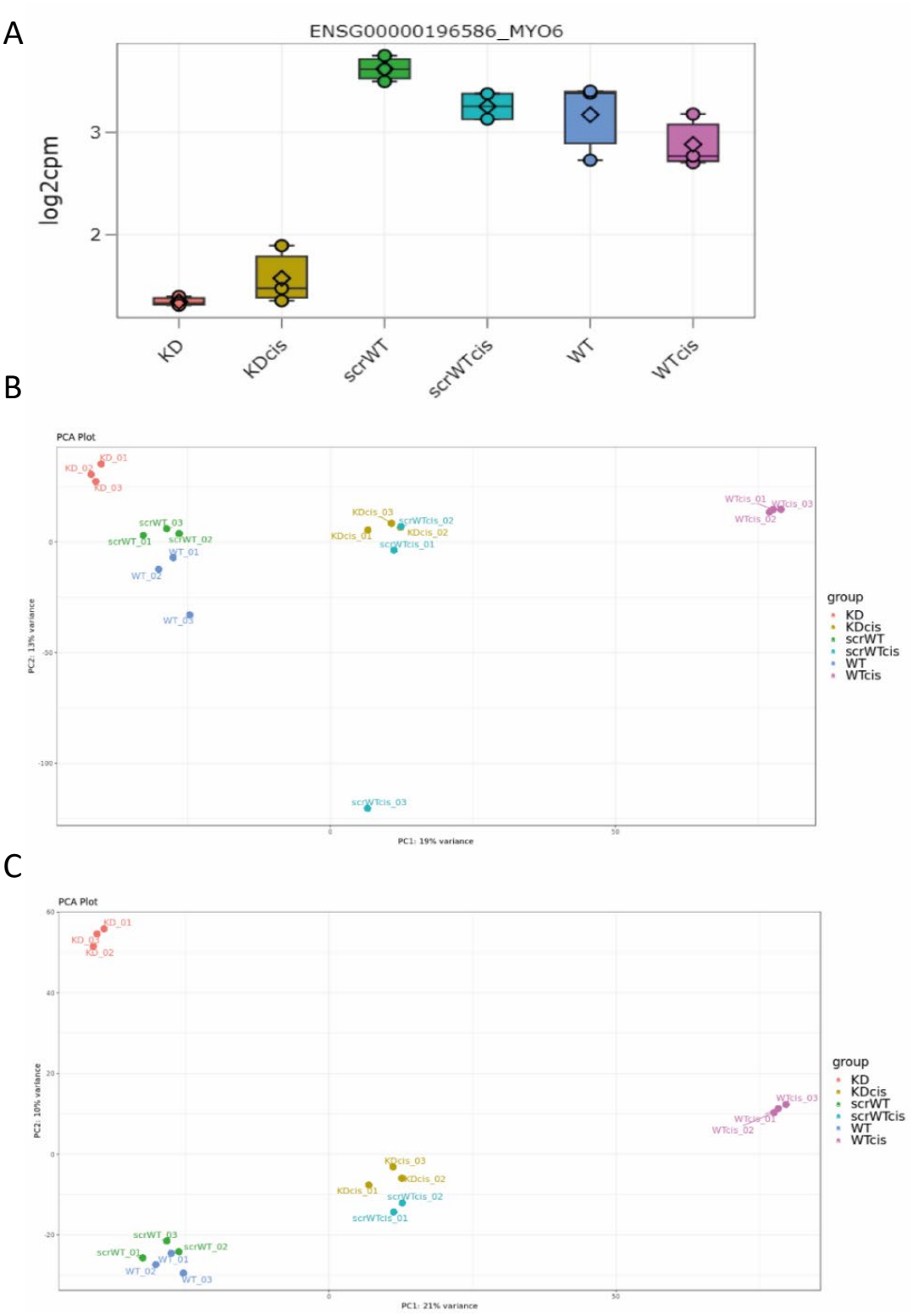


Figure 5.6. PCA analysis of the RNA-seq data.

MVI expression was first compared between all samples to ensure the KD had worked and to ensure DNA damage does not alter MVI gene expression (A). PCA analysis was then carried out between the samples (B) highlighting one sample to be an anomaly which was then removed from the data set (C).

5.2.3 Cisplatin treatment itself has the largest effect on gene regulation.

To fully appreciate the amount of genes that were affected from each condition, volcano plots have been used to represent the number of genes that were either upregulated or down regulated (Figure 5.7). After PCA analysis and the removal of the outliers, stringent statistical tests were applied to remove false discoveries as well as any gene changes that were not significant. In this study any gene that did not have a >1 log fold change (Fc) were removed as well as this, using the p adjusted value, provided any gene that did not have a p-value less than 0.05 were also removed.

Cisplatin treated mock HeLa cells generated a dataset with 4107 differentially expressed genes compared to the mock cells, which was one of the biggest effects throughout all of the conditions. After MVI KD only, there is also a global shift in transcriptomics where 1947 genes are affected by the KD. This large difference is expected due to the role of MVI in transcription and other cellular processes including binding to p53 which could alter the expression of p53 regulated genes (Jung *et al.,* 2006).

To understand how MVI KD affects the DNA damage response, cells with silenced MVI were treated with cisplatin and were then compared to the mock cisplatin condition in the RNA-seq analysis. This entailed plotting only genes that were expected to increase in transcription and instead were suppressed and vice versa. This allows the identification of genes that are specifically regulated by MVI during the DNA damage response. Here only 210 genes were transcriptionally different compared to that of mock cisplatin sample.

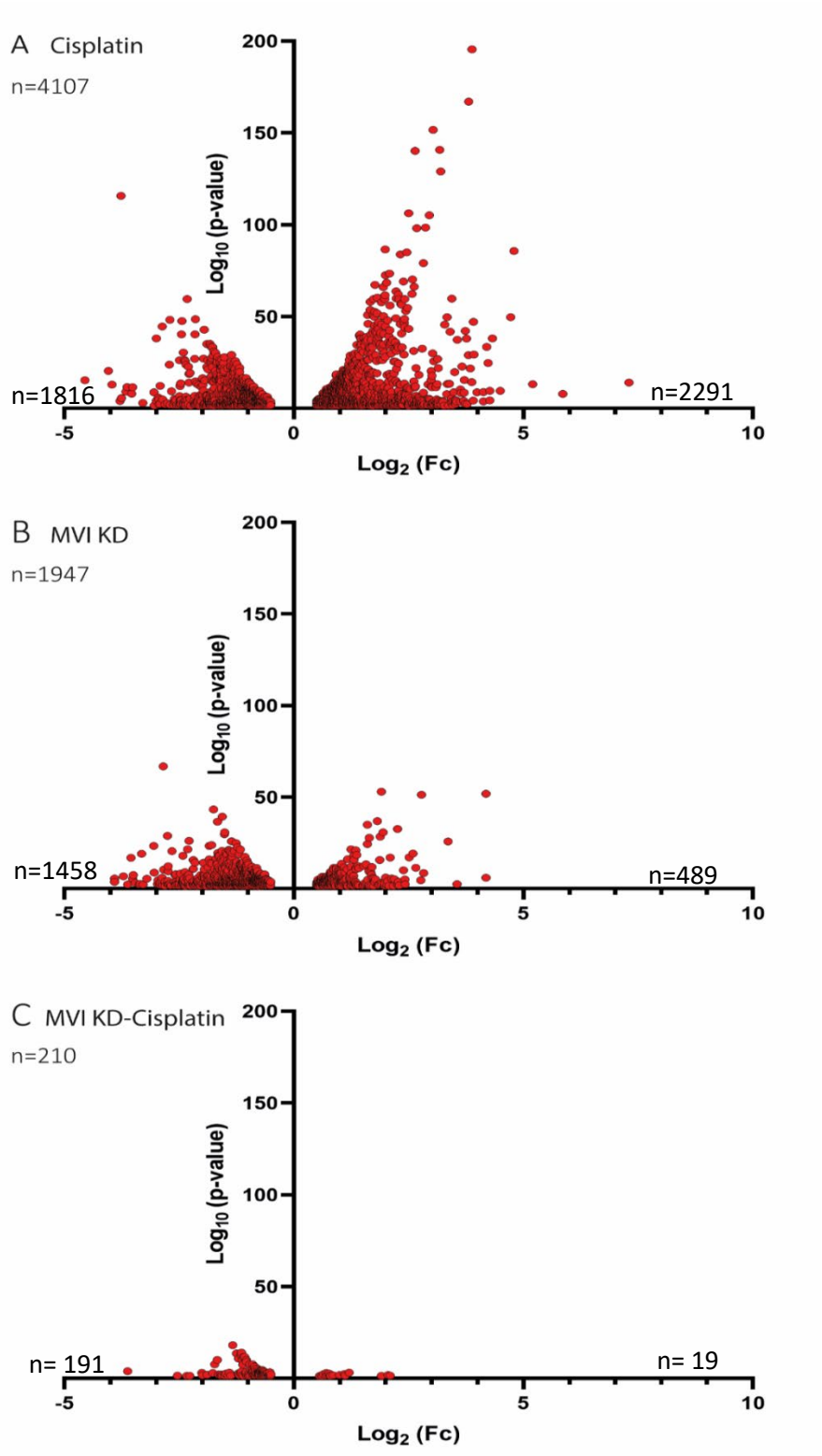


Figure 5.7. Volcano plots of upregulated and downregulated genes.

A total of the upregulated and downregulated are shown. 4107 genes were differentially expressed after cisplatin treatment (A) compared to only 1947 genes that are affected by MVI KD (B). RNA samples were then compared between the MVI KD cisplatin and cisplatin treated cells, with 210 genes having the opposite expression to cisplatin only treatment (C).

5.2.4 Cisplatin treatment alters a diverse set of genes.

To investigate how MVI may be responsible for the DNA damage response in terms of transcription it is important to first look at how cisplatin affects global gene expression. As discussed previously cisplatin treatment on mock cells alters 4107 genes. These genes can be assigned to different categories based on their molecules function, cellular localisation and various biological processes these might belong to. This classification was performed on statistically significant, differentially expressed genes from the above mentioned data set using Gene Ontology (GO) software, the results of which are represented in Figure 5.8.

Cisplatin treatment alters various biological processes as expected due to the toxicity and mode of action of the drug blocking cell replication, creating double stranded breaks and causing a large amount of stress on the cell. The processes that were affected the most by cisplatin treatment are - regulation of metabolic processes, regulation of signalling, intracellular signal transduction and cell development. These processes come as no surprise to be affected by the drug, as the cell requires a change of metabolic state so as to stall the cell development through the cell cycle, which it does by intracellular signalling. Interestingly the DNA damage biological process does not make up a significant number of genes affected by the cisplatin treatment, implying that the majority of the DNA damage response is on a protein level which then results in a change of cellular behaviour. This is also expected as a gene expression response takes far longer (Figure 5.8).

The cellular component of the genes with altered expression, are highly associated with non-membrane bound organelles of which can be ribosomes, the cytoskeleton and

chromosomes. As this GO term is relatively non-specific it is hard to identify which organelle these genes could be associated with, however it is clear that nuclear lumen associated genes are also highly affected, therefore the cell is likely responding to the damage through differential expression of genes relating to chromosomes and the nuclear envelope. This is expected with the formation of repair foci, rearrangement of chromosomes, and retention of nuclear integrity after DNA damage.

To specifically understand the expression changes from the RNA-seq data at protein level, GO molecular functions were explored. These terms highlighted how there is a major change in transcription related genes and signalling genes, such as the 423 genes found in the transcription regulatory activity and the 506 genes found in the enzyme binding function (Figure 5.9). These fit with expectations as the damage induced by cisplatin is so broad, a small localised response would not be suitable.

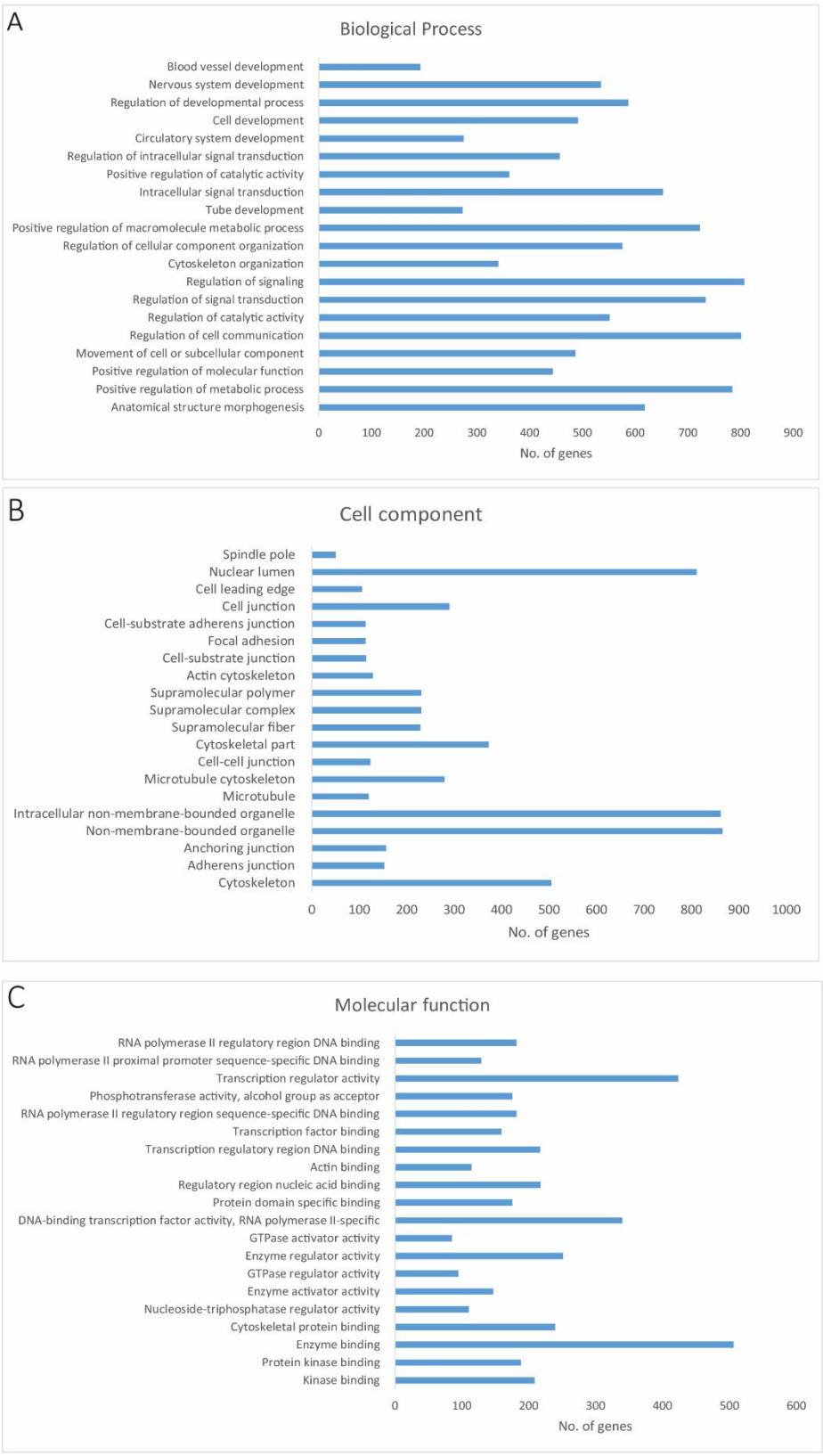


Figure 5.8. GO terms to distinguish gene expressions changed by DNA damage.

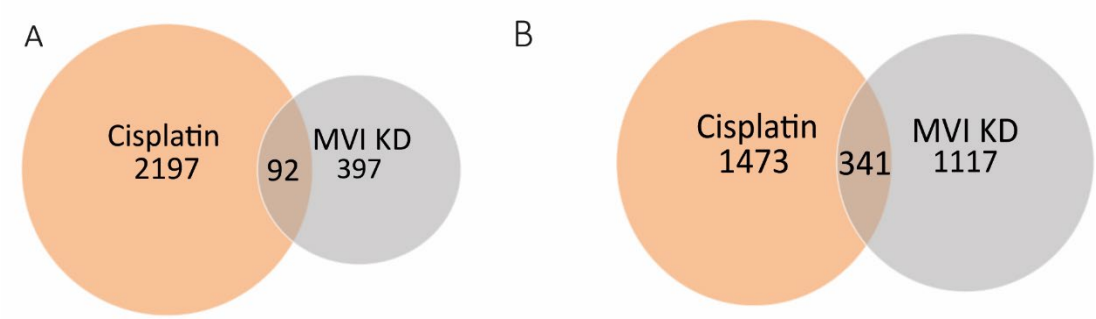
The biological processes (A), the cell component the proteins encoded by these genes (B) and the molecular function these proteins have (C) have all been plotted to show the array of genes affected by DNA damage.

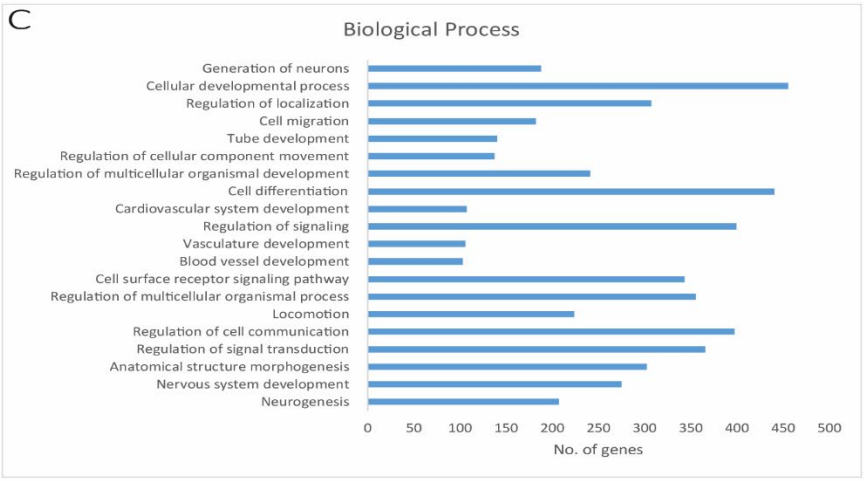
5.2.5 MVI KD effects the transcriptome differently to cisplatin treatment.

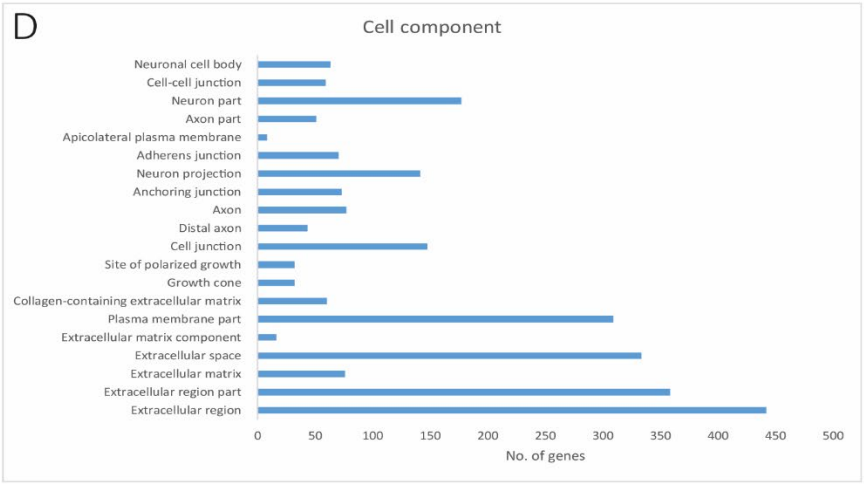
To explore if MVI KD with cisplatin treatment regulated similar cellular processes, differentially expressed genes that overlapped in both datasets were identified, that were upregulated (Figure 5.9 A) and down regulated (Figure 5.9 B). Only 92 genes were upregulated and 341 genes were downregulated in both MVI KD treatment and cisplatin treatment as compared to 397 genes upregulated and 1117 genes downregulated that were unique to the MVI KD. This shows that potentially MVI itself plays in gene regulation, due to the large number of genes that become downregulated after KD.

The difference in genes can be shown by the difference in GO biological processes (Figure 5.9 D), where the most affected are the developmental processes within the cell and its ability to differentiate, as well as cell communication. Regarding how the cell communicates with its exterior environment as well as with the extra-cellular matrix. The GO cell components also differ, where previously the cisplatin damage perturbed expression of genes relating to non-membrane bound organelles, the MVI KD affects genes regarding the extracellular region and the plasma membrane (Figure 5.9 E). This links with MVIs role in endocytosis regarding receptors on the cell surface. The most significant of GO molecular functions, that are affected, are genes responsible for producing proteins related to anion binding such as those that bind cyclic AMP, fatty acids, heparin and ATP binding (Figure 5.9 F). These could be regarding signalling proteins and spread across a large variety of cellular pathways.

It is important to note that the MVI KD does not majorly affect the DNA damage pathways, such as double strand break pathways or the p53 pathways. The cell cycle pathway is also not one of the major pathway identified to be altered either.


A
Cisplatin
2197
92
MVI KD
397
B
Cisplatin
1473
341
MVI KD
1117


C
Biological Process
Generation of neurons
Cellular developmental process
Regulation of localization
Cell migration
Tube development
Regulation of cellular component movement
Regulation of multicellular organismal development
Cell differentiation
Cardiovascular system development
Regulation of signaling
Vasculature development
Blood vessel development
Cell surface receptor signaling pathway
Regulation of multicellular organismal process
Locomotion
Regulation of cell communication
Regulation of signal transduction
Anatomical structure morphogenesis
Nervous system development
Neurogenesis
0 50 100 150 200 250 300 350 400 450 500
No. of genes


D
Cell component
Neuronal cell body
Cell-cell junction
Neuron part
Axon part
Apicolateral plasma membrane
Adherens junction
Neuron projection
Anchoring junction
Axon
Distal axon
Cell junction
Site of polarized growth
Growth cone
Collagen-containing extracellular matrix
Plasma membrane part
Extracellular matrix component
Extracellular space
Extracellular matrix
Extracellular region part
Extracellular region
0 50 100 150 200 250 300 350 400 450 500
No. of genes

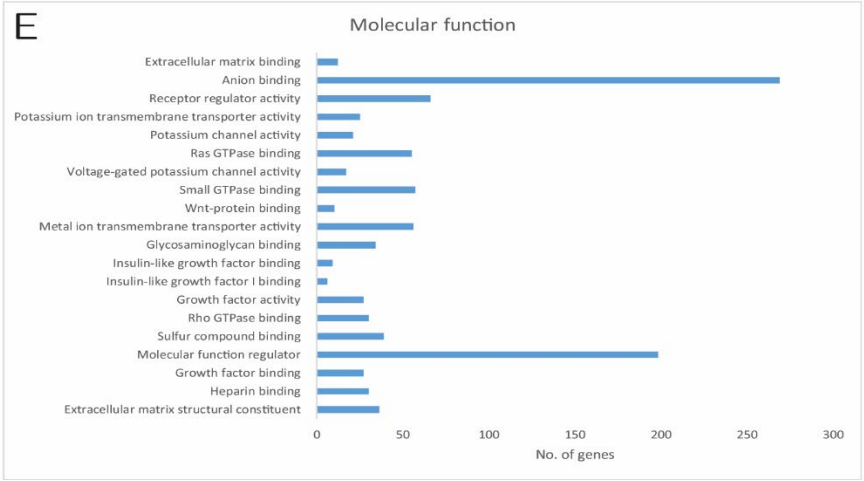

E
Molecular function
Extracellular matrix binding
Anion binding
Receptor regulator activity
Potassium ion transmembrane transporter activity
Potassium channel activity
Ras GTPase binding
Voltage-gated potassium channel activity
Small GTPase binding
Wnt-protein binding
Metal ion transmembrane transporter activity
Glycosaminoglycan binding
Insulin-like growth factor binding
Insulin-like growth factor I binding
Growth factor activity
Rho GTPase binding
Sulfur compound binding
Molecular function regulator
Growth factor binding
Heparin binding
Extracellular matrix structural constituent
0 50 100 150 200 250 300
No. of genes

Figure 5.9. Gene expression changes caused by MVI KD.

The genes upregulated during cisplatin treatment and genes upregulated during MVI KD were compared (A), where there were only 92 genes that were both upregulated in both conditions compared to 2197 unique genes due to cisplatin treatment and 397 due to MVI KD. The genes downregulated due to cisplatin and MVI KD we compared (B) where there were 341 genes that were repressed in both conditions and 1473 unique to cisplatin treatment and 1117 unique to the MVI KD. The biological processes (C), the cell component the proteins encoded by these genes (D) and the molecular function these proteins have (E) have all been plotted to show the array of genes affected by MVI KD.

5.2.6 MVI KD with cisplatin treated cells behaves similar to that of cisplatin only treated cells.

The MVI KD did not affect the genes that respond to cisplatin treatment. This study investigated if, after MVI KD and cisplatin treatment, the genes that are expected to be repressed, are still repressed, and those upregulated, are still upregulated, after cisplatin treatment only. As previously shown, only 210 genes fit into this category of opposite expression, to identify what role these handful of genes play within the cell a similar GO term comparison was carried out.

When these differentially expressed genes are grouped by their GO biological processes there is a range of processes that are affected mainly linked to stimuli (139 genes) and cell proliferation (49 genes) (Figure 5.10 A). This highlights that those genes that should respond to cisplatin and are no longer doing so due to the MVI KD are not significantly grouped under the DNA damage response.

As the stimulus process is the most affected, it is not surprising that once again the cell component GO term that contains the most genes in the sample are linked to the extracellular regions, 194 genes (Figure 5.10 B). This is also shown by the most number of

genes being grouped under receptor activity or regulation, a total of 31 genes (Figure 5.10 C).

These data show that both the MVI KD and the MVI KD with cisplatin treatment does not greatly effect a single biological process but a variation and that there is no majority of genes linked to the DNA damage response and repair pathways. This type of analyses is important, as it gives a broad overview to a large set of transcriptomics, it is however still vital that the specific pathways are looked into further detail to ensure that the MVI KD cells and the MVI KD cells treated with cisplatin do not have expression irregularities of the first responders of DNA damage, which would leave downstream DNA damage genes unaffected.

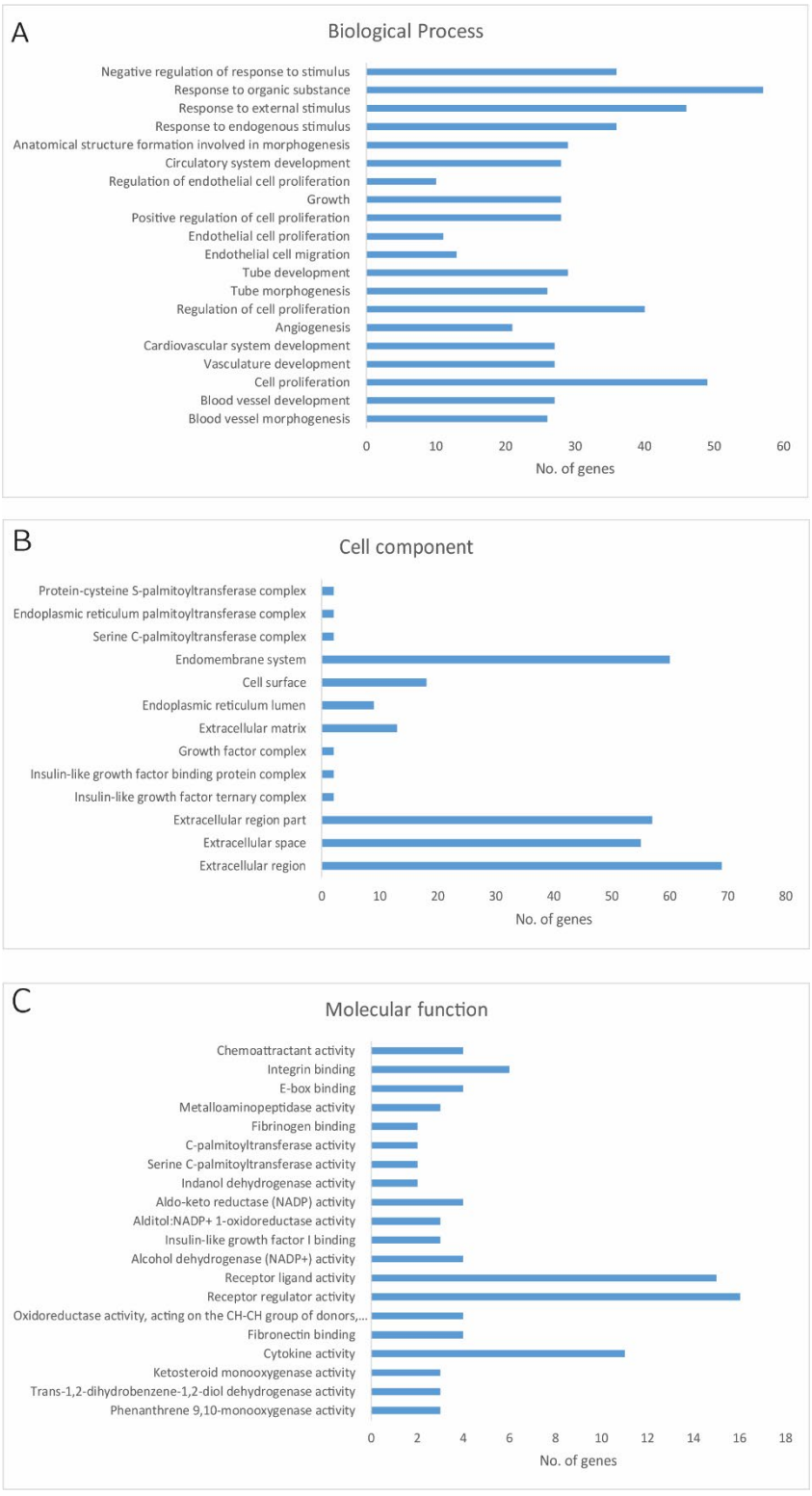


Figure 5.10. GO terms to distinguish gene expressions caused by MVI KD with cisplatin treatment.

The biological processes (A), the cell component the proteins encoded by these genes (B) and the molecular function these proteins have (C) have all been plotted to show the array of genes that behaved the opposite of cisplatin treatment due to the MVI KD.

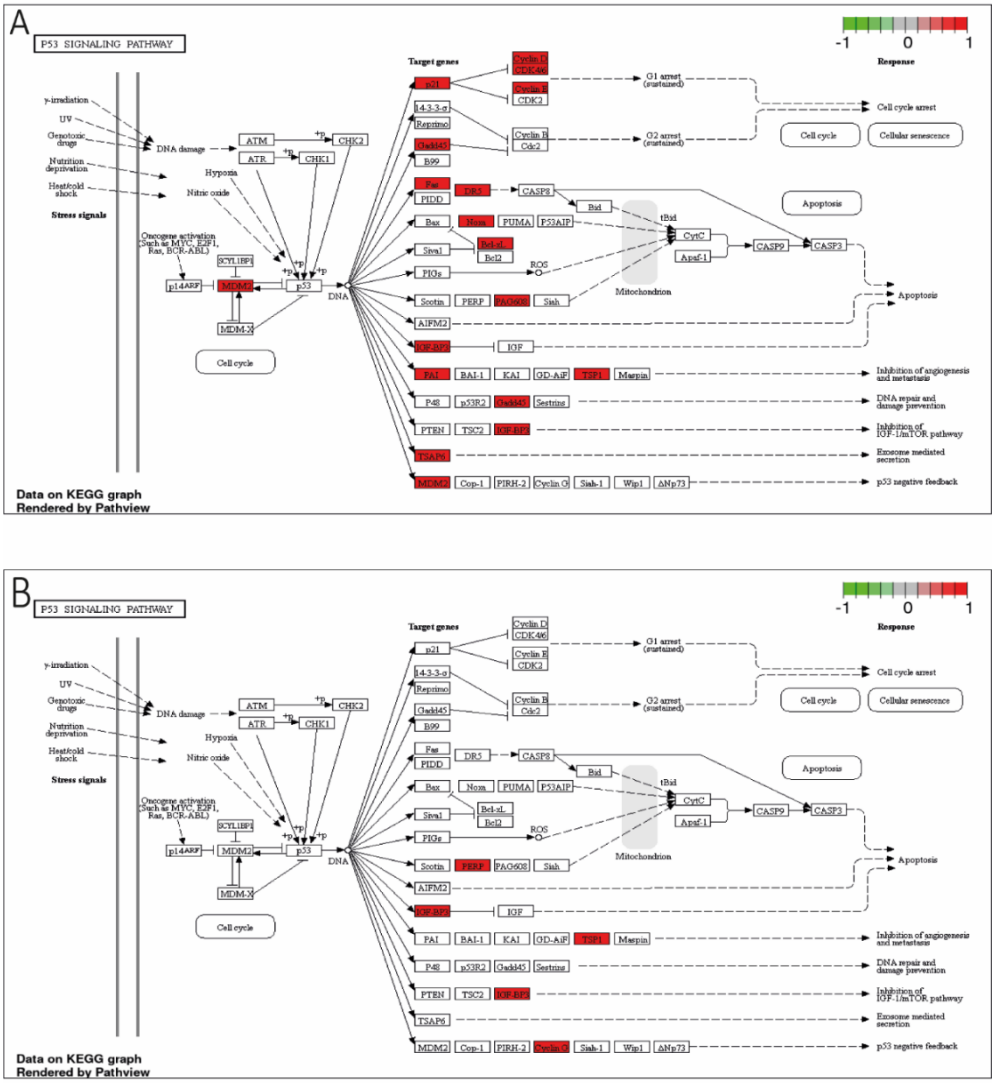
5.2.7 MVI KD with cisplatin treatment does not affect expression of genes required for the DNA damage response.

To further investigate the direct role of MVI in the DNA damage response, the genes that were upregulated due to cisplatin, were plotted onto the KEGG p53 pathway (Figure 5.11 A). Here a total of 17 genes within this pathway are upregulated after treatment with cisplatin. This list includes p21, the cell cycle inhibitor and one of the most activated proteins after DNA damage (Cazzalini *et al.,* 2010) , FAS, the cell surface death receptor that leads to apoptosis of the cell (Waring and Müllbacher, 1999) and GADD45, found in the DNA damage repair pathway (Gartel *et al.,* 2001). It is likely these genes are upregulated so the cell can respond to the multiple DSBs and stress caused by the cisplatin, allowing the cell to globally adapt to the damage, and attempt to repair the damage or proceed into apoptosis. The upregulation of these genes provide a template in which we can analyse those that have had their expression changed, due to the MVI KD after cisplatin treatment.

When the same KEGG p53 pathway is analysed with the genes that have had their expression profile altered by the MVI KD with cisplatin treatment, only 5 out of the 17 (Figure 5.11 B) were found to be differentially expressed. These include cyclin G which provide a negative feedback for the expression of p53 which in turn allows the progression of the cell cycle (Ohtsuka *et al.,* 2004) IGFBP3, the insulin-like growth factor binding protein 3 which can lead to apoptosis (Shim *et al.,* 2004), and finally thrombospondin 1 (TSP1), a protein which leads to the inhibition of metastasis and angiogenesis after DNA damage (Lawler, 2002).

It is clear that the majority of genes required for the cisplatin response are still expressed at the levels they should be, and that the MVI KD does not affect the DNA damage response at a transcriptional level as the 5 genes that are affected do not directly influence the first stages of the DNA damage response. This has also been proven through the use of classifying

these genes using GO terms that also provide the evidence that MVI has no role transcriptionally in the DNA damage response.



C

Condition	Up-regulated	Down-regulated
Cisplatin	17	0
MVI KD	0	0
MVI KD with cisplatin	0	5

Figure 5.11. P53 KEGG pathways of the RNA-seq data.

The upregulated genes within the p53 pathway caused by DNA damage show multiple genes being affected (A). After MVI KD and DNA damage those genes that behaved differently to the normal DNA damage expression profile were plotted onto the same pathway (B). This lead to a change of expression after MVI KD of only 5 genes (C).

5.2.8 The MVI interactome before treatment, is cell line independent.

To further understand how MVI reacts to DNA damage within the cell, a proteomics study was established. This study was designed to include two different cell lines, cancerous and non-cancerous. It is well known that the cervical cancer immortal cell line HeLa has a perturbed p53 pathway due to degradation of p53 by E6 (Hoppe-Seyler and Butz, 1993). Whilst this degradation allows for the quick and easy growth within laboratory conditions, it does make studying the DNA damage response and p53 pathways difficult to undertake without knowing if the pathway is behaving similar to that of other cell lines. To ensure that the MVI response to DNA damage is conserved and consistent throughout cell lines another cell line was also used, the non-cancerous epithelial breast cell, MCF10A. This cell line acts as a control where, unless mutated within laboratory conditions, the DNA damage response remains unchanged and fully functional.

During this study the proteomics data was analysed using common cut offs that have been previously published (Sennels, Bukowski-Wills, and Rappsilber, 2009). The data shown here required protein identification, to contain at least one unique peptide to reduce the false discovery rate as well as a minimum two-fold increase of protein discovered compared to that of the nonspecific binding of protein to immunoprecipitation beads without antibody. It was also required that the ANOVA p value between antibody covered beads and naked beads was at least significant to 0.05. All conditions were completed in triplicates.

It is clear that the MVI interactome is almost identical between the two cell lines when untreated, described here as WT cells (Figure 5.12 A). The WT cell lines share 362 protein interactions identified, these mainly consisted of proteins that, defined by GO terms, are found in both the cytoplasm and nucleus (Figure 5.12 B), as expected, and play a role in cell growth and maintenance (Figure 5.12 B). When the cells are not treated with any DNA damaging agent, only a small percentage ~2% of proteins were found to be interacting with

MVI that are classified to be involved in the DNA repair pathway. These 2% of proteins are also found only in the HeLa and not the MCF10A cell line, this could be due to HeLa experiencing replicative stress and thus having a small background of DNA damage compared to that of the MCF10A cell lines that have a stable genome.

5.2.9 The MVI interactome after cisplatin treatment is cell line dependent.

In WT conditions, the MVI in both cell lines interact with similar proteins, consisting of cellular maintenance and growth. After cisplatin treatment, the similarity between the cell lines dissipates and the MVI interactions completely differ. When HeLa cells are treated with 25µM of cisplatin for 24 hours, MVI changes its interactions completely, where 431 proteins can be identified that were not observed in the WT HeLa cells figure (Figure 5.12 A).

This type of global change of MVI interactions can also be seen with the MCF10A cell line. Here only 17 MVI interactions remain the same in our proteomics sample and 253 protein interactions are unique to the cisplatin treatment (Figure 5.12 A). Only 89 proteins are actually shared for the cells to respond to cisplatin treatment in both HeLa and MCF10s. This shows that whilst the MVI is responding to DNA damage, each cell line utilises MVI in a different manner, as only a small percentage of total protein interactions, be seen in both cell lines compared to that of the WT, where nearly all interactions are conserved.

In this study both cell lines have an increase of MVI interactions with proteins involved in the DNA damage response pathways, and, as classified by GO terms, cisplatin treated cells, are the only cells that have MVI protein connections within the p53 dependent and independent damage checkpoints, as well as DNA repair, including both double strand break repair and nucleotide excision repair (Figure 5.12).

After cisplatin treatment using GO terms, the molecular functions become more associated with DNA binding proteins than those without treatment. This is interesting as it is already

characterised that MVI plays a role in transcription, however as shown previously MVI has no role in transcription of DNA damage genes, and so at protein-protein level MVI is interacting not just with RNAPII but also other proteins that are capable of binding DNA that do not have a role in transcription.

By linking the images shown previously with the change of MVI within the nucleus, the fact that my RNA-seq data shows MVI silencing does not interfere with the correct transcriptional response to DNA damage, the proteomics data shown here shows that this change of MVI after DNA damage is down to the protein-protein interactions, and that MVI responds to DNA damage by altering its binding partners.

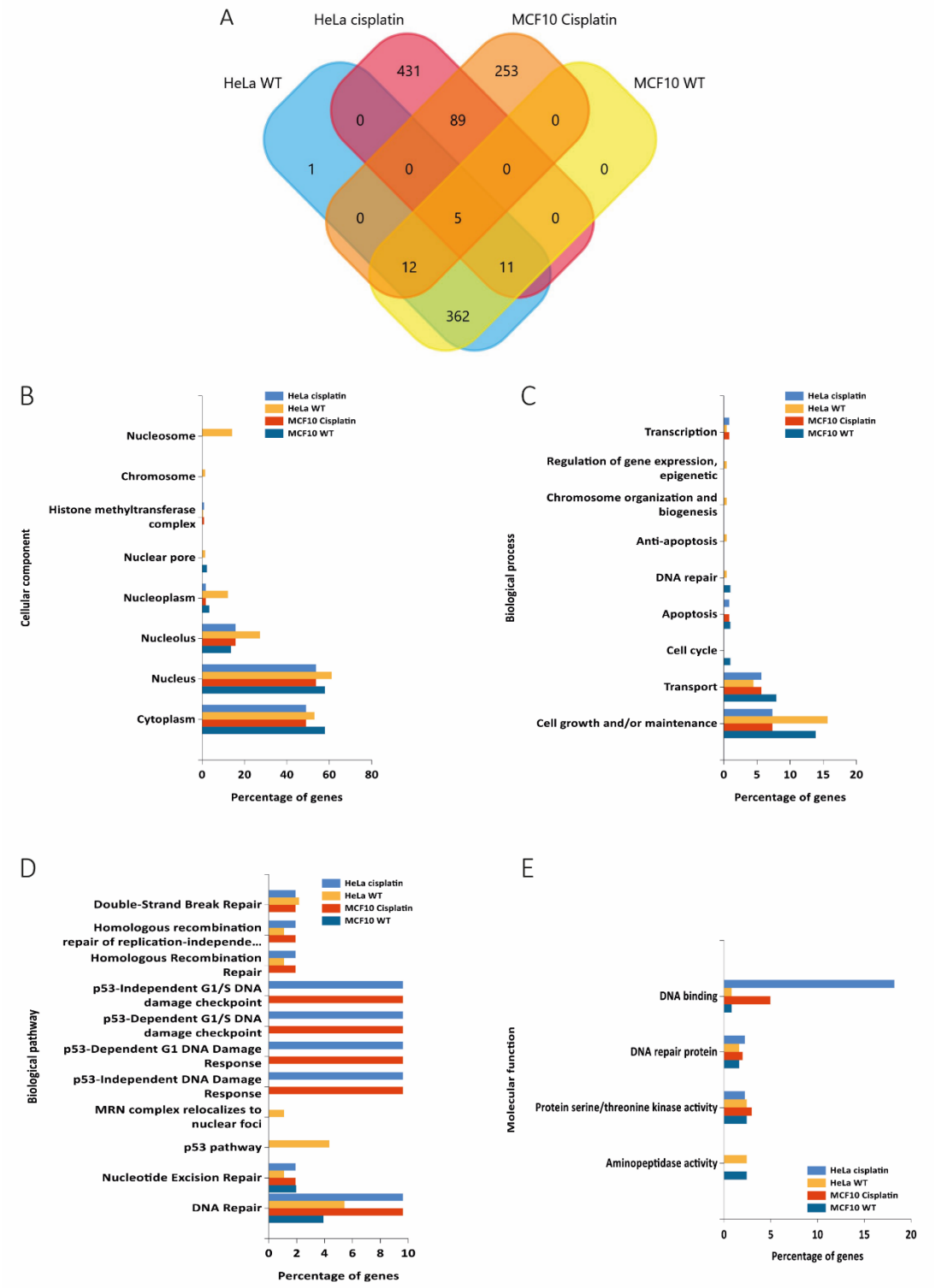


Figure 5.12. A comparison of proteomics between healthy and damaged cell lines.

A venn diagram to show the similarity of MVI interactions between WT cell lines and the difference in MVI interactions after DNA damage between cell lines (A). The MVI binding partners were then specifically defined by GO terms, identifying the cellular component (A), the biological processes (B), the biological pathways (D) and the molecular function (E) these proteins have, specifically identifying how they change after DNA damage.

5.2.10 HeLa MVI interacts with a multitude of DNA damage repair proteins.

To specifically understand how MVI interactions differ after DNA damage, using the KEGG DNA damage pathway, mapped onto the proteomics data, specific proteins required for the DNA damage response can be annotated.

To begin with, the changes within HeLa cells were annotated, all proteins interactions are visible and those marked red are part of the DNA damage pathway (Figure 5.13). Interestingly from the proteomics data set there a very few connections between the proteins and many are independent of each other. Under the GO process of DNA damage response within the untreated cells the majority of MVI interactions consist of four ubiquitinating proteins; RPL40, Ubiquitin-40S ribosomal protein S27a, Polyubiquitin-C and Ubiquitin B. These ubiquitinating proteins are responsible for marking proteins for degradation and so whilst they are required for the DNA damage response, they do not play an immediate role in signalling DSBs (Figure 5.13).

One protein can be found to interact with MVI in untreated cells that is identified not only in the DNA damage response pathway (Figure 5.13) but specifically the DSB response, is the catalytic subunit of DNA polymerase δ. This is an interesting observation as we know MVI interacts with RNA polymerase, but there are currently no reports of MVI and its binding to DNA polymerases. This polymerase is required for DNA replication and repair due to its ability to synthesise DNA from both the leading and lagging strand (Liu and Warbrick, 2006).

After cisplatin treatment the MVI-protein interactions that can be found within the DNA damage repair pathway and specifically the DSB repair pathway differ from untreated cells. Within the DNA damage pathway a total of five proteins are found in Table 5.3. Two of these proteins, ERCC6 and APEX1, are directly responsible for the nucleotide excision repair (NER) mechanism which is required when DNA inter-chelating agents bind to DNA, such as cisplatin. The two proteins used in NER found here are, DNA lyase, which is responsible for

the excision of inter-chelated nucleotides (Mol, Hosfield, and Tainer, 2000), and ERCC6, which wraps DNA around itself to modify the interaction between RNAPII and the DNA allowing NER to take place (Beerens *et al.,* 2005).

Another protein on the list is FANC1, which is involved in the DNA damage response but not the DSB pathway. This protein is a ubiquitinated protein that can be found localised to BRCA-1 DNA damage sites, as well as BRCA-1 repair foci, where multiple DNA lesions are able to repaired within a small distance of one another (Castella *et al.,* 2015). This allows cells to repair DNA damage simultaneously and as fast as possible to reduce the likelihood of tumour enhancing mutations.

Finally two MVI interacting proteins are found directly at the point of a double strand break (Figure 5.14). Rad50 and XRCC5 (Ku80). As previously discussed Rad50 is a major part of the MRN complex, which binds to the DSBs and initiates homologous recombination repair. Remarkably Ku80 also interacts with MVI, this protein initiates the non-homologous end joining, the error prone repair mechanism for DSBs. The Ku80 forms a complex with Ku70 that binds directly to the ends of DSBs and provides a scaffold for repair.

This specifically shows that after DNA damage induction in HeLa cells, MVI rapidly switches binding partners and is involved in three different repair mechanisms, nucleotide excision repair, NHEJ and HR, all of which are required when using the cancer therapeutic cisplatin.

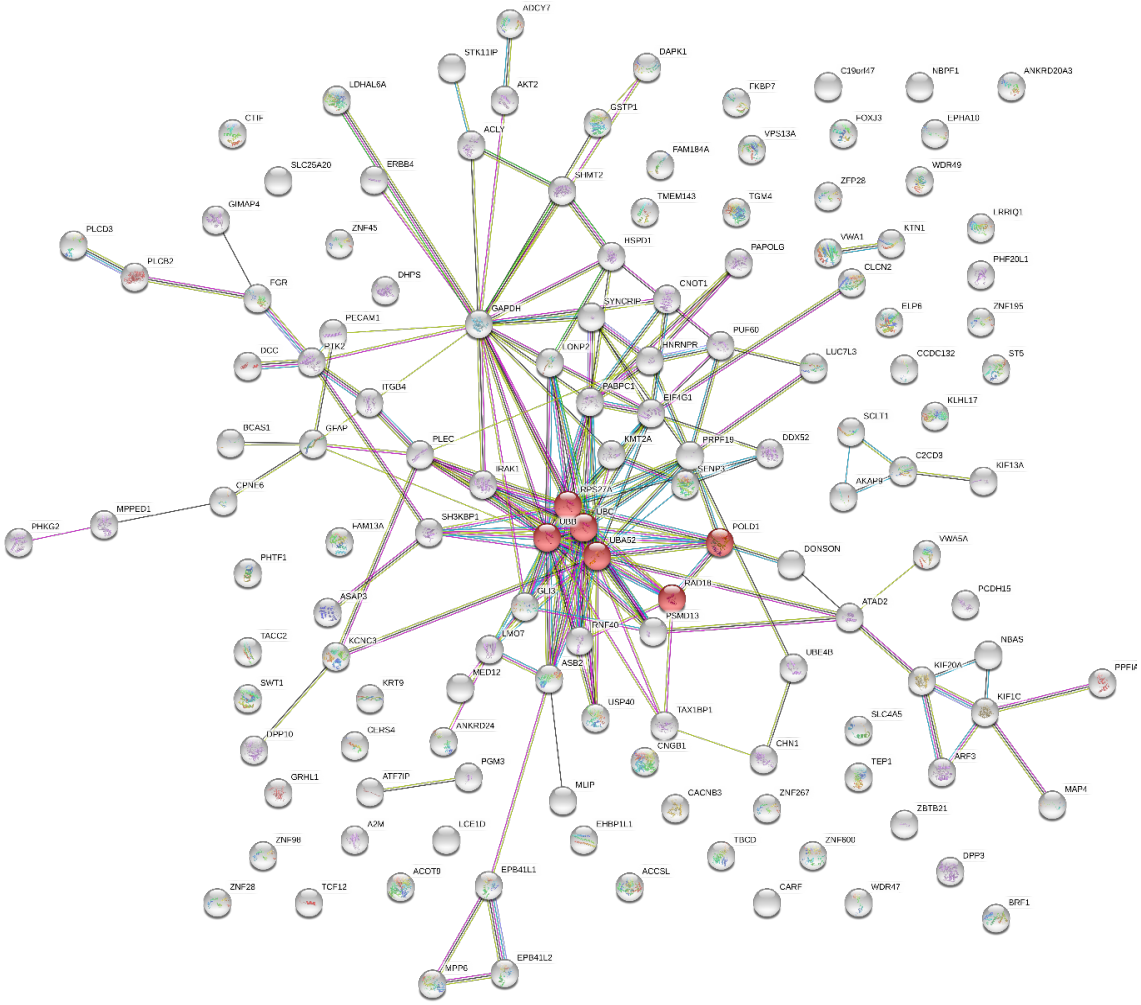


Figure 5.13. Protein network map of MVI interactions in WT HeLa.

Using the analysis software STRING. Proteins that are in the DNA damage response are highlighted red.

5.2.11 Cisplatin causes MVI to interact with chromatin remodelling complexes.

Whilst MVI clearly interacts with proteins within the first stage of DNA damage, this proteomics study has also identified two other proteins of interest MVI binds to by mapping out the DNA damage pathway (Figure 5.14), these two proteins are BRG1 and the CREB binding protein. These two proteins have roles within chromatin remodelling and histone modifications. Specifically, BRG1 is a component of the SW1/SNF chromatin remodelling complex. This complex is able to manipulate chromatin so as to signal DNA damage or alter the transcription state of the genes within the chromosome. CREB binding protein also plays a role in transcriptional regulation, where it acetylates histones for transcriptional activation. MVI chromatin interactions is a field that has not been studied, these interactions open up an interesting avenue of how MVI may affect chromosome regulation, specifically after DNA damage.

MVI also binds to multiple histones after DNA damage. It has been identified here that MVI binds to the histone linker, H1, as well as H2 and H4 (Figure 5.14). It is not clear if there is a direct link between H2AX however, these data shows that MVI can not only bind to histone modifiers but can also bind to histones themselves, this places them at the site of chromosome organisation and potentially chromosome movement which will be discussed in Chapter 6 and Chapter 7.

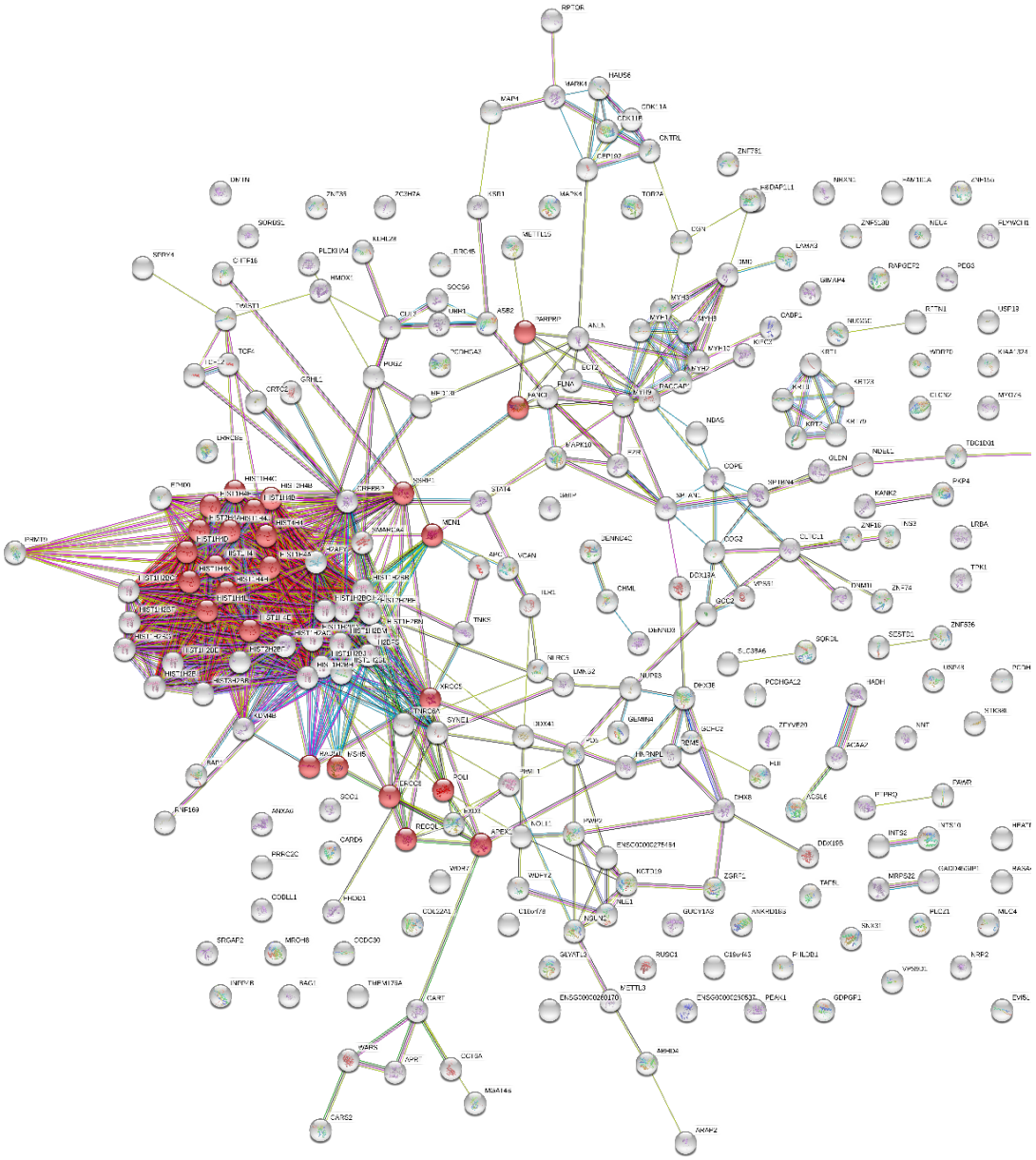


Figure 5.14. Protein network map of MVI interactions in HeLa cells treated with cisplatin.
Using the analysis software STRING. Proteins that are in the DNA damage response are highlighted red.

5.2.12 MVI interacts with the same DNA damage proteins in HeLa and MCF10A before DNA damage

As previously stated, the two cell lines do not differ when discussing their MVI interactome. This is clear when displaying the proteomics using GO analysis (Figure 5.12). Within the DNA damage response pathway, it is clear that the same proteins are binding to MVI. These proteins are the ubiquitinating proteins, RPL40, Ubiquitin-40S ribosomal protein S27a, Polyubiquitin-C and Ubiquitin B. There is also binding of MVI to the DNA polymerase δ which can be found in the specific DSB pathway (Figure 5.15). The fact that the DNA polymerase δ binding occurs across both cell lines shows that there could be a common role MVI plays when discussing either DSB repair or DNA replication. This highlights an avenue of investigation of why MVI interacts with this polymerase, as we do not see this interaction after cisplatin treatment in both cell lines (Figure 5.13 and Figure 5.16) it is possible that the MVI interaction is not required for DSB repair but more specifically DNA replication.

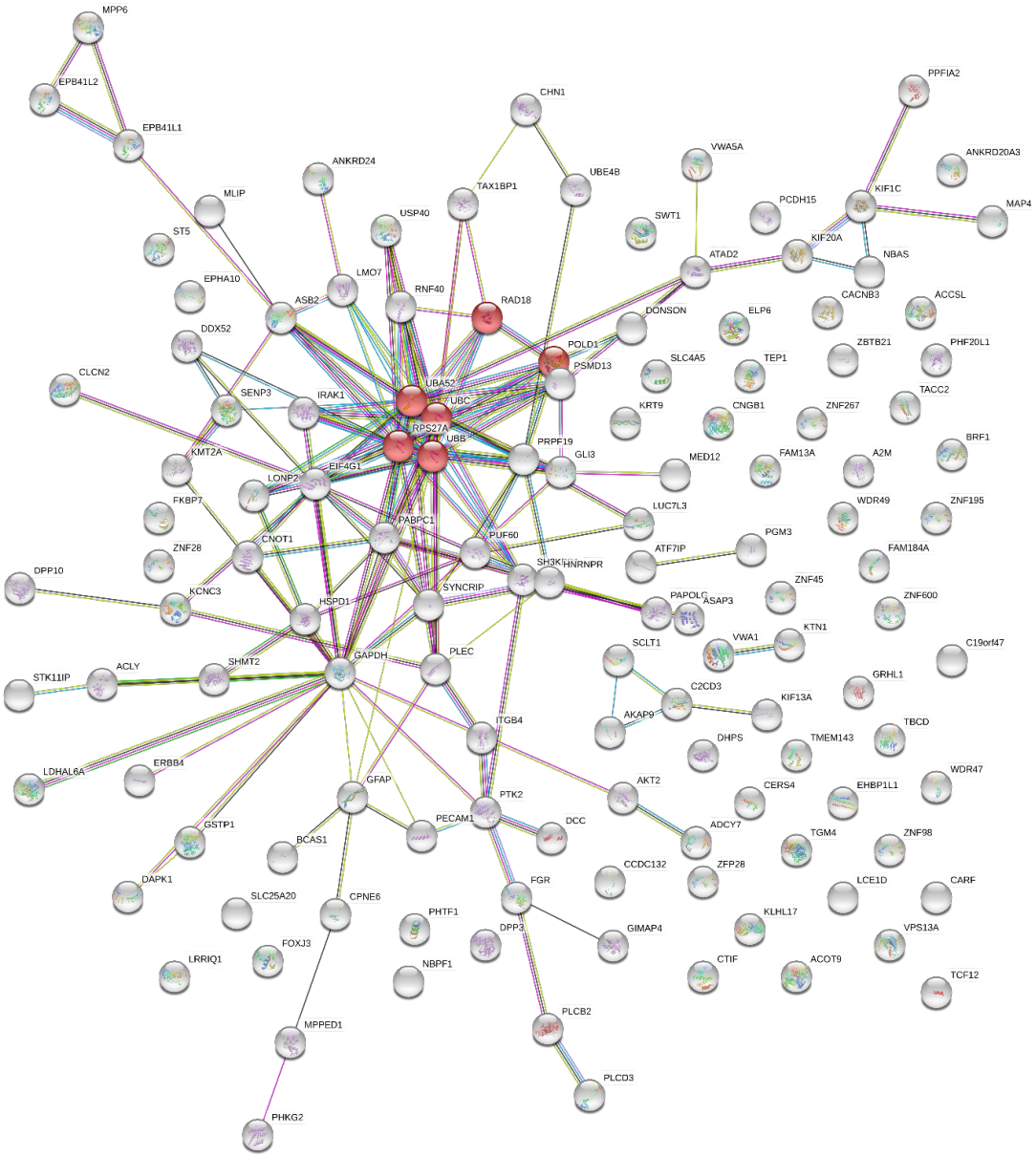


Figure 5.15. Protein network map of MVI interactions in MCF10A WT cells.

Using the analysis software STRING. Proteins that are in the DNA damage response are highlighted red.

5.2.13 MCF10A MVI does not interact with DSB specific proteins in MCF10A after DNA damage

The proteomics data of MCF10A MVI shows in this cell line, multiple DSB proteins are lost compared to that of the HeLa cell line, after cisplatin treatment. Both the Rad50 and Ku80 proteins are not found in the proteomics (Figure 5.16), however the nucleotide excision repair protein ERCC6 and the BRCA-1 repair foci protein FANC1 are still identified (Figure 5.16). This implicates MVI in the formation of repair foci as well as supporting MVIs role in the nucleotide excision repair process. As shown previously only 89 proteins are identified in both cell lines after cisplatin damage and there are 253 unique proteins to MCF10A after cisplatin treatment. This shows that whilst there are similarities of how MVI responds to DNA damage, through the NER and repair foci formation, MVIs' response differs greatly between cell lines. This proteomics data provides evidence that MVIs' response to DNA damage is not to regulate the transcription of genes through its interaction with RNAPII, but to act as a binding partner to specific DNA damage proteins.

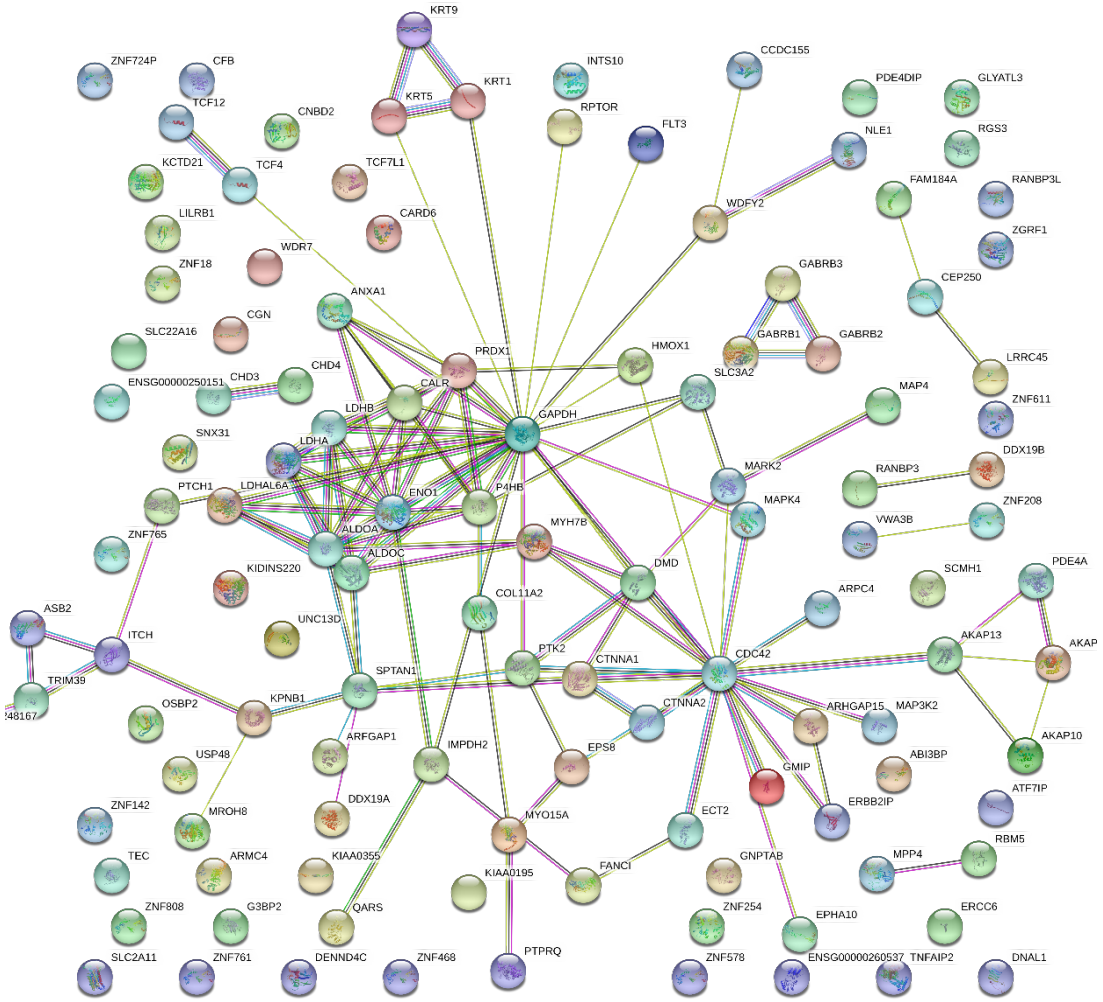


Figure 5.16. Protein network map of MVI interactions in MCF10A cells treated with cisplatin. Using the analysis software STRING. A DNA damage protein network is not identified however single DNA damage proteins are still identified.

GENE	PROTEIN	CONDITION	PATHWAY	DESCRIPTION
UBA52	Ribosomal protein L40 (RPL40)	HeLa WT, MCF10-A WT	DNA repair	Plays a role in ubiquitination of proteins in the DNA damage response
RPS27A	Ubiquitin-40S ribosomal protein S27a	HeLa WT, MCF10-A WT	DNA repair	Involved in ubiquitination of DNA damage proteins
UBC	Polyubiquitin-C	HeLa WT , MCF10-A WT	DNA repair	Involved in ubiquitination of DNA damage proteins
UBB	Ubiquitin B	HeLa WT, MCF10-A WT	DNA repair	Involved in ubiquitination of DNA damage proteins
POLD1	p125 catalytic subunit of DNA polymerase δ	HeLa WT, HeLa Cisplatin, MCF10 WT, MCF10 Cisplatin	DNA repair, DSB repair	In response to damage DNA polymerase δ is recruited to polymerase new DNA
RAD50	DNA repair protein RAD50	HeLa Cisplatin	DNA repair, DSB repair	Component of the MRN complex, involved in retaining both strands of DNA
XRCC5	Ku80	HeLa Cisplatin	DNA repair, DSB repair	Component of the Ku complex, initiates NHEJ
APEX1	DNA lyase	HeLa cisplatin	DNA repair	Acts as an endodeoxyribonuclease in base excision DNA repair and can bind Ku70/Ku80 for transcription
FANC1	FANC1	HeLa cisplatin, MCF10-A cisplatin	DNA repair	A ubiquitinated protein targeted to BRCA-1 DNA damage sites and repair foci
ERCC6	DNA excision repair protein ERCC6	HeLa cisplatin, MCF10-A cisplatin	DNA repair	Essential for transcription coupled nucleotide excision repair
SMCA4	BRG1	HeLa cisplatin	p53	Component of the SWI/SNF chromatin remodelling complex.
CREBBP	CREB binding protein	HeLa cisplatin	p53	Acetylates histones for transcriptional activation
PSMD13	26S proteasome non-ATPase regulatory subunit 13	MCF10-A WT	p53	Component of 26S proteasome targeting ubiquitinated proteins in cell cycle, DNA damage, apoptosis

Table 5.2. A table of MVI protein interactions involved in the DNA damage response.

5.3 Discussion

To fully understand how MVI responds to DNA damage this study set out to use large sale techniques such as RNA-seq and co-immunoprecipitation followed by LC-MS/MS. These techniques allow a global response to understand how MVI changes the transcription of the cell, and how it changes its binding partners. To investigate further if these changes are due to a direct role of MVI in the DNA damage response itself, or due to downstream effects from the DNA damage relating more to cell cycle stalling, cell to cell signalling and its known function in golgi structure and endocytosis. This study has shown that MVI may play a role at the exact point of DNA breaks.

5.3.1 The MVI localisation changes observed after cisplatin treatment shows a specific protein response to DNA damage.

The amount of MVI present in the nucleus increases after DNA damage. MVI expression is very low within the nuclei of normal human cells. This is mainly due to its cytoplasmic roles, that require the highest proportion of MVI to aid in endocytosis and cell signalling (Pant *et al.,* 2013). It has previously been noted that there is a specific isoform of MVI that provides the basal amounts of MVI for nuclear functions (Fili *et al.,* 2017), this isoform is the non-insert isoform that lacks a large insert of amino acids just before the cargo binding domain, and a small insert of amino acids, within the cargo binding domain.

In this study immunofluorescence has shown that the basal levels of MVI are very low and nuclei can be imaged distinctly within the cells. However, after cisplatin treatment the nucleus can no longer be determined easily as MVI is diffused across the whole cell body including the nucleus. Whilst this is visible, currently the antibody used during the immunofluorescence binds MVI isoforms non-specifically and so from this study it is not possible to identify which isoforms are causing this change of MVI within the nucleus. Further

work is required to identify the specific isoforms which can be found within the nucleus after DNA damage and by what mechanism are they entering the nucleus. This is then supported by the HCS, which shows an increase of MVI levels within the nucleus, whilst the RNA-seq data shows no change in MVI expression after DNA damage.

This type of MVI movement after a cell is stimulated has been previously reported when neurosecretory PC12 cells are stimulated with a high concentration of potassium chloride leading to the activation of genes required for the neurosecretory cells to function (Majewski *et al.,* 2018). This stimulation however was undertaken to increase transcription and thus the increase of MVI found within the nucleus was attributed to the role MVI plays in transcription. To identify if this was the case when studying the DNA damage response, RNA-seq was used to ensure that any transcriptional changes observed due to the movement of MVI could be observed at a global scale without bias.

5.3.2 Transfections change the transcriptome of cells.

To ensure that any changes in gene transcription were directly due to the MVI KD or cisplatin treatment, both samples, that had no transfection undertaken on them, and a control scrambled siRNA that should not affect any transcription were compared. As seen in this data, the difference between untransfected cells and cells transfected with scrambled siRNA is incredibly large. This could be due to the unexpected side effects of siRNA use. siRNA has been commonly used for over 20 years, however it is important to always note that the siRNA system itself is a system that is designed by the cell to respond to invasive RNAs and may increase the cell expression of genes required for interferon viral defense mechanisms (Mongkolsapaya *et al.,* 1999). That is why this study then removed the non-transfected cells from our sample group and used the scrambled siRNA transfected cells as our base line for gene expression.

5.3.3 DNA damage itself does not change the expression of DNA repair proteins.

To identify specifically how cells respond to DNA damage on a transcription level, this study has identified over 4107 genes that are differentially regulated. This number itself is not a surprise due to the major impact cisplatin can have on a cell. It is important to note that cisplatin caused DNA damage is a broad and uncontrollable event. The population of cells can be highly heterogeneous with some cells having very little damage to their genome and many cells having such a large amount the cell begins to enter apoptosis, or are already undergoing apoptosis. This produces a broad RNA-profile depending on the stage of each cell.

The RNA-seq data shown here did not have any effect on the expression of the ATM protein, required for the signalling of double stranded breaks, nor on the other DNA damage signalling proteins, ATR and DNA-PKcs. The p53 also did not have altered expression after cisplatin treatment however this can be explained by the p53 expression profile within HeLa cells. HeLa cells contain the human papillomavirus type 16 E6 protein that is consistently highly expressed. This protein itself marks p53 for degradation thus allowing the cancer phenotype of the cell (Oda *et al.,* 2000). This however makes it difficult to conclude anything when comparing p53 expression levels before and after cisplatin treatment.

Whilst the expression levels of p53 cannot be commented on, there is an increase in expression of p21, a protein that can be directly activated by p53. p21 was originally characterised by its ability to inhibit cyclins and cyclin dependent kinases, which leads to G_1/S and G_2 cell cycle stalling, stopping the cell from DNA replication whilst the genome is damaged. However, it is now known that p21 has a direct interaction within the DNA damage response, in particular within the nucleotide excision repair pathway and the DSB repair pathway (Fei, Bernhard, and El-Deiry, 2002). As well as this, it can also regulate expression of DNA damage response genes, by repressing *myc* which encodes a nuclear phosphoprotein

that plays a role in cell cycle progression and apoptosis (Maddugoda *et al.,* 2007). The RNA-seq that was performed here also saw this reduction in the *myc* gene, supporting the data shown to previously published data.

It is overall expected that DNA damage does not change the expression of DNA repair proteins, as any transcriptional changes would be unlikely based on the time response from damage to repair being almost instantaneous versus the transcription and translation lag that would delay the damage response.

5.3.4 MVI KD does not have the same transcriptional effect as cisplatin treatment.

MVI has been characterised to have a role in transcription with an interaction with RNAPII and DNA (Fili *et al.,* 2017), to identify if MVI KD causes a large scale change in gene expression, that may affect genes that are regulated during DNA damage, RNA-seq was performed on cells that have only the MVI KD without any DNA damaging drug treatment. Out of the total 1947 genes that had their expression change only 433 genes, 22% of total genes, shared a similar expression profile than that after cisplatin treatment. With regards to GO definitions, the MVI KD effects far more cellular developmental processes and cell differentiation than that of cisplatin, with the localisation of proteins that have been affected being within the extracellular regions. They also have completely different functions with the majority of genes encoding for proteins that undergo anion binding, whereas in the cisplatin treatment no proteins affected had anionic binding properties.

The MVI KD is interesting in itself, as MVI plays a large role in cell-cell adhesions, endocytosis at the plasma membrane and intracellular signalling (Chibalina *et al.,* 2009). This RNA-seq data may provide evidence for a mechanism linking MVI at the membrane to its role in RNAPII transcription, where MVI transports signals such as hormones (Loikkanen *et al.,* 2009) This observation linked with MVI movement into the nucleus after stimulation of neurosecretory cells using potassium chloride may also help elucidate how exactly MVI is

moving into the nucleus, is it being carried through with a cellular receptor or is MVI directing the receptor to the nucleus?

MVI can also be found with cadherin, at cell to cell contacts and is involved in cell adhesions (Millo et al., 2004).As we saw a reduction in genes specific to the extra-cellular region, it is possible that as MVI is not present to stabilise these junctions, the transcription of junction related proteins is not required. Further work is required to fully understand why MVI KD is having such a large effect on proteins identified in the extracellular region, and how MVI is crossing the nuclear membrane. There are no genes within the p53 pathway that have been affected by the MVI KD itself however damage stimulation was required to ensure that these genes were still transcribed as expected, after the MVI had been knocked down.

Interestingly after MVI KD, two of the largest GO processes affected were cell-cell communication and regulation of signal transduction. MVI has been attributed to these processes, more so, as a protein-protein based interaction. It has been shown that KD of MVI leads to an impairment of the exocytosis of secretory granules, and that MVI binds to these granules (Tomatis *et al.,* 2013). Yet, this study has identified possible unknown effects of MVI KD on the gene expression of signal regulators, therefore whilst MVI can be directly found during endocytosis and exocytosis, by using a MVI KD, the effect is much larger on the cell, than just losing one protein-protein interaction and rather a global shift of genes related to these processes are affected.

5.3.5 HeLa cells still transcriptionally respond to DNA damage after MVI KD.

This study set out to find any DNA damage response genes MVI may play a role in transcribing. To identify these genes, after MVI KD cells were treated with cisplatin and the RNA-seq data was compared to that of the cisplatin treated only. Any genes that were normally upregulated by cisplatin and were instead downregulated in the MVI KD cisplatin sample, were noted, as well as vice versa, any gene expected to be down regulated by

cisplatin but were instead upregulated in the KD were also noted. This lead to the identification of only 210 genes, around 5% of genes out of the 4107 genes that did not behave as expected.

The majority of these genes are involved in the stimulus response or cell proliferation processes and are once again located at the extracellular region and not within the nucleus. It can be implied that the cisplatin treatment after MVI KD, mainly effects those genes found in the MVI KD on its own, as the molecular function of the genes with differentiated expression to the cisplatin only cells are involved in receptor regulator activity and receptor ligand activity. Once again linking this idea that MVI controls the regulation of receptor genes and potentially in a response to stimuli but not the genes required for the DNA damage response pathway.

This type of receptor gene regulation MVI seems to be regulating is supported by analysing the p53 KEGG pathway previously used with the cisplatin genes. Here only 5 of the genes out of the 17 genes affected by cisplatin have their transcription changed by the MVI KD. One of these five genes, PERP that is normally upregulated by cisplatin damage becomes repressed by the MVI KD, PERP encodes a p53 apoptosis effector that regulates cell death genes, however this protein is actually found at cell-cell adhesions and leads to tumorigenesis when adhesion complexes are lost (Attardi *et al.,* 2000). Whilst this plays a role in the p53 pathway it is not directly linked to the DNA damage response and MVI most likely effects its transcription through its interactions at the cell-cell joins rather than due to MVIs response to damage.

Another of the proteins that have reduced expression following MVI KD and cisplatin treatment is IGFBP-3, the insulin like growth factor binding protein 3. Whilst this protein can play a role in apoptosis after DNA damage it is mainly found within the extracellular environment and at cellular receptors (Ogi *et al.,* 2010). This may explain why its regulation

is altered by the MVI KD after cisplatin treatment, due to the capability of MVI to bind to receptors. If the MVI is not present at these receptors they may not be enveloped into the cell and thus the cell is not stimulated. This once again supports MVIs role in endocytosis of cell receptors but also that it is not regulating genes due to the DNA damage response but through other mechanisms.

In fact, three of the genes, PERP, IGFBP3 and TSP1 that were repressed rather than expressed after cisplatin treatment in the MVI KD cells are linked with cell-cell adhesions, cell to extracellular matrix adhesions and receptor signalling. The only gene that should have been upregulated and was not is the cyclin G gene, responsible for cell cycle progression after DNA damage. Why this particular gene is affected and no other cyclins, is hard to predict and may have to do with MVIs general role in transcription and not its role in the DNA damage response.

5.3.6 MVI does not have a role transcriptionally in the DNA damage response.

The RNA-seq data has thrown some light on the role of cisplatin and MVI on transcription. Whilst cisplatin causes a global change in transcriptomics to stall the cell within its cycle and allow for repair of the DNA or apoptosis to occur, MVI has a much more specific role in the regulation of cell adhesion and cell receptor genes, non-specific to DNA damage. There is no effect on the expression of the ATM, ATR or DNA-PKcs, damage signalling genes nor any genes related to the double strand break response such as any genes found in the MRN complex or Ku70/80 genes. This suggests that the proteins immediately responsible for repair and damage signalling have an involvement at the protein level first before affecting transcription, this is likely due to the long period of time it can take to transcribe and fold a working protein that would be able to fix the DNA damage.

Whilst MVI has a role in general transcription in a cell, however it does not alter the transcription of genes involved in DNA damage, especially of those critical for p53 related

activity. As the gene levels stay the same, in particular the over expression of p21 and cyclins, it shows that at the transcriptomics level MVI does not respond to DNA damage and that the change of MVI levels in the nucleus and its response must be at the protein-protein level instead.

5.3.7 MVI binding partners are similar between cancerous and non-cancerous cell lines.

As MVI does not respond to DNA damage transcriptionally, there must be a purpose for its localisation to the nucleus. To identify if its response occurs at a protein-protein level, LC-MS/MS proteomics was carried out.

The proteomics data shown here identifies only 29 protein interactions unique to HeLa cells, the remaining 362 protein-protein interactions occur in both the cervical cancer HeLa cells and the MCF10A non-cancerous epithelial cells. This comes as a surprise as MVI amounts differ between cell lines and within cancers such as ovarian, prostate and breast. As the amount of MVI differs, unique roles of MVI within these cancer cell lines have been identified such as in prostate cancer where MVI has been attributed to the co-ordination of cell clusters during metastasis (Luo *et al.,* 2004). This may not necessarily mean that MVI does not do this in other cancer cell lines or in the clustering of healthy cells as well, and so this proteomics has shown whilst maybe the MVI levels differ between cell lines, the binding proteins identified are similar.

The number of proteins is relatively equal between cytoplasmic functions of binding partners and nuclear functions of binding partners. This further confirms MVI has a role in both the cytoplasm and the nucleus, and whilst this study only focuses on the GO related to DNA damage processes, the proteomics study identified expected interactions such as MVI with Dab2 and GIBC, well characterised binding partners of MVI for endocytosis. However, there are some limitations to this study, the MVI immunoprecipitation cannot distinguish between

MVI isomers so any protein-protein interaction identified cannot be attributed to be isomer-specific. Although LC-MS/MS is a highly sensitive protocol for proteomics, the samples were whole cell lysate and not separated by compartment, this means that lower abundant interactions such as those found in the nucleus can be hidden by more common interactions. It also does not provide a mechanism where MVI may interact with proteins that are able to cross between the nuclear membrane.

5.3.8 MVI has a role in DNA replication

As discussed MVI has a role in RNAPII transcription where it potentially acts an anchor to stabilise the complex or act as a processive motor. In both cell lines, whether DNA damage is present or not MVI interacts with DNA polymerase δ.

Polymerase δ is required for both DNA replication and chromosome organisation. It is able synthesis DNA on both the lagging and leading strands within the Okazaki fragment (Lee and Paull, 2004). Within eukaryotes replication protein A (RPA) binds to ssDNA stabilising the fragment stopping repairing of the DNA strand. Polymerase δ then binds to the lagging strand and begins synthesis of DNA using the lagging strand as template. To then complete the synthesis the lagging strand is processed by the polymerase as well as Fen1 and the DNA ligase, lig1 (Jin, 1997) .

As well DNA replication polymerase δ is involved in DNA repair, in base excision repair, mismatched-repair, nucleotide excision repair and DSB repair. In the case of base excision repair, this polymerase can be utilised to repair methylated DNA caused by methylating agents, here it repairs single base adducts 3' proximal to single stranded breaks (Folias *et al.,* 2002). In mismatched-repair, where the wrong bases are substituted in or frameshifts occur by the polymerase can be reported using the Msh2/Msh6 or Msh2/Msh3 complexes (Subramanian *et al.,* 2013). Once reported, the polymerase can bind and reintegrate the

correct nucleotide or independent of an exonuclease, Exo-1, it can melt a nicked strand identified and then continue with the correct polymerisation (Beerens *et al.,* 2005).

NER and DSB repair occurs after the use of cisplatin. In NER the polymerase is recruited to lesions that can be 25-30bp long to then polymerise the correct strand of DNA. The same is reported in the DSB response where after cleaning of and excision of the strands during homologous recombination only, polymerase δ becomes activated to polymerase the repaired DNA using the undamaged DNA as a template (Lee *et al.,* 2010).

Overall MVI was found to interact with this polymerase in all of the cell lines and conditions undertaken in this study. This implies that the MVI interaction is not necessarily damage dependent and MVI could be present at replication forks during DNA synthesis. This would be a novel role of MVI within the nucleus that is yet to be characterised. It is possible that during normal cell growth, replication stress and miss match occur, and that is why MVI is interacting with DNA polymerase δ, if this is the case then MVI may be only binding to this polymerase at the points of damage. Further work would be required to identify MVIs role with DNA polymerase δ.

5.3.9 MVI responds to DNA damage by binding to DNA damage proteins

MVIs binding partners go through a complete overhaul after DNA damage. Out of the 536 proteins identified to interact with MVI in HeLa cells after DNA damage, only 16 interactions are seen within WT (untreated) cells. Out of the 359 protein interactions identified in cisplatin treated MCF10A cells, only 17 were found within WT cells. This shows that the response to DNA damage is not just a localised phenomenon but spread throughout the whole cell activating or deactivating completely different pathways.

The data shown here identified that MVI binds specifically to proteins required for NER and the DSB response. In particular this study has identified that MVI interacts with both Rad50

and Ku80 after DNA damage in HeLa cells. These proteins form the repair scaffold around DSBs, Rad50 is directly involved in HR repair that can occur if a template of the damaged gene is available (Qi *et al.,* 2015). If the template is not available Ku80 along with Ku70 bind to the DSB forcing NHEJ to occur (Jeske and Richter, 2015).

This opens the discussion: Why is MVI there? What role does it play? And how is this interaction regulated? It is possible that this interaction occurs due to the presence of the polymerase δ at these sites and so MVI is interacting with the repair proteins so as to initiate strand synthesis. It also could be due to MVI being present at repair foci where it has these interactions. This study shows that MVI interacts with FANC1, a protein that is localised at BRCA-1 repair foci (Renodon-Corniere *et al.,* 2013). Repair foci occur when there are multiple points of damage that can be repaired simultaneously so it is interesting that MVI is binding to a protein that is present at these repair foci. It could be that MVI is using its anchoring ability to maintain and stabilise these repair foci through FANC1, Ku80 and Rad50.

Another protein identified during this proteomics is the CREB binding protein, whilst characterised as a histone acetylase it also acetylates proteins directly involved in the DNA damage response. An example of this is CREB binding protein acetylating Ku70, after DNA damage. This acetylation however does not increase DNA repair, but depletes it due to acetylated Ku70 having a lower affinity for DNA (Subramanian *et al.,* 2013). It has been hypothesised that this reduces DNA repair thus promoting apoptosis of the cell.

Both Rad50, Ku80 and the CREB binding protein were identified from the HeLa proteomics however MVI was not observed to have an interaction with either of these proteins within the MCF10A cell line. This may be due to a dynamic binding of these proteins or that HeLa cells have different repair mechanism as compared to MCF10A as in the MCF10A, MVI was still found bound to the NER protein ERCC6. This protein wraps DNA around itself to allow for the repair of the DNA followed by transcription by RNAPII (Beerens *et al.,* 2005). In this

case NER is used to repair transcriptional stress and so the MVI interaction here could be linked with the previously published data of MVI involved in RNAPII transcription.

5.3.10 MVI may play a role in chromatin reorganisation after DNA damage

As well as HeLa MVI, interacting with Rad50 and XRCC5, it has also been shown to bind to the chromosome remodelling complex BRG1 and the histone acetylase the CREB binding protein.

Here the MVI-BRG1 binding may be MVI responding to DNA damage by changing the chromatin layout within the nucleus or by rearranging chromatin to from repair foci. It is likely that the latter is the case as recently BRG1 itself promotes chromatin remodelling around the sites of DNA damage and can directly interact with the DSB signaller the histone modification γ-H2AX (Kwon *et al.,* 2015). As well as direct binding to the signaller, BRG1 aids in double stranded break repair by replacing RPA1 at sites of damage with Rad51 for homologous recombination repair (Qi *et al.,* 2015). Whether or not the MVI here is facilitating in the repair, the rearrangement of chromosomes or aiding with the interaction of Brg1 and γH2AX is yet to be elucidated and would require further work.

The CREB binding protein is able to acetylate histones to allow for the activation of particular genes local to that histone. This may link MVI back to its transcriptional activity and may allow for the transcription of downstream proteins affected by DNA damage. Due to MVI binding to both the proteins discussed here as well as FANC1 it is possible to hypothesise that if MVI is responsible for stabilising transcription complexes, then its anchoring properties may also anchor repair factories.

5.3.11 MVI responds to DNA damage at a protein-protein level and not by regulating transcription

To understand if MVI and how MVI responds to DNA damage, a change in transcription would be expected as MVI interacts directly with RNAPII and so the hypothesis begun with MVI may change the expression of DNA damage repair genes. This hypothesis has been rejected due to the RNA-seq data showing that whilst a few genes have defective transcription after MVI KD and cisplatin treatment, majority of genes for specific DNA repair proteins remain the same.

This rejection lead to the second hypothesis to explain why MVI localisation changes after DNA damage. This hypothesis was that MVI binds directly to DNA repair proteins which can now be accepted as the proteomics identified specific DNA repair proteins as well as proteins that are able to rearrange chromosomes and construct repair factories or foci. These interactions however seem to only occur in the HeLa cell line and not within the MCF10A cell line. This comes as a surprise as whilst p53 is dysfunctional within HeLa, MCF10A cells exhibit a normal response to DNA damage. This difference however might be down to the stringent conditions used through the proteomics analysis or through sample preparation. To continue to observe any differences of MVI roles between the cell lines during the DNA damage response, both cell lines were carried on for further studies.

As MVI binds directly to DNA repair proteins, it can be predicted that MVI is involved in the immediate response to DNA damage rather than the longer process of transcription, making it a vital component to study within the response to build on the mechanisms that currently exist.

Chapter 6. MVI involvement in DSB signalling

6.1 Introduction

It is now established that MVI responds to DNA damage by altering its binding partners and its localisation within the cell. Whilst DNA damage protein interactions have been identified and MVI doesn't alter the transcription of DNA damage proteins, the definitive role MVI actually plays within DNA damage is yet to be elucidated.

6.1.1 Histones and their modifications

Histones are proteins responsible for regulating DNA transcription (Sterner and Berger, 2000), chromosome organisation (Luger *et al.,* 1997), the DNA damage response (Li *et al.,* 2018) and DNA replication (Madamba, Berthet and Francis, 2017). They are able to have such a commanding role on the DNA, through their formation of nucleosomes, which consist of an octamer of histones. The histones found in the octamer are two H2A, two H2B, two H3 and two H4 histones, there can also be the H1 histone which alters the packing of the DNA but is not classified along with the other histones as part of the core complex (Takizawa *et al.,* 2018).

The nucleosome is able to wrap a strand of DNA approximately 146bp long around its core with an additional 86bp long DNA that acts as a linker strand until the next nucleosome. Whilst the DNA directly wraps around the octamer of histones, the actual regulatory role of histones is found within the long tail regions of the histones, that contain a large amount of amino acids that are readily available for post translational modifications (PTMs) (Arnaudo and Garcia, 2013). The modifications on these tails correspond specifically to the unwinding, or winding of DNA around the nucleosome that can suppress or activate gene expression. This change occurs by the PTMs, leading to a change in conformation of a histone and thus a change in affinity to the DNA it is bound to (Fenley *et al.,* 2018). As well as this, these PTMs

can then act as signallers that other proteins are able to recognise, signalling a specific pathway within the cell (Bannister and Kouzarides, 2011).

Due to the vast range of PTMs that can be undertaken on these histones, this study will only focus on some of the most well characterised PTMs of these N-terminal tail domains. For a long period of time, the general rule of PTMs was that acetylation of histones meant there was gene activation within that area, and methylation is responsible for gene repression. However there is now more evidence that depending on the number of methyl groups added to the tail, the signal changes (Pinskaya and Morillon, 2009).

Acetylation of lysine-9 on the H3 histone is a well characterised PTM and is responsible for the activation of gene transcription and elongation (Gates *et al.,* 2017), whilst the triple methylation of the very same lysine (H3K9me3) is associated with gene repression and the binding of the heterochromatin protein 1A (HP1A). This condenses the DNA from euchromatin, DNA that is freely available, to tightly compact DNA, known as heterochromatin (Gessaman and Selker, 2017). Other acetylation PTMs, such as that found on the lysine further along on the H3 histone, H3K27ac, is also linked with transcriptional activation of genes. This PTM can be found at either side of transcriptional start sites, and thought to direct the transcriptional machinery towards a gene (Rennie *et al.,* 2018).

Within DNA damage there also some alternative PTMs on different histones that are changed after DNA damage has been identified. The three so far to have been characterised are the single methylation of the lysine-20 on H4, H4K20me, and the double methylation of the lysine-36 on the H3 histone, H3K36me2, and the DNA damage signaller γH2AX. There is an increased level of H4K20me modification, 500bp, before and after a site of DNA damage which seems to be associated with the DSB NHEJ repair pathway, whilst the H3K36me2 amounts decrease +/- 500bp of the site of damage. This modification is specifically associated with the HR pathway of DSBs (Thomas Clouaire *et al.,* 2018). Whilst these PTMs

are specific to repair pathways one histone modification is central to the DNA damage response pathway and that is γH2AX.

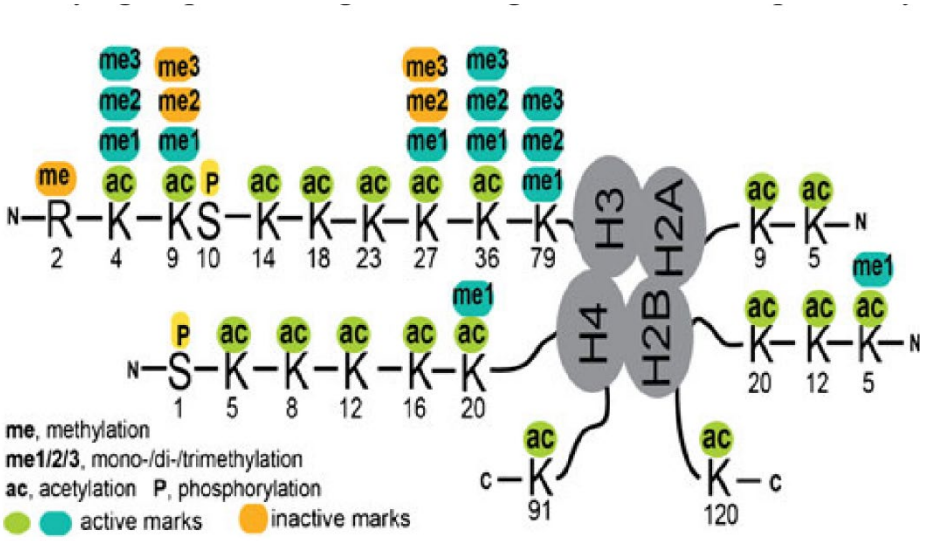


Figure 6.1. The current map of histone modifications.

All of the known histone modifications that can lead to an activation (green and blue) or inactivation (orange) of gene expression and regulation. Taken from Dai and Wang, (2014).

6.1.2 γH2AX signalling.

Often when studying DNA damage, particularly when using external stimuli such as UV, drugs or oxidative stresses, the presence of γH2AX, and the amount of γH2AX can be used as a readout of damage in terms of localisation and amount (Ivashkevich *et al.,* 2012).

γH2AX is a single phosphorylation of a serine-139 residue of the unique H2A histone variant H2AX. This variant makes up around 10-12% of the H2A histones within the nucleosome. This histone is a variant of its H2A parent by the motif SQ[E/D]Φ where Φ is a hydrophobic residue, which changes the affinity the histone has for DNA. It is the amino acid motif however, that is responsible for its role in DNA damage signalling (Song *et al.,* 2007). Due to the H2AX abundance being limited, it is possible that the integration of H2AX is either

random or directed, the random distribution would provide an H2AX variant as 1 in every 4.3 nucleosomes within a cell, which would be close enough for a DNA damage signal to travel along the chromatin (Iacovoni *et al.,* 2010).

The serine-139 found within this unique motif can become phosphorylated by the three kinases that can be activated during DSBs, the ATM kinase (Burma *et al.,* 2001), the ATR kinase (Ward and Chen*.,* 2001), and DNA-PKcs (An *et al.,* 2010). At first, the phosphorylation only occurs within the immediate location of the break, highlighting that particular region for repair, this signal can then spread across the chromatin similar to that of a chain reaction (Savic *et al.,* 2009). MDC1 is able to bind, recruiting the repair complex MRN, through its interaction with the MRN subunit Nbs1. Once the MRN complex is recruited a positive feedback loop is formed leading to further activation of the ATM kinase and thus further phosphorylation of H2AX histones (Paull *et al.,* 2000). This signalling is associated with the stabilisation of DNA damage repair proteins and complexes rather than having a direct involvement in the repair itself. Due to its ability to only signal DSBs, monitoring this reaction pathway and identifying the amount of γH2AX signals allows this study to identify if MVI plays a role in the signalling of DSBs.

6.1.3 DSB repair foci

As the signalling of γH2AX spreads across distinct areas within the nuclei, repair foci begin to form following the formation of the repair machinery. The formation of a repair foci, requires the γH2AX as this brings together and stabilises the repair proteins such as MDC1, 53BP1 and BRCA1 (Nakamura *et al.,* 2010). RAD51 however can still be found at points of damage and can form slight repair foci without γH2AX signalling, however this isn't identified until hours after the induction of DSBs. Once a repair foci is formed, the protein copies increase rapidly where it has been noted that MDC1, 53BP1, RAP80 are in their thousands and BRCA1 is in its hundreds.

The reason for this vast copy number is most likely so the cell can amplify the response to a DSB. If a few DSBs occur within the DNA, the effect on the DNA can be hugely detrimental, due to the amount of DNA the cell is required to monitor, it is likely the repair foci act as a beacon to ensure the cell cycle is stalled. If a single ATM is activated at a break point, the signalling cascade it is involved in, especially the activation of p53 would be limited, by creating a beacon, and a plethora of positive feedback loops, a single DSB can cause the whole cell cycle to become restricted. With each protein further increasing the number of active ATM proteins, there is also an increasing amount of downstream repair proteins.

When studying the formation of DSBs and how the cell responds to a DSB, it is important not just to study the first response to the break but the signalling undertaken by γH2AX and the formation of repair foci. As shown in the previous chapter, MVI has interactions with proteins responsible within all three of these stages of repair.

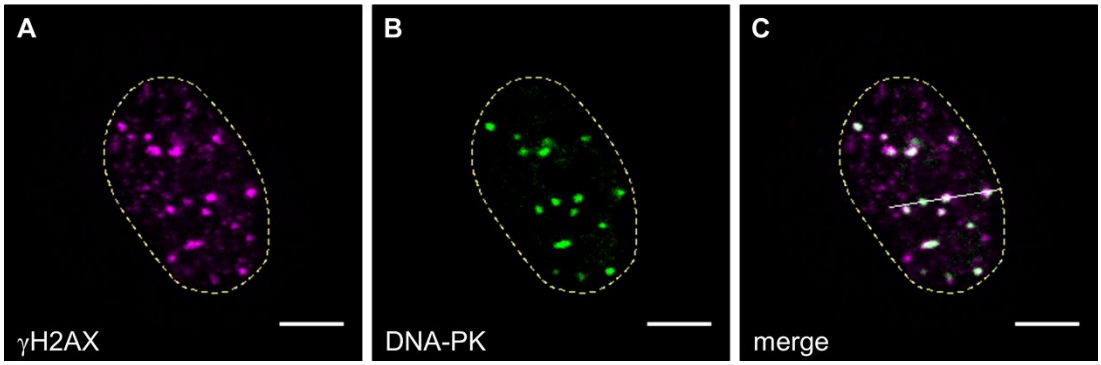


Figure 6.2. An example of visible repair foci.

30 minutes after irradiation of cells with 2 Gy, repair foci are identified using CSLM with high density of γH2AX foci (A) corresponding with the γH2AX activator DNA-PK (B,C). Taken from Sisario *et al.,* (2018).

6.1.4 2,4,6-triiodophenol (TIP) the small molecule inhibitor of MVIs motor domain.

During this study to identify the activity of MVI within the DNA damage response a small molecule inhibitor has been utilised. This small molecule is able to bind within the motor domain of MVI, in the region of amino acids 1-816. The binding of this molecule, causes a threefold inhibition of the maximum actin activated ATPase of the motor domain, which occurs in a biphasic manner, due to the two binding sites available for TIP binding (Heissler *et al.,* 2012).

It has been shown that this inhibition of the motor domain results in a deactivated MVI that is unable to undertake regular vesicle fusion with the plasma membrane, at only a working drug concentration of 5µM, having the same phenotypic result as if a MVI KD had been undertaken on the cells.

The TIP inhibitor has also been utilised when studying MVIs ability to bind to RNAPII for transcription. Here, TIP inhibition of MVI had a similar effect of inhibiting transcription by 70% to that of the MVI KD *in vitro* (Fili *et al.,* 2017; Cook *et al.,* 2018). This study highlighted that the motor activity of MVI is required for transcription.

Overall TIP as a drug inhibits MVIs motor activity, which can be used to maintain MVI levels within a cell, but identify if the motor domain of MVI is important for its role in a particular mechanism. To know if the motor domain is important for the MVI responce to DNA damage, this study has also employed the use of TIP, at previously described concentrations of 25µM.

6.1.5 Ku55933 an ATM inhibitor.

To coincide with inhibiting MVIs motor activity, this study has also used a characterised ATM inhibitor, 2-morpholin-4-yl-6-thianthren-1-yl-pyran-4-one (Ku55933). This inhibitor is an ATP competitor which binds directly within the nucleotide binding pocket. Within the DNA damage response Ku55933 only inhibits ATMs activity, and not the other DNA damage signallers, ATR and DNA-PKcs (Savic *et al.,* 2009). Once inactivated the cells are unable to phosphorylate the downstream effectors of DNA damage such as p53 and BRCA1, as well as phosphorylate the H2AX histone. In this case the ATM inhibitor has been utilised as a positive control, in which cells treated with DNA damaging agents bleomycin and cisplatin but unable to respond, can be observed alongside cells that have been treated with the MVI inhibitor.

6.1.6 Confocal microscopy

This technique uses the traditional immunofluorescence method in which a primary antibody is selected specifically for the protein of interest and a secondary is selected for the species of antibody as well as its fluorescent properties.

During this study, to gain a better understanding of where MVI localises, a more precise type of microscopy is necessary. Common microscopy techniques involve the use of widefield microscopy. This simply uses a fluorescence light source with filters to fit the excitation and emission of the fluorophore which then illuminates the whole sample non-specifically and allows for an image to be taken. However wide field itself causes high background signal that means that the resolution is very low and specific localisation of proteins is hard to predict.

To avoid this high background signal, confocal laser scanning microscopy (CSLM) can be implemented instead. Here rather than the whole sample being illuminated, a pinhole design specifically illuminates the sample. This means only the sample within the point of view is illuminated. The pinhole also reduces the scattering of light from the fluorophore (Jung *et*

al., 2015). Light scattering commonly reduces the resolution causing an image to become blurry, however the pinhole design reduces the scattering of each fluorophore and by combining this with a scanning laser, that specifically illuminates a small section of sample at a time reduces the background further.

Whilst the use of this microscopy technique allows for co-localisation studies and high-resolution imaging, it is unable to define the localisation of a single molecule which is where other microscopy techniques can employed.

6.1.7 Stochastic Optical Reconstruction Microscopy (STORM)

STORM imaging provides single molecule imaging with an incredibly high resolution. All microscopy techniques are restricted by the resolution of an image, this resolution can be defined by Abbes criteria (Neice, 2010);

Equation 6.1 Abbes resolution criteria

$$d = \frac{\lambda}{2NA}$$

Where d, is the resolving power, λ, is the wavelength and NA is the numerical aperture of the microscope. This equation stipulates that to resolve two points of emission there is a limit to the resolution. To obtain a resolution that allows for single molecule imaging i.e. a resolution of single nm, a single signal that produces enough photons that is at least 200nm from another similar emitting molecule is required. As this type of separation of molecules is rare to find within a biological sample, especially within a single cell, the fluorophores are required to be switched “on” and “off” (van de Linde and Sauer, 2014).

This switching relies on how fluorescence emission works. Fluorescence emission is produced by a molecule when electrons in their stable state become excited by a photon at the correct wavelength. Once excited there is a small change in energy down through the

excited states, this process is called internal conversion and vibrational relaxation. After this, the electron returns to its stable state and it is this loss of energy that produces fluorescent photons. This process of excitation and emission takes within the picosecond range, and so current camera technologies will identify a single emission of fluorescence. To obtain blinking of a fluorophore, the fluorophore has to be forced into its dark state, this dark state occurs when the electrons are excited they transfer not immediately back to their stable state but progressively down through alternative systems. This is known as intersystem crossing (van de Linde and Sauer, 2014).

To encourage an electron to travel into this dark state, a reducing agent is required, commonly β-mercaptoethanol (BME) is used, to enhance the dark state lifetime and to avoid photobleaching of a fluorophore, an oxygen scavenger such as glucose oxidase (GOX) is used to keep the fluorescent molecule in the dark state. This dark state however is not infinite and eventually the electrons will return to their stable state and become re-excited thus causing a cyclic motion of fluorescence on and then off. This blinking provides that 200nm distance between fluorescent signals at a single time.

Once a signal is identified a point-spread function is applied to that signal (von Tiedemann *et al.,* 2006). This function fits a gaussian function, where a fluorescent signal is brightest within the centre of the signal and the fluorescence decreases around this point. By applying this fitting alongside the subtraction of any surrounding signal through the blinking properties, it is possible to identify a single molecule within approximately 1nm to 20nm depending on the amount of photons collected from that point.

This technique allows for the complete mapping of single molecules within a cell and the identification of any co-localisation between molecules if the signals are within 10nm of each

other. It also allows a quantitative measure, as it is possible to count individual molecules within a region of interest.

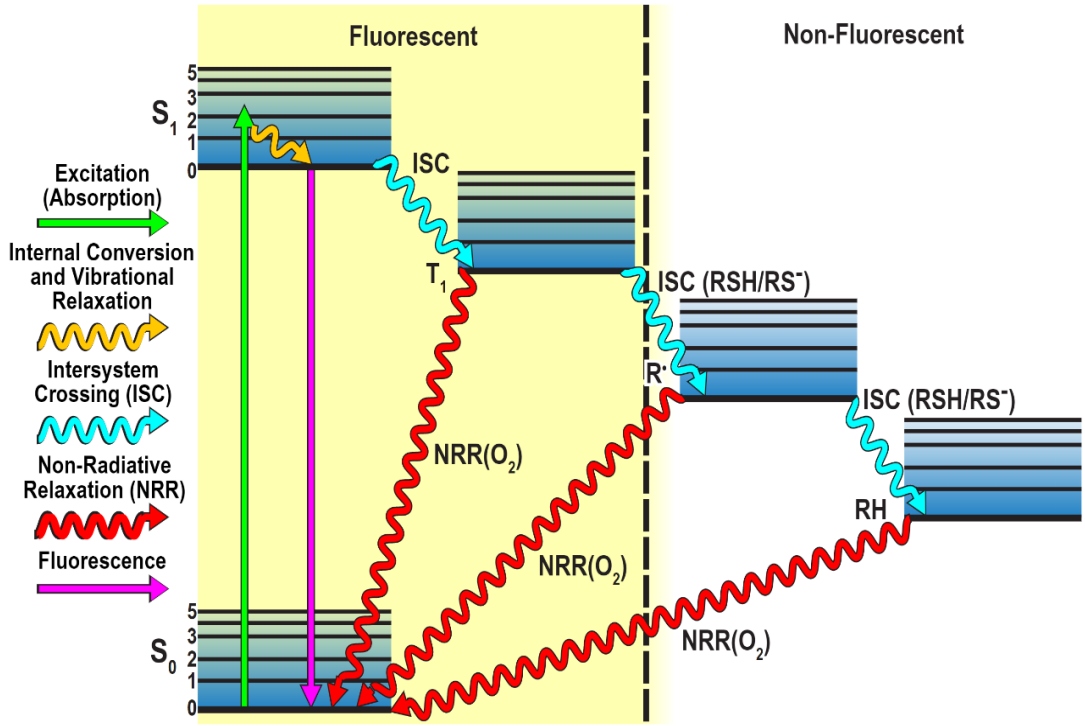


Figure 6.3. A simplified Jablonski diagram.

A Jablonski diagram showing the direction of electron energy changes from S_0 the stable state to S_1 the excited state and the transfer of energy down the intersystem states into the dark non fluorescent state and back to the stable state. Taken from Microscopy U, Nikon (2019).

6.1.8 Cluster analysis with degree of colocalization (Clus-Doc)

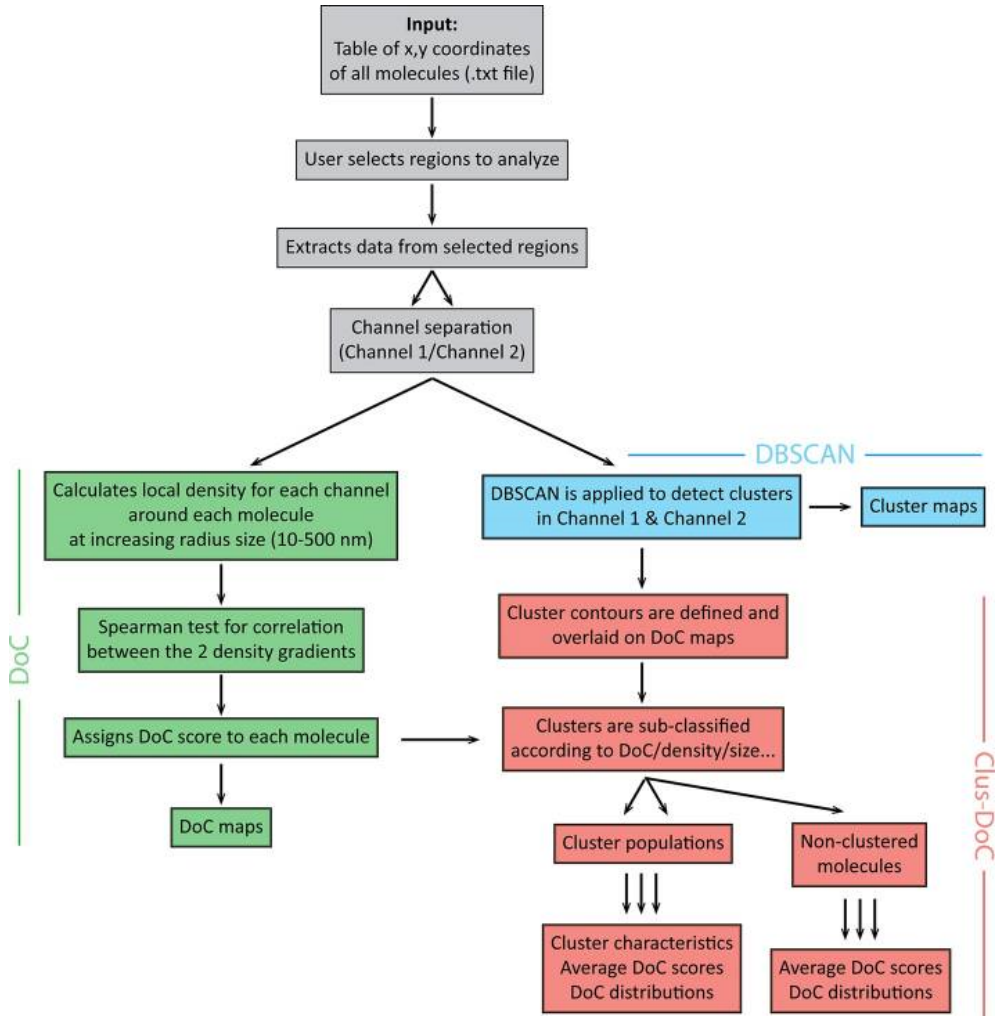


Figure 6.4. A work flow of Clus-DoC.

The work flow of the analysis software Clus-Doc, and the data output at each stage. Taken from Pageon *et al.,* (2016).

In addition to using STORM to identify single molecules, further analysis is required to identify the number of molecules, whether or not these molecules cluster together, the density of these clusters and the area of these clusters.

To complete this analysis, the data provided by STORM imaging allocates a single molecule to have an x and y coordinate. This is directly inputted into the Clus-Doc software which is then able to identify the Ripley K function to provide an average of clustering across the region of interest (Pageon *et al.,* 2016).

The Ripley K function is as defined as:

Equation 6.2. Ripley K function

$$\widehat{K}(t) = \lambda^{-1} \sum_{i \neq j} \frac{I(d_{ij} < t)}{n}$$

Where d_{ij} is the Elucidean distance between the i^{th} and j^{th} points in a data set of n points, t is the search radius, λ is the average of density of points and I is the indicator function.

Once the Ripley K function is defined for each data point, they are then processed through the DBSCAN algorithm which segments these points into clusters. This identifies if one species of molecules are clustered or separated from each other.

A degree of colocalization (DoC) score is then defined for each data point, where the search for other points within a certain radius is identified and can define the local density around each molecule. With each molecule being provided with a surrounding density score. These data can be partnered with a second species, i.e the second image channel and then overlaid.

Overall this process not only provides the clustering of molecules within a single channel, the location of these clusters and scores the clusters, but it allows for both channels to be overlaid on top of each other, providing information of protein-protein localisation and protein cluster-protein cluster localisation. This type of information is important to obtain when discussing protein clusters such as those found within repair foci of DSBs.

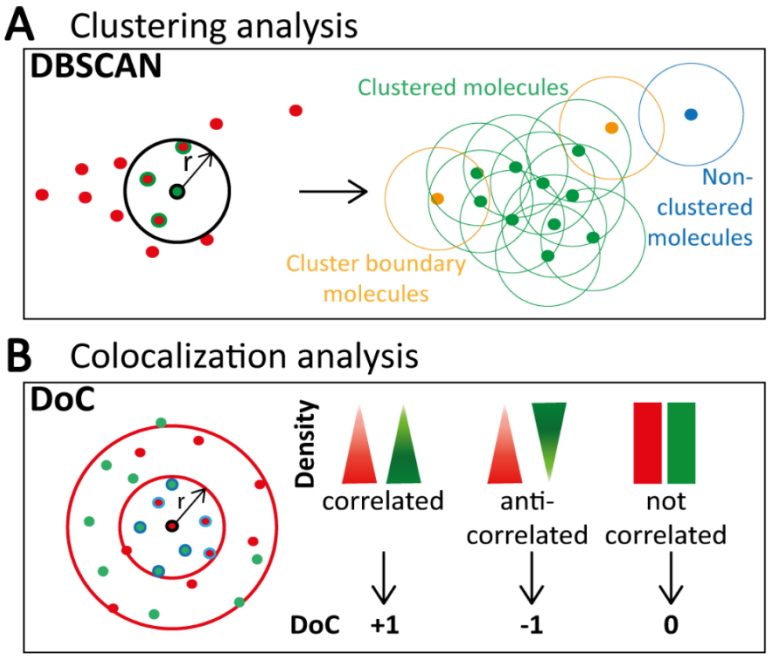


Figure 6.5. A comparison of clustering analysis and colocalisation analyses.

Clus-Doc begins with identifying clustered proteins using a defined radius (A). After this clustering analysis colocalisaion of clusters are then defined between two channels (B). Taken from Pageon *et al.,* (2016).

6.1.9 Studying apoptosis

After DNA damage, cells have the potential to enter apoptosis. If the MVI motor domain is required for the cell to respond to DNA damage, then by inhibiting it, a change in apoptosis signals may occur. This type of change can be measured through the exposure of phosphatidylserine at the outer cellular membrane. This protein is normally embedded on the inner leaflet of the plasma membrane, however as a cell undergoes apoptosis, scrambalase, a translocating enzyme, flips the phospholipid to the outer surface of the cell which in a mammalian organism, would lead to macrophage engulfment of the cell (Mariño and Kroemer, 2013).

This presentation of phosphatidyl serine allows for the measurement of apoptosis. To measure the abundance of this molecule, a fluorescently labelled protein, annexin V, can be utilised as a reporter, where annexin V binds to this phosphatidyl serine, changing its conformation leading to an increase of fluorescence (Kapty *et al.,* 2012) . This is a common protocol where the reagents can now be purchased commercially.

6.1.10 The aims of this study

Now that it is know that MVI localisation changes throughout the cell in response to DNA damage and that whilst it does not change the transcription of DNA damage response genes it does change its interactions, so that MVI interacts directly with DNA damage response proteins after damage. To identify the role it may have in the DNA damage response and in particular DSBs, microscopy techniques have been implemented to identify if the MVI co-localises with DSBs, if it has an involvement in the DNA damage signalling the repair of DNA damage, and if the MVI is found within the repair foci, or alters the apoptosis pathway of the cell.

6.2 Results

6.2.1 MVI inhibited HeLa, respond to DNA damage.

After identifying that MVI binds to DNA damage, and DSB proteins through studying the MVI interactome, the next step was to observe how cells respond to damage if MVI is perturbed. As it has previously been shown that the motor activity of MVI is needed for transcription (Fili *et al.,* 2017), and so it may be required for the DNA damage response.

HeLa cells were first grown in non-treated media (WT), media treated with cisplatin; bleomycin, TIP, and Ku55933 (ATM inhibitor) (Figure 6.6). The cells showed background DNA damage in the WT HeLa cells, which is likely due to replicative stress placed on the cells and their innate chromosome instability. The DNA damaging drugs, cisplatin and bleomycin worked as expected, as shown by the increase of γH2AX signals, and the formation of γH2AX foci. The TIP treatment itself does not cause any further damage than the background seen under normal growth conditions. Therefore MVI perturbation does not preclude the cells to damage. As expected, cells treated with the ATM inhibitor, showed no γH2AX signals at all, which is once again expected as there is no damage to cause the phosphorylation of the H2AX histone.

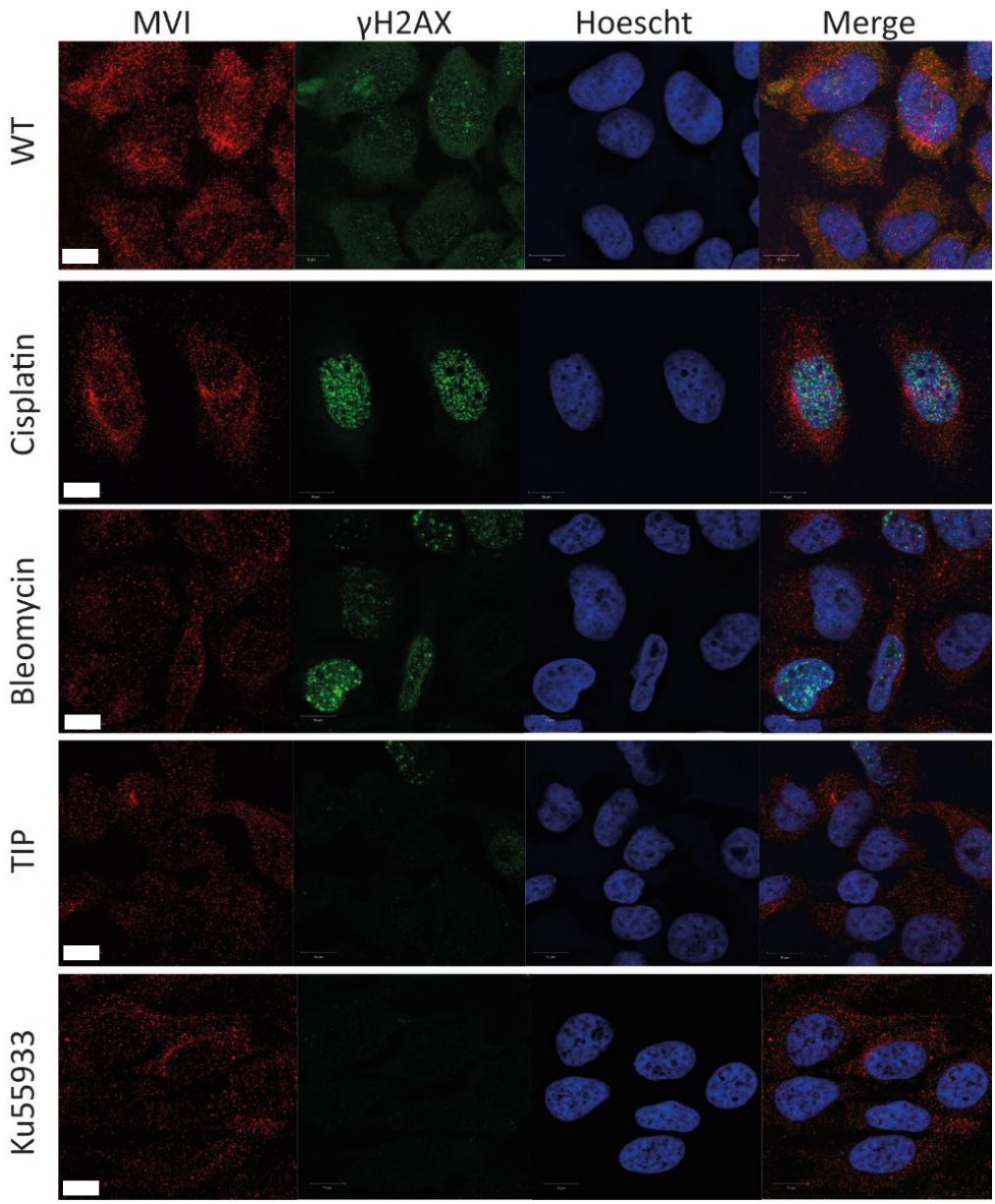


Figure 6.6. Confocal microscopy of HeLa cells with single treatments.

Damage is observed through the increase of γH2AX signal. HeLa cells show no damage by the two inhibitors used during this study. Scale bar =10µm

When HeLa cells have been treated with a combination of the TIP inhibitor and DNA damaging drug, or Ku55933 and DNA damaging drug there are no changes in the expected phenotype (Figure 6.7). The samples are still able to signal DNA damage after the MVI motor domain has been inhibited. Whereas, agreeing with previously published work, the cells are

unable to signal DNA damage using γH2AX when Ku55933 has been used, as this inhibits the ATM, and so the phosphorylation of the histone.

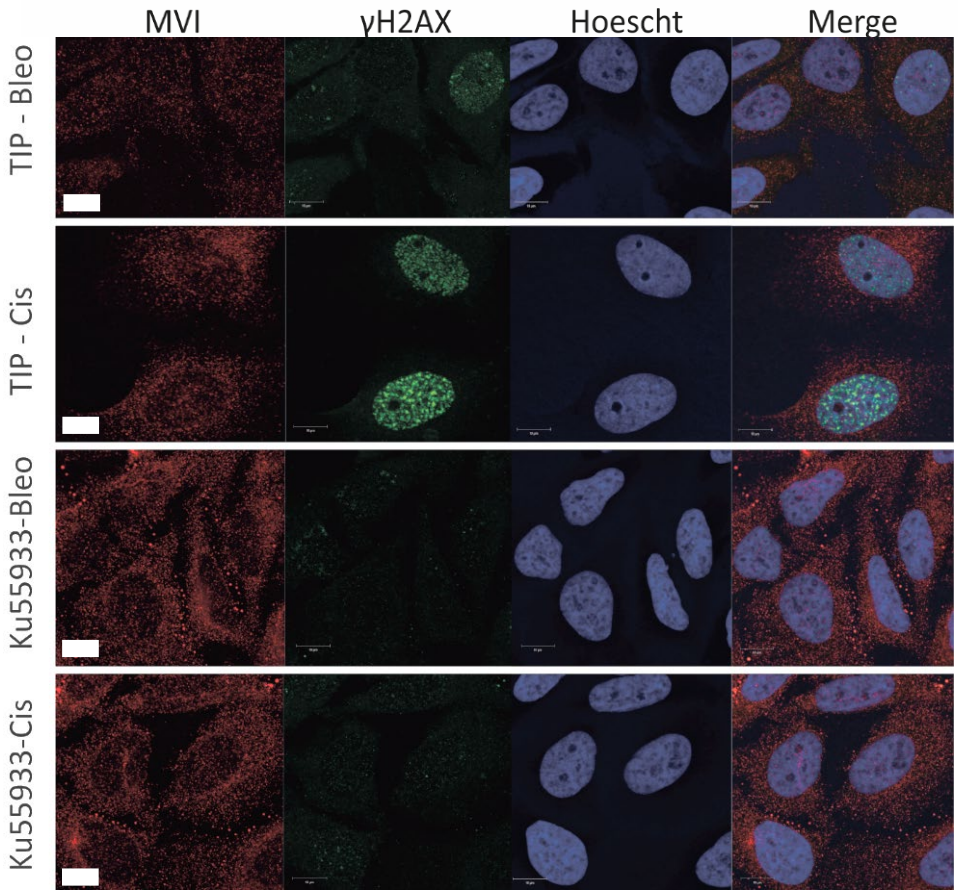


Figure 6.7. Confocal microscopy of HeLa cells with double treatments.

Damage is observed through the increase of γH2AX signal when MVI has been inhibited by TIP. The Ku55933 inhibitor functioned as expected and inhibited γH2AX signalling after DNA damage. Scale bar =10µm.

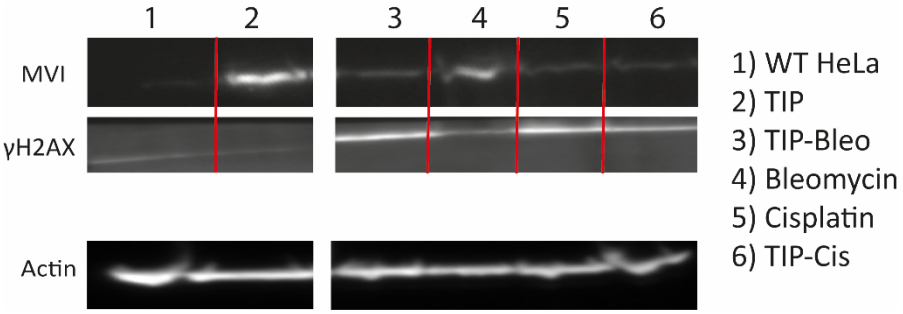


Figure 6.8. A western blot of DNA damage proteins in HeLa.

The western blot shows an increase in γH2AX levels within all of the samples treated with a DNA damaging agent. However the MVI levels are not consistent.

When using the MVI inhibitor TIP, the HeLa cells do not activate their DNA damage response, as is expected, as the TIP itself should not create any DSBs. When cells have been treated with both the TIP and the DNA damaging agents, the cells were still able to produce the γH2AX signal, as well as produce repair foci seen by clustering of the γH2AX.

As expected the ATM inhibitor Ku55933 is capable of inhibiting the DSB response caused by cisplatin and bleomycin. The inhibitor here shows reduced γH2AX after treatment with DNA damaging agents (Figure 6.7).

To compliment the microscopy western blots were performed. There are increases in γH2AX signals when cells are either treated with bleomycin and cisplatin compared to the WT γH2AX amount. When using a DNA damaging agent with TIP there are similar increases in the western blot, which agrees with the images (Figure 6.7).

As well as this MVI amounts increase in all conditions compared to the WT. As shown in the RNA-seq data the expression profile of MVI does not change after DNA damage, this suggests that after DNA damage MVI becomes far more stable, possibly through its interactions, inhibiting degradation of the protein. Even the TIP treatment itself causes an increase of MVI amounts within the sample, which could be due to to the inability of the cell to mark it for degradation due to the motor domain being blocked by the presence of the inhibitor, however further experiments would be required to understand this mechanism. However this would require further work to fully quantify the amounts. Due to the variability of this western blot, especially within the amounts of MVI between samples, high content screening was further undertaken within this study to provide statistical measurements.

6.2.2 The motor activity of MVI is required for DNA damage signalling in MCF10A cells.

As the HeLa cells showed no difference in DNA damaging signalling when the motor capabilities of MVI had been inhibited, this study then looked at the non-cancerous, genomically stable cell line to ensure that both responded in a similar manner. Firstly, MCF10A cells respond similar to HeLa, as, when there is DNA damage an increase of γH2AX occurs, and once again using TIP and Ku55933 does not causes γH2AX signalling (Figure 6.9).

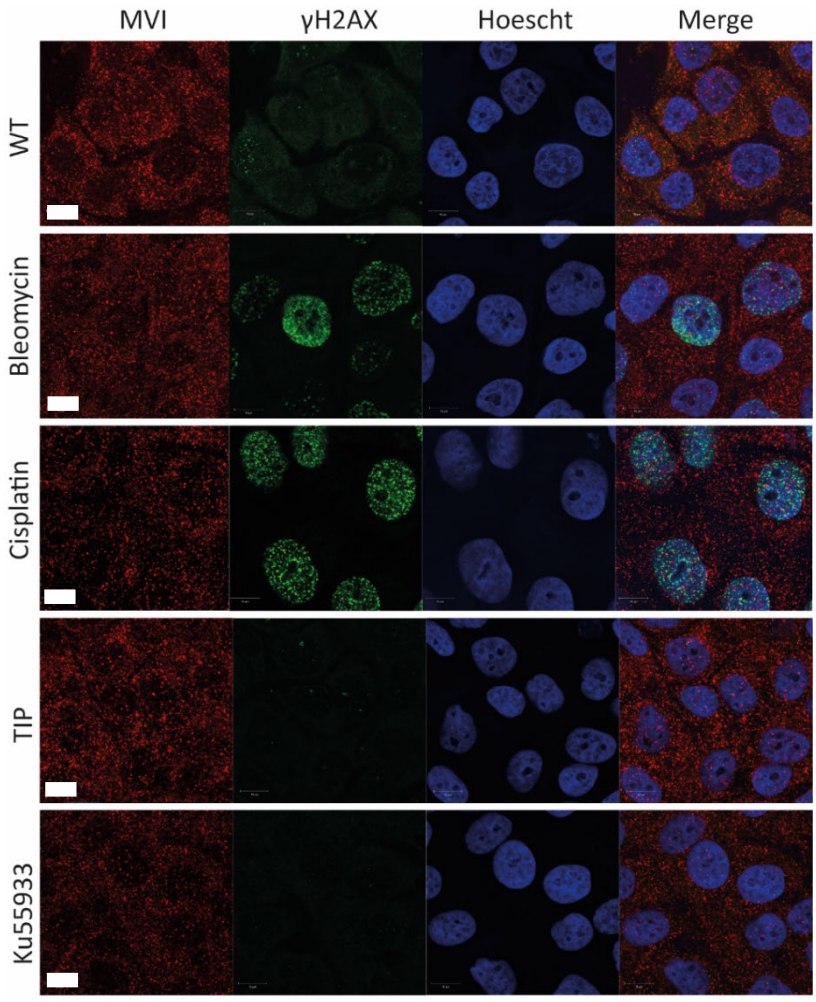


Figure 6.9. Confocal microscopy of MCF10A cells with single treatments.

As expected there is an increase of γH2AX signals after cells are treated with cisplatin and bleomycin. Whilst the inhibitor treatments, TIP and Ku55933 do not cause DNA damage alone. Scale bar =10µm.

If however, the cells are treated with a combination of the DNA damaging agents and TIP, then the cells lack the γH2AX signal for DSBs (Figure 6.11).

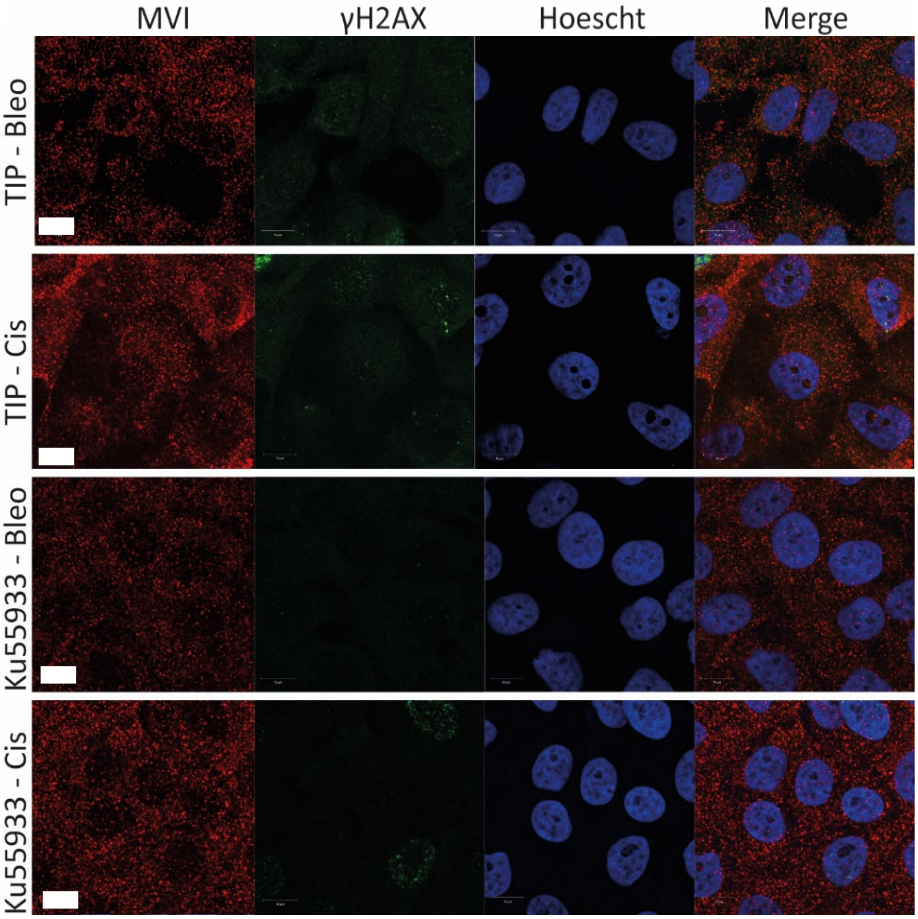


Figure 6.11. Confocal microscopy of MCF10A cells after double treatments.

When cells are treated with both TIP and a DNA damaging agent, the cells exhibit little γH2AX staining. The Ku55933 with DNA damaging agents, also show less γH2AX compared to DNA damaging drug treatments on their own. Scale bar = 10µm

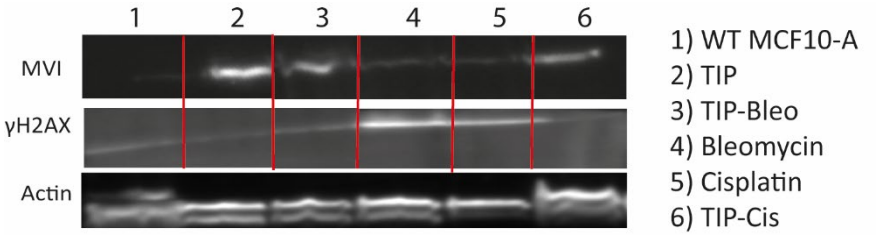


Figure 6.10. A western blot of DNA damage proteins in MCF10A cells.

The western blot shows that there are basal levels of γH2AX within the WT and TIP treated cells, after DNA damage drugs are used there is an increase of γH2AX. Yet when a DNA damaging agent with TIP was used there was no increase in γH2AX signal. However there is large variation in the western blot within MVI.

This lack of γH2AX, was then checked using western blot. After cisplatin and bleomycin treatment, the intensity of the γH2AX bands increase. When the TIP inhibitor has been used the amount of γH2AX reduces to basal levels (Figure 6.10). This agrees with the images that after treating cells with a DNA damaging agent and TIP there is a reduction of γH2AX signalling. Once again the MVI levels varied between samples, therefore due to this variation and the fact the proteins amounts are not quantifiable using western blot, HCS was utilised further on in this study (Figure 6.10).

6.2.3 MVI is capable of entering the nucleus of HeLa cells after TIP treatment.

To further understand if MVI is required for DNA damage signalling in both the HeLa and MCF10A cell lines, and due to the western blot variation, HCS was utilised. This type of screening using immunofluorescence ensures any observations made during confocal microscopy is happening across the whole sample and most importantly is quantifiable. It also allows for the identification of localisation of proteins. When studying the localisation of MVI, a mask was created that contained the whole nucleus known as the circle mask. Once this mask had been designed to fit suitable nuclei, a second mask was created. This mask was designed to identify if the population in the immediate area on the external side of the nuclear membrane has a change in MVI signal intensity as done in the previous chapter (Figure 6.12). This would allow for the comparison of MVI population inside the nucleus and at nuclear membrane.

γH2AX signals were analysed in a different manner. As the γH2AX signals for DSBs are always nuclear the circle mask was designed to fit the majority of the nucleus, leaving only the periphery of the nucleus to be mapped using the ring mask (Figure 6.12 B). This type of analyses shows if there is any preference for the histone modifications to reside at the nuclear periphery, often where euchromatin can be found, or within the nuclear centre, favoured by heterochromatin formation. Once all the masks had been designed the

fluorescence intensity of each mask was measured globally, with any imaging variables fixed, to allow for direct comparisons between samples.

In the HeLa cell line, there is no distinguishable difference of the DNA damage response with and without the use of TIP. When cells are treated with the motor domain inhibitor of MVI, less MVI can be found at the external side of the nuclear membrane, however the amount of MVI found within the circle mask, the nucleus, remain at the basal level. As expected after treatment of HeLa cells with bleomycin both the amount of MVI within nucleus increases by 2.4 fold. This data confirms the observations previously made about the MVI responding to DNA damage. However with the addition of TIP the levels of MVI still increase within the nucleus after DNA damage similar to that of drug treatment on its own by 3.1 fold.

The γH2AX levels follow the same pattern as the MVI levels, where there is an increase after bleomycin treatment, by 2.8 fold, and when the cells are treated with both the inhibitor and drug also by 2.8 fold. Interestingly there was no preference of γH2AX localisation either at the nuclear periphery or interior showing that the damage occurring is not specific to euchromatin or heterochromatin and the formation of repair foci can occur across the whole of the nucleus rather than at specific locations. Albeit, based upon 2D analysis.

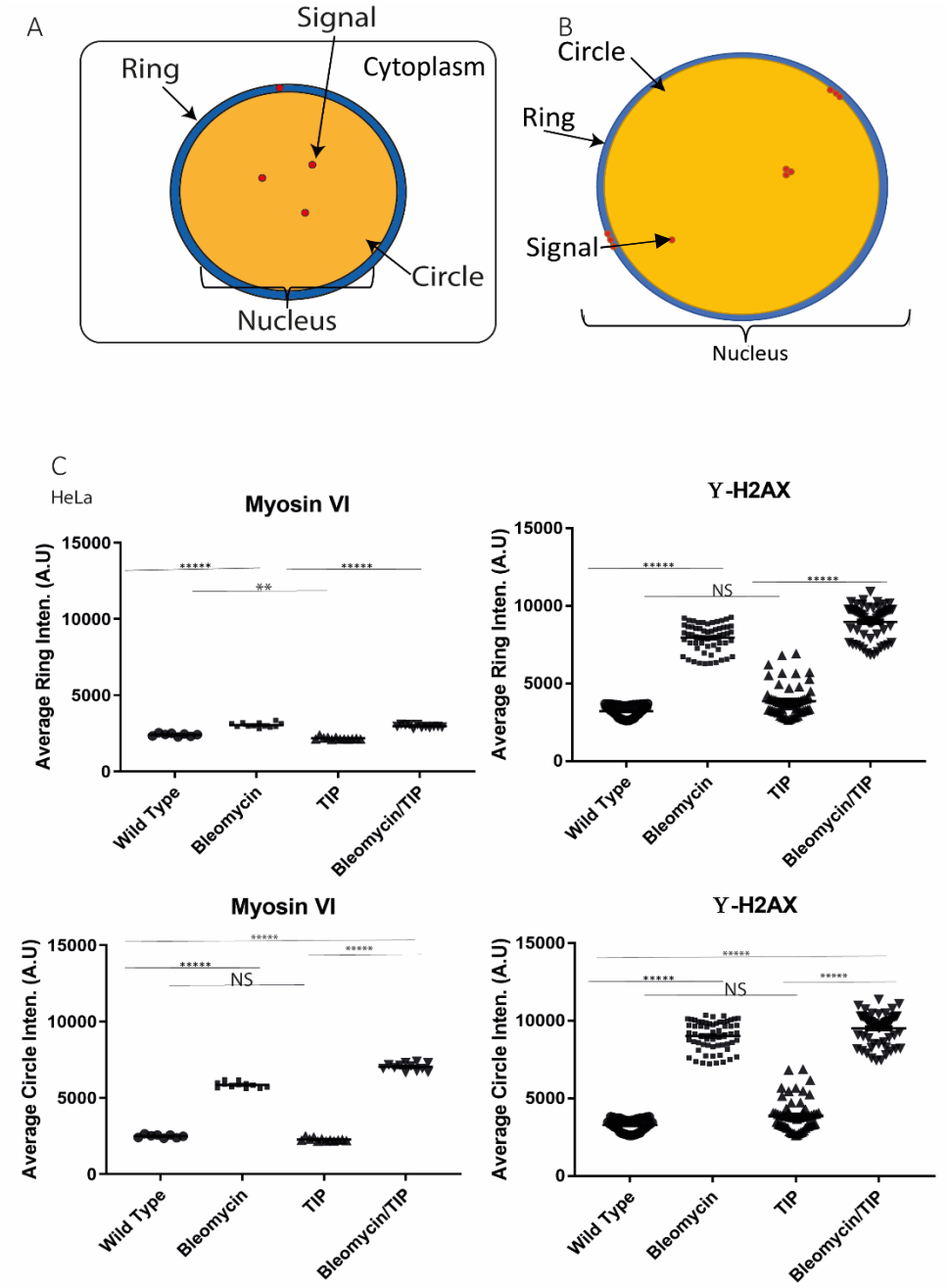


Figure 6.12. HCS of HeLa cells.

HCS analysis allows the making of masks defined as ring and circle. When studying MVI localisation the ring was placed just outside of the nucleus whilst the circle was the entire nucleus (A). When studying γH2AX localisation the nuclear periphery was analysed using the ring and the nuclear interior was analysed using the circle (B). The amount of fluorescence intensity was measured with fix capture settings and compared between conditions. Here MVI increases alongside γH2AX levels in both bleomycin treatments (C). Each data point is an average of 1,000 nuclei and the conditions were compared using an ordinary one-way ANOVA with Sidaks multiple comparisons test. ****** signify a $p<0.0001$ and ** signify a $p<0.001$. N=2

6.2.4 MCF10A cell line requires MVI for phosphorylation of H2AX.

After observing a lack of H2AX phosphorylation after TIP treatment, as shown in the confocal images, HCS was employed to ensure the observations could be supported statistically. Like with the HeLa samples, two masks were created the ring and circle, using the exact parameters used for the previous analysis. To fully fit the nuclei, a mask is created that uses the hoescht DNA dye signal, for the formation of a mask that has a round score of above 0.6. This means as many of the nuclei are quantified allowing for their diverse shapes. The ring, which can be classified as the nuclear periphery is so designed that from the masks periphery a 0.1µM edge is created. In the case of MVI this ring was created 0.1µM away from the hoescht mask, whilst in the case of histone modifications this ring was created 0.1µM inside the hoescht mask. This allows some separation of signals from being in the case of MVI on the outside of the nucleus and for histone modifications, residing near the nuclear periphery.

The first observation is similar to that found in HeLa, where after bleomycin treatment for four hours, there is a significant increase of MVI within the nucleus by 1.3 fold and a significant reduction of MVI surrounding the nucleus. Interestingly the TIP treatment reduced the amount of MVI within the nucleus and the surrounding area by 0.3 fold. The amount of γH2AX directly corresponds with the amount of MVI inside the nucleus. Where drug treatment increases the amount of γH2AX, 2.1 fold, and this coincides with the increase of MVI (Figure 6.13). Whilst the fold increase of MVI is lower than that of in HeLa, the average intensities in the WT conditions differ in HeLa and MCF10A, 2493 A.U and 4636 A.U respectively, suggesting that MCF10A cells maintain a higher basal level of MVI within their nuclei.

If there is however little MVI inside the nucleus and the motor domain is inhibited there is the same amount of γH2AX signal found as the basal level within the WT cells. Therefore it

is proven that the motor domain of MVI is vital for the phosphorylation of H2AX and the formation of γH2AX signalled repair foci.

Once again there is no preference of the γH2AX signals to be found within the nuclear periphery or interior with both masks identifying the same fluorescence intensities within both regions. Implying the damage is occurring throughout the genome and there is no preference for the formation of repair foci (Figure 6.13).

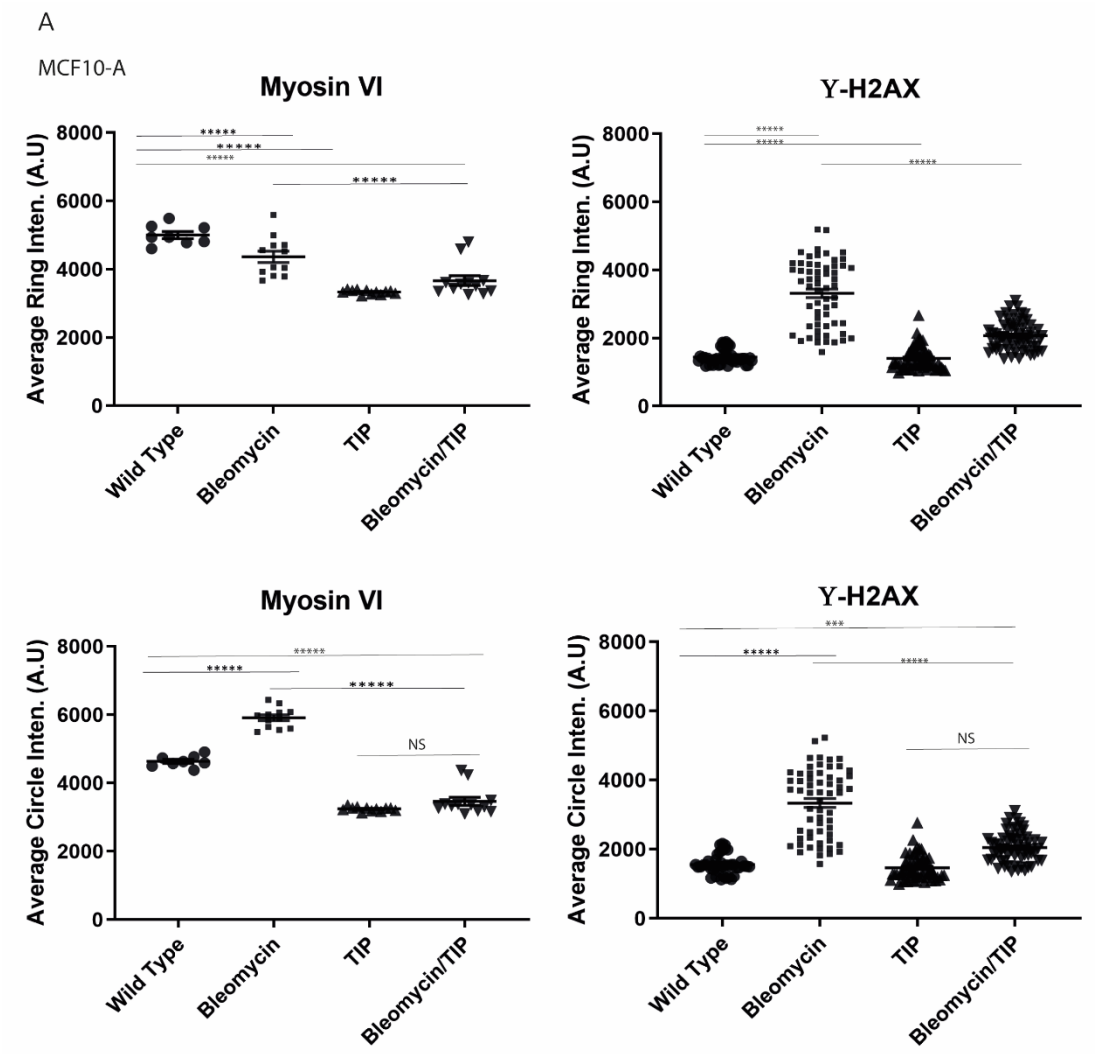


Figure 6.13. HCS analyses of MCF10A cells.

The amount of fluorescence intensity was measured with fixed capture settings and compared between conditions (A). Here MVI increases significantly after bleomycin treatment, however when MVI is inhibited with TIP and then treated with bleomycin the cells there is no significant increase in γH2AX. Each data point is an average of 1,000 nuclei and the conditions were compared using an ordinary one-way ANOVA with Sidaks multiple comparisons test. ****** signify a $p<0.0001$. N=2

6.2.5 MVI inhibition causes a greater change to DNA damage histone modifications than damage itself.

If in MCF10A cell lines MVI is involved in the phosphorylation of H2AX histones, then it could be involved in the two other histone modifications found related to the DNA damage response, the double methylation found on lysine-36 of the H3 histone (H3K36me2) and the single methylation found on lysine-20 on histone H4 (H4K20me). Previously published work identified an increase in H4K20me and a reduction of H3K36me2 surrounding DSBs (Thomas Clouaire *et al.,* 2018).

In both cell lines however this study identified that both modifications increase after bleomycin treatment (Figure 6.14. and Figure 6.15). Using HCS at a 20X magnification as well as drugs that cause DSBs randomly, it is hard to predict if these modifications sit +/- 500bp of a DSB.

Within HeLa cells (Figure 6.14) the H3K36me2 modification became more abundant after TIP treatment compared to bleomycin treatment, with an average intensity increasing from 5869 to 8848. Cells that were treated with both the drug and TIP had similar amounts of H3K36me2 modifications, than the TIP treatment on its own, with average intensities being 9495 and 8848 respectively. This shows that the MVI has a larger role in regulating this histone modification than DNA damage itself. Following the masking of the images with the ring and circle using the same dimensions as the γH2AX analyses, it is clear there is no specific localisation of these modifications, either within heterochromatin or euchromatin and these modifications can occur spread throughout the nucleus. These data suggest MVI may have a wider role in chromosome organisation and chromatin remodelling which will be discussed in Chapter 7.

Whilst TIP has the largest impact on H3K36me2 modifications, when studying the H4K20me modification, its observed that bleomycin causes a similar increase of modification to that of

TIP and TIP bleomycin treatment, with average intensities being 8708, 8286 and 10197 respectively, with the WT having an average intensity of 5042. So whilst there is an increase in methylation on lysine-20 compared to the WT there is no difference between TIP and bleomycin. Once again there is no difference of localisation within the nuclei of this signal, where it is found to be spread across the entirety of the nucleus.

The MCF10A cell lines (Figure 6.15) behaves identical to that of the HeLa, where there is an increase of H3K36 double methylation after bleomycin treatment, of 344 A.U, however there is a larger increase of this modification after cells have been treated with TIP and TIP with bleomycin of 1696 A.U and 1555 A.U respectively, with the two TIP treatments not being significantly different from each other. H4K20me levels also increase after bleomycin treatment by 475 A.U, however TIP can cause a similar increase of 698 A.U, and the TIP with bleomycin treated cells have no significant difference in the amount of single methylation on H4K20 than the other drug conditions. Overall there is no preference of localisation of these signals as shown by the same amount of fluorescence being identified in both masks. This impact on DNA damaging histone modifications, shows that the impact MVI has on γH2AX signalling within MCF10A cells, has a broader effect when it comes to a global response to damage and chromatin remodelling.

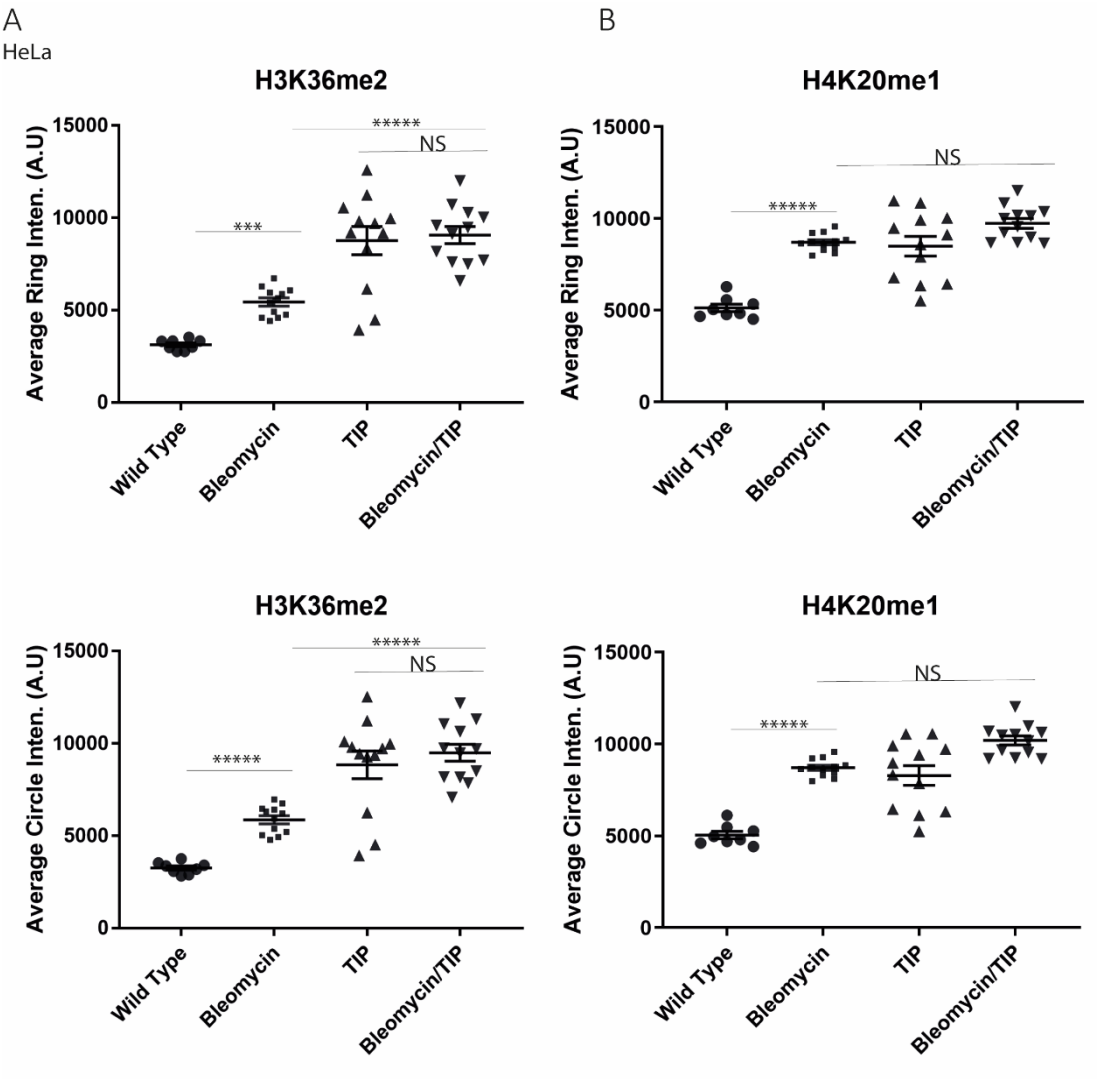


Figure 6.14. HCS analyses of DSB histone modifications in HeLa.

The amount of fluorescence intensity was measured with fix capture settings and compared between conditions (A). Each data point is an average of 1,000 nuclei and the conditions were compared using an ordinary one-way ANOVA with Sidaks multiple comparisons test. ****** signify a $p<0.0001$. N=2

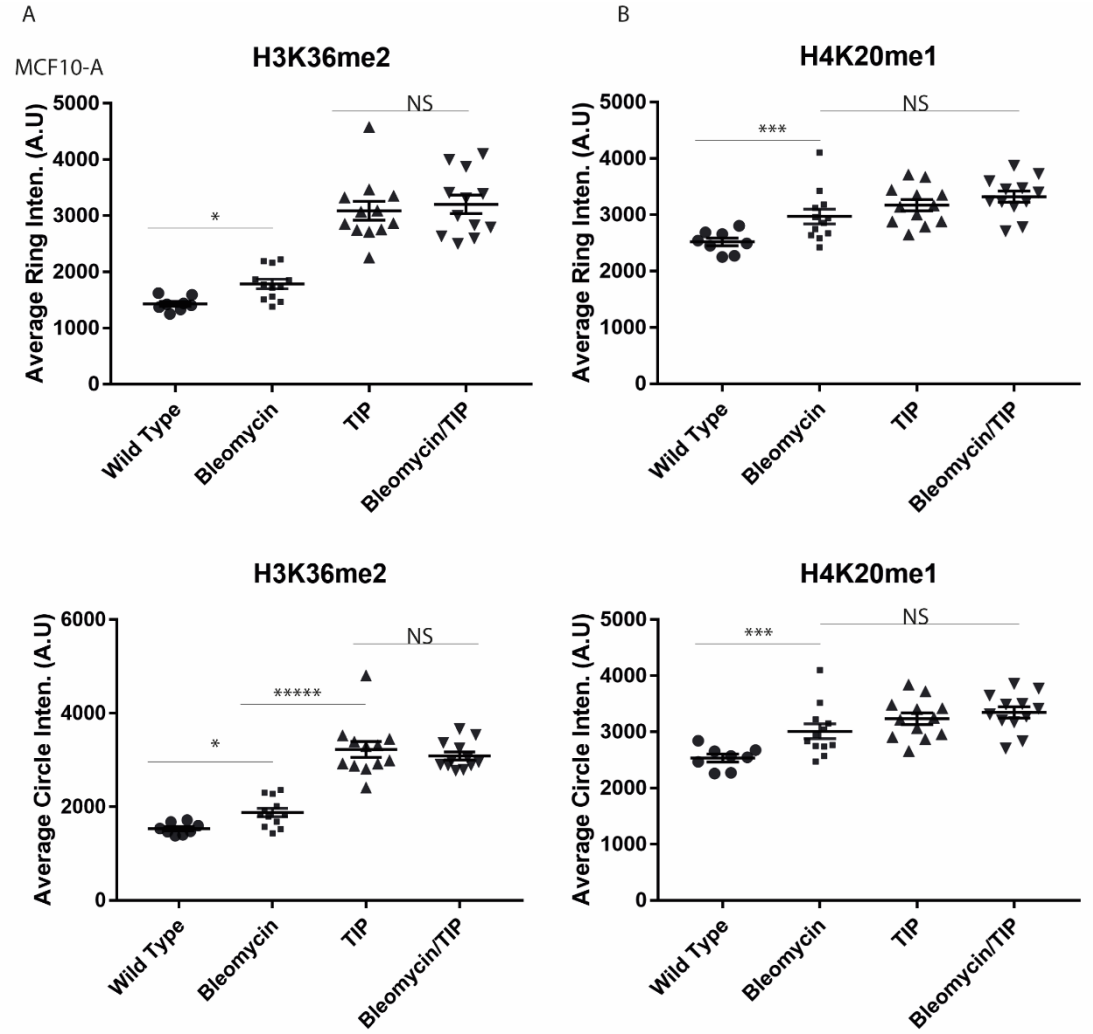


Figure 6.15. HCS analyses of DSB histone modifications in MCF10A cells.

The amount of fluorescence intensity was measured with fix capture settings and compared between conditions (A). Each data point is an average of 1,000 nuclei and the conditions were compared using an ordinary one-way ANOVA with Sidaks multiple comparisons test. ****** signify a $p<0.0001$. N=2

6.2.6 Using Clus-DoC for data analysis on MCF10A cells.

There is a clear difference of how MVI responds to DNA damage between the cell lines with MCF10A cells requiring a functioning motor domain of MVI to produce γH2AX signals and HeLa not, due to this difference the next study focused solely on the MCF10A cell line. To understand if MVI can be found at sites DNA repair, STORM imaging was carried out and then analysed using the Clus-Doc analysis software (Pageon *et al.,* 2016). This study has already shown that MVI responds to DNA damage by changing its protein-protein interactions, and by using the motor domain inhibitor TIP, the MCF10A cells are unable to import MVI into the nucleus and signal DNA damage using γH2AX. To gain insight into why MVI is required, the next step is to identify where MVI is found precisely within the nucleus, its organisation and if it is found colocalised with γH2AX after DNA damage.

The process of analysing STORM data is shown in Figure 6.16. Firstly cells are imaged using epifluorescence, this allows identification of a cell without the need of high power lasers. The cells are then imaged following the STORM technique under HiLo illumination, allowing the identification of single molecules, the nucleus is then specified within the Clus-DoC analysis software. Once the region of interest has been determined, the software provides an average Ripley K result for each single molecule as shown in figure 5.2.11 C. This provides information of the average radius of a cluster of molecules with the maximum amount of molecules within that radius. If a Ripley K value of less than 0 occurs, each single molecule is functionally separate and they deliberately do not cluster. If the Ripley K value is 0 there is complete random clustering and if it is above 0 then the molecules have a tendency to cluster (Stoyan and Stoyan, 1994). Once all of the single molecules have been mapped (Figure 6.16 D), clusters, that contain a minimum of five molecules, are then plotted (Figure 6.16 E). From this data it is possible to learn if the molecules cluster, the size of the cluster and how many

molecules can be identified in one cluster. As an example a histogram of the number of MVI molecules in a single cluster within the nucleus has been shown in Figure 6.16 E.

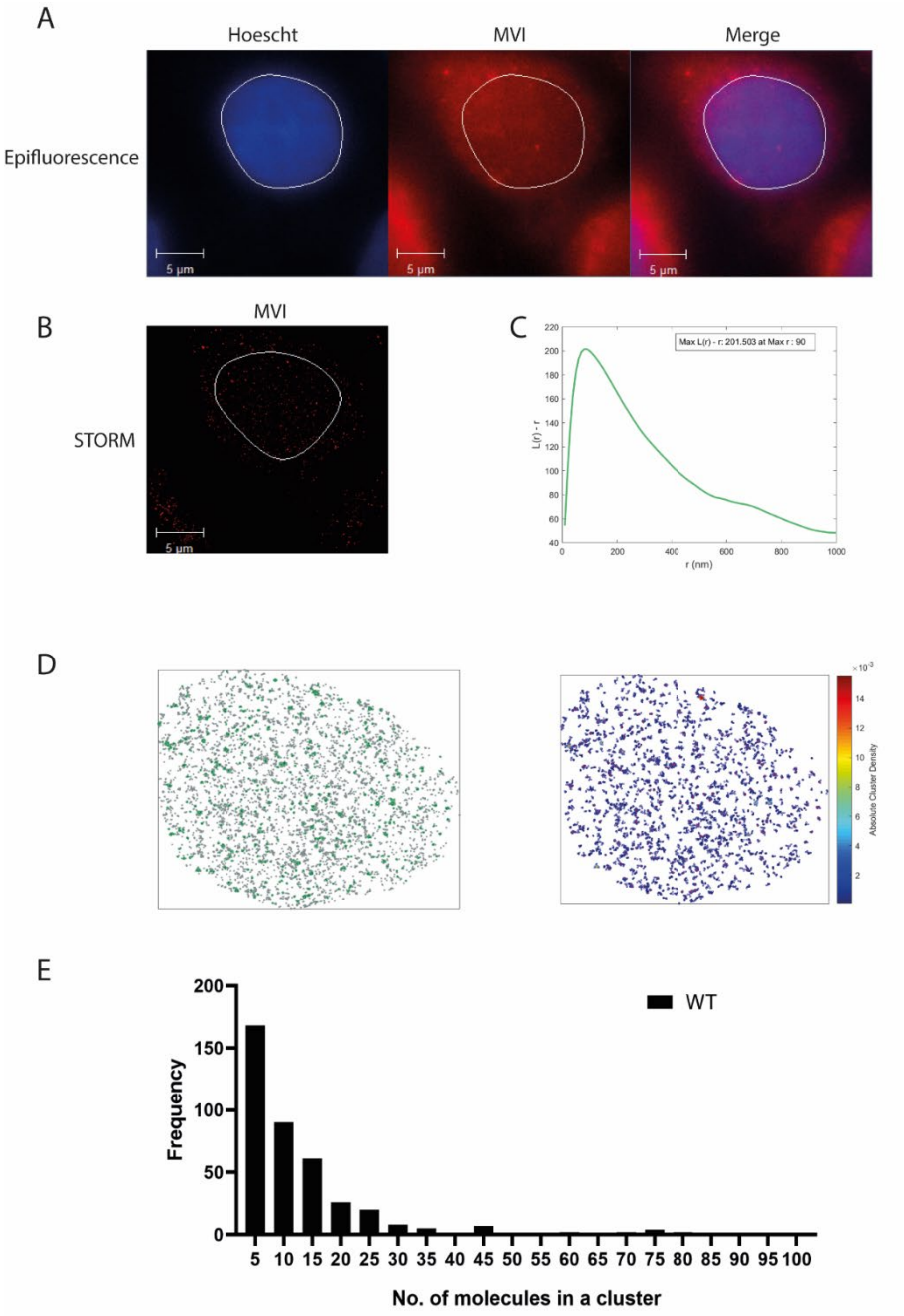


Figure 6.16. A workflow of Cluster analyses.

STORM and cluster analysis was performed on MCF10A cells. Cells are first imaged using epifluorescence (A) and the nucleus is defined. STORM imaging is then completed (B) and the average Ripley K function is defined for all molecules (C). Maps of all molecules are then produced followed by a cluster map, where the high absolute cluster densities are marked red and molecules with low density are blue (D). The clusters can then be binned by

6.2.7 MVI forms larger clusters after DNA damage in MCF10A cells

MVI molecules are equally likely to cluster before and cisplatin damage. The Ripley K function has shown that MVI is likely to have a clustered formation rather than a random distribution around the nucleus (Figure 6.17). DNA damage itself does not change MVIs probability of clustering compared to WT cells as shown by a similar maximum r value of 100.

Whilst the likelihood of clustering is unaffected the Ripley K value itself does not provide any detailed information on the clusters themselves. The number of MVI clusters after DNA damage reduces significantly compared to the WT cells, with the average number of clusters of MVI in a WT nucleus being 442, and after DNA damage the average number of clusters is reduced to 87. Whilst the number of MVI clusters reduces after DNA damage, the clusters that do exist are larger with an average of 51 molecules, compared to undamaged cells that contain on average 22 molecules. This shows that whilst the number of clusters is reduced there are overall larger clusters. This is supported by the increase of the actual size of clusters where before damage, MVI clusters within the nucleus, on average have an area of 2008nm^2, whereas after DNA damage this area increases significantly to an average of 3266nm^2.

This data shows that DNA damage causes a reduction in the number of MVI clusters inside the nucleus, however this reduction is due to the increase of cluster size and the number of molecules within a cluster, showing that MVI molecules are likely to aggregate together and it is possible this aggregation is required for correct DNA damage signalling. As this study has shown MVI has multiple roles within the nucleus, this switch of clustering could be MVI being diverted from its role in transcription to repair sites. It is known activated ATM inhibits transcription (Jang *et al.,* 2010), this could allow this switching of roles to take place, freeing the MVI from the transcription machinery.

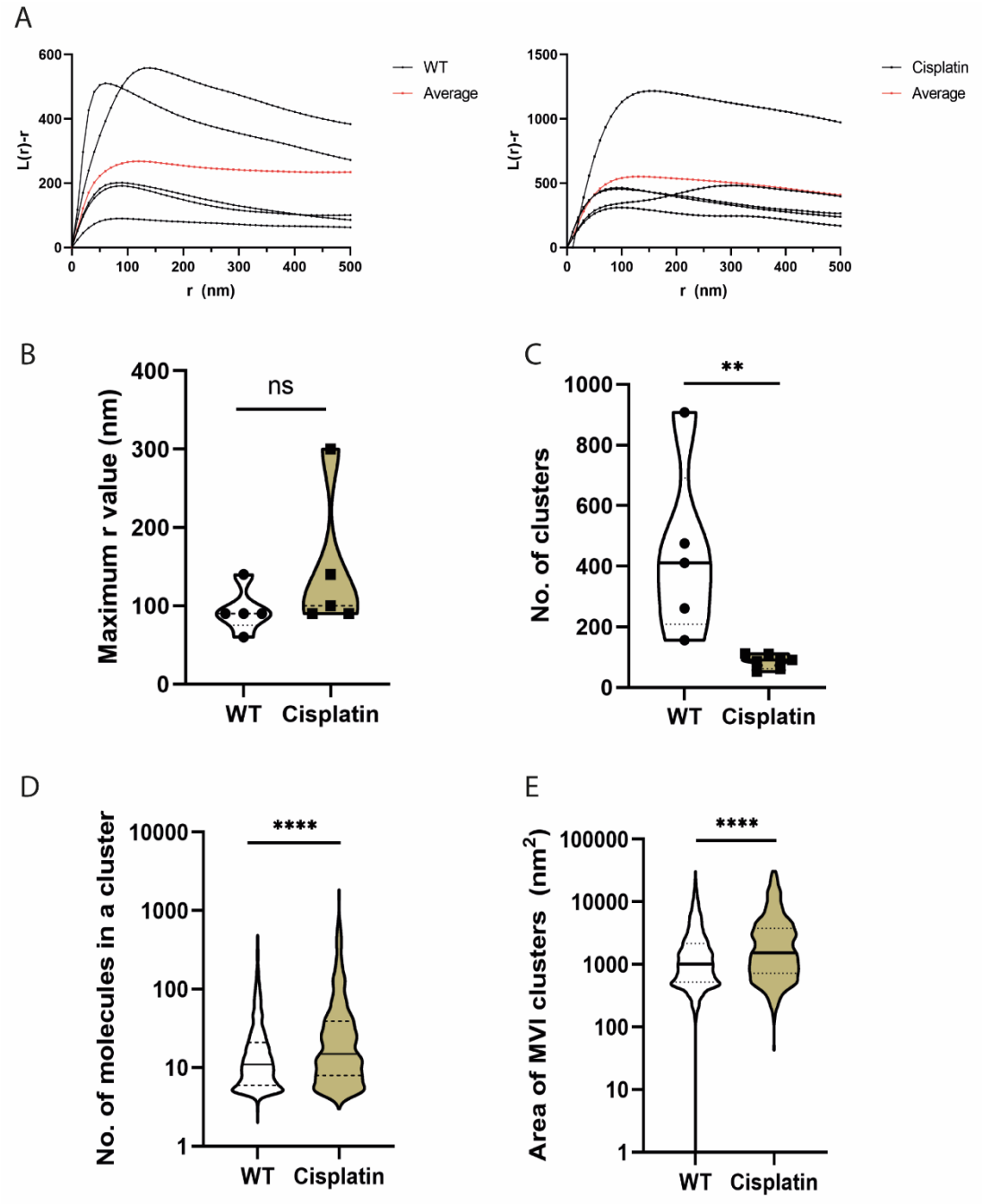


Figure 6.17. The effect of cisplatin on MVI nuclear clustering.

STORM and cluster analysis was performed on MCF10A cells. An average of Ripley K functions was calculated per molecule per cell which identifies the likelihood of molecules clustering (A). This can be defined by the maximum radius between two molecules (B), which shows no variation of MVIs chance of clustering after damage. The number of clusters drop significantly after DNA damage (C) however the number of molecules in these clusters increase (D) along with the total area of the clusters (E). A students T-test was carried out to confirm significance where ** represents $p<0.01$ and **** $p<0.0001$. N=2

6.2.8 Clus-DoC provides information on the colocalization of protein clusters in MCF10A cells

To identify if MVI is colocalising with γH2AX or if it can be found within repair foci, Clus-DoC analyses was completed on the nuclei of cells as before, however this time both channels were taken into account and analysed.

Firstly the software overlays each channel, allowing for the visualisation of MVI and γH2AX single molecules (Figure 6.18 A), next each molecule is defined if it is within a cluster or not (Figure 6.18, B and Figure 6.18 C), similar to that shown when studying just MVI clusters. The two channels are then overlaid onto each other providing information of the amount of MVI clusters that colocalise with γH2AX clusters (Figure 6.18 D) and vice versa the clusters of γH2AX that colocalise with MVI clusters (Figure 6.18 E).

This type of analysis will provide information on how MVI and γH2AX interact with each other and if they have any colocalization at all.

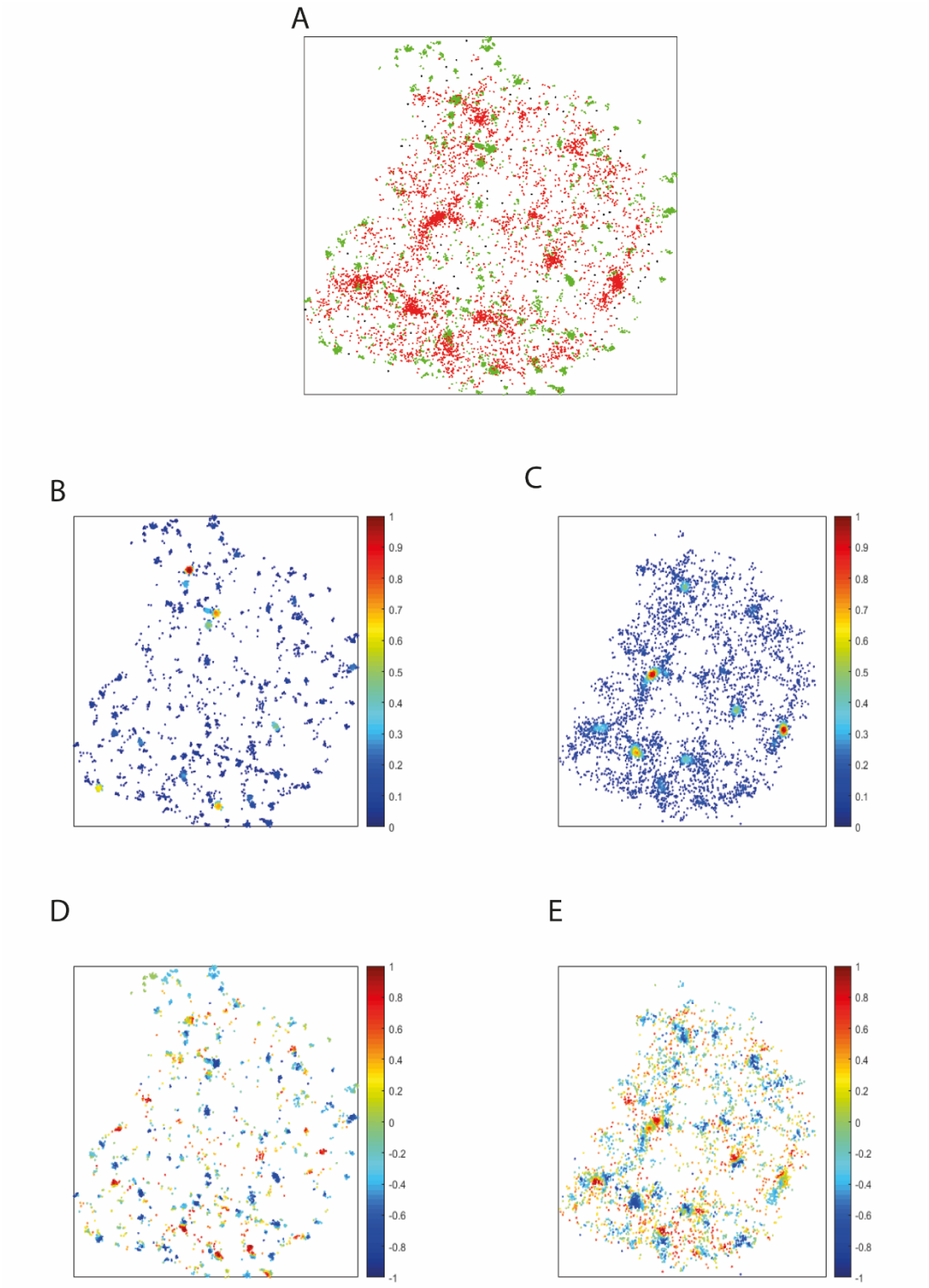


Figure 6.18. A work flow of DoC analyses.

STORM and cluster analysis was performed on MCF10A cells. The clusters of both MVI (green) and γH2AX (red) can be mapped onto each other (A). Then the clusters are defined by their normalised scores 1 is highly clustered, 0 is no clustering for MVI(B) and γH2AX (C). Finally the two cluster maps can be overlaid and scored where 1 is colocalisation and -1 is functional separation. This is done where MVI is overlaid onto γH2AX clusters (D) and γH2AX is overlaid onto MVI clusters (E).

6.2.9 γH2AX clusters vary within the nucleus in MCF10A cells.

As discussed previously the phosphorylation of the H2AX histone on the serine-139 occurs as close to the point of a DSB as possible, from this point the signal then spreads along other H2AX histones spread throughout the chromatin (Firsanov, Solovjeva and Svetlova, 2011) . With cisplatin causing nonspecific DSBs there can often be overlapping of these distal signals as well the formation of large repair foci which can be seen by the large clustering of γH2AX signals (Figure 6.19).

It has been observed that cisplatin treatment leads to clustering of γH2AX molecules in small clusters of around five to ten molecules, this clustering does not imply large formation of repair foci but small signals at the points of damage, however whilst the majority of γH2AX is found at these small clusters, there are some clusters that can be far larger with some as large as 1000 molecules in a cluster (Figure 6.19).

The area of these clusters differ significantly as well, the clusters can range from an area of approximately $5nm^2$ to the largest being observed as large as approximately $1\mu m^2$ which is a substantial part of the nucleus. Finally the number of clusters observed between nuclei vary after cisplatin treatment. This can be expected as depending on the drug uptake of the cell and the cell cycle stage it is in, can affect the damage caused by cisplatin. On average a nuclei has 18 clusters of at least 5 γH2AX molecules, however cells were observed to have up to 60 clusters of γH2AX, it is possible that nuclei with this larger amount of γH2AX would be at the beginning of apoptosis.

6.2.10 MVI clustering increases around areas of dense γH2AX in MCF10A cells

To identify if MVI clusters and γH2AX clusters colocalise the two channels were analysed using Clus-DoC which provides a degree of colocalisation (DoC) score. If this score is above 0 then there is definite clustering of the two proteins, if the score is 0, then there is no clustering between the two protein clusters and if the score is less than 0 then the clusters are functionally separate to each other (Pageon *et al.,* 2016) .

When the clusters of MVI are overlaid onto the γH2AX clusters the average DoC score is 0.147 showing that on average the clusters of MVI are deliberately apart from γH2AX clusters and is not due to random distribution of clusters (Figure 6.19). The same can be said when the γH2AX clusters are overlaid onto MVI clusters where the average DoC score is -0.121, where on average the clusters are within an area that MVI is not.

However whilst the DoC scores are below 0 for both proteins, if each cluster is looked at individually then more information can be obtained. The average number of MVI clusters that colocalise with γH2AX clusters is significantly smaller than the number of MVI clusters that do not colocalise, with an average of 9 and 46 clusters per nuclei respectively. This shows that the majority of MVI clusters are not found near γH2AX. There is however no significant difference between the number of γH2AX foci that overlap with MVI clusters and those that don't, with an average of 3 and 12 clusters respectively (Figure 6.19).

The number of molecules of MVI within clusters that are categorised as colocalised with γH2AX clusters is significantly higher than the number of molecules in non-colocalised clusters, with an average of 287 molecules and 45 molecules respectively. The average number of molecules of γH2AX that colocalises with MVI however does not significantly differ between colocalised clusters and non-colocalised clusters, with an average of 332 and 59 molecules respectively. This shows that there are a similar amount of molecules in clusters that do colocalise with MVI than do not, yet there are more MVI molecules per colocalised

cluster. This is interesting as when there is colocalisation between the two proteins the clusters of MVI are far larger, compared to when MVI clusters are on their own there are far less molecules.

This is supported by the fact that colocalised clusters of MVI have a much larger area on average than those that are not colocalised, their areas on average are 11766nm^2 compared to the non-colocalised MVI cluster area being 3687nm^2. The same can be observed with the average size of γH2AX foci. When γH2AX clusters are found with MVI nearby there area on average is 14705nm^2 compared to the average size of non-colocalised clusters being 2762nm^2. This shows that the two protein only colocalise when the clusters are of a large enough size, and when there are small clusters of either proteins they are kept functionally apart from each other (Figure 6.19). This implies MVI is part of multi break foci, creating repair factories, around the points of damage, but not at the diffuse γH2AX signals, as shown in Figure 6.19.

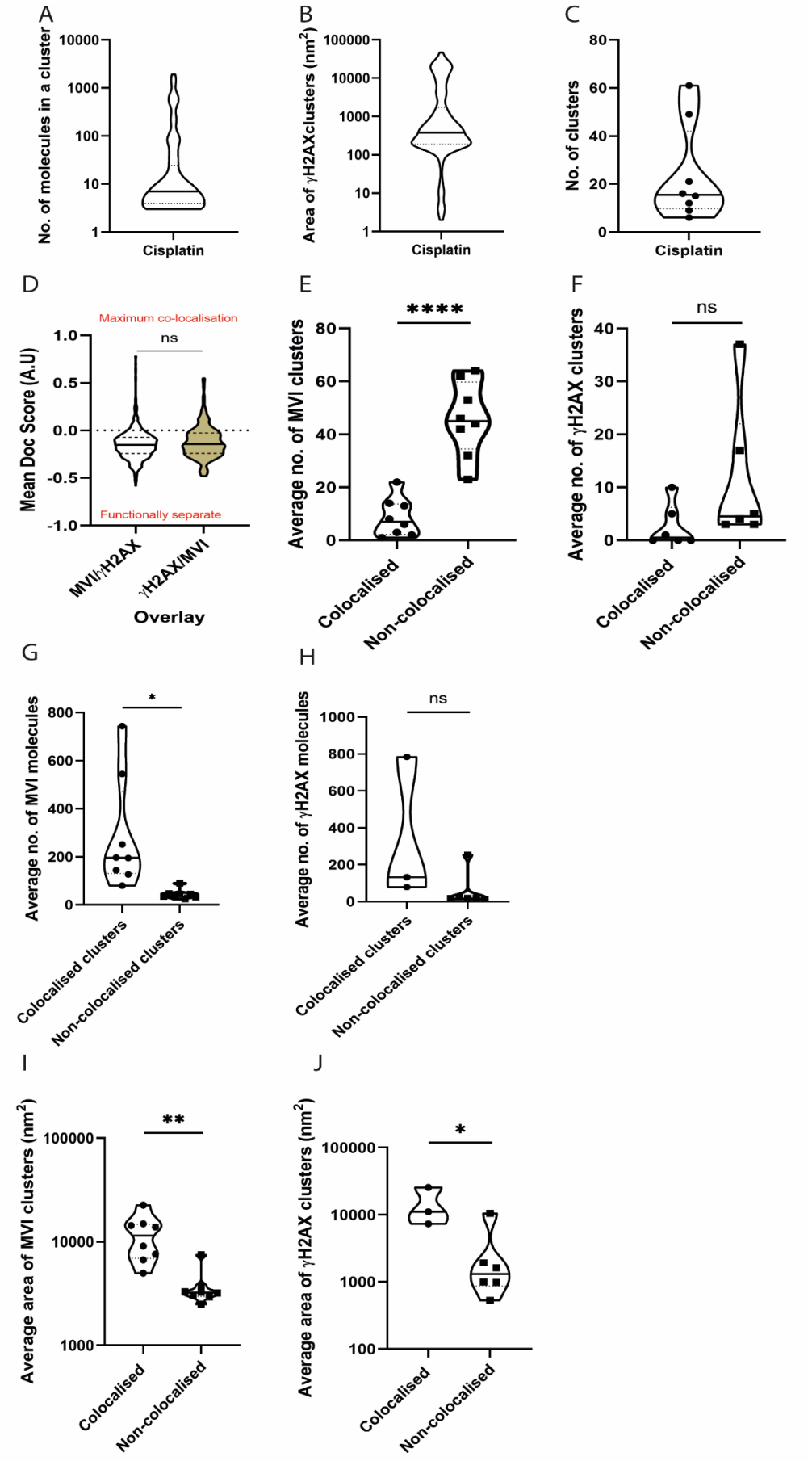

A
No. of molecules in a cluster
10000
1000
100
10
1
Cisplatin
B
Area of γH2AXclusters (nm²)
100000
10000
1000
100
10
1
Cisplatin
C
No. of clusters
80
60
40
20
0
Cisplatin
D
Maximum co-localisation
ns
Mean Doc Score (A.U)
1.0
0.5
0.0
-0.5
-1.0
Functionally separate
MVI/γH2AX
γH2AX/MVI
Overlay
E
****
Average no. of MVI clusters
80
60
40
20
0
Colocalised
Non-colocalised
F
ns
Average no. of γH2AX clusters
40
30
20
10
0
Colocalised
Non-colocalised
G
*
Average no. of MVI molecules
800
600
400
200
0
Colocalised clusters
Non-colocalised clusters
H
ns
Average no. of γH2AX molecules
1000
800
600
400
200
0
Colocalised clusters
Non-colocalised clusters
I
**
Average area of MVI clusters (nm²)
100000
10000
1000
Colocalised
Non-colocalised
J
*
Average area of γH2AX clusters (nm²)
100000
10000
1000
100
Colocalised
Non-colocalised

Figure 6.19. Violin plots showing the colocalisation of MVI and γH2AX.

STORM and cluster analysis was performed on MCF10A cells. γH2AX clusters were analysed and the number of molecules in a cluster (A), the size of these clusters (B) and the number of clusters have been calculated (C). The DoC score of MVI overlaid on γH2AX clusters and vice versa showed no difference between overlays with the mean being less than 0, thus the majority of clusters do not colocalise (D). The number of MVI clusters were calculated (E) showing a significant number non-colocalised clusters. There is similar amount of γH2AX clusters that do or do not colocalise with MVI clusters (F). There are more molecules of MVI in clusters that colocalise with γH2AX that do not (G) and there is no difference in the number of molecules found in the γH2AX clusters that either colocalise with MVI clusters or not (H). There is a significantly larger area of MVI clusters (I) that colocalise with γH2AX clusters as well as a significantly larger clusters of γH2AX that colocalise with MVI clusters (J). All data was tested with the students T-test where **** $p<0.0001$, ** $p<0.001$ and * $p<0.05$. N=2

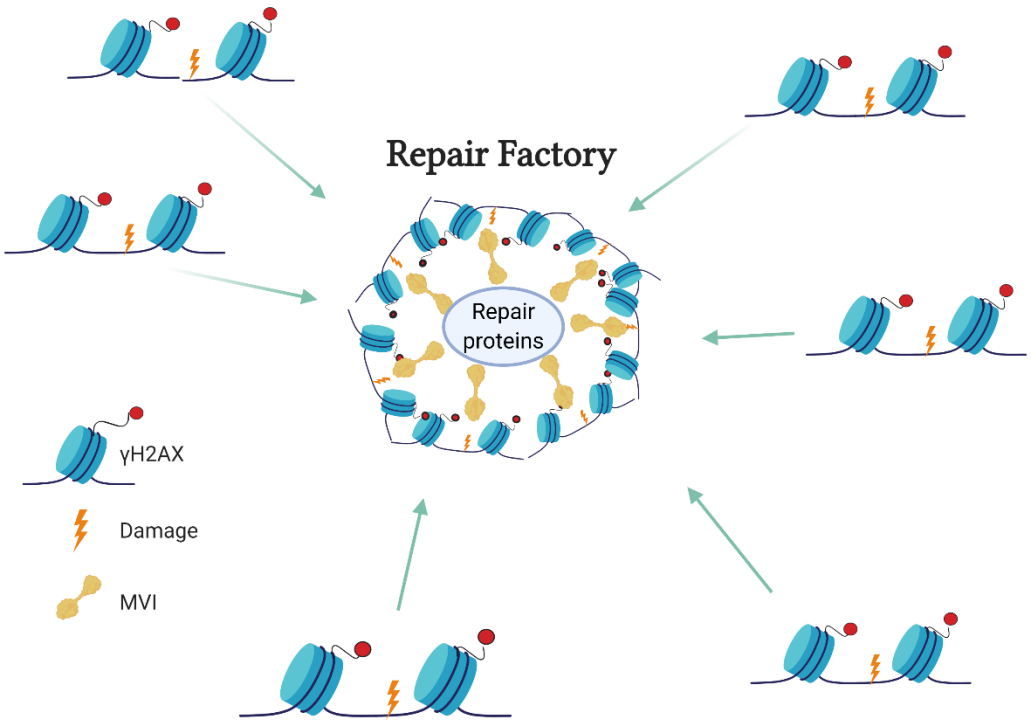


Figure 6.20. A cartoon depicting MVI inside repair foci.

Points of damage labelled with γH2AX move into repair foci where clusters of MVI can be found, which stabilise repair factories for simultaneous repair of DNA.

6.2.11 Studying apoptosis requires further work

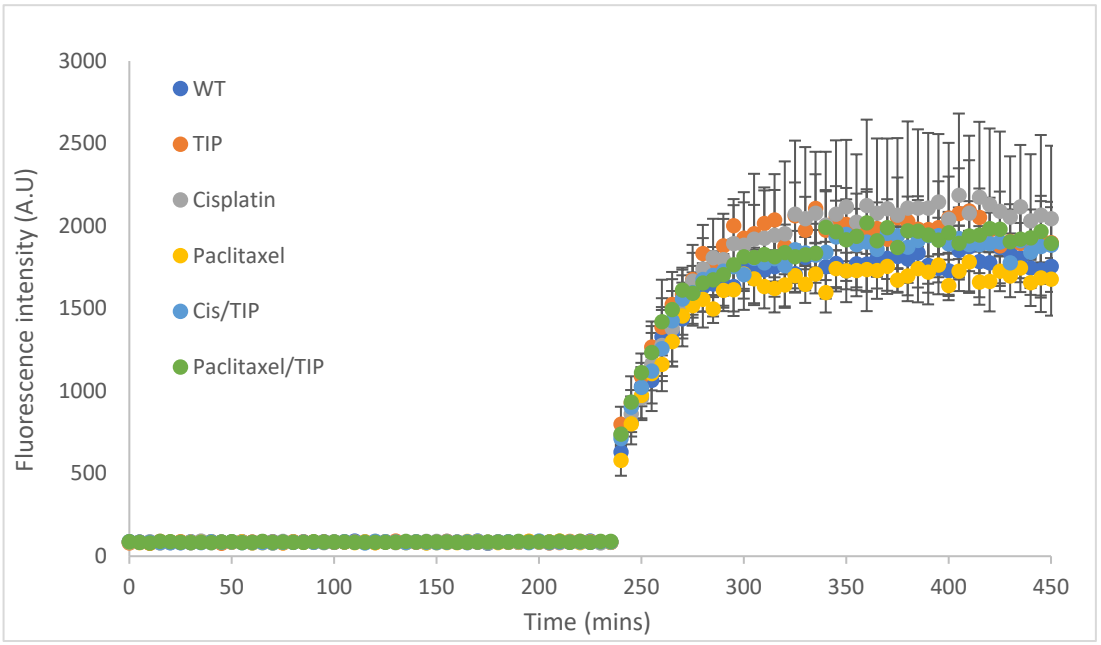


Figure 6.21. Apoptosis report of HeLa cells.

Fluorescence measurements measured following the manufacturers' protocol. Cells were incubated in 5% CO_2 at 37°C before drug induction, each drug was diluted into the appropriate medium at t=0 mins. There was no significant difference between each condition, and so it the apoptosis kit did not work. Error bars = SD.

During microscopy and HCS, visual inspection showed that HeLa displayed high cell death when treated with TIP and a DNA damaging agent. To provide statistics to this observation, the RealTime-Glo™ Annexin V apoptosis kit (Promega, Cat no.JA1011) was used. This kit provides a real time readout of cellular apoptosis, whereas the cells present their phosphotidylserine, fluorescently tagged annexin V binds and its fluorescence increases. Here, this study found no difference in apoptosis between any samples, including when using the apoptotic inducer, paclitaxel. All of the samples produced a similar hyperbolic curve where there is an exponential increase of apoptotic signal at time point 240 minutes after drug treatment until a plateau at time point 325 minutes (Figure 6.21). After visual inspection of the samples, the paclitaxel treated cells showed high cell death compared to the untreated sample, yet this was not detected whilst using the kit. This assay requires further work to

ensure the fluorescent readout matches the observations made for each condition and that the kit is working correctly.

6.3 Discussion

This study has focused on the particular role MVI may play in the DNA damage response and how this role may be regulated. It builds on the data previously shown that whilst MVI doesn't affect the transcription of DNA damage response proteins, it does bind directly to certain repair proteins. Also previously discussed is that MVI localisation changes, where it moves into the nucleus due to DNA damage. This study has attempted to build on this information and understand exactly why MVI would move into the nucleus and change its binding partners after DNA damage.

6.3.1 MVI motor domain inhibitor TIP prevents nuclear localisation of MVI.

In this study it has been identified that the motor domain is vital for the movement of MVI into the nucleus within MCF10A cells, however not necessarily in HeLa cells. When MCF10A cells were treated with TIP for a 24 hour period there is a clear loss of MVI inside the nucleus as shown by the HCS. This highlights the motor domain of MVI as a potential regulator of nuclear localisation. Published work has shown that MVI has seven nuclear localisation signals, however no work was undertaken to identify which of these signals are responsible for the movement of MVI into the nucleus. One such NLS identified is the PRKSKLA amino acid sequence found at positions 559-566 within MVI (Majewski *et al.,* 2018). These amino acid residues are found directly within the motor domain. It is possible that the TIP inhibitor is blocking this site for recognition of nuclear importins.

It has been shown recently that the nuclear isoform of MVI, the non-insert isoform, is able to back fold (Fili *et al.,* 2017). This back folding ability inactivates the MVI until a suitable binding partner binds, the MVI then folds open and the protein can then dimerise with a

binding partner as the mediator (Fili *et al.,* 2017). It is possible that TIP itself interferes with this back folding mechanism, where MVI may need to be in the folded confirmation to be able to cross the nuclear membrane and that the TIP, inhibits this backfolding keeping the MVI stuck in its open state restricting the localisation of MVI.

Interestingly MVI localisation within HeLa does not seem to be impacted by the presence of TIP, as shown by the confocal microscopy and the use of HCS. This may provide more information on the mechanism of MVI translocation. As discussed previously HeLa have high chromosome instability and contain the E6 viral protein that marks p53 for degradation (DeFilippis *et al.,* 2003). It is known that MVI interacts with p53 around the nuclear periphery particularly at the golgi apparatus (Jung *et al.,* 2006), it is possible that MVI is able to move into the nucleus due to this loss of a binding partner and the motor domain is not necessarily required for the crossing of MVI into the nucleus, but the movement along actin filaments from the cell periphery towards the nucleus. The previous proteomics showed very little variation between cell lines of untreated cells MVI binding partners so it is possible that TIP inhibiting the motor domain of MVI is causing a knock on effect of other proteins required for nuclear movement that HeLa cell lines do not require.

Further work is required to get a complete grasp on nuclear localisation of not only MVI but other nuclear myosins as well. Currently it is hypothesised that MVI moves across the nucleus through the same importins required for NM1 movement into the nucleus, yet no binding partners or mechanism has been observed within a cell (Majewski *et al.,* 2018).

6.3.2 MCF10A cells rely on nuclear MVI to signal DSBs.

Confocal imaging, western blotting and HCS have all shown that cells treated with TIP and then treated with either cisplatin or bleomycin are completely unable to produce the correct γH2AX signalling. As expected, after treating both lines with bleomycin and cisplatin there was an increase of γH2AX signal due to the induction of DSBs by these drugs, however after treatment with TIP, HeLa is still able to produce γH2AX foci yet MCF10A cells cannot. This could be due to the TIP not affecting the nuclear localisation of MVI within HeLa whilst inhibiting nuclear movement of MVI in MCF10A cells. It does also introduce a new mechanistic step into the recognition of DSBs and the activation of the ATM kinase that is responsible for the phosphorylation of H2AX after a DSB occurs.

The DSB response is a well-known response where the MRN complex, consisting of Mre11, Rad50 and Nbs1 bind to a break. These proteins are the first responders to DSBs where they bind to the DNA at the precise location of the break and then begin to repair the break. Whilst this is occurring it has been shown that Nbs1, the protein responsible for nucleotide dependent DNA binding and ATP-dependent unwinding of the DNA (Paull and Gellert, 1999), causes the autophosphorylation of the ATM kinase which then in turn monomerises and phosphorylates the H2AX histone as well as p53, Brca1 and other cell cycle checkpoint proteins (Difilippantonio *et al.,* 2005). In this study γH2AX signalling is lost without MVI, this implicates MVI within the first stages of DSB response. MVI might have a role between the activation of the ATM kinase and it phosphorylating H2AX. This allows the hypothesis that MVI is in some way interacting with the MRN complex and is regulating either the autophosphorylation of ATM or the phosphorylation of H2AX.

It is possible that MVI is required to stabilise the MRN complex on the DSB through its ability to act as an anchor when bound to actin when high forces are applied (Altman, Sweeney and Spudich, 2004). The high forces could be introduced by the large repair complex binding to

myosin or through the forces required to pull the two broken strands together. It may also be acting as a transporter within the nucleus where it locates, binds to a component of the MRN complex and then move this binding partner towards a point of damage. Further work, such as live cell imaging of MVI movement would be required to understand if it is acting as an anchor as described in transcription or as a motor.

Another theory is that phosphorylation of γH2AX occurs however the phosphorylation itself is not stable without MVI. Live cell imaging would provide information if this is the case, as the γH2AX signal would be incredibly brief.

6.3.3 MVIs motor is required to regulate histone modifications.

Previous work has shown that specifically two histones respond to DNA damage the H3K36me2 modification and the H4K20me1 (Clouaire *et al.,* 2018). In both the HeLa and MCF10A cell lines these modifications were increased by the induction of damage by bleomycin. Yet the increase observed was higher when MVI is inhibited by TIP. This increase must be due to MVI interacting with histone modifiers directly as it occurs both in the TIP and TIP with bleomycin treatments, and in both cell lines, even though HeLa cells have a functional DNA damage response after TIP treatment.

How MVI may be interacting with these protein is still yet to be defined. Similar to the MRN complex, discussion above, MVI could be acting as an anchor for histone methylaters providing support for the reaction to occur or by working as a transporter within the nucleus. Further work to understand if MVI is affecting global histone modifications or just those that have been attributed with DNA damage would be required. It is known that the methylation of histones causes the activation of gene expression (Zhang and Reinberg, 2001), so the role MVI is playing here may not be down to DNA damage but down to a transcription regulatory process. It is known that NM1 binds to the B-WICH complex that regulates chromatin

modifications around the activation of rDNA transcription (Sarshad *et al.,* 2013). It is possible that MVI may be playing a similar role.

6.3.4 MVI can be found at γH2AX repair foci.

To identify if the loss of γH2AX signalling is because the H2AX histone has a colocalisation with MVI, STORM imaging was utilised. This provided precise single molecule colocalisation analysis. After DNA damage there was an increase in MVI clustering which coincided with an increase of cluster size and the number of molecules within a cluster. As no γH2AX signalling occurs if there is no DNA damage it is impossible to identify the difference in clustering before and after DNA damage, however what can be seen is two distinct types of clusters, those that co-localise with MVI and those that do not.

The clusters of γH2AX that do not colocalise with MVI have equal number of molecules and equal occurrence than those that do colocalise however the area they take up within the nucleus is significantly smaller than the clusters that do colocalise with MVI. These large clusters of MVI and γH2AX, may be a product of MVI switching its role from transcription to a role in DNA repair.

Interestingly the fact that there is an increase in cluster size between the MVI clusters colocalised to γH2AX clusters to those that are not imply that MVI is most likely in small clusters that provide a function within the nucleus and the large clusters provide a function within the DNA damage response. The fact that only large clusters of MVI and large clusters of γH2AX can be found together may implicate MVI as a stabiliser of repair factories. This would rely on the motor protein acting as an anchor once again to hold together multiple points of breaks and multiple scaffolds together. Unfortunately due to the lack of γH2AX signals after inhibiting the MVI motor domain it is not possible to comment on the exact mechanism. The HeLa cells may be a more suitable cell line to identify if MVI clusters

colocalising to γH2AX clusters is a product of a functioning motor domain, or due to a MVI binding partner being embedded within these repair foci.

Whilst it was observed the HeLa cells have increased cell death when treated with a DNA damaging agent and TIP, the apoptosis assay did not provide any further information. Such as, how TIP with drug treatment affects the cells ability to enter apoptosis rather than stalling its cell cycle. This would require more time and further work to optimise the conditions necessary for assay to work.

Overall MVI plays a vital role within the DSB repair signalling process and cells that have an inhibited motor domain show a significant phenotype. During this study however it is not possible to distinguish if the role MVI plays inhibits the whole DNA damage response process along with cell cycle inhibition and an activation of apoptosis or it only impacts the γH2AX signalling, and the cells are able to repair the DNA with or without MVI.

Chapter 7. Linking the roles of NM1 and MVI in the nucleus

7.1 Introduction

So far this study has focused on further characterising NM1, as well as identifying the importance of MVI in the DNA damage response. Both these myosins are able to cross the nuclear membrane, and their protein levels within the nucleus can be enhanced after stimuli (Maly and Hofmann, 2016; Majewski *et al.,* 2018). Whilst the structure of these two myosins differ, both are able to act as transporters. So far it is known that both these myosins are involved within transcription and now DNA damage, how they may work together is still yet to be defined.

7.1.1 Chromosome territories.

Originally it was believed that during interphase, chromosomes were not defined within the nucleus and they were free to move. However as time has progressed it has become apparent that each chromosome within an interphase cell actually has a designated region known as a chromosome territory (CT) (Cremer and Cremer, 2010). Fluorescence in Situ Hybridisation (FISH) has opened up this field of CTs, as each chromosome has been able to be individually mapped. 3D FISH has then shown full spatial organisation (Bolzer *et al.,* 2005)(Sehgal et al., 2015) It has been shown that these CTs can be adjusted depending on the transcriptional activity of the chromosome, the replication timing and the GC content of each chromosome (Mahy *et al.,* 2002) . Whilst CTs are defined it does not mean they are the same globally in a cell line, for example it is not possible to predict which chromosome would be adjacent to another, and currently there is no theme of genes consistently identified on the periphery or interior of CTs (Heride *et al.,* 2010). These territories are also able to intermingle, which allows for long rearrangements and organisation within a 3D space (Szczepińska et al., 2019). However to ensure chromosomes do not become entangled and to potentially slow down the movement of chromosomes, it is vital that chromosomes are

able to form attachments to the nuclear envelope (Kinney et al., 2018). This information does however, provide evidence that an interphase nucleus is highly organised and relies on the large pool of post-translational modifiers for histone management,, as well as chromatin remodelling complexes found within a mammalian cell .

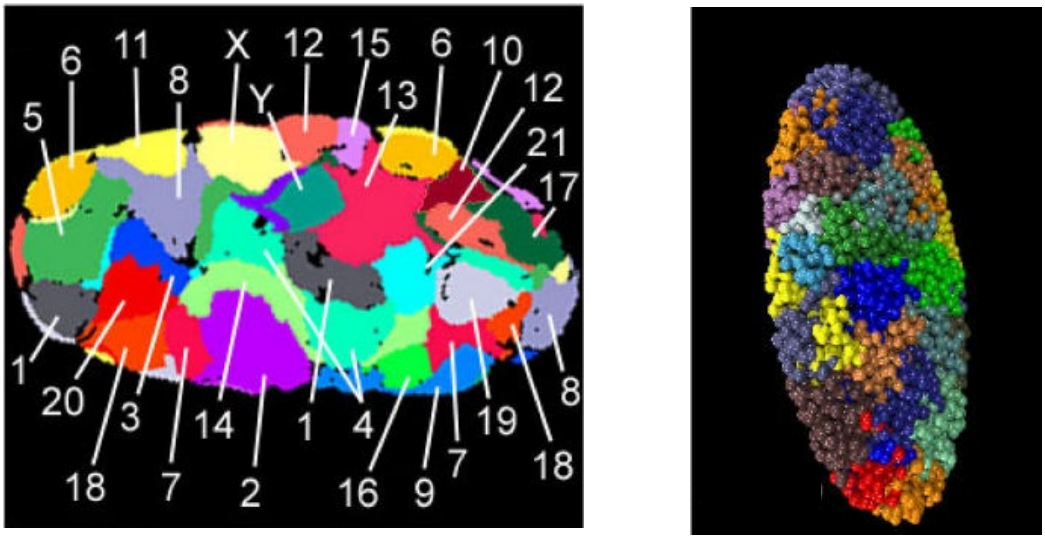


Figure 7.1. A generalised map of chromosome territories.
Each chromosome has been painted with a different colour and then plotted in 3D space. Adapted from Bolzer *et al.,* (2005).

7.1.2 Histone modifications shape chromatin

Histone modifications, as discussed previously, are post translational modifications that occur on the "tails" of histones (Zhang and Reinberg, 2001). Often these modifications can signal other proteins towards the DNA or change the affinity the histone has for DNA, either by loosening its grip on the DNA or tightening it. This process allows for gene expression to be tightly regulated by allowing the DNA to be accessed by the polymerase complexes. The histones that have been studied here, revolve around the transcriptional landscape, as this is the specific difference between heterochromatin (Volpe *et al.,* 2002), tightly packed often unreadable DNA, and euchromatin, consisting of transcriptionally active genes (Collins *et al.,* 2004).

Histone acetyltransferases (HATs) are responsible for the acetylation of histones often linked with gene activation (Lee and Workman, 2007). H3K9ac and H3K27ac are both found either side of active genes (Creyghton *et al.,* 2010), and can be acetylated by the CREB-binding protein when gene expression is required (Yuan *et al.,* 2013). To ensure a gene is transcriptionally repressed methylation occurs on the histone tails (Curradi *et al.,* 2002). One such methylated histone is H3K9me3, which is regulated by SUV39H1 and SUV39H2 which methylate the tail three times on the same lysine. This modification in turn, activates the heterochromatin protein 1 (HP1) which causes the chromatin to compact and become inaccessible (Schuhmacher *et al.,* 2015; Maison *et al.,* 2016).

7.1.3 Actin has a direct interaction with chromatin organisers

Whilst the types of actin found within the nucleus is still heavily debated, it is agreed that the presence of β-actin within the nucleus is a definite (Kelpsch and Tootle, 2018). To understand how nuclear myosins may play a role in the organisation of chromosomes, it is necessary to keep in mind the state of actin in the nucleus. The requirement for actin in chromosome organisation has already been well characterised, where it has been found to bind directly to chromatin remodelling complexes (Kapoor *et al.,* 2013; Schubert *et al.,* 2013). Mammalian cells contain multiple chromatin restructuring complexes, two common complexes are the SWI/SNF remodelling complex, BRG1. Other proteins that bind to these complexes and allow for the functionality of these proteins are grouped together, known as BAFs, BRG or BRM associated factors.

It has been found that the 53kDa BAF subunit can be defined as an actin related protein (Arp) and that not only does actin bind to this subunit but actin itself is a subunit of the complex (Rando *et al.,* 2002). If actin polymerisation is blocked using latrunculin B, then the whole BRG1 complex including the 53kDa BAF subunit and actin, are unable to bind to chromatin (Nishimoto *et al.,* 2012)

Actin has also been identified in other roles; as part of the INO80 remodelling complex used in histone translocation for transcription, within the SWR1 complex, which is involved in DSB repair (Kapoor *et al.,* 2015) where it is required for the replacement of H2A histones (Wu *et al.,* 2009) with H2A.Z to activate transcription and finally actin is found in the NuA4 complex (Doyon *et al.,* 2004), which is an acetylator of the H4 histone modifier, which is necessary for DSB repair and cell cycle control. Within these complexes actin often plays a stabilising role, however if actin is present on these complexes, then there is potential for the binding of a nuclear myosin.

Following DSBs, INO80 is recruited to γH2AX through its interaction with actin (Kapoor *et al.,* 2015), also during this recruitment the NuA4 complex acetylates H2AX histones which in turn leads to an increase of the SWI/SNF (BAF) histone modifier which increases the amount of γH2AX signals surrounding the DSB (Jha, Shibata and Dutta, 2008). Here, all three complexes require their Arps for their recruitment and so it is known that at points of damage, actin is present.

As both chromatin regulatory complexes and actin are found at the points of damage, it is more than likely nuclear myosins, can also be found within these regions due to their high affinity to actin.

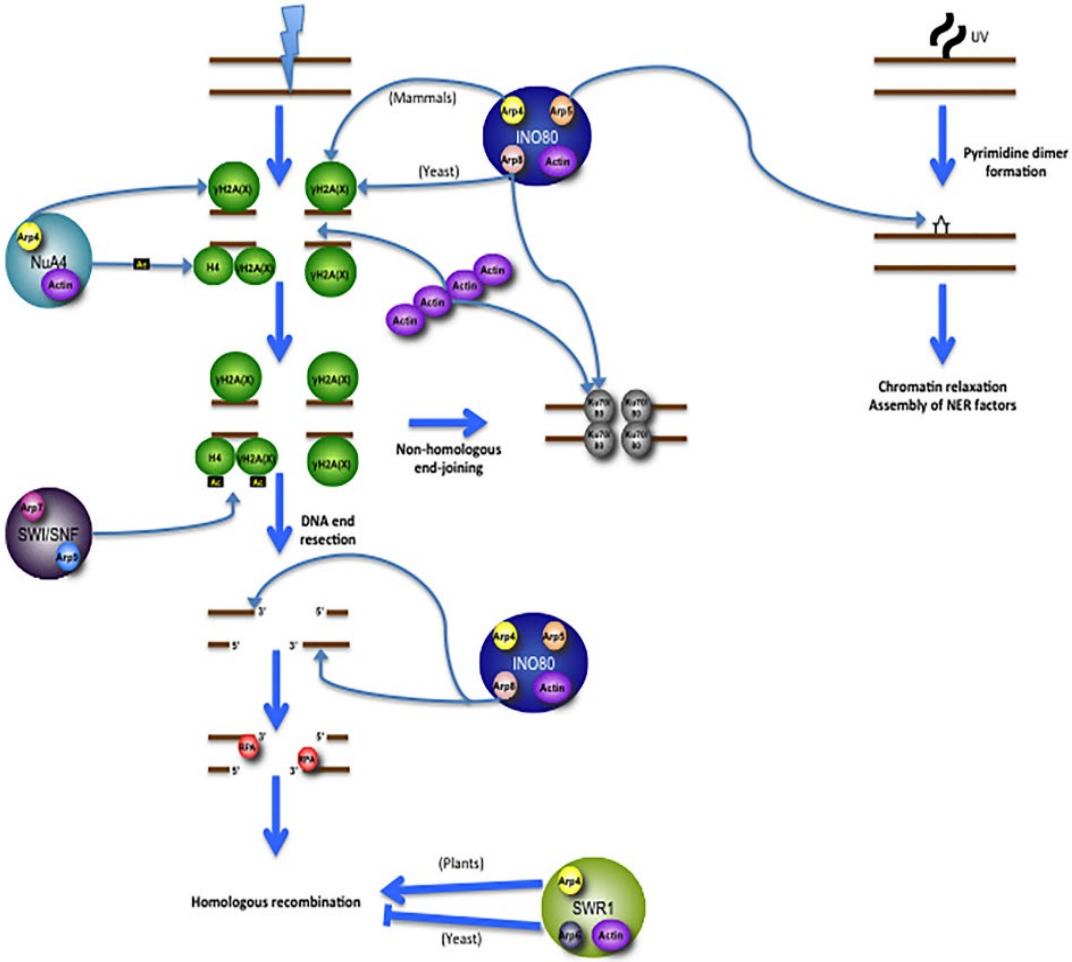


Figure 7.2. Chromatin remodelling complexes in DSBs.

Ino80 first identify γH2AX due to the actin present at a DSB. This recruits NuA4 to cause a spread of γH2AX signals. If the repair is HR then SWI/SNF is also recruited, if not the repair follows the NHEJ pathway. Taken from Klages-Mundt *et al.,* (2018).

7.1.4 NM1 binds directly to chromatin remodelling complexes.

As discussed previously NM1 plays a vital role in transcription. Within RNAPI transcription NM1 binds directly to a chromatin remodelling complex that contains SNF2h and WSTF, known as B-WICH (Percipalle *et al.,* 2006). It is hypothesised that this interaction, allows for the recruitment of B-WICH to the points of rDNA transcription, which then changes chromosome organisation for the successful transcription. Not only does NM1 bind to SNF2h and WSTF in RNAPI transcription but also in RNAPII transcription (Almuzzaini *et al.,* 2015). This binding allows for the recruitment of these subunits to transcriptionally active sites that in turn employ histone acetyl transferases (HATs) to acetylated local histones such as lysine-9 on the H3 histone (H3K9ac). This provides stability to the site of transcription and ensures the DNA is loosely wrapped around the nucleosomes. This is evidence of a nuclear myosin being involved in multiple steps of transcription, where it provides a clear pathway for the progression of the RNAP complexes along previously compacted DNA.

7.1.5 Nuclear myosins are involved in long-range chromatin movements.

It has been shown that nuclear myosins can organise specific areas of chromatin to allow for transcription, NM1 has also been implicated in the long-range movement of chromosomes (Chuang *et al.,* 2006). During interphase, chromatin was imagined to be relatively static, and only during cell division was DNA moved with intention. However more recently Chuang *et al.,* (2006) observed chromatin moving 5µm with a velocity of 0.1-0.9µm/min which is larger and faster than can be explained by simple Brownian motion. This movement has been attributed to the formation of F-actin, which NM1 is able to the bind along with the DNA and travel along these filaments.

Not only is movement of DNA required during general cell maintenance, it is also observed after DSB induction with the use of cisplatin. Overall, in human dermal fibroblasts (DHFs) five different chromosomes have been shown to move, these are chromosomes; 19, 17, 20, 12

and 15. Here these chromosomes move either from the nuclear periphery towards the nuclear interior, or vice versa (Mehta *et al.,* 2013). These translocations require γH2AX signalling, and once a DSB is signalled, it is hypothesised that NM1 moves the chromosomes to allow for the formation of repair foci and the matching of homologous chromosomes. Inhibition of NM1s motor domain removes all capability for the cell to rearrange these chromosomes (Kulashreshta *et al.,* 2016). Whilst this work has showed that inhibiting γH2AX signals also stops the movement of chromosomes, there is no mechanism provided of how does γH2AX signalling regulate NM1s activity and how is the direction of movement decided.

Myosin V another myosin that can be found inside the nucleus, has also been attributed with movement of heterochromatic breaks (Caridi *et al.,* 2018). Filamentous actin is formed at the location of a DSB through activation of the Arp2/3 proteins, it then linearises towards the nuclear periphery towards repair foci. The myosin activator Unc45 and myosin V as well as NM1, can all be found at the site of damage and removal of either myosin causes a depletion in heterochromatin transportation along actin filaments (Caridi *et al.,* 2018). If the movement is inhibited in some way, then the γH2AX signals persist continuously until an alternative repair mechanism to homologous recombination is utilised. This study however did not comment on the redundancy between these two myosins and hints that both myosins are required for transport. How these myosins are able to communicate between each other and why two different myosins are required is still unknown. This does however provide evidence for the first time in the nucleus that myosins are able to cooperate.

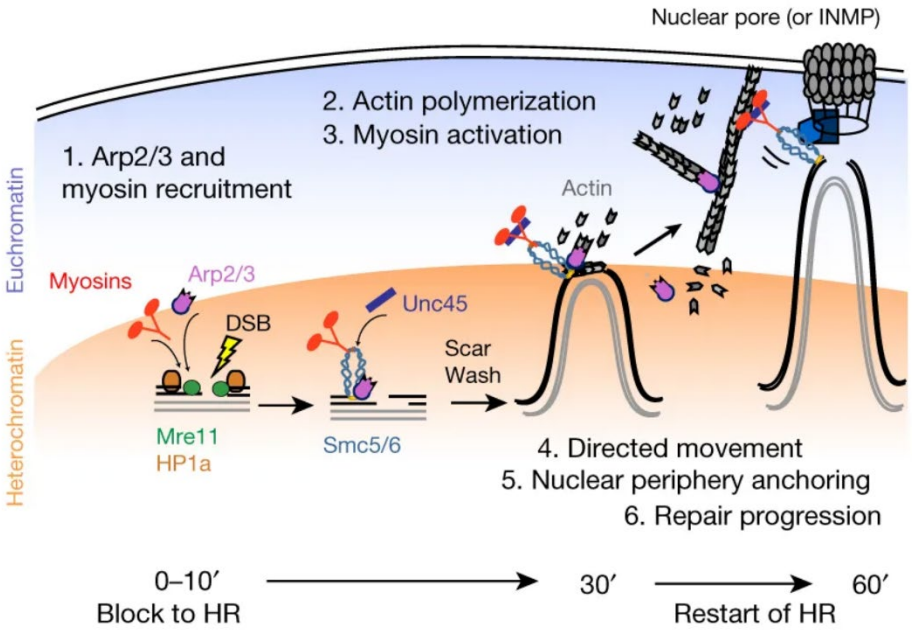


Figure 7.3. Acting and myosins translocating DSBs.

The arp2/3 complex and myosin V or NM1 bind to a DSB and the Unc45 activates the myosins causing directed movement of the heterochromatin towards the euchromatin region at the nuclear membrane for repair. Taken from Caridi *et al.,* (2018).

7.1.6 Myosin I and MVI cooperate within the cytoplasm of the cell.

If MVI and NM1 are to work together within the nucleus, it is interesting to identify any other cellular activities where both these type of myosins can be seen together. During phagocytosis, a whole host of myosins are required for the completion of this process; myosin I, 2, 5, 7, 9b and 10 all play a role (Papadopulos *et al.,* 2013). During the invagination of clathrin coated vesicles both MVI and myosin I are necessary (Derwerchin *et al.,* 2014). This study utilised the virally infected macrophages to then study the internalisation of antibodies at the cell membrane. At the cell periphery when an antigen is recognised myosin I allows for invagination occurs, following this, the vesicle needs to pass through the cortical actin corridor. Here myosin I does not transport the vesicle but MVI binds and carries the cargo along the network of actin filaments. Once the vesicle is through the actin filament

MVI disassociates from the vesicle, leaving myosin I and a microtubule motor to then transport the vesicle to the microtubule organising centre.

MVI is most likely utilised here for its ability to travel along actin from the pointed end to the barbed end to travel through the cortical corridor, where myosin I is incapable of this movement. This provides some evidence for the two myosins being utilised within one mechanism, however having two different functions. Whether or not this could be so in the nucleus is yet to be determined.

7.1.7 Using Fluorescence in Situ Hybridisation (FISH) for studying chromosome locations.

One method used here to study the locations of chromosomes before and after damage is FISH. To study whole chromosome locations fluorophores are attached to a group of specific DNA sequences that are unique to each chromosome. These fluorescently labelled sequences are hybridised onto the samples. In interphase cells if the karyotype of the cell is a regular diploid, two signals should be apparent per chromosome paint and in interphase cells these signals are spread throughout the chromosome territory (Bishop, 2010).

To analyse the images obtained, and provide information on the chromosome location, whether it is at the nuclear periphery, in an intermediate state or within the nuclear interior, a nuclear morphology analysis software was used. This software designates a location of a fluorescence signal within the nucleus, by dividing the nucleus into subshells. The number of subshells can be decided and the amount of signal detected in each subshell depicts the most common location of a chromosome (Skinner *et al.,* 2019).

This analysis allows chromosome movements to be mapped without the use of live cell technology and any nonspecific DNA stress caused by DNA dyes.

7.1.8 The aims of this study.

So far NM1 has been further characterised biochemically, and MVI has been studied concerning its role in DNA damage. As both myosins have been found at the points of active transcription, it could be possible that they also both function within the DNA damage response. It is known NM1 regulates chromatin organisation in both normal and damaged cells, this study sets out to investigate if the same is true for MVI by using high content screening, and FISH techniques. If both myosins do truly share roles within the nucleus, STORM microscopy will identify any colocalising molecules.

7.2 Results

7.2.1 HeLa and MCF10A cells modify their histones differently after DNA damage

It is known that NM1 is able to bind to the B-WICH complex for transcriptional activation of genes (Vintermist *et al.,* 2011). There is yet to be a study if MVI is required for histone modifications other than the γH2AX modifications, and DNA damage modifications as shown in Chapter 6. To understand if MVI alters the chromatin landscape similar to that of NM1, HCS was once again utilised.

Firstly the DNA damage drug bleomycin, led to an increase of intensity by 584 A.U, in the transcriptional repressor histone modification H3K9me3 (Figure 7.6) which in turn leads to a decrease in acetylation of the same lysine (H3K9ac), by 1051 A.U, which could mark transcription activation within the MCF10A cell lines (Figure 7.5). The HeLa cells lines responded in an opposite fashion where this lysine has an increase in acetylation by 1847 A.U (Figure 7.5), which could increase transcriptional activity, and the triple methylation on the same lysine residue is actually no different to the non-treated cells (Figure 7.6). This shows that whilst the MCF10A cell lines are responding as expected to DNA damage by

possibly reducing transcription, the HeLa in turn react in the opposite manner, where acetylation of histones increases.

There is however no difference between the cells lines in H3K27ac signals , as after bleomycin treatment, there is reduction of this signal in both MCF10A and HeLa cells (Figure 7.5), 544 A.U and 669 A.U respectively, compared to the non-treated cells.

7.2.2 Nuclear MVI is responsible for correct histone modifications

When DNA damage free cells, are treated with the MVI motor domain inhibitor TIP, the histone landscape is affected in both MCF10A cells and HeLa cells (Figure 7.5 and Figure 7.6). Here the TIP treatment itself causes a significant decrease in both H3K9ac, by 1973 A.U in MCF10As and 1488 A.U in HeLa, and H3K27ac, by 1556 A.U in MCF10As and 644 A.U, and a significant increase of H3K9me3, by 1190 A.U in MCF10As and 5400 A.U in HeLa. The changes seen in the TIP treatment compared to that of WT cells, shows that the inhibition of the motor domain of MVI and most likely its nuclear localisation is responsible for the control of histone modifications.

After treating MCF10A cells with a DNA damaging agent as well as TIP, the cells are unable to respond appropriately with the effects of DNA damage on histone modifications being masked by the inhibition of MVI. This would be expected as TIP treatment on its own would impact histone modifications due to the direct role of MVI in transcription. It is clear that the simple loss of MVI has a far greater influence compared to that of the bleomycin. The MCF10A cells after both drug and TIP treatment remain, with a reduction in H3K9ac, by 1998 A.U and H3K27ac by 1536 A.U respective to untreated cells (WT).

TIP also has an effect on the HeLa cell lines as after WT cells have been treated with TIP there is a significant reduction in H3K9ac -by 1488 and H3K27ac - by 644.9 A.U and a significant increase in H3K9me3 levels – by 5400 A.U. Yet, when the cells are treated with both

bleomycin and TIP the cells still respond to the DNA damage by increasing their H3K9ac to an average intensities of 6151 A.U, but not to the levels seen with just bleomycin treatment, where cells have an average intensity of 6436 A.U. This shows once again how the different cell lines utilise MVI for their response to DNA damage. Compared to the MCF10A cells who lose their histone modification response when MVI is inhibited, the HeLa cells are still able to respond to. It is clear the NM1 is not the only nuclear myosin involved in histone modifications.

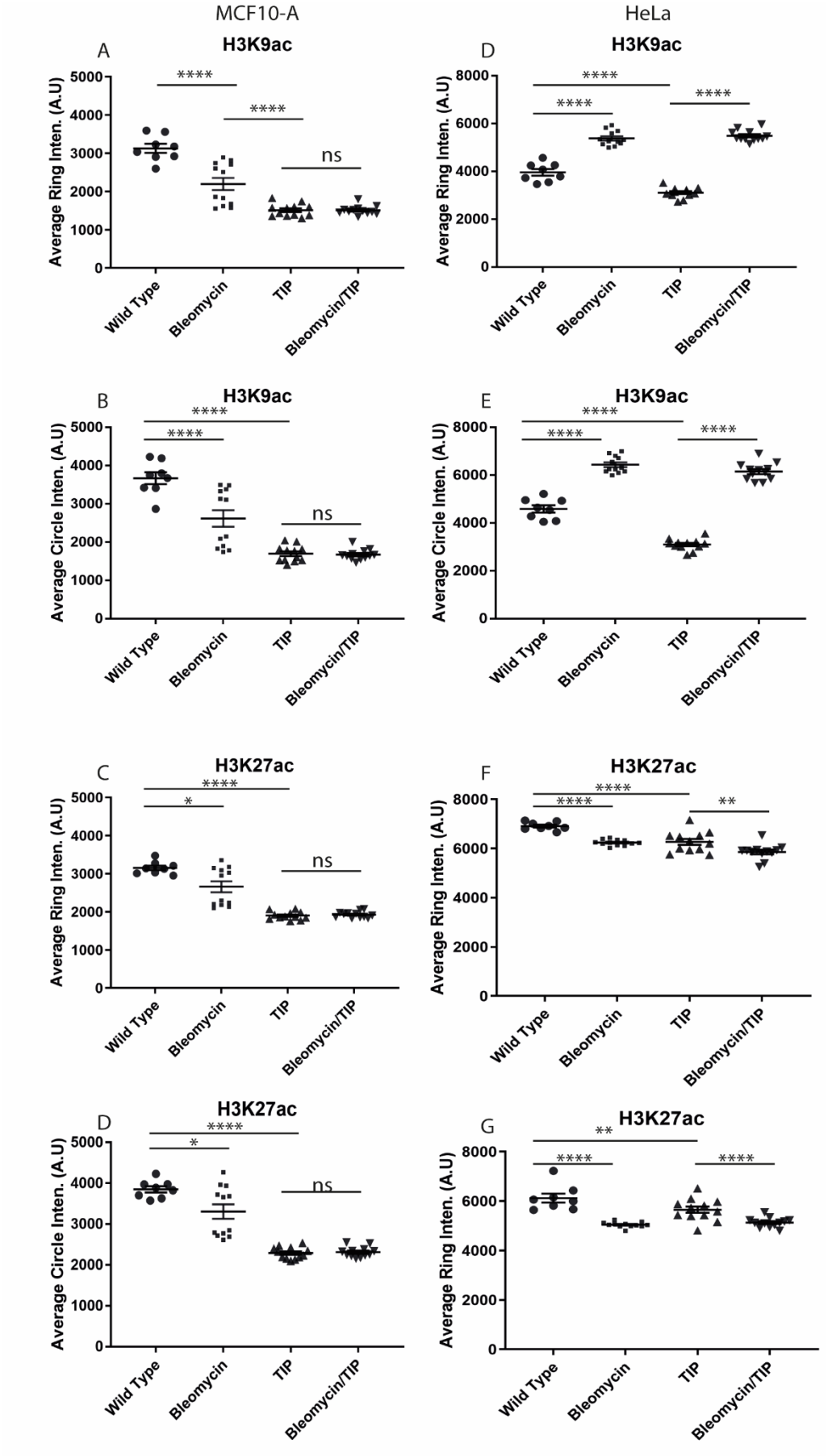

MCF10-A
HeLa
A
H3K9ac
Average Ring Inten. (A.U)
B
H3K9ac
Average Circle Inten. (A.U)
C
H3K27ac
Average Ring Inten. (A.U)
D
H3K27ac
Average Circle Inten. (A.U)
D
H3K9ac
Average Ring Inten. (A.U)
E
H3K9ac
Average Circle Inten. (A.U)
F
H3K27ac
Average Ring Inten. (A.U)
G
H3K27ac
Average Ring Inten. (A.U)
Wild Type
Bleomycin
TIP
Bleomycin/TIP
****
*
**
ns

Figure 7.5. HCS of acetyl histone modifications.

MCF10A and HeLa cells were treated with bleomycin, TIP or bleomycin and TIP. The fluorescence intensities were measured where each data point is a minimum of 1000 nuclei. MCF10A cells had a global decrease after bleomycin and TIP treatments of H3K9ac (A,B) and H3K27ac (C,D). HeLa had an increase of H3K9ac (E,F) and H3K27ac (G,H) which were both reduced after TIP treatment but then increased again after TIP with bleomycin treatment. The SD is shown and significance was calculated using ordinary one-way ANOVA with Sidaks multiple comparisons test, where * p<0.05, ** p<0.01, **** p<0.001. N=2

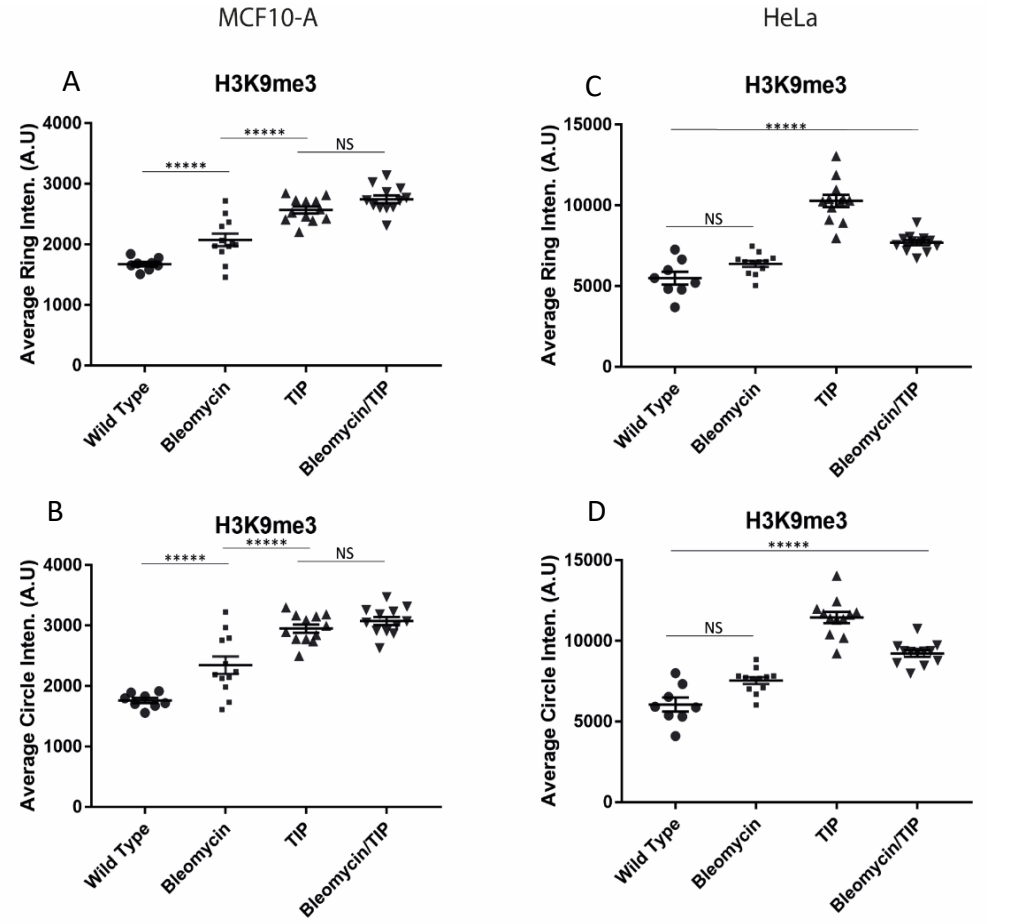


Figure 7.6. HCS of methyl histone modifications.

MCF10A and HeLa cells were treated with bleomycin, TIP or bleomycin and TIP. The fluorescence intensities were measured where each data point is a minimum of 1000 nuclei. MCF10A cells had a global increase after bleomycin and TIP treatments of H3K9me3 (A,B). HeLa had no change of its H3K9me3 after DNA damage however it does increase after TIP and bleomycin with TIP treatments again after TIP with bleomycin treatment (C,D). The SD is shown and significance was calculated using ordinary one-way ANOVA with Sidaks multiple comparisons test, where, **** p<0.001. N=2

7.2.3 HeLa chromosome territories differ to human dermal fibroblasts

It is already published that NM1 is required for the rearrangement of chromosome territories after DNA damage, and this rearrangement requires the γH2AX signalling pathway (Kulashreshtha *et al.,* 2016). As MVI inhibits the γH2AX signals within MCF10A cells, HeLa cells were utilised, as they still produce γH2AX without MVI, to study if MVI is also required for chromatin rearrangements after damage.

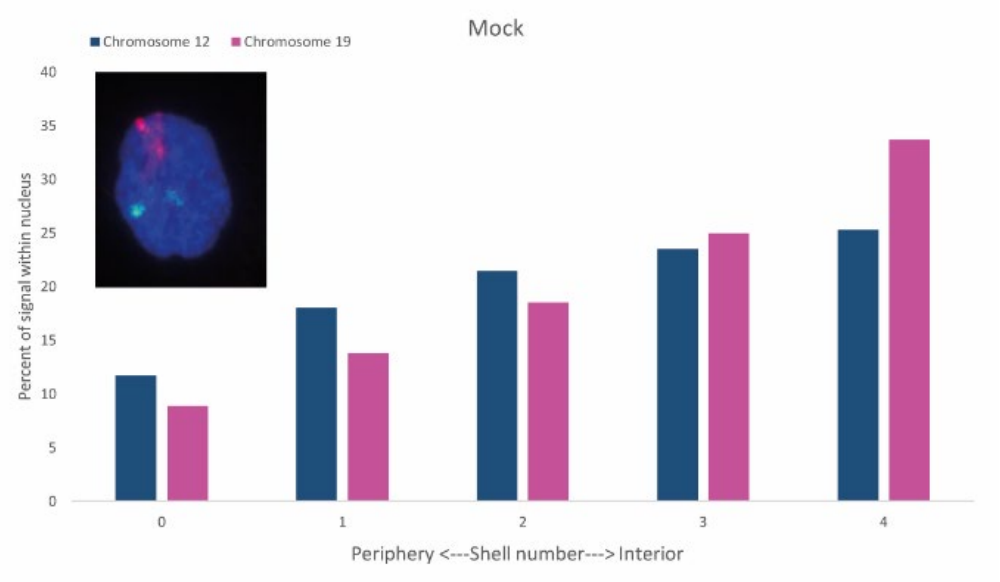
2D FISH alongside the analysis software, nuclear morphology analysis, has allowed the mapping of chromosome territories within one focal plane of a HeLa nucleus. Previously published work involving human dermal fibroblasts identified two chromosomes that move after DNA damage, these are chromosome 12 and chromosome 19 (Mehta *et al.,* 2013), which move from the periphery to the interior and the interior to the periphery of the nucleus, respectively. However after completing the analysis of WT HeLa cells which contain a heavily unstable karyotype, this study has found that both chromosome 19 and chromosome 12 are more commonly found within the interior of the nucleus and not at opposite localisations (Figure 7.7,A).

Whilst the locations differ to that observed in human dermal fibroblasts, the response to DNA damage is the same. After cells have been treated with cisplatin, the chromosome territories of 12 and 19 both have a preference for the periphery of the nucleus rather than the interior. This shows the HeLa cells are responding to the DNA damage through whole chromosome territory reorganisation (Figure 7.7,B).

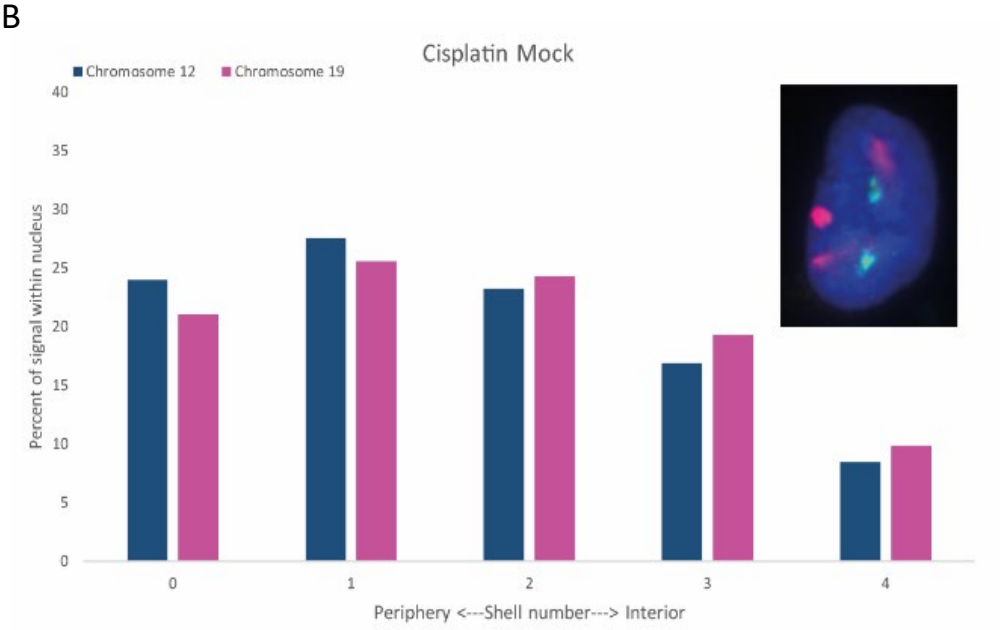
7.2.4 MVI is required for CT organisation both before and after DNA damage

To understand if MVI is required for normal chromosome organisation, a MVI KD was performed on cells which were then separated for RNA-seq analysis and FISH. Both chromosome 12 and 19 had their locations mapped using the nuclear morphology analysis software. After MVI KD there is a larger percentage of chromosome within the nuclear centre than that of the nuclear periphery as shown in Figure 7.7 C. After treating MVI KD cells, with cisplatin for 24 hours there is no shift of these chromosome territories towards the nuclear periphery (Figure 7.7 D). This shows that without MVI the HeLa cells are unable to move the chromosome territories as expected due to the DNA damage, as the HeLa cells still produce the γH2AX signals after DNA damage, it must be solely down to the loss of MVI these chromosomes are unable to move.

A


Mock
Chromosome 12
Chromosome 19
Percent of signal within nucleus
0
5
10
15
20
25
30
35
40
0
1
2
3
4
Periphery <---Shell number---> Interior

B


Cisplatin Mock
Chromosome 12
Chromosome 19
Percent of signal within nucleus
0
5
10
15
20
25
30
35
40
0
1
2
3
4
Periphery <---Shell number---> Interior

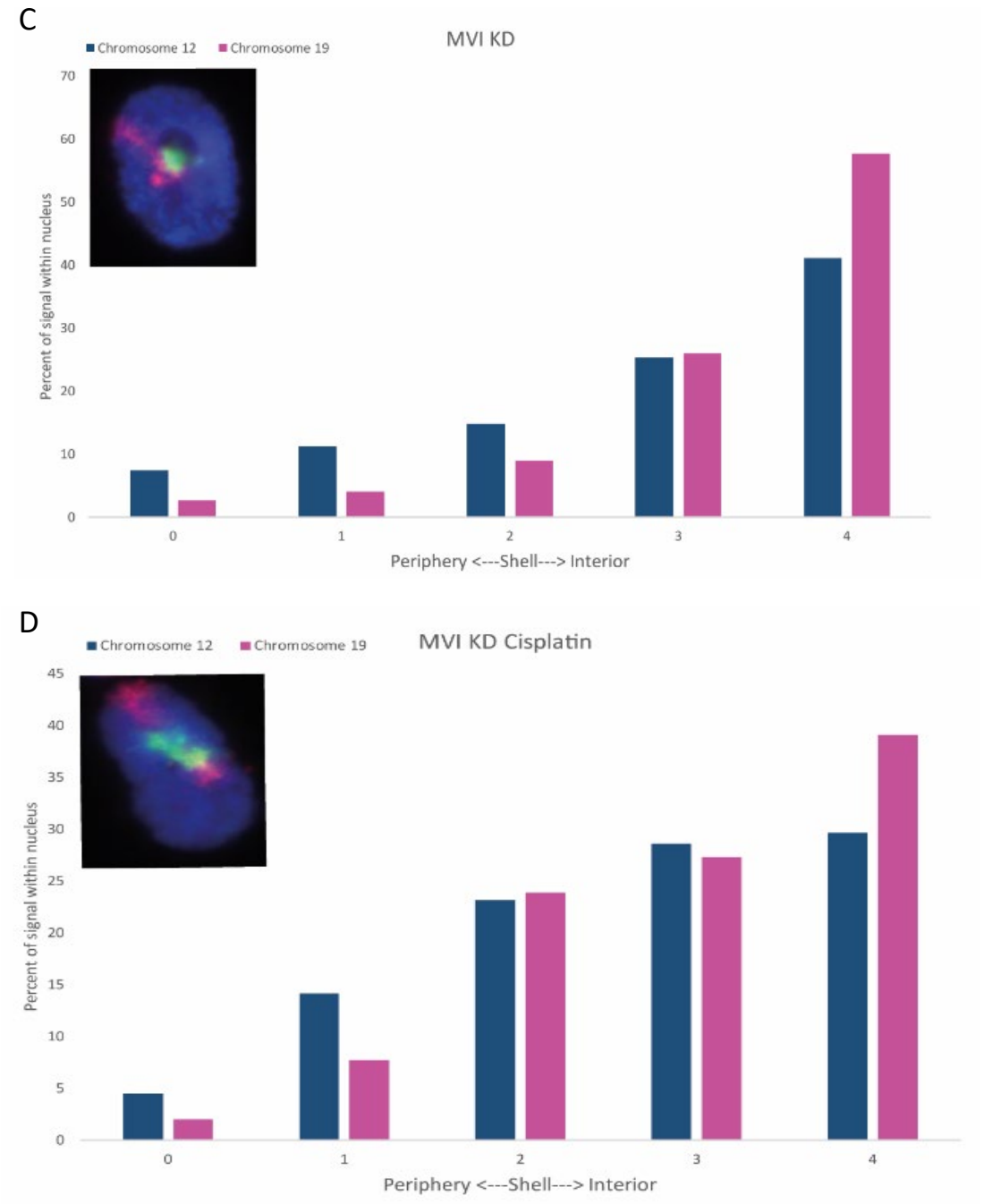


Figure 7.7. 2D FISH of whole painted chromosome 12 (blue) and 19 (pink).

In mock cells, both chromosomes (images; green and red respectively) remain within the interior of the nucleus, after cisplatin treatment these then shift away from the nuclear interior (B). After MVI KD the chromosomes become concentrated in the nuclear interior (C) and after cisplatin damage with a MVI KD the chromosomes remain relatively in the centre of the nucleus (D). N for each condition = 50.

7.2.5 Neither NM1 or MVI nuclear clustering is affected by TIP

As it is now established MVI is required for correct histone modifications as well correct chromosome territory organisation, it is possible that these two myosins can affect the functionality of each other. To study this hypothesis, STORM microscopy alongside Clus-DoC analysis has provided information on how TIP can effect MVI, and how this may in turn impact upon NM1 within the nucleus of HeLa cells. Within HeLa cells Figure 7.8, shows that both MVI and MIC staining, which is able to stain the three isoforms of the protein, MIC A, MIC B (NM1) and MIC C, are found all throughout the cell and within the nucleus. The nuclear levels of each protein is far lower than observed at the plasma membrane of the cell.

After treating HeLa cells with TIP, the amount of clusters and the number of molecules within them, is unchanged. As well as this, the area of these clusters also remains unchanged, therefore the TIP treatment itself does not affect MVIs ability to cluster within the nucleus. NM1 also follows the same pattern that after TIP treatment its ability to clusters, the number of molecules within a cluster and the overall size of these clusters remains the same.

This implies that NM1 is acting independently of MVI and that its ability to enter the nucleus and cluster together does not rely on the motor activity of MVI agreeing with the results shown in Chapter 6.

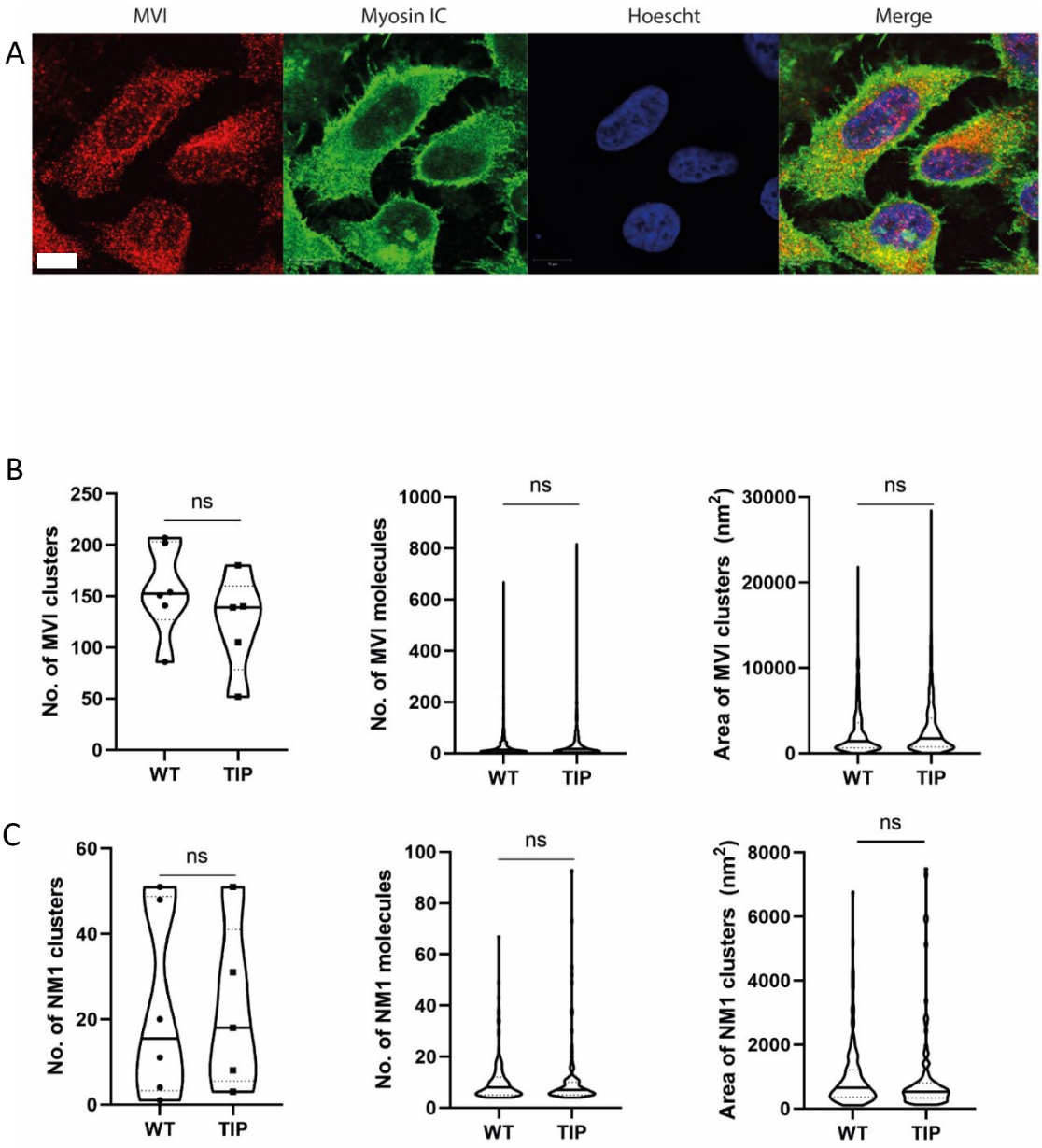


Figure 7.8. NM1 and MVI clustering analysis.

Confocal imaging shows where MVI and all myosin IC isoforms including NM1 are located (A). Scale bar 10µm. Using STORM and Clus-DoC analysis the number of clusters, the number of molecules found inside these clusters and the area of the clusters were calculated for MVI (B) and NM1 (C). A students T test was used and found all to be not significantly different (ns) before and after TIP treatment. N=3 n=10

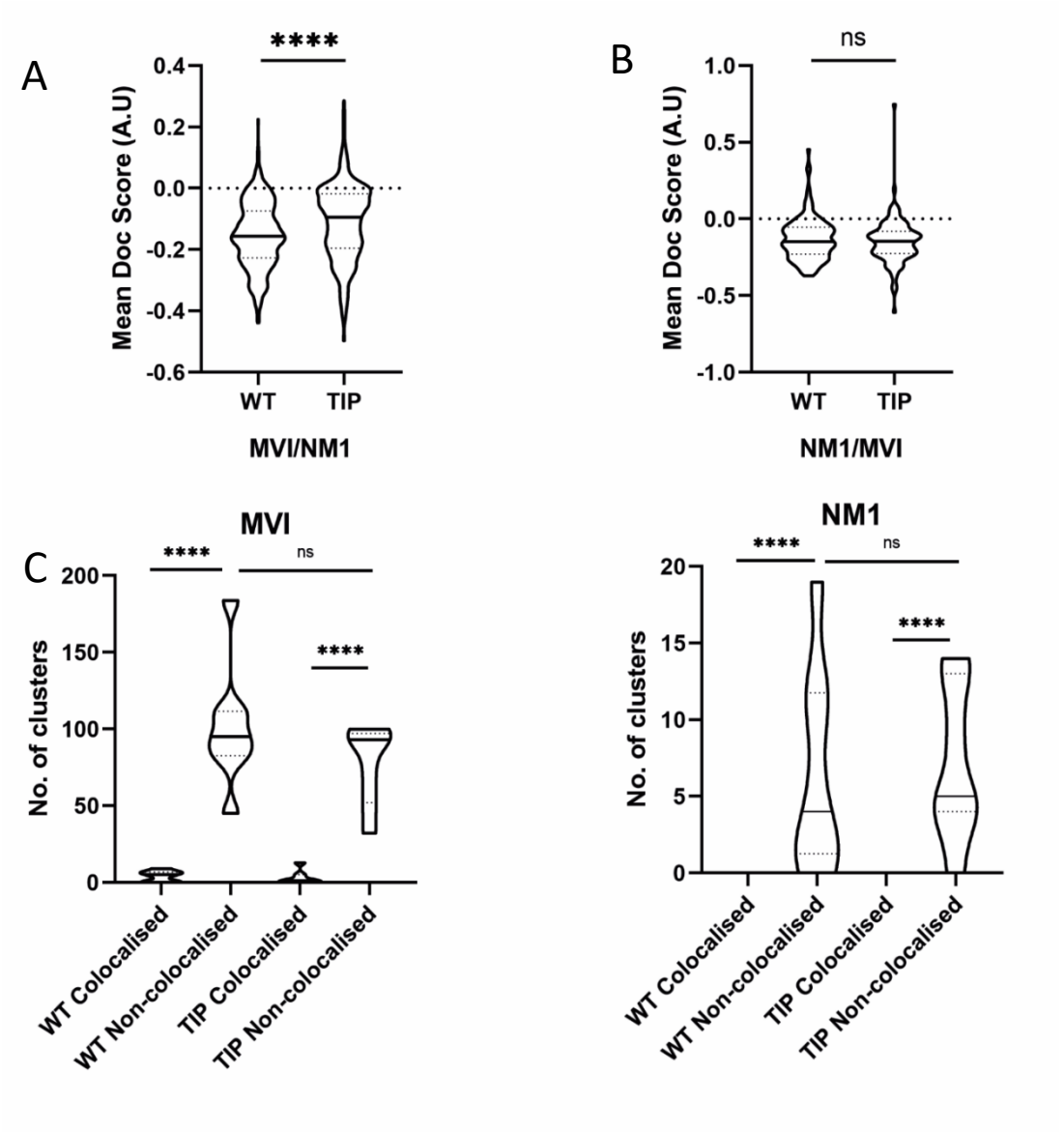
7.2.6 MVI and NM1 clusters are often segmented

As previously shown, the clusters of both MVI and NM1 can be superimposed onto each other and then each cluster can be scored by their colocalisation, their DoC score. If the DoC score is closer to -1 the two signals are functionally separate from each other, meaning the cell is specifically segmenting the two proteins, if the score is +1 the clusters colocalise completely together. When MVI clusters are overlapped onto NM1 clusters, the mean DoC score -0.1533 and when NM1 is overlapped onto MVI the mean DoC score is -0.1292 (Figure 7.9 A and B). This shows that the average MVI cluster is found not only not colocalised, but functionally separate from NM1 clusters.

After TIP treatment the MVI clusters have increased DoC scores with an average of -0.11, and so are more likely to colocalised with NM1 however the average score is still below 0, therefore it is likely all the clusters except a few are kept apart from NM1. TIP treatment has no effect on the overlap of NM1 clusters onto MVI clusters, once again showing that the MVIs functionality does not affect NM1s likelihood to be found adjacent to a MVI molecule.

The number of clusters found colocalised is significantly lower than the clusters that do not colocalise with each other, as well as the number of molecules found in these clusters and their areas (Figure 7.9 D). Once again, TIP has no effect on the size of these clusters or the number of molecules found in them. This confirms that these two proteins are both able to form clusters however, these clusters are kept functionally separate from each other.

The amount of NM1 molecules within nuclei is far less than MVI with an average of 984 and 8106 molecules respectively, and the average number of both NM1 and MVI molecules are similar after TIP treatment, 983 and 6527 respectively.


A
****
Mean Doc Score (A.U)
0.4
0.2
0.0
-0.2
-0.4
-0.6
WT
TIP
MVI/NM1
B
ns
Mean Doc Score (A.U)
1.0
0.5
0.0
-0.5
-1.0
WT
TIP
NM1/MVI
C
MVI
****
ns
****
No. of clusters
200
150
100
50
0
WT Colocalised
WT Non-colocalised
TIP Colocalised
TIP Non-colocalised
NM1
****
ns
****
No. of clusters
20
15
10
5
0
WT Colocalised
WT Non-colocalised
TIP Colocalised
TIP Non-colocalised

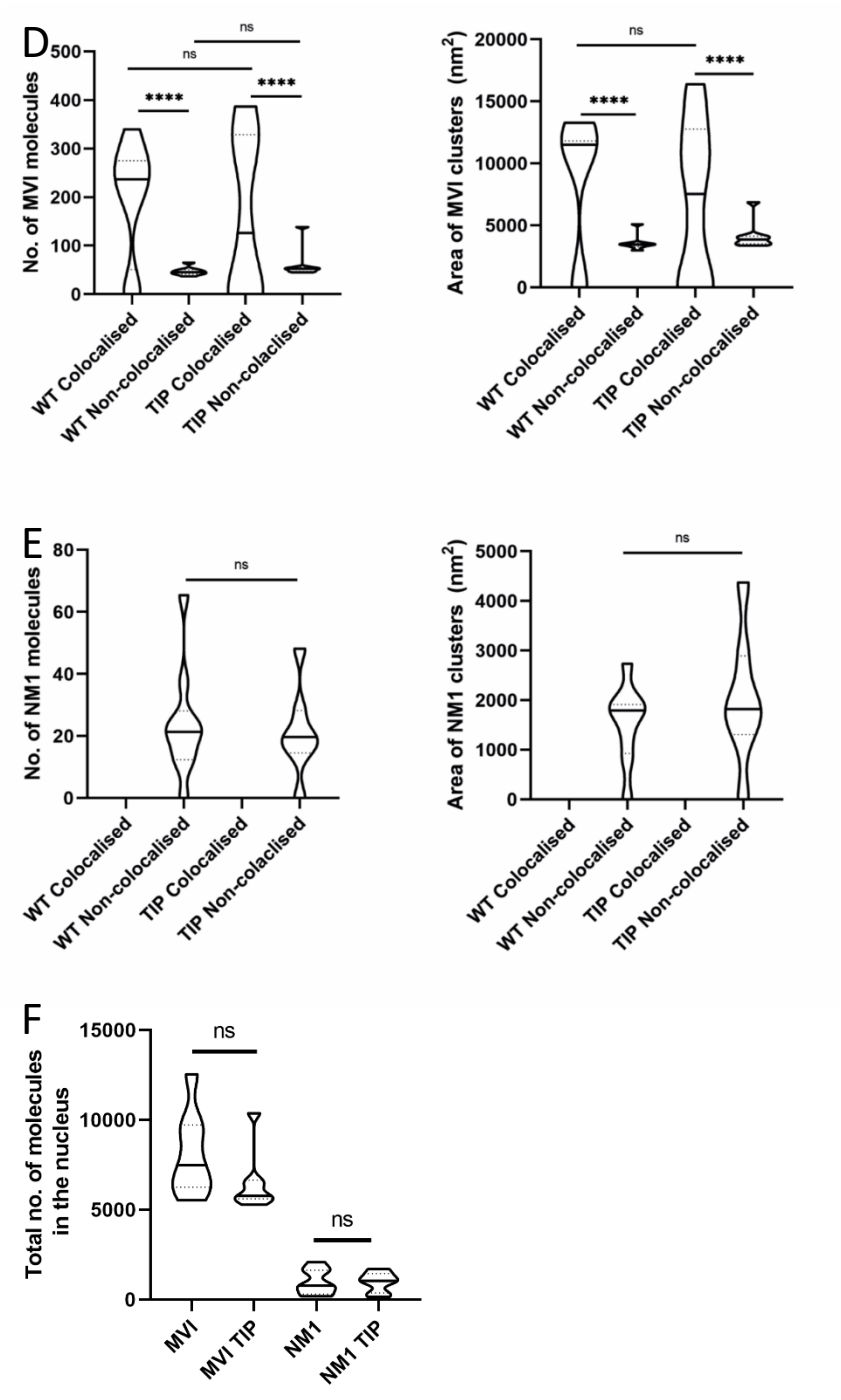


Figure 7.9. Clus-DoC analysis of the colocalisation of MVI and NM1 clusters.

STORM imaging and Clus-DoC analysis was used to identify the degree of colocalisation between MVI overlaid on NM1 (A) and NM1overlaid on MVI (B). The number of clusters that colocalised (C) was calculated alongside the number of molecules in these clusters and the area of MVI (D) and NM1 (E). The total no. of molecules in the nucleus is shown both before and after TIP (F) A normal ANOVA supplemented with Sidaks multiple comparions test is shown where ns is not significant or where **** is when $p<0.001$. N=3 n=10

7.3 Discussion

This study set out to identify if MVI and NM1 are linked in their roles within the nucleus. Both myosins within the cytoplasm can be used as transporters, and have been shown to colocalise at the cell periphery for endocytosis (Derwerchin *et al.,* 2014). Within the nucleus, it is now known that both myosins are required for RNAPII transcription through their interactions with the polymerase complex itself (Fili *et al.,* 2017; Almuzzaini *et al.,* 2015), and in NM1s case its ability to interact with the histone modification complex B-WICH (Vintermist *et al.,* 2011). If the two myosins are present at transcription sites, it is possible that the two myosins may also be linked within the DNA damage response.

7.3.1 Scientific research is cell line dependent

Often within scientific research, when an observation is made, it is quickly forgotten, in which cell line this observation relates to. It is assumed that if the role of protein is identified in one cell line, then it is the same for others. The same can be said about treatments to mammalian cells, if a cisplatin treatment causes a cell to produce a phenotype, it is often assumed this is the case for other mammalian cell lines. It is clear from the changes in histone modifications in this study that, both HeLa and MCF10A cells have a different response to bleomycin treatment. With HeLa increasing acetylation modifications whilst MCF10A cells are reducing these modifications, there needs to be more emphasis of context within cell biology research on the type of cell being used.

Immortal cancer cell lines have their limitations within laboratory research. They are indeed, easy to maintain, simple to manipulate and are well characterised, but they also have their downsides. They are not homogenous between laboratories, depending on the age and source of the cells, effects their genome, which could lead to unique phenotypes that other

laboratories do not observe. They also behave very differently to normal mammalian cells that are very difficult to maintain and perturb.

This study has shown how inhibiting MVI inhibits γH2AX in MCF10A cells and not HeLa, therefore, it is always of great importance to take into account cell lines and mutations when discussing an experimental result.

7.3.2 NM1 and MVI may both play a role in transcription regulation

It is published that NM1 allows the chromosome landscape to shift allowing for the progression of transcription from initiation to elongation (Almuzzaini *et al*, 2015). It does this by first binding to the RNAPII complex and actin, whilst bound to actin it then switches to bind to a histone modifier, which allows the correct modifications for transcription to occur.

Using HCS this study has followed gene activation through acetylation of the lysine-9 and lysine-27 on the H3 histone. Within MCF10A cells after bleomycin treatment the cells reduce these signals which may cause a repression of gene expression. When the MVI motor domain is inhibited and the MVI can no longer enter the nucleus the levels of H3K9ac and H3K27ac reduce significantly, more than seen after DNA damage. If both TIP and bleomycin treatments are undertaken together in MCF10A cells, these reductions are the same as TIP treatment only.

This shows that the cells may have a greater response transcriptionally to MVI inhibition than DNA damage, which was also been observed in the RNA-seq data. It is possible that the full role of MVI within transcription is yet to be elucidated, and that whilst it is seen MVI binds to the RNAPII complex, it may also act similar to NM1 where once RNAPII transcription has begun it is then recruited to a histone modifying complex to allow for further gene activation. It may also be that because KD of MVI changed the transcriptome of the cell, as shown in the RNA-seq data, the cell is responding to the fact it is unable to undergo

transcription, by reducing gene activation, focusing its resources on the most vital of genes. This can be observed through the increase of triple methylations found on lysine-9 of the H3 histone. Due to the increase of this signal, it is not possible to comment if MVI controls these methylations in a repressive way, or that due to MVI unable to carry out gene activation the cell automatically signals gene suppression.

7.3.3 HeLa cells do not require functioning MVI for their histone response to DNA damage

HeLa cells responded to DNA damage in an opposite fashion to the MCF10A cells, where originally the acetylated histones were reduced due to bleomycin treatment, in HeLa cells increase of acetylation occurred. This may provide information of the HeLa cell's ability to survive within the stressful environment of tumour growth, as well some cancers ability to become resistant to chemotherapeutics, as these changes in modifications may increase gene expression, through activation, the cell could be producing proteins vital to their survival.

After TIP treatment, the cells respond similar to that of MCF10A cells where it is observed acetylation is reduced and methylation is increased. This once again shows MVI may have some regulation over global gene expression changes within HeLa. This study is unable to produce a mechanism, as further work is required to fully understand if this is linked with MVIs ability to bind RNAPII or it acts independently of RNAPII and binds solely to histone modifiers.

After treating the cells with both the DNA damaging agent bleomycin and TIP, the HeLa cells respond to the DNA damage as though the MVI is not inhibited. This study sees a readjustment of histone signals so that there is once again an increase of H3K9ac and a reduction of H3Kme3, which may coincide with gene activation. This suggests that either the MVI is not required for the DNA damage response within HeLa, which has been shown by

the cells ability to still produce γH2AX signals after cisplatin and TIP treatment, or there is an alternative mechanism for MVI to be recruited into the nucleus, that does not require a functioning motor domain. Once again, this study has shown that a cells response to DNA damage is completely dependent on the cell line and that by comparing a non-cancerous cell line to a cancerous one, may identify the differences in their survival after DNA damage.

7.3.4 MVI is required for CT relocations after DNA damage

It is already known that NM1 has an ability to relocate CTs after DNA damage (Kulashreshtha *et al.,* 2016), in a mechanism that relies on γH2AX signalling. This movement of chromosomes most likely allows for the formation of repair foci as well as the matching of chromatin to allow for homologous recombination, and thus the repair of a DSB. This study set out to identify if CT relocation may also be dependent on MVI. It is known that after DNA damage, actin filaments can form within the nucleus, and that by inhibiting this formation, movement of chromatin does not occur and heterochromatic breaks are unable to repaired (Caridi *et al.,* 2018). This information provides a mechanism for how NM1 is able to transport such a large cargo by utilising strong actin tracks. MVI on the other hand travels along actin in the opposite direction to all other myosins, where it travels from the barbed end to the pointed end.

In this study a movement of two chromosomes, chromosome 12 and 19, which have been shown to move after DNA damage, were analysed before and after DNA damage. It is clear that these two chromosomes begin within the interior of the nucleus and after DNA damage move towards the nuclear periphery, whilst the positions of these chromosomes differ from previously published work it is likely that the HeLa cells have chromosome differences compared to normal human dermal fibroblast cells. This movement of chromosomes does not occur after DNA damage if the MVI motor domain inhibitor TIP is used alongside cisplatin. Therefore, MVI is required for chromosome movement just as NM1 is required.

It is likely MVI is required for its capability to travel in the opposite direction along actin filaments. Currently little characterisation work has been completed on these actin filaments within nuclei after DNA damage. It is unknown if the direction of filament formation occurs in a structured fashion, or randomly from the points of damage. It is likely NM1 transports chromosomes along these filaments in one direction and MVI may be recruited to transport these chromosomes in the opposite direction. However as discussed previously MVI becomes an anchor when a high force load is applied to it (Altman *et al.,* 2004), how the cell stops MVI becoming an anchor, when bound to such a large cargo as chromatin cannot be commented on, it is possible that a large cluster of MVI molecules would be able to move this cargo. By utilising multiple types of myosin for this movement of chromosomes, the cell can control direction of chromatin movement along actin filaments. It is also necessary to broaden the research into multiple chromosomes and multiple cell types, to identify if they undergo the same changes observed here.

7.3.5 NM1 and MVI are kept apart from each other

Using STORM imaging and a clustering and colocalisation analysis software, Clus-DoC, this study has been able to characterise if the two myosins are found together within a nucleus or functionally separate from each other. Currently there is no commercial antibody developed in mice, that is specific to the NM1 protein, therefore an antibody that recognises all three myosin IC isoforms has been utilised and the nucleus has been specifically highlighted as the region of interest.

Both NM1 and MVI are capable of clustering within the nucleus and neither are affected by the use of TIP. There are however, differences between MVI and NM1. MVI forms more clusters compared to that of NM1, and these clusters contain more molecules as well, being far larger. This could be related to their functions within the nucleus, where MVI can act as an anchor. This anchoring property may allow MVI molecules to cluster together to maintain

transcription factories or to cluster other proteins together, compared to NM1 that acts as a transporter and may need less than five molecules within a mechanism to perform its function, such as in transcription where it may act as an auxiliary motor. There are far less NM1 molecules within the nucleus compared to MVI, this may explain why the co-localisation events of NM1 is so rare.

After studying the co-localisation of these two molecules, it was found that the majority of MVI clusters do not overlap with NM1, and no NM1 clusters overlap with MVI clusters, along with this information a clustering score was provided, which determined that the clusters of these two proteins are deliberately separate. This separation may occur due to the two myosins being able to travel along actin filaments in different directions and thus need to be located at either end of the filaments to then allow transportation. It may also be to inhibit any cross talk between the myosins, as this study has found both myosins are involved in the DNA damage response and previous work has shown both to be involved in transcription. Therefore, it is possible the cell does not want the functions of these two myosins to be mixed. Finally, MVI is yet to be identified within the nucleolus of cells whereas NM1 is vital for the rDNA transcription, this may lead to clustering of MVI outside of the nucleoli yet in the nucleus and NM1 only clustering specifically within the nucleoli.

As discussed, both proteins have been linked with RNAPII transcription and both have been found to interact with the polymerase complex itself, therefore there should be some colocalisation of molecules, it is important to state that the analysis software here focused on the colocalisation of clusters that contained a minimum of five of each protein, therefore any small colocalisation between single molecules has not been identified and would require further work.

The TIP within this study has no effect on the colocalisation between the proteins and their clusters, therefore a functioning MVI motor domain is not required for the formation of these clusters and is most likely binding partners that generate the formation of these groups.

Overall, this study has found that MVI and NM1 have similar roles within the nucleus; both proteins have a role in the post translational modifications of histones, and can alter the global transcription activity of both MCF10A cells and HeLa cells. MVI has a similar role in the reorganisation of chromosome territories both before and after damage like NM1, which may be linked with the myosins ability to change histone modifications. Finally whilst these two myosins have similar roles, if there are groups larger than five molecules of one myosin then it will not colocalise with the other myosin, leading to the hypothesis that these two proteins have similar roles but may act in opposite manners within a mechanism, further work would be required to fully understand the relationship between the two myosins.

Chapter 8. General Discussion

8.1 Summary

Both NM1 and MVI are structurally different, and their roles within the cytoplasm are different, with only one observation of the two myosins working together (Dewerchin *et al.,* 2014). Often NM1 is found in a monomeric state (Manceva *et al.,* 2007), whilst MVI can form dimers (Hasson 2003), NM1 also acts solely as a transporter (McIntosh and Ostap, 2016), whilst MVI is a transporter when bound to low load bearing cargo, or an anchor when under high molecular forces (>2pN) (Chuan *et al.,* 2011). Whilst these myosins behave differently to each other, within the nucleus their roles seem to be intertwined during DNA damage.

8.2 Myosin self-regulation aids its nuclear localisation

This thesis has focused on the ability of myosins to enter the nucleus to perform specific functions within the nucleus. Currently within the nuclear myosin field there is some discussion as to how NM1 and MVI are able to enter the nucleus, including experiments that show shuttling of nuclear myosins (Maly and Hofmann, 2016), as well as cells pooling nuclear myosins (Nevzorov *et al.,* 2018), so that NM1 is maintained within the nucleus, without losing it back to the cytoplasm.

NM1 has been proposed to move into the nucleus through two different mechanisms, one utilising its phosphoinositol binding capabilities (Nevzorov *et al.,* 2018), where it first enters the golgi apparatus and then uncontrollably diffuses through the nuclear pore complexes. The second mechanism requires the specific NLS found embedded within the flexible neck region of the myosin, specifically the second IQ region. Here a loss of CaM is required for the NM1 to travel through importin beta, importin 5 and importin 7. Meanwhile MVI contains seven NLS sites and one predicted NES site, where ivermectin, an inhibitor of α/β-mediated nuclear importers blocks the import of MVI, following the rule of controlled import of nuclear myosins (Maly and Hofmann, 2016).

This study identified a folding capability of NM1 that may aid in its nuclear import by inhibiting the binding of CaM to the IQ region and thus allowing the NLS sequence to be identified by importins, moving the myosin into the nucleus. By using well understood biochemical techniques and recombinant protein purification, it is clear the N-terminus of NM1 can bind to the neck and tail region of itself, which may regulate its ability to transport into the nucleus. MVI is also capable of self-regulation through folding (Fili *et al.,* 2017), and with one NLS being identified within the IQ domain of the protein (Majewski *et al.,* 2018), it is possible it may act in the opposite manner, where a folded confirmation is unable to enter the nucleus due to the blocked NLS, however so far only the non-insert isoform is found in the nucleus and this is unable to back fold. Therefore a myosins structure plays an important role in its ability to become nuclear.

8.3 MVI is vital to the DNA damage response

This thesis has focused on the unknown roles of MVI in the nucleus, by comparing the already characterised roles of NM1 after DNA damage.

It is known MVI is able to respond to certain stimuli (Majewski *et al.,* 2018) by localising into the nucleus, and DNA damage can now be added to the growing list. An increase of MVI in the nucleus observed through HCS and confocal imaging can be attributed to MVI localisation, as there is no change of MVI gene expression, after cisplatin treatment, this would be reasonable as the cell would wish to respond to the DNA damage rapidly. If the response was transcriptionally based there would be a minimum lag time before the cell could respond.

This lag time also correlates with the KD of MVI having little effect on the expression of DNA damage proteins found at the start of the DNA damage response, thus implying MVIs role in transcription is not relevant to the immediate response. Therefore, protein-protein

interactions drive the MVI response leading its nuclear recruitment. During the proteomics study within this thesis, MVI was found to bind multiple DNA repair proteins, and within HeLa it was found specifically bound to Rad50, a subunit of the MRN complex that repairs DNA, which also plays a role in ATM activation (Lee and Paull, 2004). Interestingly MVI was found to bind not only DSB repair proteins, but others found within base excision repair and nucleotide excision repair. This opens up the idea that MVI is not specifically responding to DSBs, but is used globally to repair multiple types of damage, the remit of this thesis did not extend as far as other repair mechanisms, however the data provides enough evidence for further work to be carried out.

A significant discovery has been the necessity of MVI nuclear localisation to signal DSBs through the phosphorylation of the H2AX histone in MCF10A cells. This phosphorylation event occurs, due to the auto-phosphorylation of the ATM kinase at the point of a DSB, which then phosphorylates the H2AX histone (Firsanov *et al.,* 2011). As shown when the motor domain of MVI has been inhibited in MCF10A cells using TIP, the MVI is unable to translocate into the nucleus and there is no γH2AX signalling. This lack of γH2AX places MVI at the very beginning of DSB signalling.

So far multiple activations of ATM have been identified, all of which must occur rapidly for the accumulation of ATM around sites of damage. One such activation of ATM is through the Rad50 subunit of the DSB repair complex, MRN. Here, both the coiled-coil domain and zinc hook found on Rad50, whose conformation changes are ATP driven can cause ATM activation (Limbo *et al.,* 2018). Interestingly, in the proteomics presented in this thesis, Rad50 was one protein found bound to MVI. Another method of ATM activation, which may occur previous to this step, is the acetylation of the ATM dimer (inactive ATM), at lysine-3016 (Sun *et al.,* 2007). This acetylation however can be blocked by the acetylation found on lysine-9 on the H3 histone (Meyer *et al.,* 2016). This thesis identified a change in H3K9me3 amounts after

both TIP treatment and DNA damage, and could put MVI within this step of ATM activation. Other activations of ATM occur after the first signal of DSBs is initiated, and contribute to the spread of signal and stabilisation of repair foci.

So why the movement of MVI? MVI is always present in the nucleus, however this has been prescribed to its role in transcription and its interactions with RNAPII (Fili *et al.,* 2017). It is possible the cell is simply recruiting more MVI into the nucleus to provide enough MVI to regulate transcription, as well as being present at sites of DNA damage. DNA damage itself may switch MVI from its role in transcription, to a role in DNA damage, thus resulting in the change of multiple small clusters of the protein, to a reduced amount of clusters of larger size. It may however have a binding partner within the cytoplasm of the cell in which it is responsible for translocating into the nucleus after a DSB, or its binding partners movement into the nucleus, brings with it MVI. There are multiple proteins found within the DSB signalling and repair, that can be found within the cytoplasm of the cell, however due to the rapid response necessary for repair, these cytoplasmic proteins can often be found downstream of γH2AX signalling, such as p53, BRCA1, NFκB (Bennetzen *et al.,* 2018). ATM is also found in the cytoplasm, but is yet to be characterised in terms of DSBs but for its role in controlling reactive oxygen species (Kozlov *et al.,* 2016). So it is possible that MVI is required to transport a key protein into the nucleus, for γH2AX signalling.

Finally, what is signalling MVI to move into the nucleus after DNA damage? One possible signal for the recruitment of MVI is ATM itself. MVI has three identified phosphorylation sites within its structure, and so far one site in particular has been characterised in its role within the motor domain (Yoshimura *et al.,* 2001). Threonine-405 within MVIs motor domain, when phosphorylated, weakens MVIs ability to bind actin. Therefore one such theory is activated ATM crosses the nuclear membrane into the cytoplasm where it would normally phosphorylate p53 and other downstream proteins, and as well as this, it phosphorylates the

motor domain of MVI. MVI then rapidly dissociates from cytoplasmic actin and is now freely available to move into the nucleus where it then plays a role in γH2AX signalling. For this hypothesis to be proven, the phosphorylated ATM would need to be followed after induction of DSBs. This would identify if the loss of γH2AX is down to a loss of phospho-ATM in the nucleus or the loss of γH2AX signalling only and the remaining cellular response to DNA damage still continues.

8.4 Nuclear myosins play a significant role in chromosome organisation

As discussed previously, NM1 directly influences histone modifications during transcription where it binds directly to the Snf2h/WSTF complex which forms the B-WICH chromatin remodelling complex (Almuzzaini *et al.,* 2015). This complex in turn recruits the histone acetyltransferase (HAT) Set1/Ash2 to maintain H3K9 acetylation and H3K4 tri-methylation for active transcription. As well as this, NM1, is able to move chromatin territories large distances across the nucleus after DNA damage, and this movement is strictly controlled by γH2AX signalling (Kulashreshta *et al.,* 2016). This movement of chromatin, allows the cell to undergo homologous recombination with sister chromatids as well the formation of repair foci.

This thesis provided data that not only MVI affects γH2AX signalling but also by inhibiting its motor domain in both MCF10A and HeLa cell lines, the levels of H3K9ac, H3K9me3, H3K27ac, H3K36me2 and H4K20me are all affected. This global response to a loss of MVI within the nucleus shows that MVI plays a larger role within the nucleus than first thought. Whilst NM1 interacts with the HAT Set1/Ash2, MVI must interact with a larger pool of HATs and histone methyl transferases (HMTs). Using the HCS approach here, a phenotype has been identified, however little else can be further elucidated. The proteomics did see MVI binding directly to BRG1, which can be found associated with transcriptional repressors and activators, as well

as histones themselves, which may explain why it is vital for such a broad array of histone modifications.

Finally like NM1, MVI is required for the relocation of chromosome territories after DNA damage, in this scenario it is likely the MVI is acting as a transporter similar to NM1 that is able to move large pieces of chromatin across large distances for the organisation of homologous recombination and the formation of repair foci.

8.5 DNA damage response is cell line dependent

This thesis has identified a clear difference between the cervical cancer cell line, HeLa, and the non-cancerous breast cell line, MCF10A, and how they respond to DNA damage. It is clear that the motor domain of MVI is vital for MCF10A to signal damage through γH2AX however a functioning motor domain within HeLa was not. This difference highlights not just the importance of MVI, but the need to study cellular responses in a cell line specific manner.

Gene expression analysis of HeLa cells, has shown that out of the large set of over-expressed genes compared to normal human cell lines, the DNA repair pathway contains the most (Frattini *et al.,* 2015). Interestingly each DNA repair pathway contained at least one aberrated component, yet the cells were still able to contain and repair the damaged sites. This highlights the flexibility and redundancy that has been created through this highly mutated cell line.

HeLa also contain the E6 protein from oncogenic HPV type 18 which directly represses the activity of p53 (Hoppe-Seyler and Butz, 1993) as discussed previously in certain cell lines, MVI interacts with p53 and is able to stabilise the activated phospho-p53 allowing the cell to respond to cell stresses whilst in others, MVI expression reduced p53 stabilisation and expression (Cho and Chen, 2010). It is possible that by inhibiting the motor domain of MVI using TIP, in turn the supressed p53 is reactivated or further repressed. This variation in p53

response makes understanding the mechanism as to why exactly the two cell lines behave differently difficult, especially as HeLa, with a non-functioning p53, and debilitated damage repair pathway, is still able to repair and divide after DNA damage and the inhibition of MVI.

8.6 Improving research practices

The nuclear myosin field is currently at a turning point, with the general agreement of actin within the nucleus, the possible forms it may take, and the identification of 8 types of myosins within the nucleus (de Lanerolle, 2012), it is vital that the research undertaken is thorough. Published work to this point have often identified a phenotype after KO or KD of a nuclear myosin without understanding the full mechanism of its role. It is easy to observe NM1 or MVI at transcription sites but far harder to assign a function. To do this, biophysical, biochemical and cellular chemistry are all required. Myosins can only function within their biophysical restraints: are they able to withhold a force? Are they kinetically viable? Do their structures allow for that binding confirmation? These questions then need to link with the biochemistry, is it possible to have a myosin and another protein interacting? And finally the cellular biology, where are the myosins located within the nucleus? These questions provide a basis of where to begin however all nuclear myosins have cytoplasmic counterparts, so by removing a myosin from a system, you not only affect the role that is being studied but the cytoskeleton, endo- and exocytosis, transcription, chromatin organisation. This is why in this thesis, both RNA-seq and proteomics provided a base of understanding of the cells behaviour before drawing any conclusions.

Finally this thesis highlighted the importance of cell lines when studying cellular biology. It is far too common practice within research that if a mechanism has been discovered in one cell line, it would be observable in most other cell lines. However here, this has clearly not been the case. The difference of MCF10A cells requiring MVI and HeLa not for γH2AX signalling,

highlights how each cell line needs to be analysed as its own separate class if the resources allow it.

8.7 Further work

To fully understand the function of MVI in the DNA damage response, further work would need to be carried out by using live cell imaging techniques and infra-red radiation. This would make it possible to track MVI from the cytoplasm to the nucleus in real time to gain a better understanding of how it is signalled into the nucleus. As well as this, further work into the phosphorylation sites of MVI may provide further information, therefore using biochemical techniques *in vitro*, it could be possible that ATM itself can directly phosphorylate MVI. Further work is required to understand the relationship between NM1 and MVI, if DNA damage is caused, do the two proteins then colocalise or are they functionally independent of each other during the DSB response? Fluorescence recovery after photobleaching (FRAP) measurements would allow the visualisation of the myosins as they move into the nucleus, and so this will provide further information on the shuttling status of both proteins before and DNA damage. Finally more cell lines will need to be studied to understand the broad role MVI and NM1 play within the nucleus, specifically comparing genomically stable cell lines to cancerous cell lines, for therapeutic advances.

Chapter 9. References

Adamek, N., Coluccio, L. M. and Geeves, M. A. (2008) “Calcium sensitivity of the cross-bridge cycle of Myo1c, the adaptation motor in the inner ear.,” *Proceedings of the National Academy of Sciences of the United States of America*, 105(15), pp. 5710–5. doi: 10.1073/pnas.0710520105.

Adams, R. J. and Pollard, T. D. (1989) “Binding of myosin I to membrane lipids,” *Nature*, 340(6234), pp. 565–568. doi: 10.1038/340565a0.

Alexander, J. L. and Orr-Weaver, T. L. (2016) “Replication fork instability and the consequences of fork collisions from rereplication,” *Genes and Development*. Cold Spring Harbor Laboratory Press, 30(20), pp. 2241–2252. doi: 10.1101/gad.288142.116.

Almuzzaini, B., Sarshad, A. A., Farrants, A.-K. Ö., *et al.* (2015) “Nuclear myosin 1 contributes to a chromatin landscape compatible with RNA polymerase II transcription activation,” *BMC Biology*, 13(1), p. 35. doi: 10.1186/s12915-015-0147-z.

Altman, D., Sweeney, H. L. and Spudich, J. A. (2004) “The mechanism of myosin VI translocation and its load-induced anchoring.,” *Cell*, 116(5), pp. 737–49. Available at: http://www.ncbi.nlm.nih.gov/pubmed/15006355.

An, J. *et al.* (2010) “DNA-PKcs plays a dominant role in the regulation of H2AX phosphorylation in response to DNA damage and cell cycle progression.,” *BMC molecular biology*, 11, p. 18. doi: 10.1186/1471-2199-11-18.

Aparicio, T., Baer, R. and Gautier, J. (2014) “DNA double-strand break repair pathway choice and cancer,” *DNA Repair*. Elsevier, 19, pp. 169–175. doi: 10.1016/j.dnarep.2014.03.014.

Arif, E. *et al.* (2016) “Structural Analysis of the Myo1c and Neph1 Complex Provides Insight into the Intracellular Movement of Neph1,” *Molecular and Cellular Biology*. American Society for Microbiology, 36(11), pp. 1639–1654. doi: 10.1128/mcb.00020-16.

Arnaudo, A. M. and Garcia, B. A. (2013) 'Proteomic characterization of novel histone post-translational modifications', *Epigenetics & Chromatin*, 6(1), p. 24. doi: 10.1186/1756-8935-6-24.

Attardi, L. D., Reczek, E. E., Cosmas, C., Demicco, E. G., McCurrach, M. E., Lowe, S. W., & Jacks, T. (2000). PERP, an apoptosis-associated target of p53, is a novel member of the PMP-22/gas3 family. *Genes & development*, 14(6), 704–718.

Babu, Y. S., Bugg, C. E. and Cook, W. J. (1988) "Structure of CaM refined at 2.2 Å resolution," *Journal of Molecular Biology*. Academic Press, 204(1), pp. 191–204. doi: 10.1016/0022-2836(88)90608-0.

Bae, W. *et al.* (2019) "Single-strand annealing mediates the conservative repair of double-strand DNA breaks in homologous recombination-defective germ cells of Caenorhabditis elegans.," *DNA repair*, 75, pp. 18–28. doi: 10.1016/j.dnarep.2019.01.007.

Bähler, M. and Rhoads, A. (2002) 'Calmodulin signaling via the IQ motif', *FEBS Letters*, 513(1), pp. 107–113. doi: 10.1016/S0014-5793(01)03239-2.

Bahloul, A. *et al.* (2004) "The unique insert in myosin VI is a structural calcium-CaM binding site," *Proceedings of the National Academy of Sciences of the United States of America*, 101(14), pp. 4787–4792. doi: 10.1073/pnas.0306892101.

Balakrishnan, L., Gloor, J. W. and Bambara, R. A. (2010) "Reconstitution of eukaryotic lagging strand DNA replication.," *Methods (San Diego, Calif.)*, 51(3), pp. 347–57. doi: 10.1016/j.ymeth.2010.02.017.

Bamburg, J. R. and Bernstein, B. W. (2010) "Roles of ADF/cofilin in actin polymerization and beyond," *F1000 Biology Reports*. doi: 10.3410/B2-62.

Bannister, A. J. and Kouzarides, T. (2011) “Regulation of chromatin by histone modifications,” *Cell Research*, pp. 381–395. doi: 10.1038/cr.2011.22.

Batters, C. *et al.* (2016) “Calcium can mobilize and activate myosin-VI,” *Proceedings of the National Academy of Sciences of the United States of America*. National Academy of Sciences, 113(9), pp. E1162–E1169. doi: 10.1073/pnas.1519435113.

Batters, C. and Veigel, C. (2016) “Mechanics and Activation of Unconventional Myosins,” *Traffic*, 17(8), pp. 860–871. doi: 10.1111/tra.12400.

Beerens, N. *et al.* (2005) “The CSB protein actively wraps DNA.,” *The Journal of biological chemistry*, 280(6), pp. 4722–9. doi: 10.1074/jbc.M409147200.

Belin, B. J., Lee, T. and Mullins, R. D. (2015) “DNA damage induces nuclear actin filament assembly by formin-2 and spire-1/2 that promotes efficient DNA repair,” *eLife*. eLife Sciences Publications Ltd, 4(AUGUST2015). doi: 10.7554/eLife.07735.

Bennetzen, M. V *et al.* (2018) ‘DNA damage-induced dynamic changes in abundance and cytosol-nuclear translocation of proteins involved in translational processes, metabolism, and autophagy’, *Cell Cycle*, 17(17), pp. 2146–2163. doi: 10.1080/15384101.2018.1515552.

Beucher, A. *et al.* (2009) “ATM and Artemis promote homologous recombination of radiation-induced DNA double-strand breaks in G2.,” *The EMBO journal*, 28(21), pp. 3413–27. doi: 10.1038/emboj.2009.276.

Bezanilla, M. *et al.* (2015) “Cytoskeletal dynamics: A view from the membrane,” *Journal of Cell Biology*. Rockefeller University Press, pp. 329–337. doi: 10.1083/jcb.201502062.

Boguslavsky, S. *et al.* (2012) “Myo1c binding to submembrane actin mediates insulin-induced tethering of GLUT4 vesicles,” *Molecular Biology of the Cell*, 23(20), pp. 4065–4078. doi: 10.1091/mbc.E12-04-0263.

Bolzer, A. *et al.* (2005) “Three-dimensional maps of all chromosomes in human male fibroblast nuclei and prometaphase rosettes,” *PLoS Biology*, 3(5), pp. 0826–0842. doi: 10.1371/journal.pbio.0030157.

Bose, A. *et al.* (2004) “Unconventional Myosin Myo1c Promotes Membrane Fusion in a Regulated Exocytic Pathway,” *Molecular and Cellular Biology*. American Society for Microbiology, 24(12), pp. 5447–5458. doi: 10.1128/mcb.24.12.5447-5458.2004.

Brandstaetter, H., Kendrick-Jones, J. and Buss, F. (2012) “Myo1c regulates lipid raft recycling to control cell spreading, migration and Salmonella invasion,” *Journal of Cell Science*, 125(8), pp. 1991–2003. doi: 10.1242/jcs.097212.

Bugreev, D. v, Mazina, O. M. and Mazin, A. v (2006) “Rad54 protein promotes branch migration of Holliday junctions.,” *Nature*, 442(7102), pp. 590–3. doi: 10.1038/nature04889.

Burgess, S. *et al.* (2002) “The prepower stroke conformation of myosin V,” *The Journal of Cell Biology*, 159(6), pp. 983–991. doi: 10.1083/jcb.200208172.

Burma, S. *et al.* (2001) “ATM Phosphorylates Histone H2AX in Response to DNA Double-strand Breaks,” *Journal of Biological Chemistry*, 276(45), pp. 42462–42467. doi: 10.1074/jbc.C100466200.

Bussa, F. and Kendrick-Jonesb, J. (2011) “Multifunctional myosin VI has a multitude of cargoes,” *Proceedings of the National Academy of Sciences of the United States of America*, pp. 5927–5928. doi: 10.1073/pnas.1103086108.

Buss, F. *et al.* (2001) “Myosin VI isoform localized to clathrin-coated vesicles with a role in clathrin-mediated endocytosis,” *EMBO Journal*, 20(14), pp. 3676–3684. doi: 10.1093/emboj/20.14.3676.

Buss, F., Spudich, G. and Kendrick-Jones, J. (2004) “MYOSIN VI: Cellular Functions and Motor Properties,” *Annual Review of Cell and Developmental Biology*. Annual Reviews, 20(1), pp. 649–676. doi: 10.1146/annurev.cellbio.20.012103.094243.

Cameron, R. S., Liu, C. and Pihkala, J. P. S. (2013) “Myosin 16 levels fluctuate during the cell cycle and are downregulated in response to DNA replication stress,” *Cytoskeleton*, 70(6), pp. 328–348. doi: 10.1002/cm.21109.

Caridi, C. P. *et al.* (2018) “Nuclear F-actin and myosins drive relocalization of heterochromatic breaks,” *Nature*. doi: 10.1038/s41586-018-0242-8.

Castella, M. *et al.* (2015) “FANCI Regulates Recruitment of the FA Core Complex at Sites of DNA Damage Independently of FANCD2.,” *PLoS genetics*, 11(10), p. e1005563. doi: 10.1371/journal.pgen.1005563.

Caswell, P. T. and Zech, T. (2018) “Actin-Based Cell Protrusion in a 3D Matrix,” *Trends in Cell Biology*. Elsevier Ltd, pp. 823–834. doi: 10.1016/j.tcb.2018.06.003.

Cazzalini, O. *et al.* (2010) “Multiple roles of the cell cycle inhibitor p21CDKN1A in the DNA damage response,” *Mutation Research - Reviews in Mutation Research*, pp. 12–20. doi: 10.1016/j.mrrev.2010.01.009.

Chesarone, M. A. and Goode, B. L. (2009) “Actin nucleation and elongation factors: mechanisms and interplay,” *Current Opinion in Cell Biology*, pp. 28–37. doi: 10.1016/j.ceb.2008.12.001.

Chibalina, M. v. *et al.* (2009) “Potential roles of myosin VI in cell motility,” in *Biochemical Society Transactions*, pp. 966–970. doi: 10.1042/BST0370966.

Cho, S. J. and Chen, X. (2010) “Myosin VI Is Differentially Regulated by DNA Damage in p53- and Cell Type-dependent Manners,” *Journal of Biological Chemistry*, 285(35), pp. 27159–27166. doi: 10.1074/jbc.M110.142117.

Chrisanthar, R. *et al.* (2008) “CHEK2 mutations affecting kinase activity together with mutations in TP53 indicate a functional pathway associated with resistance to epirubicin in primary breast cancer,” *PLoS ONE*, 3(8). doi: 10.1371/journal.pone.0003062.

Chuang, C.-H. *et al.* (2006) “Long-range directional movement of an interphase chromosome site.,” *Current biology : CB*, 16(8), pp. 825–31. doi: 10.1016/j.cub.2006.03.059.

CHUAN, P., SPUDICH, J. A. & DUNN, A. R. 2011. Robust mechanosensing and tension generation by myosin VI. Journal of molecular biology, 405, 105-112.

Collins, F. S. *et al.* (2004) “Finishing the euchromatic sequence of the human genome,” *Nature*, 431(7011), pp. 931–945. doi: 10.1038/nature03001.

Cook, A., Hari-Gupta, Y. and Toseland, C. P. (2018) ‘Application of the SSB biosensor to study in vitro transcription’, *Biochemical and Biophysical Research Communications*, 496(3), pp. 820–825. doi: 10.1016/j.bbrc.2018.01.147.

Cortez, D. *et al.* (1999) “Requirement of ATM-dependent phosphorylation of brca1 in the DNA damage response to double-strand breaks.,” *Science (New York, N.Y.)*, 286(5442), pp. 1162–6. doi: 10.1126/science.286.5442.1162.

Cramer, L. (2008) “Organelle transport: dynamic actin tracks for myosin motors.,” *Current biology : CB*, 18(22), pp. R1066-8. doi: 10.1016/j.cub.2008.09.048.

Creyghton, M. P. *et al.* (2010) “Histone H3K27ac separates active from poised enhancers and predicts developmental state,” *Proceedings of the National Academy of Sciences of the United States of America*, 107(50), pp. 21931–21936. doi: 10.1073/pnas.1016071107.

Curradi, M. *et al.* (2002) “Molecular Mechanisms of Gene Silencing Mediated by DNA Methylation,” *Molecular and Cellular Biology*. American Society for Microbiology, 22(9), pp. 3157–3173. doi: 10.1128/mcb.22.9.3157-3173.2002.

Cyr, J. L., Dumont, R. A. and Gillespie, P. G. (2002) “Myosin-1c interacts with hair-cell receptors through its CaM-binding IQ domains.,” *The Journal of neuroscience : the official journal of the Society for Neuroscience*, 22(7), pp. 2487–95. doi: 20026242.

Dasari, S. and Bernard Tchounwou, P. (2014) “Cisplatin in cancer therapy: Molecular mechanisms of action,” *European Journal of Pharmacology*. Elsevier, pp. 364–378. doi: 10.1016/j.ejphar.2014.07.025.

Dasbiswas, K. *et al.* (2018) “Ordering of myosin II filaments driven by mechanical forces: experiments and theory.,” *Philosophical transactions of the Royal Society of London. Series B, Biological sciences*, 373(1747). doi: 10.1098/rstb.2017.0114.

Davies, L. *et al.* (2011) “PERP expression stabilizes active p53 via modulation of p53-MDM2 interaction in uveal melanoma cells,” *Cell Death and Disease*, 2(3). doi: 10.1038/cddis.2011.19.

DeFilippis, R. A. *et al.* (2003) “Endogenous Human Papillomavirus E6 and E7 Proteins Differentially Regulate Proliferation, Senescence, and Apoptosis in HeLa Cervical Carcinoma Cells,” *Journal of Virology*. American Society for Microbiology, 77(2), pp. 1551–1563. doi: 10.1128/jvi.77.2.1551-1563.2003.

Denessiouk, K. *et al.* (2014) “Two structural motifs within canonical EF-hand calcium-binding domains identify five different classes of calcium buffers and sensors,” *PLoS ONE*. Public Library of Science, 9(10). doi: 10.1371/journal.pone.0109287.

Dewerchin, H. L. *et al.* (2014) “Myosins 1 and 6, myosin light chain kinase, actin and microtubules cooperate during antibody-mediated internalisation and trafficking of membrane-expressed viral antigens in feline infectious peritonitis virus infected monocytes,” *Veterinary Research*, 45(1). doi: 10.1186/1297-9716-45-17.

Difilippantonio, S. *et al.* (2005) ‘Role of Nbs1 in the activation of the Atm kinase revealed in humanized mouse models’, *Nature Cell Biology*, 7(7), pp. 675–685. doi: 10.1038/ncb1270.

Donovan, K. W. and Bretscher, A. (2012) “Myosin-V is activated by binding secretory cargo and released in coordination with Rab/exocyst function.,” *Developmental cell*, 23(4), pp. 769–81. doi: 10.1016/j.devcel.2012.09.001.

Dorr, R. T. (1992) “Bleomycin pharmacology: mechanism of action and resistance, and clinical pharmacokinetics.,” *Seminars in oncology*, 19(2 Suppl 5), pp. 3–8. Available at: http://www.ncbi.nlm.nih.gov/pubmed/1384141 (Accessed: September 29, 2019).

Doyon, Y. *et al.* (2004) “Structural and Functional Conservation of the NuA4 Histone Acetyltransferase Complex from Yeast to Humans,” *Molecular and Cellular Biology*. American Society for Microbiology, 24(5), pp. 1884–1896. doi: 10.1128/mcb.24.5.1884-1896.2004.

DUENSING, S. & MÜNGER, K. 2002. Human papillomaviruses and centrosome duplication errors: modeling the origins of genomic instability. Oncogene, 21, 6241-6248.

Duncan, B. K. and Miller, J. H. (1980) “Mutagenic deamination of cytosine residues in DNA,” *Nature*, 287(5782), pp. 560–561. doi: 10.1038/287560a0.

Dzijak, R. *et al.* (2012) “Specific nuclear localizing sequence directs two myosin isoforms to the cell nucleus in CaM-sensitive manner,” *PLoS ONE*, 7(1). doi: 10.1371/journal.pone.0030529.

Eddinger, T. J. and Meer, D. P. (2007) “Myosin II isoforms in smooth muscle: heterogeneity and function,” *American Journal of Physiology-Cell Physiology*, 293(2), pp. C493–C508. doi: 10.1152/ajpcell.00131.2007.

Einarsdóttir, K. *et al.* (2006) “Comprehensive analysis of the ATM, CHEK2 and ERBB2 genes in relation to breast tumour characteristics and survival: A population-based case-control and follow-up study,” *Breast Cancer Research*, 8(6). doi: 10.1186/bcr1623.

Eliezer, Y. *et al.* (2014) “Interplay between the DNA damage proteins MDC1 and ATM in the regulation of the spindle assembly checkpoint,” *Journal of Biological Chemistry*. American Society for Biochemistry and Molecular Biology Inc., 289(12), pp. 8182–8193. doi: 10.1074/jbc.M113.532739.

Evdokimova, V. N. *et al.* (2018) “Nuclear myosin/actin-motored contact between homologous chromosomes is initiated by ATM kinase and homology-directed repair proteins at double-strand DNA breaks to suppress chromosome rearrangements,” *Oncotarget*. Impact Journals LLC, 9(17), pp. 13612–13622. doi: 10.18632/oncotarget.24434.

Fei, P., Bernhard, E. J. and El-Deiry, W. S. (2002) “Tissue-specific induction of p53 targets in vivo.,” *Cancer research*, 62(24), pp. 7316–27. Available at: http://www.ncbi.nlm.nih.gov/pubmed/12499275 (Accessed: September 26, 2019).

Fenley, A. T. *et al.* (2018) “Modulation of nucleosomal DNA accessibility via charge-altering post-translational modifications in histone core,” *Epigenetics and Chromatin*. BioMed Central Ltd., 11(1). doi: 10.1186/s13072-018-0181-5.

Fili, N. *et al.* (2017) “NDP52 activates nuclear myosin VI to enhance RNA polymerase II transcription,” *Nature Communications*. Springer US, 8(1), p. 1871. doi: 10.1038/s41467-017-02050-w.

Fili, N., Hari-Gupta, Y., ... Toseland, C.P, (2019). Binding partner regulation of Myosin VI: Loss of tumour-suppressor Dab2 leads to enhanced activity of nuclear myosin. bioRxiv 639963. doi:10.1101/639963

Fincham, V. J., Brunton, V. G. and Frame, M. C. (2000) "The SH3 domain directs acto-myosin-dependent targeting of v-Src to focal adhesions via phosphatidylinositol 3-kinase.," *Molecular and cellular biology*, 20(17), pp. 6518–36. doi: 10.1128/mcb.20.17.6518-6536.2000.

Firsanov, D. v., Solovjeva, L. v. and Svetlova, M. P. (2011) "H2AX phosphorylation at the sites of DNA double-strand breaks in cultivated mammalian cells and tissues," *Clinical Epigenetics*, pp. 283–297. doi: 10.1007/s13148-011-0044-4.

Fleming, A. M., Ding, Y. and Burrows, C. J. (2017) "Oxidative DNA damage is epigenetic by regulating gene transcription via base excision repair," *Proceedings of the National Academy of Sciences of the United States of America*. National Academy of Sciences, 114(10), pp. 2604–2609. doi: 10.1073/pnas.1619809114.

Folias, A. *et al.* (2002) "BRCA1 interacts directly with the Fanconi anemia protein FANCA.," *Human molecular genetics*, 11(21), pp. 2591–7. doi: 10.1093/hmg/11.21.2591.

Fragkos, M., Jurvansuu, J. and Beard, P. (2009) "H2AX Is Required for Cell Cycle Arrest via the p53/p21 Pathway," *Molecular and Cellular Biology*. American Society for Microbiology, 29(10), pp. 2828–2840. doi: 10.1128/mcb.01830-08.

Frattini, A. *et al.* (2015) "High variability of genomic instability and gene expression profiling in different HeLa clones," *Scientific Reports*. Nature Publishing Group, 5. doi: 10.1038/srep15377.

Friederich, E. *et al.* (1999) “Villin function in the organization of the actin cytoskeleton. Correlation of in vivo effects to its biochemical activities in vitro.,” *The Journal of biological chemistry*, 274(38), pp. 26751–60. doi: 10.1074/jbc.274.38.26751.

Frontera, W. R. and Ochala, J. (2015) “Skeletal Muscle: A Brief Review of Structure and Function,” *Calcified Tissue International*, 96(3), pp. 183–195. doi: 10.1007/s00223-014-9915-y.

Gartel, A. L. *et al.* (2001) “Myc represses the p21 (WAF1/CIP1) promoter and interacts with Sp1/Sp3,” *Proceedings of the National Academy of Sciences of the United States of America*, 98(8), pp. 4510–4515. doi: 10.1073/pnas.081074898.

Gates, L. A. *et al.* (2017) “Acetylation on histone H3 lysine 9 mediates a switch from transcription initiation to elongation,” *Journal of Biological Chemistry*. American Society for Biochemistry and Molecular Biology Inc., 292(35), pp. 14456–14472. doi: 10.1074/jbc.M117.802074.

Geeves, M. A. and Holmes, K. C. (1999) “Structural Mechanism of Muscle Contraction,” *Annual Review of Biochemistry*, 68(1), pp. 687–728. doi: 10.1146/annurev.biochem.68.1.687.

Gessaman, J. D. and Selker, E. U. (2017) “Induction of H3K9me3 and DNA methylation by tethered heterochromatin factors in Neurospora crassa,” *Proceedings of the National Academy of Sciences of the United States of America*. National Academy of Sciences, 114(45), pp. E9598–E9607. doi: 10.1073/pnas.1715049114.

Gieni, R. S. and Hendzel, M. J. (2009) “Actin dynamics and functions in the interphase nucleus: Moving toward an understanding of nuclear polymeric actin,” *Biochemistry and Cell Biology*, pp. 283–306. doi: 10.1139/O08-133.

Goode, B. L. *et al.* (2001) “Activation of the Arp2/3 complex by the actin filament binding protein Abp1p.,” *The Journal of cell biology*, 153(3), pp. 627–34. doi: 10.1083/jcb.153.3.627.

Greenberg, M. J. *et al.* (2015) “Mechanochemical tuning of myosin-I by the N-terminal region,” *Proceedings of the National Academy of Sciences of the United States of America*. National Academy of Sciences, 112(26), pp. E3337–E3344. doi: 10.1073/pnas.1506633112.

Gupta, P. *et al.* (2017) “Myosin-1 inhibition by PClP affects membrane shape, cortical actin distribution and lipid droplet dynamics in early Zebrafish embryos,” *PLoS ONE*. Public Library of Science, 12(7). doi: 10.1371/journal.pone.0180301.

Hartlerode, A. J. *et al.* (2015) “Recruitment and activation of the ATM kinase in the absence of DNA-damage sensors,” *Nature Structural and Molecular Biology*. Nature Publishing Group, 22(9), pp. 736–743. doi: 10.1038/nsmb.3072.

Hartman, M. A. and Spudich, J. A. (2012) “The myosin superfamily at a glance,” *Journal of Cell Science*, 125(7), pp. 1627–1632. doi: 10.1242/jcs.094300.

Hasson, T. (2003) “Myosin VI: Two distinct roles in endocytosis,” *Journal of Cell Science*. doi: 10.1242/jcs.00669.

Heissler, S. M. *et al.* (2012) ‘Kinetic properties and small-molecule inhibition of human myosin-6’, *FEBS Letters*. Federation of European Biochemical Societies, 586(19), pp. 3208–3214. doi: 10.1016/j.febslet.2012.07.014.

Heride, C. *et al.* (2010) “Distance between homologous chromosomes results from chromosome positioning constraints,” *Journal of Cell Science*. Company of Biologists Ltd, 123(23), pp. 4063–4075. doi: 10.1242/jcs.066498.

Hofmann, W. A. *et al.* (2004) “Actin is part of pre-initiation complexes and is necessary for transcription by RNA polymerase II,” *Nature Cell Biology*, 6(11), pp. 1094–1101. doi: 10.1038/ncb1182.

Hokanson, D. E. and Ostap, E. M. (2006) “Myo1c binds tightly and specifically to phosphatidylinositol 4,5-bisphosphate and inositol 1,4,5-trisphosphate,” *Proceedings of the National Academy of Sciences of the United States of America*, 103(9), pp. 3118–3123. doi: 10.1073/pnas.0505685103.

Holmes, K. C. *et al.* (1990) “Atomic model of the actin filament.,” *Nature*, 347(6288), pp. 44–9. doi: 10.1038/347044a0.

Hoppe-Seyler, F. and Butz, K. (1993) “Repression of endogenous p53 transactivation function in HeLa cervical carcinoma cells by human papillomavirus type 16 E6, human mdm-2, and mutant p53.,” *Journal of virology*, 67(6), pp. 3111–7. Available at: http://www.ncbi.nlm.nih.gov/pubmed/8388491 (Accessed: September 29, 2019).

Houdusse, A. *et al.* (2006) “Crystal structure of apo-CaM bound to the first two IQ motifs of myosin V reveals essential recognition features,” *Proceedings of the National Academy of Sciences of the United States of America*, 103(51), pp. 19326–19331. doi: 10.1073/pnas.0609436103.

Houdusse, A., Silver, M. and Cohen, C. (1996) “A model of Ca2+-free CaM binding to unconventional myosins reveals how CaM acts as a regulatory switch,” *Structure*, 4(12), pp. 1475–1490. doi: 10.1016/S0969-2126(96)00154-2.

Houdusse, A. and Sweeney, H. L. (2016) “How Myosin Generates Force on Actin Filaments,” *Trends in Biochemical Sciences*. Elsevier Ltd, pp. 989–997. doi: 10.1016/j.tibs.2016.09.006.

Hu, J. *et al.* (2016) “Cisplatin DNA damage and repair maps of the human genome at single-nucleotide resolution,” *Proceedings of the National Academy of Sciences of the United States of America*. National Academy of Sciences, 113(41), pp. 11507–11512. doi: 10.1073/pnas.1614430113.

Hu, Q. *et al.* (2008) “Enhancing nuclear receptor-induced transcription requires nuclear motor and LSD1-dependent gene networking in interchromatin granules.,” *Proceedings of the National Academy of Sciences of the United States of America*, 105(49), pp. 19199–204. doi: 10.1073/pnas.0810634105.

Iacovoni, J. S. *et al.* (2010) “High-resolution profiling of gammaH2AX around DNA double strand breaks in the mammalian genome.,” *The EMBO journal*, 29(8), pp. 1446–57. doi: 10.1038/emboj.2010.38.

Ikebe, M. *et al.* (2001) “The Tip of the Coiled-coil Rod Determines the Filament Formation of Smooth Muscle and Nonmuscle Myosin,” *Journal of Biological Chemistry*, 276(32), pp. 30293–30300. doi: 10.1074/jbc.M101969200.

Ivashkevich, A. *et al.* (2012) “Use of the γ-H2AX assay to monitor DNA damage and repair in translational cancer research,” *Cancer Letters*, pp. 123–133. doi: 10.1016/j.canlet.2011.12.025.

Iwabuchi, K. *et al.* (1998) “Stimulation of p53-mediated transcriptional activation by the p53-binding proteins, 53BP1 and 53BP2.,” *The Journal of biological chemistry*, 273(40), pp. 26061–8. doi: 10.1074/jbc.273.40.26061.

Jackson, S. P. (2002) “Sensing and repairing DNA double-strand breaks,” *Carcinogenesis*. Oxford University Press (OUP), 23(5), pp. 687–696. doi: 10.1093/carcin/23.5.687.

Jang, E. R. *et al.* (2010) 'ATM modulates transcription in response to histone deacetylase inhibition as part of its DNA damage response', *Experimental and Molecular Medicine*. Nature Publishing Group, 42(3), p. 195. doi: 10.3858/emm.2010.42.3.020.

Jeske, H. and Richter, K. S. (2015) 'KU80, a key factor for non-homologous end-joining, retards geminivirus multiplication', *Journal of General Virology*, 96(9), pp. 2913–2918. doi: 10.1099/jgv.0.000224.

Jin, S. (1997) "Double-strand break repair by Ku70 requires heterodimerization with Ku80 and DNA binding functions," *The EMBO Journal*. Wiley, 16(22), pp. 6874–6885. doi: 10.1093/emboj/16.22.6874.

Jung, D. S. *et al.* (2015) "Anti-confocal versus confocal assessment of the middle ear simulated by Monte Carlo methods," *Biomedical Optics Express*. The Optical Society, 6(10), p. 3820. doi: 10.1364/boe.6.003820.

Jung, E. J. *et al.* (2006) "Myosin VI Is a Mediator of the p53-Dependent Cell Survival Pathway," *Molecular and Cellular Biology*, 26(6), pp. 2175–2186. doi: 10.1128/MCB.26.6.2175-2186.2006.

Kang, J. *et al.* (2005) "Functional Interaction of H2AX, NBS1, and p53 in ATM-Dependent DNA Damage Responses and Tumor Suppression," *Molecular and Cellular Biology*. American Society for Microbiology, 25(2), pp. 661–670. doi: 10.1128/mcb.25.2.661-670.2005.

Kapoor, P. *et al.* (2013) "Evidence for monomeric actin function in INO80 chromatin remodeling.," *Nature structural and molecular biology*, 20(4), pp. 426–32. doi: 10.1038/nsmb.2529.

Kapoor, P. *et al.* (2015) “Phosphorylation-Dependent Enhancement of Rad53 Kinase Activity through the INO80 Chromatin Remodeling Complex,” *Molecular Cell*, 58, pp. 863–869. doi: 10.1016/j.molcel.2015.03.032.

Kapty, J. *et al.* (2012) “Evaluation of phosphatidylserine-binding peptides targeting apoptotic cells,” *Journal of Biomolecular Screening*, 17(10), pp. 1293–1301. doi: 10.1177/1087057112453313.

Kelpsch, D. J. and Tootle, T. L. (2018) “Nuclear Actin: From Discovery to Function.,” *Anatomical record (Hoboken, N.J. : 2007)*, 301(12), pp. 1999–2013. doi: 10.1002/ar.23959.

Kittelberger, N. *et al.* (2016) “The role of myosin 1c and myosin 1b in surfactant exocytosis,” *Journal of Cell Science*. Company of Biologists Ltd, 129(8), pp. 1685–1696. doi: 10.1242/jcs.181313.

KINNEY, N. A., SHARAKHOV, I. V. & ONUFRIEV, A. V. 2018. Chromosome–nuclear envelope attachments affect interphase chromosome territories and entanglement. Epigenetics & Chromatin, 11, 3.

Kolodner, R. D. and Marsischky, G. T. (1999) “Eukaryotic DNA mismatch repair,” *Current Opinion in Genetics and Development*. Current Biology Ltd, 9(1), pp. 89–96. doi: 10.1016/S0959-437X(99)80013-6.

Korn, E. D. (2000) “Coevolution of head, neck, and tail domains of myosin heavy chains,” *Proceedings of the National Academy of Sciences*, 97(23), pp. 12559–12564. doi: 10.1073/pnas.230441597.

Kozlov, S. V *et al.* (2016) ‘Reactive Oxygen Species (ROS)-Activated ATM-Dependent Phosphorylation of Cytoplasmic Substrates Identified by Large-Scale Phosphoproteomics

Screen', *Molecular and Cellular Proteomics*, 15(3), pp. 1032–1047. doi: 10.1074/mcp.M115.055723.

Kulashreshtha, M. *et al.* (2016) "Chromosome territory relocation during DNA repair requires nuclear myosin 1 recruitment to chromatin mediated by ϒ-H2AX signaling," *Nucleic Acids Research*, 44(17), pp. 8272–8291. doi: 10.1093/nar/gkw573.

Kurosawa, A. *et al.* (2013) 'DNA Ligase IV and Artemis Act Cooperatively to Suppress Homologous Recombination in Human Cells: Implications for DNA Double-Strand Break Repair', *PLoS ONE*. Edited by K. Yu, 8(8), p. e72253. doi: 10.1371/journal.pone.0072253.

Kwon, S.-J. *et al.* (2015) 'ATM-mediated phosphorylation of the chromatin remodeling enzyme BRG1 modulates DNA double-strand break repair', *Oncogene*, 34(3), pp. 303–313. doi: 10.1038/onc.2013.556.

de Lanerolle, P. (2012) "Nuclear actin and myosins at a glance," *Journal of Cell Science*, 125(21), pp. 4945–4949. doi: 10.1242/jcs.099754.

Lawler, J. (2002) "Thrombospondin-1 as an endogenous inhibitor of angiogenesis and tumor growth," *Journal of Cellular and Molecular Medicine*. Journal of Cellular and Molecular Medicine, pp. 1–12. doi: 10.1111/j.1582-4934.2002.tb00307.x.

Lee, H. S. *et al.* (2010) "A cooperative activation loop among SWI/SNF, γ-H2AX and H3 acetylation for DNA double-strand break repair," *EMBO Journal*, 29(8), pp. 1434–1445. doi: 10.1038/emboj.2010.27.

Lee, J. H. and Paull, T. T. (2004) "Direct Activation of the ATM Protein Kinase by the Mre11/Rad50/Nbs1 Complex," *Science*, 304(5667), pp. 93–96. doi: 10.1126/science.1091496.

Lee, K. K. and Workman, J. L. (2007) “Histone acetyltransferase complexes: One size doesn’t fit all,” *Nature Reviews Molecular Cell Biology*, pp. 284–295. doi: 10.1038/nrm2145.

Lee, S. *et al.* (1995) “p53 and its 14 kDa C-terminal domain recognize primary DNA damage in the form of insertion/deletion mismatches,” *Cell*, 81(7), pp. 1013–1020. doi: 10.1016/S0092-8674(05)80006-6.

Leoni, L. M. *et al.* (1998) “Induction of an apoptotic program in cell-free extracts by 2-chloro-2’-deoxyadenosine 5’-triphosphate and cytochrome c,” *Proceedings of the National Academy of Sciences of the United States of America*. National Academy of Sciences, 95(16), pp. 9567–9571. doi: 10.1073/pnas.95.16.9567.

Lestourgeon, W. M. *et al.* (1975) “Contractile proteins. Major components of nuclear and chromosome non-histone proteins.,” *Biochimica et biophysica acta*, 379(2), pp. 529–52. Available at: http://www.ncbi.nlm.nih.gov/pubmed/1091294 (Accessed: September 19, 2019).

van Lierop, J. E. *et al.* (2002) “Activation of smooth muscle myosin light chain kinase by CaM. Role of LYS30 and GLY40,” *Journal of Biological Chemistry*, 277(8), pp. 6550–6558. doi: 10.1074/jbc.M111404200.

Li, J. *et al.* (2017) “Ca 2+ -Induced Rigidity Change of the Myosin VIIa IQ Motif-Single α Helix Lever Arm Extension,” *Structure*. Elsevier Ltd., 25(4), pp. 579-591.e4. doi: 10.1016/j.str.2017.02.002.

Limbo, O., Yamada, Y. and Russell, P. (2018) ‘Mre11-Rad50–dependent activity of ATM/Tel1 at DNA breaks and telomeres in the absence of Nbs1’, *Molecular Biology of the Cell*. American Society for Cell Biology, 29(11), pp. 1389–1399. doi: 10.1091/mbc.E17-07-0470.

van de Linde, S. and Sauer, M. (2014) “How to switch a fluorophore: From undesired blinking to controlled photoswitching,” *Chemical Society Reviews*, pp. 1076–1087. doi: 10.1039/c3cs60195a.

Lindsay, A. J. and McCaffrey, M. W. (2009) “Myosin Vb localises to nucleoli and associates with the RNA polymerase I transcription complex,” *Cell Motility and the Cytoskeleton*, 66(12), pp. 1057–1072. doi: 10.1002/cm.20408.

Liu, G. and Warbrick, E. (2006) “The p66 and p12 subunits of DNA polymerase δ are modified by ubiquitin and ubiquitin-like proteins,” *Biochemical and Biophysical Research Communications*, 349(1), pp. 360–366. doi: 10.1016/j.bbrc.2006.08.049.

Li, Z. *et al.* (2018) “Destabilization of linker histone H1.2 is essential for ATM activation and DNA damage repair,” *Cell Research*. Nature Publishing Group, 28(7), pp. 756–770. doi: 10.1038/s41422-018-0048-0.

Loikkanen, I. *et al.* (2009) “Myosin VI is a modulator of androgen-dependent gene expression.,” *Oncology reports*, 22(5), pp. 991–5. doi: doi.org/10.3892.

LOUIS-JEUNE, C., ANDRADE-NAVARRO, M. A. & PEREZ-IRATXETA, C. 2012. Prediction of protein secondary structure from circular dichroism using theoretically derived spectra. Proteins: Structure, Function, and Bioinformatics, 80, 374-381.

Lu, C. H. *et al.* (2018) “Swi5-Sfr1 stimulates Rad51 recombinase filament assembly by modulating Rad51 dissociation,” *Proceedings of the National Academy of Sciences of the United States of America*. National Academy of Sciences, 115(43), pp. E10059–E10068. doi: 10.1073/pnas.1812753115.

Lu, Q. *et al.* (2014) “Structure of myosin-1c tail bound to CaM provides insights into calcium-mediated conformational coupling.” doi: 10.1038/nsmb.2923.

Luger, K. *et al.* (1997) “Crystal structure of the nucleosome core particle at 2.8 A resolution.,” *Nature*, 389(6648), pp. 251–60. doi: 10.1038/38444.

Luo, J. *et al.* (2004) “The actin motor protein myosin VI is over-expressed in human prostate cancer and correlates with cancer invasion.,” *Cancer Research*, 64(7 Supplement).

Madamba, E. V., Berthet, E. B. and Francis, N. J. (2017) “Inheritance of Histones H3 and H4 during DNA Replication In Vitro,” *Cell Reports*. Elsevier B.V., 21(5), pp. 1361–1374. doi: 10.1016/j.celrep.2017.10.033.

Maddugoda, M. P. *et al.* (2007) “Myosin VI and vinculin cooperate during the morphogenesis of cadherin cell-cell contacts in mammalian epithelial cells,” *Journal of Cell Biology*, 178(3), pp. 529–540. doi: 10.1083/jcb.200612042.

Mahy, N. L. *et al.* (2002) “Spatial organization of active and inactive genes and noncoding DNA within chromosome territories,” *Journal of Cell Biology*, 157(4), pp. 579–589. doi: 10.1083/jcb.200111071.

Maison, C. *et al.* (2016) “The methyltransferase Suv39h1 links the SUMO pathway to HP1α marking at pericentric heterochromatin,” *Nature Communications*. Nature Publishing Group, 7. doi: 10.1038/ncomms12224.

Majewski, L. *et al.* (2018) “Myosin VI in the nucleus of neurosecretory PC12 cells: Stimulation-dependent nuclear translocation and interaction with nuclear proteins,” *Nucleus*, 9(1), pp. 125–141. doi: 10.1080/19491034.2017.1421881.

Maly, I. v. and Hofmann, W. A. (2016) “Calcium-regulated import of myosin IC into the nucleus,” *Cytoskeleton*, 73(7), pp. 341–350. doi: 10.1002/cm.21310.

Manceva, S. *et al.* (2007) “Calcium regulation of CaM binding to and dissociation from the Myo1c regulatory domain,” *Biochemistry*, 46(42), pp. 11718–11726. doi: 10.1021/bi700894h.

Mariño, G. and Kroemer, G. (2013) “Mechanisms of apoptotic phosphatidylserine exposure,” *Cell Research*, pp. 1247–1248. doi: 10.1038/cr.2013.115.

Martin, J. L. and Baxter, R. C. (1986) “Insulin-like growth factor-binding protein from human plasma. Purification and characterization.,” *The Journal of biological chemistry*, 261(19), pp. 8754–60. Available at: http://www.ncbi.nlm.nih.gov/pubmed/3722172 (Accessed: September 27, 2019).

Mazloum, N. and Holloman, W. K. (2009) “Second-End Capture in DNA Double-Strand Break Repair Promoted by Brh2 Protein of Ustilago maydis,” *Molecular Cell*, 33(2), pp. 160–170. doi: 10.1016/j.molcel.2008.12.023.

Mehta, I. S. *et al.* (2010) “Rapid chromosome territory relocation by nuclear motor activity in response to serum removal in primary human fibroblasts,” *Genome Biology*, 11(1). doi: 10.1186/gb-2010-11-1-r5.

Mehta, I. S. *et al.* (2013) “Chromosome territories reposition during DNA damage-repair response,” *Genome Biology*, 14(12), p. R135. doi: 10.1186/gb-2013-14-12-r135.

Melli, L. *et al.* (2018) “Bipolar filaments of human nonmuscle myosin 2-A and 2-B have distinct motile and mechanical properties,” *eLife*. eLife Sciences Publications Ltd, 7. doi: 10.7554/eLife.32871.

Ménétrey, J. *et al.* (2005) “The structure of the myosin VI motor reveals the mechanism of directionality reversal,” *Nature*, 435(7043), pp. 779–785. doi: 10.1038/nature03592.

Meyer, B. *et al.* (2016) 'Histone H3 Lysine 9 Acetylation Obstructs ATM Activation and Promotes Ionizing Radiation Sensitivity in Normal Stem Cells', *Stem Cell Reports*. Cell Press, 7(6), pp. 1013–1022. doi: 10.1016/j.stemcr.2016.11.004.

Millo, H., Leaper, K., Lazou, V. & Bownes, M. 2004. Myosin VI plays a role in cell–cell adhesion during epithelial morphogenesis. Mechanisms of Development, 121, 1335-1351.

Mol, C. D., Hosfield, D. J. and Tainer, J. A. (2000) "Abasic site recognition by two apurinic/apyrimidinic endonuclease families in DNA base excision repair: The 3' ends justify the means," *Mutation Research - DNA Repair*. Elsevier, 460(3–4), pp. 211–229. doi: 10.1016/S0921-8777(00)00028-8.

Mongkolsapaya, J. *et al.* (1999) "Structure of the TRAIL-DR5 complex reveals mechanisms conferring specificity in apoptotic initiation.," *Nature structural biology*, 6(11), pp. 1048–53. doi: 10.1038/14935.

Morrical, S. W. (2015) "DNA-pairing and annealing processes in homologous recombination and homology-directed repair," *Cold Spring Harbor Perspectives in Biology*. Cold Spring Harbor Laboratory Press, 7(2). doi: 10.1101/cshperspect.a016444.

Morris, S. M. *et al.* (2002) "Myosin VI binds to and localises with Dab2, potentially linking receptor-mediated endocytosis and the actin cytoskeleton.," *Traffic (Copenhagen, Denmark)*, 3(5), pp. 331–41. Available at: http://www.ncbi.nlm.nih.gov/pubmed/11967127 (Accessed: September 19, 2019).

Morriswood, B. *et al.* (2007) "T6BP and NDP52 are myosin VI binding partners with potential roles in cytokine signalling and cell adhesion," *Journal of Cell Science*, 120(15), pp. 2574–2585. doi: 10.1242/jcs.007005.

Mukherjea, M. *et al.* (2014) “Myosin VI Must Dimerize and Deploy Its Unusual Lever Arm in Order to Perform Its Cellular Roles,” *Cell Reports*. Elsevier, 8(5), pp. 1522-1532,. doi: 10.1016/j.celrep.2014.07.041.

Nash, J. E. *et al.* (2010) “Disruption of the interaction between myosin VI and SAP97 is associated with a reduction in the number of AMPARs at hippocampal synapses.,” *Journal of neurochemistry*, 112(3), pp. 677–90. doi: 10.1111/j.1471-4159.2009.06480.x.

Neice, A. (2010) “Methods and limitations of subwavelength imaging,” *Advances in Imaging and Electron Physics*. Academic Press Inc., 163(C), pp. 117–140. doi: 10.1016/S1076-5670(10)63003-0.

Nevzorov, I. *et al.* (2018) “Myosin-1C uses a novel phosphoinositide-dependent pathway for nuclear localization,” *EMBO reports*, 19(2), pp. 290–304. doi: 10.15252/embr.201744296.

Nishikawa, M. *et al.* (2006) “A unique mechanism for the processive movement of single-headed myosin-IX,” *Biochemical and Biophysical Research Communications*, 343(4), pp. 1159–1164. doi: 10.1016/j.bbrc.2006.03.057.

Nishimoto, N. *et al.* (2012) “Heterocomplex formation by Arp4 and β-actin is involved in the integrity of the Brg1 chromatin remodeling complex,” *Journal of Cell Science*, 125(16), pp. 3870–3882. doi: 10.1242/jcs.104349.

Nowak, G. *et al.* (1997) “Evidence for the presence of myosin I in the nucleus,” *Journal of Biological Chemistry*, 272(27), pp. 17176–17181. doi: 10.1074/jbc.272.27.17176.

Oda, E. *et al.* (2000) “Noxa, a BH3-only member of the Bcl-2 family and candidate mediator of p53-induced apoptosis.,” *Science (New York, N.Y.)*, 288(5468), pp. 1053–8. doi: 10.1126/science.288.5468.1053.

Odronitz, F. and Kollmar, M. (2007) “Drawing the tree of eukaryotic life based on the analysis of 2,269 manually annotated myosins from 328 species,” *Genome Biology*, 8(9), p. R196. doi: 10.1186/gb-2007-8-9-r196.

Ogi, T. *et al.* (2010) “Three DNA polymerases, recruited by different mechanisms, carry out NER repair synthesis in human cells.,” *Molecular cell*, 37(5), pp. 714–27. doi: 10.1016/j.molcel.2010.02.009.

Ohtsuka, T. *et al.* (2004) “The negative role of cyclin G in ATM-dependent p53 activation,” *Oncogene*, 23(31), pp. 5405–5408. doi: 10.1038/sj.onc.1207693.

Ostap, E. M. *et al.* (2002) “Mechanism of regulation of Acanthamoeba myosin-IC by heavy-chain phosphorylation,” *Biochemistry*, 41(41), pp. 12450–12456. doi: 10.1021/bi0262193.

Pageon, S. v *et al.* (2016) “Clus-DoC: a combined cluster detection and colocalization analysis for single-molecule localization microscopy data.,” *Molecular biology of the cell*, 27(22), pp. 3627–3636. doi: 10.1091/mbc.E16-07-0478.

Pant, V. *et al.* (2013) “The p53-Mdm2 feedback loop protects against DNA damage by inhibiting p53 activity but is dispensable for p53 stability, development, and longevity,” *Genes and Development*, 27(17), pp. 1857–1867. doi: 10.1101/gad.227249.113.

Paudyal, S. C. *et al.* (2017) “Dna2 initiates resection at clean DNA double-strand breaks.,” *Nucleic acids research*, 45(20), pp. 11766–11781. doi: 10.1093/nar/gkx830.

Paull, T. T. *et al.* (2000) “A critical role for histone H2AX in recruitment of repair factors to nuclear foci after DNA damage,” *Current Biology*. Current Biology Ltd, 10(15), pp. 886–895. doi: 10.1016/S0960-9822(00)00610-2.

Paull, T. T. and Gellert, M. (1999) “Nbs1 potentiates ATP-driven DNA unwinding and endonuclease cleavage by the Mre11/Rad50 complex.,” *Genes and development*, 13(10), pp. 1276–88. doi: 10.1101/gad.13.10.1276.

Percipalle, P. *et al.* (2006) “The chromatin remodelling complex WSTF–SNF2h interacts with nuclear myosin 1 and has a role in RNA polymerase I transcription,” *EMBO reports*, 7(5), pp. 525–30. doi: 10.1038/sj.embor.7400657.

Pestic-Dragovich, L. *et al.* (2000) “A myosin I isoform in the nucleus.,” *Science (New York, N.Y.)*, 290(5490), pp. 337–41. doi: 10.1126/science.290.5490.337.

Philimonenko, V. v *et al.* (2004) “Nuclear actin and myosin I are required for RNA polymerase I transcription.,” *Nature cell biology*, 6(12), pp. 1165–72. doi: 10.1038/ncb1190.

Pinskaya, M. and Morillon, A. (2009) “Histone H3 Lysine 4 di-methylation: A novel mark for transcriptional fidelity?” doi: 10.4161/epi.4.5.9369.

Pomerantz, R. T. and O’Donnell, M. (2008) “The replisome uses mRNA as a primer after colliding with RNA polymerase,” *Nature*, 456(7223), pp. 762–767. doi: 10.1038/nature07527.

Qi, W. *et al.* (2015) “BRG1 promotes the repair of DNA double-strand breaks by facilitating the replacement of RPA with RAD51,” *Journal of Cell Science*. Company of Biologists Ltd, 128(2), pp. 317–330. doi: 10.1242/jcs.159103.

Ramakrishnan, S. *et al.* (2018) “Single-strand annealing between inverted DNA repeats: Pathway choice, participating proteins, and genome destabilizing consequences,” *PLoS Genetics*. Public Library of Science, 14(8). doi: 10.1371/journal.pgen.1007543.

Rando, O. J. *et al.* (2002) “Phosphatidylinositol-dependent actin filament binding by the SWI/SNF-like BAF chromatin remodeling complex,” *Proceedings of the National Academy of*

Sciences of the United States of America, 99(5), pp. 2824–2829. doi: 10.1073/pnas.032662899.

Rennie, S. *et al.* (2018) "Transcription start site analysis reveals widespread divergent transcription in D. melanogasterand core promoter-encoded enhancer activities," *Nucleic Acids Research*. Oxford University Press, 46(11), pp. 5455–5469. doi: 10.1093/nar/gky244.

Renodon-Cornire, A. *et al.* (2013) "New Potential Therapeutic Approaches by Targeting Rad51- Dependent Homologous Recombination," in *New Research Directions in DNA Repair*. InTech. doi: 10.5772/53973.

Ripoll, L. *et al.* (2018) "Myosin VI and branched actin filaments mediate membrane constriction and fission of melanosomal tubule carriers," *Journal of Cell Biology*. Rockefeller University Press, 217(8), pp. 2709–2726. doi: 10.1083/jcb.201709055.

Rogakou, E. P. *et al.* (1998) "DNA double-stranded breaks induce histone H2AX phosphorylation on serine 139," *Journal of Biological Chemistry*, 273(10), pp. 5858–5868. doi: 10.1074/jbc.273.10.5858.

Roos, W. P. and Kaina, B. (2006) "DNA damage-induced cell death by apoptosis.," *Trends in molecular medicine*, 12(9), pp. 440–50. doi: 10.1016/j.molmed.2006.07.007.

Saito, S. N. I. *et al.* (2002) "ATM mediates phosphorylation at multiple p53 sites, including Ser 46 , in response to ionizing radiation," *Journal of Biological Chemistry*, 277(15), pp. 12491–12494. doi: 10.1074/jbc.C200093200.

Sakamoto, T. *et al.* (2005) "Step-Size Is Determined by Neck Length in Myosin V †," *Biochemistry*, 44(49), pp. 16203–16210. doi: 10.1021/bi0512086.

Sarshad, A. *et al.* (2013) “Nuclear Myosin 1c Facilitates the Chromatin Modifications Required to Activate rRNA Gene Transcription and Cell Cycle Progression,” *PLoS Genetics*. Edited by G. P. Copenhaver, 9(3), p. e1003397. doi: 10.1371/journal.pgen.1003397.

Savic, V. *et al.* (2009) “Formation of Dynamic γ-H2AX Domains along Broken DNA Strands Is Distinctly Regulated by ATM and MDC1 and Dependent upon H2AX Densities in Chromatin,” *Molecular Cell*, 34(3), pp. 298–310. doi: 10.1016/j.molcel.2009.04.012.

Schubert, H. L. *et al.* (2013) “Structure of an actin-related subcomplex of the SWI/SNF chromatin remodeler,” *Proceedings of the National Academy of Sciences of the United States of America*, 110(9), pp. 3345–3350. doi: 10.1073/pnas.1215379110.

Schuhmacher, M. K. *et al.* (2015) “Activity and specificity of the human SUV39H2 protein lysine methyltransferase.,” *Biochimica et biophysica acta*, 1849(1), pp. 55–63. doi: 10.1016/j.bbagrm.2014.11.005.

Sehgal, N., Fritz, A. J., Vecerova, J., Ding, H., Chen, Z., Stojkovic, B., Bhattacharya, S., Xu, J. & Berezney, R. 2015. Large-scale probabilistic 3D organization of human chromosome territories. Human Molecular Genetics, 25, 419-436.

Sennels, L., Bukowski-Wills, J. C. and Rappsilber, J. (2009) “Improved results in proteomics by use of local and peptide-class specific false discovery rates,” *BMC Bioinformatics*, 10. doi: 10.1186/1471-2105-10-179.

Serebryannyy, L. A. *et al.* (2016) “The effects of disease models of nuclear actin polymerization on the nucleus,” *Frontiers in Physiology*. Frontiers Media S.A., 7(OCT). doi: 10.3389/fphys.2016.00454.

Shim, M. L. *et al.* (2004) “Insulin-like growth factor binding protein-3 is a novel mediator of apoptosis in insulin-secreting cells,” *Growth Hormone and IGF Research*. Churchill Livingstone, 14(3), pp. 216–225. doi: 10.1016/j.ghir.2003.12.009.

Sielski, N. L. *et al.* (2014) “Tissue specific expression of Myosin IC Isoforms,” *BMC Cell Biology*. BioMed Central Ltd., 15(1). doi: 10.1186/1471-2121-15-8.

Skvaril, F. 1976. The question of specificity in binding human IgG subclasses to protein A-sepharose. Immunochemistry, 13, 871-872.

So, A. *et al.* (2017) “Genomic rearrangements induced by unscheduled DNA double strand breaks in somatic mammalian cells.,” *The FEBS journal*, 284(15), pp. 2324–2344. doi: 10.1111/febs.14053.

Somlyo, A. v. *et al.* (2004) “Smooth muscle myosin: Regulation and properties,” *Philosophical Transactions of the Royal Society B: Biological Sciences*, 359(1452), pp. 1921–1930. doi: 10.1098/rstb.2004.1562.

Song, X. *et al.* (2007) “Phosphorylation of the SQ H2A.X Motif Is Required for Proper Meiosis and Mitosis in Tetrahymena thermophila,” *Molecular and Cellular Biology*. American Society for Microbiology, 27(7), pp. 2648–2660. doi: 10.1128/mcb.01910-06.

So, S., Davis, A. J. and Chen, D. J. (2009) “Autophosphorylation at serine 1981 stabilizes ATM at DNA damage sites,” *Journal of Cell Biology*, 187(7), pp. 977–990. doi: 10.1083/jcb.200906064.

Stack, S. M., Brown, D. B. and Dewey, W. C. (1977) “Visualization of interphase chromosomes,” *Journal of Cell Science*, 26(1).

Sterner, D. E. and Berger, S. L. (2000) “Acetylation of Histones and Transcription-Related Factors,” *Microbiology and Molecular Biology Reviews*. American Society for Microbiology, 64(2), pp. 435–459. doi: 10.1128/mmbr.64.2.435-459.2000.

Stoyan, Dietrich. and Stoyan, Helga. (1994) *Fractals, random shapes, and point fields : methods of geometrical statistics*. Wiley.

Subramanian, C. *et al.* (2013) “CREB-Binding protein regulates Ku70 acetylation in response to ionization radiation in neuroblastoma,” *Molecular Cancer Research*, 11(2), pp. 173–181. doi: 10.1158/1541-7786.MCR-12-0065.

Sun, H. Q. *et al.* (1999) “Gelsolin, a multifunctional actin regulatory protein,” *Journal of Biological Chemistry*, pp. 33179–33182. doi: 10.1074/jbc.274.47.33179.

Sun, Y. *et al.* (2007) ‘DNA Damage-Induced Acetylation of Lysine 3016 of ATM Activates ATM Kinase Activity’, *Molecular and Cellular Biology*. American Society for Microbiology, 27(24), pp. 8502–8509. doi: 10.1128/mcb.01382-07.

Szczepińska, T., Rusek, A. M. & Plewczynski, D. 2019. Intermingling of chromosome territories. Genes, chromosomes & cancer, 58, 500-506.

Takata, M. *et al.* (1998) “Homologous recombination and non-homologous end-joining pathways of DNA double-strand break repair have overlapping roles in the maintenance of chromosomal integrity in vertebrate cells,” *EMBO Journal*, 17(18), pp. 5497–5508. doi: 10.1093/emboj/17.18.5497.

Takizawa, Y. *et al.* (2018) “Cryo-EM structure of the nucleosome containing the ALB1 enhancer DNA sequence,” *Open Biology*. Royal Society Publishing, 8(3). doi: 10.1098/rsob.170255.

Terrak, M. *et al.* (2003) “Two distinct myosin light chain structures are induced by specific variations within the bound IQ motifs--functional implications,” *The EMBO Journal*, 22(3), pp. 362–371. doi: 10.1093/emboj/cdg058.

Thomas Clouaire, A. *et al.* (2018) “Comprehensive Mapping of Histone Modifications at DNA Double-Strand Breaks Deciphers Repair Pathway Chromatin Signatures.” doi: 10.1016/j.molcel.2018.08.020.

von Tiedemann, M. *et al.* (2006) “Image adaptive point-spread function estimation and deconvolution for in vivo confocal microscopy.,” *Microscopy research and technique*, 69(1), pp. 10–20. doi: 10.1002/jemt.20261.

Tomatis, V. M. *et al.* (2013) “Myosin vi small insert isoform maintains exocytosis by tethering secretory granules to the cortical actin,” *Journal of Cell Biology*, 200(3), pp. 301–320. doi: 10.1083/jcb.201204092.

Tumbarello, D. A. *et al.* (2012) ‘Autophagy receptors link myosin VI to autophagosomes to mediate Tom1-dependent autophagosome maturation and fusion with the lysosome’, *Nature Cell Biology*, 14(10), pp. 1024–1035. doi: 10.1038/ncb2589.

Turgeon, M.-O., Perry, N. J. S. and Poulogiannis, G. (2018) ‘DNA Damage, Repair, and Cancer Metabolism’, *Frontiers in Oncology*. Frontiers Media S.A., 8(FEB). doi: 10.3389/fonc.2018.00015.

Venit, T. *et al.* (2013) “Mouse Nuclear Myosin I Knock-Out Shows Interchangeability and Redundancy of Myosin Isoforms in the Cell Nucleus,” *PLoS ONE*. Edited by A. van Wijnen, 8(4), p. e61406. doi: 10.1371/journal.pone.0061406.

Venkatachalam, G., Surana, U. and Clément, M. V. (2017) “Replication stress-induced endogenous DNA damage drives cellular senescence induced by a sub-lethal oxidative

stress," *Nucleic Acids Research*. Oxford University Press, 45(18), pp. 10564–40582. doi: 10.1093/nar/gkx684.

Vignard, J., Mirey, G. and Salles, B. (2013) "Ionizing-radiation induced DNA double-strand breaks: a direct and indirect lighting up.," *Radiotherapy and oncology : journal of the European Society for Therapeutic Radiology and Oncology*, 108(3), pp. 362–9. doi: 10.1016/j.radonc.2013.06.013.

Vintermist, A. *et al.* (2011) "The chromatin remodelling complex B-WICH changes the chromatin structure and recruits histone acetyl-transferases to active rRNA genes," *PLoS ONE*, 6(4). doi: 10.1371/journal.pone.0019184.

Volpe, T. A. *et al.* (2002) "Regulation of heterochromatic silencing and histone H3 lysine-9 methylation by RNAi," *Science*, 297(5588), pp. 1833–1837. doi: 10.1126/science.1074973.

Vreugde, S. *et al.* (2006) "Nuclear Myosin VI Enhances RNA Polymerase II-Dependent Transcription," *Molecular Cell*. Elsevier Inc., 23(5), pp. 749–755. doi: 10.1016/j.molcel.2006.07.005.

Walklate, J., Ujfalusi, Z. and Geeves, M. A. (2016) "Myosin isoforms and the mechanochemical cross-bridge cycle," *The Journal of Experimental Biology*, 219(2), pp. 168–174. doi: 10.1242/jeb.124594.

Wang, Hongyan *et al.* (2005) "Complex H2AX phosphorylation patterns by multiple kinases including ATM and DNA-PK in human cells exposed to ionizing radiation and treated with kinase inhibitors.," *Journal of cellular physiology*, 202(2), pp. 492–502. doi: 10.1002/jcp.20141.

Ward, I. M. and Chen, J. (2001) 'Histone H2AX Is Phosphorylated in an ATR-dependent Manner in Response to Replicational Stress', *Journal of Biological Chemistry*, 276(51), pp. 47759–47762. doi: 10.1074/jbc.C100569200.

Waring, P. and Müllbacher, A. (1999) "Cell death induced by the Fas/Fas ligand pathway and its role in pathology," *Immunology and Cell Biology*. Blackwell Publishing, pp. 312–317. doi: 10.1046/j.1440-1711.1999.00837.x.

Wells, A. L. *et al.* (1999) "Myosin VI is an actin-based motor that moves backwards.," *Nature*, 401(6752), pp. 505–8. doi: 10.1038/46835.

Wilkie, A. R., Lawler, J. L. and Coen, D. M. (2016) "A role for nuclear F-actin induction in human cytomegalovirus nuclear egress," *mBio*. American Society for Microbiology, 7(4). doi: 10.1128/mBio.01254-16.

Wollscheid, H. P. *et al.* (2016) "Diverse functions of myosin VI elucidated by an isoform-specific α-helix domain," *Nature Structural and Molecular Biology*. Nature Publishing Group, 23(4), pp. 300–308. doi: 10.1038/nsmb.3187.

Woolner, S. and Bement, W. M. (2009) 'Unconventional myosins acting unconventionally', *Trends in Cell Biology*, 19(6), pp. 245–252. doi: 10.1016/j.tcb.2009.03.003.

Xie, X. *et al.* (2018) "β-Actin-dependent global chromatin organization and gene expression programs control cellular identity," *FASEB Journal*. FASEB, 32(3), pp. 1296–1314. doi: 10.1096/fj.201700753R.

Xu, J., Fu, Y. and Xiao, Y. (2018) "Endonuclease IV recognizes single base mismatch on the eighth base 3' to the abasic site in DNA strands for ultra-selective and sensitive mutant-type DNA detection," *RSC Advances*. Royal Society of Chemistry, 8(48), pp. 27016–27020. doi: 10.1039/c8ra04552f.

Xu, L. *et al.* (2017) “Mechanism of DNA alkylation-induced transcriptional stalling, lesion bypass, and mutagenesis,” *Proceedings of the National Academy of Sciences of the United States of America*. National Academy of Sciences, 114(34), pp. E7082–E7091. doi: 10.1073/pnas.1708748114.

Xu, P. *et al.* (1997) “The myosin-I-binding protein Acan125 binds the SH3 domain and belongs to the superfamily of leucine-rich repeat proteins,” *Proceedings of the National Academy of Sciences*, 94(8), pp. 3685–3690. doi: 10.1073/pnas.94.8.3685.

Yaginuma, Y., Yoshimoto, M., Eguchi, A., Tokuda, A. & Takahashi, S. 2015. The human papillomavirus18 E7 protein inhibits CENP-C binding to α-satellite DNA. Virus research, 205, 27-32

Ye, J. *et al.* (2008) “Nuclear myosin I acts in concert with polymeric actin to drive RNA polymerase I transcription,” *Genes and Development*, 22(3), pp. 322–330. doi: 10.1101/gad.455908.

Yoshimura, M. *et al.* (2001) ‘Dual Regulation of Mammalian Myosin VI Motor Function’, *Journal of Biological Chemistry*, 276(43), pp. 39600–39607. doi: 10.1074/jbc.M105080200.

Yuan, H. *et al.* (2013) “Involvement of p300/CBP and epigenetic histone acetylation in TGF-β1-mediated gene transcription in mesangial cells,” *American Journal of Physiology - Renal Physiology*, 304(5). doi: 10.1152/ajprenal.00523.2012.

Yu, C. *et al.* (2009) “Myosin VI Undergoes Cargo-Mediated Dimerization,” *Cell*. Elsevier Ltd, 138(3), pp. 537–548. doi: 10.1016/j.cell.2009.05.030.

Zattelman, L. *et al.* (2017) “N-terminal splicing extensions of the human MYO1C gene fine-tune the kinetics of the three full-length myosin IC isoforms,” *Journal of Biological Chemistry*, 292(43), pp. 17804–17818. doi: 10.1074/jbc.M117.794008.

Zhang, S. *et al.* (2007) “A novel DNA damage response: Rapid degradation of the p12 subunit of DNA polymerase δ,” *Journal of Biological Chemistry*, 282(21), pp. 15330–15340. doi: 10.1074/jbc.M610356200.

Zhang, X. *et al.* (2019) “Structure and functional interactions of INO80 actin/Arp module.,” *Journal of molecular cell biology*, 11(5), pp. 345–355. doi: 10.1093/jmcb/mjy062.

Zhang, Y. and Reinberg, D. (2001) “Transcription regulation by histone methylation: Interplay between different covalent modifications of the core histone tails,” *Genes and Development*, pp. 2343–2360. doi: 10.1101/gad.927301.

Zhao, R. *et al.* (2000) “Analysis of p53-regulated gene expression patterns using oligonucleotide arrays,” *Genes and Development*. Cold Spring Harbor Laboratory Press, 14(8), pp. 981–993. doi: 10.1101/gad.14.8.981.

Zhao, X. *et al.* (2017) “Cell cycle-dependent control of homologous recombination.,” *Acta biochimica et biophysica Sinica*, 49(8), pp. 655–668. doi: 10.1093/abbs/gmx055.

Zhou, H. *et al.* (2017) “NBS1 is regulated by two kind of mechanisms: ATM-dependent complex formation with MRE11 and RAD50, and cell cycle-dependent degradation of protein,” *Journal of Radiation Research*. Oxford University Press, 58(4), pp. 487–494. doi: 10.1093/jrr/rrx014.

Zhou, W. and Doetsch, P. W. (1993) “Effects of abasic sites and DNA single-strand breaks on prokaryotic RNA polymerases,” *Proceedings of the National Academy of Sciences of the United States of America*. National Academy of Sciences, 90(14), pp. 6601–6605. doi: 10.1073/pnas.90.14.6601.

Zhou, Y. *et al.* (2017) “Regulation of the DNA Damage Response by DNA-PKcs Inhibitory Phosphorylation of ATM,” *Molecular Cell*. Cell Press, 65(1), pp. 91–104. doi: 10.1016/j.molcel.2016.11.004.

Zorca, C. E. *et al.* (2015) “Myosin VI regulates gene pairing and transcriptional pause release in T cells,” *Proceedings of the National Academy of Sciences*, 112(13), pp. E1587–E1593. doi: 10.1073/pnas.1502461112.

Chapter 10. Appendix

GENE	PEPTIDE COUNT	UNIQUE PEPTIDES	CONFIDENCE SCORE	ANOVA (P)	Q VALUE	MAX FOLD CHANGE	POWER	CONDITION	NORMALISED ABUNDANCE SAMPLE 1	SAMPLE 2	SAMPLE 3
UBA52	10	7	32.0367	0.00038	0.02097	3.379244293	1	HeLa WT	8666.052	10718.0	9346.06
RPS27A	15	4	63.7867	0.0336	0.24654	43.02299919	0.666618	HeLa WT	4471.886	472.916	12672.1
UBC	1	1	6.347	0.02707	0.221112	8.414918893	0.723636	HeLa WT	1100.448	5016.16	943.473
UBB	7	3	30.2928	0.01112	0.148277	5.958422657	0.908102	HeLa WT	6487.459	6621.91	10593.5
POLD1	9	4	39.7908	0.04986	0.289713	5.476827536	0.557656	HeLa WT	774.8179	294.781	1559.32
RAD50	12	2	5.1811	0.0828	0.422448	29.27276128	0.420048	HeLa Cis	118.2932	1859.11	986.837
XRCC5	11	3	76.7765	0.17049	0.494852	2.138908431	0.251688	HeLa Cis	212755	70073.8	72710.1
APEX1	4	4	26.2618	0.00236	0.140623	2.748897974	0.998317	HeLa Cis	94600.04	78196.0	75821.7
FANC1	4	2	20.8731	0.14664	0.481737	2.217086619	0.283191	HeLa Cis	6212.764	11755.9	21434.0
ERCC6	14	3	5.2642	0.30497	0.56171	2.680359558	0.150161	HeLa Cis	3153.796	6857.60	895.267
SMCA4	8	2	5.1291	0.3739	0.590335	Infinity	0.122249	HeLa Cis	2375.46	3828.67	2503.58
CREBBP	4	1	10.505	0.01826	0.342766	10.85604685	0.817382	HeLa Cis	124873.8	31819.3	21750.8
PSMD13	6	4	29.959	0.00442	0.092905	6.195014874	0.986959	MCF10 WT	34938.58	34689.4	24903.5

Appendix table 1. The progenesis output for the DNA damage proteins, from the mass-spectrometry data as shown in table 5.3.